University of Southampton

FACULTY OF NATURAL AND ENVIRONMENTAL SCIENCES

Ocean and Earth Sciences

Mechanisms of Ca^{2+} Signalling in Diatoms

by

Friedrich Hans Kleiner

ORCID ID 0000-0002-8429-0636

Thesis for the degree of Doctor of Philosophy

October 2020

University of Southampton

Abstract

FACULTY OF NATURAL AND ENVIRONMENTAL SCIENCES

Ocean and Earth Sciences

Thesis for the degree of Doctor of Philosophy

Mechanisms of Ca^{2+} Signalling in Diatoms

by

Friedrich Hans Kleiner

Diatoms are unicellular algae characterised by their two intercalating cell walls made of silica. Diatoms are among the most abundant phytoplankton in the oceans and are key players in the oceanic and global ecosystem, providing a significant contribution to global photosynthetic productivity and oceanic nutrient cycling. Despite their importance and ecological success, little is known on how individual diatom cells monitor abiotic changes in their environment - a crucial undertaking to ensure cell survival. This study presents novel insight into how Ca^{2+} signalling, a highly versatile and strongly conserved signalling system based on the Ca^{2+} ion as cellular messenger and initiator of cell responses, helps diatoms to quickly respond and adapt to abiotic changes in their environment. In this study, the centric diatom *Thalassiosira pseudonana* and the green alga *Chlamydomonas reinhardtii* were transformed to express fluorescent Ca^{2+} biosensors. This succeeded for *T. pseudonana* and the R-GECO1 biosensor, which complemented the existing R-GECO1 reporter strain in the pennate diatom *Phaeodactylum tricornutum*. Using both strains, this study shows that diatom cells exhibit complex spatio-temporal cytosolic Ca^{2+} elevations in response to hypo-osmotic and cold shocks. *P. tricornutum* was examined in more detail, which exhibits strongly graded Ca^{2+} elevations depending on the magnitude and change-rate of the decrease in osmolarity and temperature, including localised apical Ca^{2+} elevations and propagating Ca^{2+} waves. For hypo-osmotic shock, these Ca^{2+} elevations are vital for cell survival, and also differ between genetically identical yet physiologically different pelagic fusiform and benthic oval morphotype of *P. tricornutum*. The role of the graded cold shock-induced Ca^{2+} elevations is not yet resolved, but bear many similarities to cold-shock induced Ca^{2+} elevations in plants, known to facilitate acclimation to low temperatures. An investigation of diatom ion channels revealed a novel class of two-pore channel (TPCL) that localised to the vacuole membrane. TPCL was only found in diatom genomes and differs significantly from other TPC channels, including an atypical ion selective motif with negatively charged amino-acid substitutions, suggesting a specialised but yet unknown function in diatoms. Although they are unicellular organisms, diatoms therefore likely exhibit complex signal perception, transduction and deduction pathways rivalling those of more complex multicellular organisms.

Table of Contents

Table of Contents

Table of Tables

Table of Figures

Table of Figures

Research Thesis: Declaration of Authorship

Print name: Friedrich Hans Kleiner

Title of thesis: Mechanisms of Ca^{2+} signalling in diatoms

I declare that this thesis and the work presented in it are my own and has been generated by me as the result of my own original research.

I confirm that:

1. This work was done wholly or mainly while in candidature for a research degree at this University;
2. Where any part of this thesis has previously been submitted for a degree or any other qualification at this University or any other institution, this has been clearly stated;
3. Where I have consulted the published work of others, this is always clearly attributed;
4. Where I have quoted from the work of others, the source is always given. With the exception of such quotations, this thesis is entirely my own work;
5. I have acknowledged all main sources of help;
6. Where the thesis is based on work done by myself jointly with others, I have made clear exactly what was done by others and what I have contributed myself;
7. None of this work has been published before submission.

Signature: ..... Date: .....

Acknowledgements

"Men of Athens, there is not much time for exhortation,
but to the brave a few words are as good as many."
Hippocrates of Athens, 424 BC (to his soldiers before the battle of Delium)

I dedicate this work to my deceived grandfather Heinz Liedtke. You actively cultivated all my interests and told me the joys of curiosity. Thank you.

I want to thank the European Research Council and consequently all EU-citizens for funding this work. I am grateful to live in these relatively prosperous and peaceful times allowing me to pursuit the luxury of fundamental research. I want to thank the University of Southampton, the Marine Biological Association and the citizens of the United Kingdom for hosting me. I also appreciate the travel grant awarded by the Plymouth Marine Science and Education Foundation which allowed me to present my work to an international audience.

I want to thank Colin Brownlee for entrusting me with this project, for his advice, patience and extraordinary support. I also want to thank you for your benevolence regarding travel costs and conference fees which allowed me to enjoy multiple conferences and associated activities. I want to thank Glen Wheeler for his excellent supervision in daily matters and his devotion for my topic. No matter how I entered your offices, I always left it with a smile. I am unsure on how exactly to formulate my gratefulness and appreciation for the both of you, and I don't have much space left, so please just think of some nice words on your own (see the quote above). I guess it would be adequate to say that you are idols I would consider aiming for if I were to stay in science in the long run.

I talk now short like as if I in Germany would be; complete with Big- and Smallwriting and togetherput Words. Many, many thank to Colin and Glen for the Patience in Correctionreading mine Thesis and for the Improving the Clarity, Wordchoice and general speaky Elegance. Also when I still not perfect English speak and write, I have much learned, and it was a good Decision to(nach) England to(zu) come to(um) from Motherspeakers to learn.

Acknowledgements

I want to thank Peter Smith and Mary Smith from Southampton University for their assistance (and patience) in bureaucratic matters. I want to thank Katherine Helliwell (MBA Plymouth) for her advice on Ca^{2+} signalling and imaging. I want to thank Amanda Hopes (Mock lab, UEA Norwich) for her insightful introduction to *T. pseudonana* transformation and Golden Gate cloning. I want to thank the Mike Allen lab (PML Plymouth) for their assistance in fluorescent *T. pseudonana* cell sorting. I want to thank Payam Mershahi (Smith Lab, Cambridge University, UK) for his insight into *C. reinhardtii* transformation troubleshooting. I want to thank Shiri Graff Gaikwad (Assaf Vardi lab, Israel) for the mutual exchange in golden gate plasmids and discussion of transformation troubleshooting. I want to thank Trupti Gaikwad (MBA Plymouth) for assistance in *T. pseudonana* transformation. I want to thank Abdul Chachri for the attempted electrophysiological characterisation of TPCs. I want to thank Klaus Valentin of AWI Bremen for his insightful crash course in low temperature and its potential effects on photosynthesis, a field of study I did not know a lot of one year ago! I want to thank Mieszkowska lab for their temperature recordings in rock pools. I also would like to thank the technical assistants Angela Ward, Shay Bayley and Tyrone Roberts for keeping the labs such a tidy and productive workplace.

The small size of the MBA led to a very warm and personal atmosphere which I will miss. I want to thank my co-workers and fans of the Friedrich-Friday-mails™ for the much appreciated appraisal of my excellent humour, as well as the much appreciated tolerance of my awful humour. I would like to highlight Jack Dickenson and Kim Bird in particular with whom I associate excellent memories with, be it professional advice, emotional support, entertainment, exciting travels or heated political arguments. You and the MBA made Plymouth a place I actually liked to spend 4 years at.

Also thanks to Mama, Papa and Oma for your varied support. The contents of your supply-packages demonstrate that you took my complaints about the lacking variety of sausages in the UK to the heart, and I was glad to be reminded on the better weather in Germany.

Lastly, I want to thank Kronenbourg, Staropramen, Anastasiia, Proper Job et al. for their patience, comfort, understanding, time, loyalty and loveliness. It was a good time, but I am definitely looking forward for Pilsner Urquell, Flensburger, Anastasiia and Krombacher et al. in the near future. It has been difficult being separated for so long and I cannot wait to hold you in my arms again!

University of Southampton Research Repository

Copyright © and Moral Rights for this thesis and, where applicable, any accompanying data are retained by the author and/or other copyright owners. A copy can be downloaded for personal non-commercial research or study, without prior permission or charge. This thesis and the accompanying data cannot be reproduced or quoted extensively from without first obtaining permission in writing from the copyright holder/s. The content of the thesis and accompanying research data (where applicable) must not be changed in any way or sold commercially in any format or medium without the formal permission of the copyright holder/s.

When referring to this thesis and any accompanying data, full bibliographic details must be given, e.g.

Thesis: Friedrich Kleiner (2021) "Mechanisms of Ca^{2+} Signalling in Diatoms", University of Southampton, National Oceanography Centre, PhD Thesis, pagination.

Definitions and Abbreviations

ABA - abscisic acid
ANOVA - analysis of variance
AP - action potential
ASW - artificial seawater
ATP - adenosine triphosphate

$BacNa_V$ - bacterial voltage-gated sodium channels

Cas9 - CRISPR associated protein 9
CatSper - cation channel of sperm
Ca_V - four-domain voltage gated Ca^{2+} channel
CAX - Ca^{2+}/H^+ exchanger
CBF - core binding factor (group of transcription factors)
CDPK - Ca^{2+}-dependent protein kinase
CFP - cyan fluorescent protein
CHT - cyclohexanetetrol
CIP - alkaline Phosphatase, Calf Intestinal
CIPK - calcineurin B-like -interacting protein kinase
CNGC - cyclic nucleotide-gated channel
COR - cold-responsive
CRISPR - clustered regularly interspaced short palindromic repeats

DD - (2*E*,4*E/Z*)-decadienal
DMSO - dimethyl sulfoxide
DMSP - dimethylsulfoniopropionate
DNA - deoxyribonucleic acid
DREB - dehydration-responsive element-binding protein

EGFP - enhanced green fluorescent protein
EGTA - ethylene glycol-bis(β-aminoethyl ether)-N,N,N',N'-tetraacetic acid
EPS - extracellular polysaccharides
ER - endoplasmatic reticulum
EukCat - 1D Voltage-Gated Cation Channels

FCP - fucoxanthin-chlorophyll binding protein
FRET - Förster resonance energy transfer
GFP - green fluorescent protein
GLR - glutamate receptor-like channel

HEK - human embryo kidney
HEPES - 4-(2-hydroxyethyl)-1-piperazineethanesulfonic acid
HSP70 - heat-shock protein 70

IP_3R - inositol trisphosphate receptor channel
ISM - ion selective motif

JGI - joint genome institute

LHC - light harvesting complex

MCA - mechanosensitive channel (in plant literature)
MCU - mitochondrial Ca^{2+} uniporter
MMETSP - marine microbial eukaryote transcriptomic database
mRNA - messenger RNA
MscS - mechanosensitive channel (in bacteria literature)

NAADP - nicotinic acid adenine dinucleotide phosphate
NAT - gene conferring nourseotricine resistance
Na_V - four-domain voltage gated Na^{2+} channel
NCBI - national centre for biotechnology information
NCX - Ca^{2+}/Na^{+} antiporter
NO - nictric oxide

OSCA - hyperosmolarity-gated Ca^{2+} permeable channels
OST1 - open stomata 1 (*A. thaliana* protein kinase)

PCR - polymerase chain reaction
PIP_2 - phosphatidylinositol 4,5-bisphosphate
$PI(3,5)P_2$ - phosphatidylinositol 3,5-bisphosphate
PsaD - photosystem I protein D
PtR1 - *P. tricornutum* strain expressing RGECO1

RbcS2 - ribulose 1,5 bisphosphate carboxylase subunit
RGECO - red genetically encoded Ca^{2+} indicator
RNA - ribonucleic acid
RNAi - RNA interference
ROI - region of interest
ROS - reactive oxygen species
RRed - ruthenium red
RyR - ryanodine receptor channel

SEM - standard error of the mean
sgRNA - single guide RNA

TAP - tris-acetate-phosphate medium
TPC - two-pore cation channel
TPCL - two-pore cation-like channel
TRP - transient receptor potential channel

VDCC - voltage dependent cation channel

Wt - wildtype

Chapter 1 Calcium signalling in diatoms

1.1 Introduction to diatoms

"Alga" is a relative unspecific term used to address various phylogenetically diverse organisms distinct from land plants, mosses and ferns which are or were able to perform photosynthesis (Figueroa-Martinez et al., 2015). The ecologic success of the first photosynthetic cyanobacteria formed an oxidising atmosphere which caused the first mass extinction, and as a result, most ecosystems on earth are now dependent on photosynthetic organisms (Blankenship, 2010). Within these ecosystems, uni- and/or multicellular photosynthetic organisms form the basis of many food chains. Despite their small size, microalgae have a significant impact, and it is cautiously estimated that they are responsible for 50 % of global photosynthetic activity (Field et al., 1998; Regaudie-de-Gioux et al., 2014). Indeed, the primary production of oceans is dominated by microalgae, and an exceptionally important group of among these are diatoms.

Diatoms (Bacillariophyceae) are unicellular microalgae belonging to the superphylum of heterokonts. Some diatoms also organise in chains of several individual cells or are part of biofilms (Bahulikar *et al.,* 2008, Musielak *et al.,* 2009). It is generally accepted that a diatom ancestor acquired the ability to perform photosynthesis through endosymbiotic assimilation of a eukaryotic red alga. This made diatoms highly successful: At least 100,000 species are estimated to exist, making diatoms the most species-rich group of microalgae (Malviyaa et al., 2016). Furthermore, diatoms are estimated to be responsible for up to 50 % of the oceanic photosynthetic which translates as a fifth of global photosynthetic activity (Falkowski et al., 1998; Field et al., 1998).

The hallmark of diatoms is their highly delicate silicified bipartite cell walls of various shapes and symmetries called frustules, which are thought to help maintain buoyancy (Miklasz and Denny, 2010; Raven and Waite, 2004), increase photosynthesis efficiency or to protect against grazers (Zhang et al., 2017). Evidence of frustules in fossil records date back to the Jurassic period (Sims et al., 2006).

Two major groups of diatoms are distinguished through their symmetry. The first, more ancient and mostly marine branch are centric diatoms which are further divided into

diatoms of radial or multipolar symmetry (Sims et al., 2006). The second, evolutionarily younger branch are pennate diatoms of bilateral symmetry. Within these, the sub-branch of raphid pennates is known to glide on surfaces using their frustule as slide and secreted substances as lubricant (Poulsen et al., 1999).

An additional testament to the success of diatoms is their broad distribution. They may be found in open and coastal sea regions (and may dominate algae blooms there), in Polar Regions and sea ice environments, in estuarine regions such as mudflats, in freshwater and wet soils (Malviyaa et al., 2016). In some of these areas, diatoms may experience rapid fluctuations in abiotic factors including salinity, nutrient availability, temperature and light, or may need to coordinate biotic interactions with grazers, parasites or mates.

To coordinate adjustments to metabolism and initiate protective measures to these stressors and stimuli, a system of perception and signalling pathways is necessary which detects the stimulus and translate it into an appropriate cell response. An exceptionally important and versatile signalling system broadly utilised in eukaryotes is based on the element calcium.

1.2 Introduction to Ca^{2+} signalling

Calcium is an alkaline earth metal and the fifth most abundant element of Earth's crust. Throughout living nature, calcium is broadly established as a major building block through a process called biomineralization, and is thus a key component for bones, seashells, corals or the calcified plates of a different successful group of microalgae called coccolithophores (Currey, 2005; Kocot et al., 2016; Westbroek et al., 2007). Besides these structural applications, the calcium ion, Ca^{2+}, is also very important for cellular physiology and biochemistry.

All currently known organisms of the three major branches of life (Bacteria, Archaea and Eukarya) share a very low cytosolic free Ca^{2+} concentration (~100 nM) in relation to their environment (1-5 mM in vertebrate serum, 10 mM in seawater, 0.02-2 mM in freshwater (Campbell, 2015)). Since Ca^{2+} ions cannot pass bio-membranes, and considering the up to 10000-fold difference between intra- and extracellular free Ca^{2+} concentration, Ca^{2+} has a

very large inwardly-directed electrochemical potential gradient driving Ca^{2+} into the cytoplasm of cells. This gradient is actively maintained by Ca^{2+} pumps and/or transporters located either at the plasma membrane or membranes of intracellular organelles which actively remove Ca^{2+} from the cytosol. The Ca^{2+} efflux system is likely an ancient feature of cells and is necessary to prevent harmful Ca^{2+}-related toxicity effects such as calcium phosphate precipitation or protein aggregation (Campbell, 2015). Ca^{2+} quickly enters the cytosol if the plasma membrane barrier is breached through damage, and it is proposed that this led to the recruitment of Ca^{2+} ions as a signalling agent for cell damage, and later, for a broad range of other stimuli (Marchadier et al., 2016).

Thus, sophisticated Ca^{2+} signalling pathways emerged, which all follow the same principle:

1.3 The Ca^{2+} signalling toolkit and its components

The basic concept of Ca^{2+}-based signalling involves three major steps (Edel et al., 2017):

1. Influx: Given a trigger, ion channels open, resulting in a relatively fast passive influx of free Ca^{2+} ions down their electrochemical potential gradient into the cytosol (up to 10^8 ions /s may pass in an animal action potential, (Raghavan et al., 2019)). Ion channels can show varying ion selectivity depending on channel type and may be located at the plasma membrane or at the membrane of intracellular organelles. The trigger necessary to open an ion channel is again dependent on channel type, and may include membrane potential (voltage gated channels), the binding of ligands, or changes in membrane tension. Multiple opening stimuli may need to apply at once, and some channels also have auxiliary subunits which further affect channel activity (Campiglio and Flucher, 2015; Haworth and Brackenbury, 2019). Channel-mediated Ca^{2+} entry leads to an increase in cytosolic Ca^{2+} from sub-micromolar resting levels to levels greater than micromolar (Bagur and Hajnóczky, 2017). This elevation of cytosolic Ca^{2+} concentration can be very rapid and can underlie very fast physiological processes, such as rapid muscular contraction in animals, which can occur over millisecond time scales (Hill-Eubanks et al., 2011).

2. Efflux: Cytosolic excess Ca^{2+} is then quickly and actively removed from the cytosol to extracellular space or intracellular compartments (e.g. mitochondria, endoplasmatic reticula (ER) or vacuoles) utilising an arsenal of ATP-driven Ca^{2+} pumps (McAinsh and Pittman, 2009) or Ca^{2+} symporters (Sharma et al., 2013). In animals, pumps have generally high affinity for Ca^{2+} but low transport rates, whereas symporters have opposite properties, indicating that cells may have different demands for Ca^{2+} efflux (Carafoli, 2002; Clapham, 2007). Eventually, Ca^{2+} transporters shift the cytosolic Ca^{2+} concentration back towards low "resting"-state levels.

3. Decoding: Cytosolic Ca^{2+} acts as a reversible on- and off switch to a broad range of Ca^{2+} binding proteins, e.g. calmodulins, calcineurins or annexins (Yáñez et al., 2012). When activated, these Ca^{2+} sensors can then regulate downstream responses, e.g. through phosphorylation or binding of the sensor to target proteins (Edel et al., 2017). Not all Ca^{2+} binding proteins have an inherent function in signal decoding, as some merely act as Ca^{2+} buffers, while others such as Ca^{2+} binding ion channels may actively contribute to the intensity or progression of the Ca^{2+} elevation (Carafoli, 2002; Purves et al., 2001).

Two major theories for the interpretation of the cytosolic Ca^{2+} influx and efflux kinetics exist. According to the Ca^{2+} signature hypothesis, the duration, intensity, intervals and also location of these signatures will be a vital part in decoding the type and strength of stimulus (Whalley and Knight, 2013). The alternative is that Ca^{2+} acts as on-off switch for a cell response in which the signature of a Ca^{2+} elevation has a negligible role (Scrase-Field and Knight, 2003). These hypotheses are not necessarily mutually exclusive and it likely depends on the stimulus and organism which of the signature decoding theories is favoured.

The exemplary plant cell shown in Fig. 1.1 presents a versatile array of Ca^{2+} channels, efflux proteins and Ca^{2+} sensors. The Ca^{2+} signalling toolkit of other organisms such as diatoms may differ in type, abundance and number of components (Armbrust et al., 2004; Bowler et al., 2008).

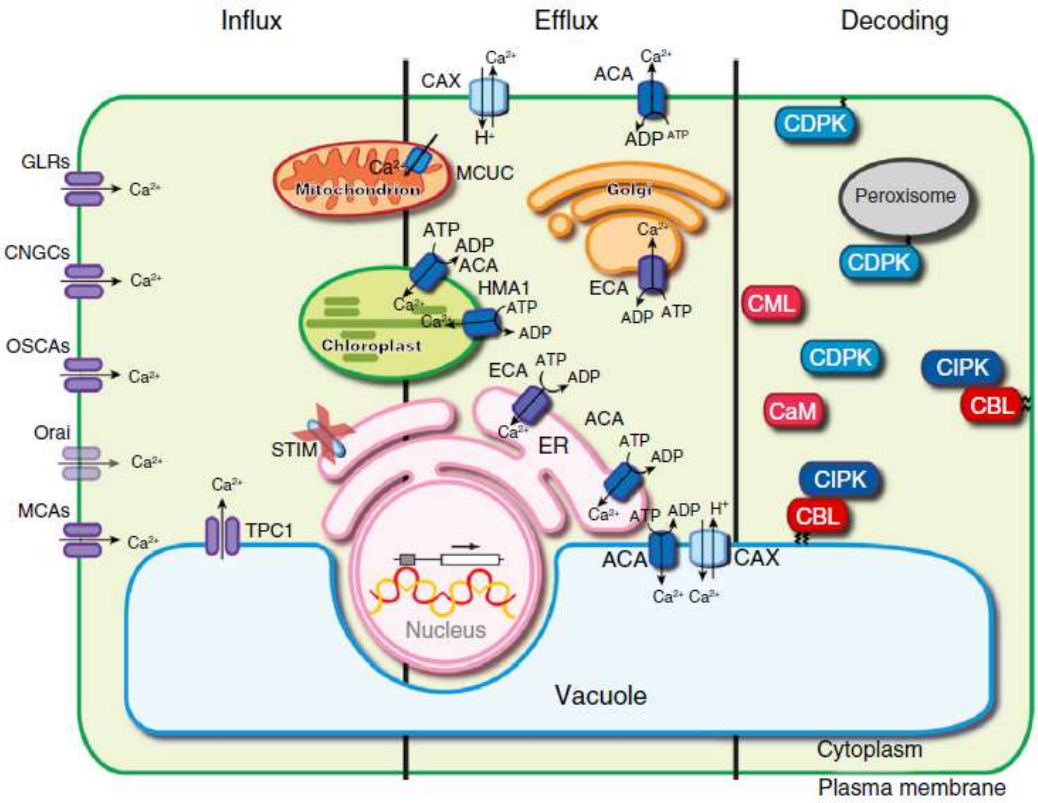

Figure 1.1: Schematic of Ca^{2+} signalling toolkit in a plant cell.

Influx systems: Cyclic nucleotide-gated channels (CNGCs), glutamate receptor-like channels (GLRs), two-pore channels (TPCs), mechanosensitive channels (MCAs), reduced hyperosmolality-induced Ca^{2+} increase channels (OSCAs) and potentially by Orai channels (at least in plants outside of the angiosperm group). Efflux systems: autoinhibited Ca^{2+}-ATPases (ACAs), ER-type Ca^{2+}-ATPases (ECAs), P1-ATPases (HMA1), mitochondrial calcium uniporter complex (MCUC) and Ca^{2+}/H^{+} exchangers (CAX). Decoding systems: calcium-dependent protein kinases (CDPKs), calcineurin B-like (CBL) protein kinases (CIPKs) and calmodulin (CaM) and CaM-like proteins (CMLs) and more (not shown). Fig. from (Edel et al., 2017).

1.4 The Ca^{2+} signalling toolkit in plants, animals and algae

Plants and animals differ in their perception and responses to environmental stimuli in a number of ways. For example, multicellular animals generally show neuromuscular activity, allowing rapid movement and behaviour-based responses. In contrast, plants are generally non-motile and thus need to integrate a wide range of external stimuli into appropriate growth and adaptive responses. Moreover, photosynthesizing plants have the added requirement to regulate their complex metabolism in the face of rapid changes in environmental conditions including light, temperature, water availability and osmotic environment.

The resulting different signalling requirements between animals and plants also manifest in differences in their Ca^{2+} signalling toolkit. Recent increase in sequenced genomes revealed that the Ca^{2+} signalling toolkit in unicellular algae may show homologs of components found in animals or plants, but also may show exclusive components (Verret et al., 2010; Wheeler et al., 2019; Wheeler and Brownlee, 2008). For example, previous studies revealed that the pennate diatom *P. tricornutum* and centric diatom *T. pseudonana* possess a diverse range of ion channels.

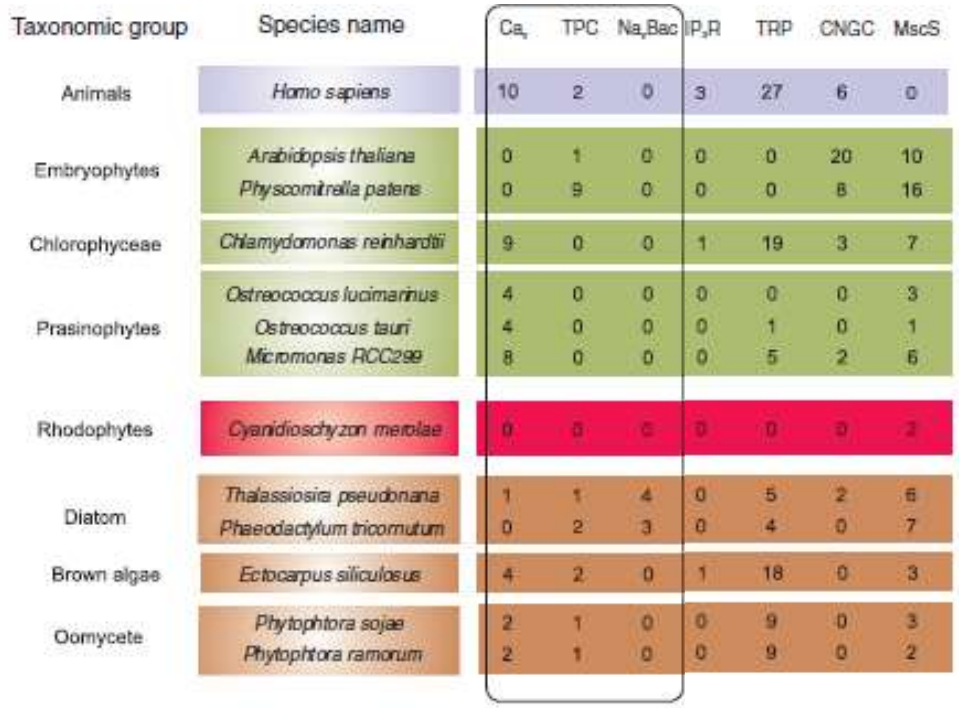

Taxonomic group	Species name	Ca_v	TPC	Na_vBac	IP_3R	TRP	CNGC	MscS
Animals	*Homo sapiens*	10	2	0	3	27	6	0
Embryophytes	*Arabidopsis thaliana*	0	1	0	0	0	20	10
	Physcomitrella patens	0	9	0	0	0	8	16
Chlorophycese	*Chlamydomonas reinhardtii*	9	0	0	1	19	3	7
Prasinophytes	*Ostreococcus lucimarinus*	4	0	0	0	0	0	3
	Ostreococcus tauri	4	0	0	0	1	0	1
	Micromonas RCC299	8	0	0	0	5	2	6
Rhodophytes	*Cyanidioschyzon merolae*	0	0	0	0	0	0	2
Diatom	*Thalassiosira pseudonana*	1	1	4	0	5	2	6
	Phaeodactylum tricornutum	0	2	3	0	4	0	7
Brown algae	*Ectocarpus siliculosus*	4	2	0	1	18	0	3
Oomycete	*Phytophtora sojae*	2	1	0	0	9	0	3
	Phytophtora ramorum	2	1	0	0	9	0	2

Figure 1.2: Overview of Ca^{2+}-permeable channels in several photosynthetic lineages.

Ca_v = voltage dependent Ca^{2+}-channel, TPC = Two-pore channel, Na_vBac = single-domain bacterial-type channel, IP_3R = inositol-1,4,5 trisphosphate receptor, TRP = transient receptor channel, CNGC = cylic nucleotide gated channel, MscS = mechanosensitive ion channel. Fig. modified from (Verret et al., 2010).

Plants are relatively well characterised and reveal differences in their signalling toolkit compared to animals (Fig. 1.2). The major classes of currently known Ca^{2+} channels in plants are ionotropic glutamate receptors (GLRs), mechanosensitive channels (MscS), cyclic nucleotide-gated channels (CNGG), and two pore channels (TPCs) (Ali et al., 2007; Hetherington and Brownlee, 2004; Peiter et al., 2005; Qi et al., 2006). The relative low variety in Ca^{2+} channels in plants compared to animals and some algae is proposed to be compensated by an increased diversity within the present ion channel classes, such as CNGCs, and increased variety in efflux-components and especially Ca^{2+} binding proteins (Kleist et al., 2014; Weinl and Kudla, 2009; Zhu et al., 2015). The distribution of some ion channels classes and Ca^{2+} signalling components will be further presented below.

1.4.1 Four-domain voltage gated Ca^{2+} channels

Ca_V channels in animals are known for exceptionally transient Ca^{2+} elevations required for muscle contraction and neurotransmitter release in synapses. Within algae, the current pattern of Ca_V channel abundance suggest a role in motility. In the green alga *C. reinhardtii*, the Ca_V-2 channel is important for flagella beating (Brunet and Arendt, 2016), but the role of the other eight Ca_V channels is less understood. In diatoms, Ca_V channels are only evident in centric species. Notably, centric diatoms perform sexual reproduction involving flagellated male gametes (Nanjappa et al., 2017), whereas pennate diatoms which lack gametes with flagella appear to lack Ca_V channels (Verret et al., 2010; Wheeler and Brownlee, 2008). However, it is unknown whether Ca_V channels in centric diatoms are responsible for flagella activity.

An exception to this pattern may occur in the green lineage. Ca_V channels appear absent in plants (Edel and Kudla, 2015; Verret et al., 2010; Wheeler and Brownlee, 2008), and land plants do not have cells with flagella during their vegetative phase (Bhattacharya and Medlin, 1998; Hodges et al., 2012). However, the more basal land plants (bryophytes, pteridophytes, some cycads and *ginkgo*) still have flagellated male gametes (Hodges et al., 2012) but also lack Ca_V channels (Verret et al., 2010).

1.4.2 Two-pore channels

TPCs are generally found at the membrane of intracellular organelles of acidic lumina, such as vacuoles in plants and endolysosomes in animals (Hedrich et al., 2018). They appear to be not highly selective for Ca^{2+}, but are nonetheless thought to cause or reinforce cytosolic Ca^{2+} elevations through Ca^{2+} release in plants and animals and to facilitate Ca^{2+} dependent endolysosomic vesicle trafficking in animal cells (Grimm et al., 2017; Guo et al., 2017). Curiously, they appear to have been lost in many unicellular archaeplastidan lineages. The major groups within the stramenopiles (diatoms, oomycetes, brown algae) all have TPCs, but their role is unknown (see Chapter 4).

1.4.3 EukCat channels

The $BacNa_V$ channels presented in Fig. 1.2 represent a novel class of single-domain voltage gated Ca^{2+} channels designated as EukCats (Helliwell et al., 2019). EukCats are related but distinct to other single domain channels such as bacterial $BacNa_V$ or animal CatSper channels. No direct homologs of EukCat were found in animals and plants, but presence in haptophytes, pelagophytes, cryptophytes and dinoflagellates demonstrate a broad distribution among unicellular algae with the exclusion of archaeplastidans (Helliwell et al., 2019).

1.4.4 Transient receptor potential channels

Transient receptor potential channels (TRPs) are a versatile group of predominantly mechanosensitive channels, but certain members are known for their highly polymodal way of function (Zheng, 2013). As such, some TRPs can also be affected by membrane potential and/or act as receptors for chemical compounds. Members of this channel class are important for vision, and sensing of temperature, taste, pain and osmotic stress in animals (Zheng, 2013).

While absent in embryophytes, TRPs are found in many algae including chlorophytes and stramenopiles such as diatoms, brown algae and oomycetes (Verret et al., 2010). *P. tricornutum* has four and T*. pseudonana* has five TRPs, indicating that this channel class plays an important role in diatoms.

1.4.5 Hyperosmolarity-gated Calcium permeable channels

Hyperosmolarity-gated Calcium permeable channels (OSCA) are mechanosensitive channels found in the plasmamembrane of plants and are also present in other archaeplastidans including red- and green algae (Edel and Kudla, 2015; Murthy et al., 2018). In plants, OSCAs infer hyperosmotic induced Ca^{2+} elevations (Yuan et al., 2014), but it is not known if they also have this role in microalgae. There is evidence of several OSCAs in

diatoms (Armbrust et al., 2004; Bowler et al., 2008), but their role has not been investigated.

1.4.6 Intracellular Ca^{2+} release systems

Inositol trisphosphate receptor-channels (IP_3Rs) are important Ca^{2+} release channels mostly found on the ER membrane and were shown to translate external stimuli into complex intracellular Ca^{2+} elevations in animals, including oscillations and Ca^{2+} waves (Yoshida and Imai, 1997). IP_3R are present in chlorophytes and brown algae, but absent in plants and diatoms (Cock et al., 2010; Verret et al., 2010). The role of IP_3Rs in algae has not been investigated.

Ryanodine receptor channels (RyR) channels are also an important class of intracellular Ca^{2+} release channels and are important for muscle and neuron activity in animals (Lanner et al., 2010). In algae, RyR channels are evident in some stramenopiles such as the brown alga *Ectocarpus* and omycetes but appear absent in diatoms (Cock et al., 2010; Verret et al., 2010; Zheng and Mackrill, 2016). Lacking IP_3R and RyR-channels, diatoms must therefore either not rely on or possess a currently unknown functional homolog facilitating Ca^{2+} release from internal stores.

1.4.7 Channels and transporters at the mitochondrion membrane

Besides the ER and the vacuole, mitochondria can also act as intracellular Ca^{2+} store. Mitochondrial Ca^{2+} uniporters (MCU) are a highly conserved family of Ca^{2+} efflux proteins transporting cytosolic Ca^{2+} into the mitochondrion and are thought to be involved in signalling, energy metabolism and cell death (Bick et al., 2012). MCU and its conserved regulatory associate MICU1 are evident for plants and animals, and presence within oomycetes suggest a broad distribution (Wheeler et al., 2019). Conversely, MCU and MICU1 were lost in some fungal and protozoan lineages, the latter including the red alga *C. merolae* and the diatoms *P. tricornutum* and *T. pseudonana*. This suggests that novel Ca^{2+} uptake mechanisms for the mitochondrion developed in diatoms (Bick et al., 2012; Wheeler et al., 2019).

1.4.8 Ca^{2+} efflux systems

There are also differences in the distribution of Ca^{2+} efflux proteins. Animals mainly possess Ca^{2+}/Na^{+} antiporters (NCX), whereas plants additionally have Ca^{2+}/H^{+} antiporters (CAX) (Bose et al., 2011; Wang et al., 2016a). CAX were also found in several algae including the haptophyte *Emiliania huxleyi*, the green alga *Chlamydomonas reinhardtii* and the diatom *P. tricornutum* (Emery et al., 2012; Mackinder et al., 2010; Wheeler et al., 2019). There is no evidence for NCX in the diatom *P. tricornutum* (Emery et al., 2012).

1.4.9 Ca^{2+} binding proteins

Ca^{2+} binding proteins also vary in distribution. Some are widespread and found in plants and animals (e.g. calmodulin *H. sapiens* n = 30, *A. thaliana* n = 54), some are restricted to animals (e.g. S100, calbindin, troponin c), and some are restricted to plants (e.g. CDPK, CIPK) (Nagata et al., 2004; Weinl and Kudla, 2009). In plants, CDPKs and CIPKs are known to play important roles in biotic and abiotic Ca^{2+} responses (Weinl and Kudla, 2009). Homologs of CDPKs and CIPKs were found in coccolithophores and diatoms (Edel and Kudla, 2015; Talevich et al., 2011), but their roles are poorly understood.

CIPKs are absent and CDPKs are poorly distributed in red algae. Instead, a novel and distinct class of Ca^{2+} sensor kinases was identified in red algae known as CDTKLs (Brawley et al., 2017; Wheeler et al., 2019).

There are far more components of the Ca^{2+} signalling toolkit, but the above examples may suffice to highlight the conserved importance of Ca^{2+} as versatile messenger and to reveal substantial differences in the Ca^{2+} signalling toolkit of animals, plants and algae.

1.5 Animal-specific Ca^{2+} signalling

Ca^{2+} signalling in animals is involved in a plenitude of signalling pathways and orchestrate muscle activity (Kuo and Ehrlich, 2015), fertilisation of eggs (Whitaker, 2006), sperm motility (Jimenez-Gonzalez et al., 2006) and proliferation, migration, differentiation and death of cells (Stewart and Davis, 2019; Whitaker, 2006). In neuron cells, Ca^{2+} modulates synaptic signal transmission through Ca_V dependent exocytosis of vesicles containing neurotransmitters (Südhof, 2012) and regulates nerve function and memory through the calmodulin binding protein CaMKII (Carafoli, 2002; Yamauchi, 2005). More typical roles of Ca^{2+} signalling in animal cells include sensing of oxidative stress in muscle cells (calcineurin, (Ermak and Davies, 2002)), temperature in neurons (TRP, (Wetsel, 2011)), osmotic stress in muscle cells (TRP in muscle cells, (Apostol et al., 2009)), endolysosomal vesicle trafficking (TPC, (Marchant and Patel, 2015) or cell damage (Cheng et al., 2015).

A prominent example for complexity of Ca^{2+} signalling in animals as well as the Ca^{2+} signature hypothesis are smooth muscle cells. Ca^{2+} regulates both relaxation and contraction depending on whether the Ca^{2+} responses occur locally or globally (Berridge et al., 1999). Relaxation is facilitated by spontaneous Ca^{2+} sparks below the plasma membrane which in turn activate K^+ channels leading to membrane hyperpolarisation, whereas contraction is facilitated through coordination of Ca^{2+} sparks into RyR2-mediated Ca^{2+} waves which propagate the cell and activates the contractile components (Berridge et al., 1999; Hill-Eubanks et al., 2011). Another particular impressive example are IP_3R-mediated highly delicate rotating or meandering Ca^{2+} waves in *X. laevis* oocytes (Atri et al., 1993; Tang et al., 2008).

This demonstrates that Ca^{2+} is recruited to orchestrate “animal-exclusive” activities but is also preserved as a signalling agent for more basic stimuli – although underlying channels and mechanisms may vary from other organisms.

1.6 Plant-specific Ca^{2+} signalling

Plants also show complex Ca^{2+} elevations. They may be single and transient or repetitively oscillate between a few seconds to several hours (Allen and Schroeder, 2001; Carpaneto et al., 2007; Dodd et al., 2005; Hayashi et al., 2006). Mostly, these Ca^{2+} elevations are not as fast as in animals, but rapid animal-like action potentials (although involving Cl^- instead of Na^+) were observed in the rapid turgor-driven movements of *Mimosa pudica* and the Venus flytrap *Dionaea muscipula* (Hedrich and Neher, 2018)

In terms of function, it has been shown so far that plant Ca^{2+} signalling is involved in mechanical and osmotic stimuli, in oxidative stress, in response to *Rhizobium* nodulation factors, pathogen- and plant-hormone signalling, light and temperature shock responses (Fasano et al., 2002; Kiegle et al., 2000; Knight et al., 1997; Knight et al., 1992; Miwa et al., 2006; Pei et al., 2000; Rudd and Franklin-Tong, 2001; Takahashi et al., 1997).

1.7 Ca^{2+} signalling in algae

In contrast to the well-characterised signalling systems of animals and plants, relatively little is known about Ca^{2+} signalling in unicellular algae. However, some microalgae have provided substantial insight which will be briefly discussed below.

1.7.1 Ca^{2+} signalling in the green alga ***Chlamydomonas reinhardtii***

The green freshwater alga *C. reinhardtii* is a highly important model protist (see Chapter 2). In *C. reinhardtii*, Ca^{2+} signalling is mostly investigated with respect to flagella function and cell motility (Wheeler 2017).

The two flagella of *C. reinhardtii* beat in a breast-stroke motion to propel the cell body in liquids (Bickerton et al., 2016). *C. reinhardtii* is known to adjust its swimming behaviour towards or away from light sources (phototaxis) and to exhibit a brief backwards-swimming movement in response to brief impulses of intense light (photoshock). Ca^{2+} plays a key role in this: While smaller changes in intraflagellar Ca^{2+} independently affect beating

frequencies resulting in change of swimming direction (Kamiya and Witman, 1984), a large Ca^{2+} increase changes the breast-stroke beating to an undulating beating, reversing movement direction (Bessen et al., 1980; Okita et al., 2005). Both responses are based on light-dependent depolarisation of plasma membrane light-gated cation cannels called channelrhodopsins, and in case of the photoshock response these channelrhodopsins were shown to further activate Ca_V2 channels in the flagellum (Fujiu et al., 2009; Harz and Hegemann, 1991). Intraflagellar Ca^{2+} hereby binds to axonemal motor protein complexes called dyneins which are in contact with microtubules (Sakato et al., 2007), leading to a conformation change and overall change in flagellum performance (DiPetrillo and Smith, 2013; Pazour et al., 2005; Sakato et al., 2007).

C. reinhardtii may also use its flagella to maintain contact or react to surfaces, objects and mates. Surface gliding is realised through adhesive glycoproteins (FMG-1B) located in the plasmamembrane of the flagellum which are in contact with a different type of intraflagellar dyneins than used for swimming (Collingridge et al., 2013). The involvement of Ca^{2+} in gliding was directly proven through employment of flagellum-localised Ca^{2+} sensitive dyes monitored with total internal reflection fluorescence microscopy (Collingridge et al., 2013), revealing that individual flagella may exhibit propagating Ca^{2+} waves and that coordination of these elevations is important for gliding direction. Voltage-gated or mechanosensitive Ca^{2+} channels were suggested to underlie these Ca^{2+} waves (Collingridge et al., 2013). Ca^{2+} as also been implicated in signalling during mating which includes the entanglement of flagella, though the underlying mechanisms are unknown (Goodenough et al., 1993). TRP11 is proposed to infer mechanoception to the proximal region of the flagella given that low TRP11 expression resulted in loss of the collision-avoidance reaction (Fujiu et al., 2011).

Ca^{2+} also plays a role in maintenance and growth of flagella. Knock-down of *C. reinhardtii* CDPK1 led to a phenotype with reduced flagellum length (Liang and Pan, 2013). Moreover, deflagellation caused by organic acids or elevated Ca^{2+} concentrations in the medium coincided with a rapid elevation of cytosolic Ca^{2+} in the apical region of the cell, showing a connection between apical Ca^{2+} signalling and deflagellation (Aiyar et al., 2017; Wheeler et al., 2008). Capsaicin induced deflagellation was partially inhibited when the TRP channel ADF1 was knocked out (Wada 2020). The heat- and PIP_2 (Phosphatidylinositol 4,5-

bisphosphate) sensitive TRP1 channel is down-regulated during deflagellation, but its definite role remains unknown (Arias-Darraz et al., 2015; McGoldrick et al., 2019).

Ca^{2+} also is important for responses unrelated to flagella activity in *C. reinhardtii*, but the understanding of underlying signalling pathways remains fragmented. Hypo- and hyperosmotic stress led to dose-dependent transient and repetitive Ca^{2+} elevations in the cytosol, respectively (Bickerton et al., 2016). Ca^{2+}-binding CDPKs were upregulated and showed increased intracellular mobility in response to acetate, phosphate and nitrogen starvation (Motiwalla et al., 2014). Similar to plants, Ca^{2+} plays a role in photosynthesis related photoprotection and carbon availability. RNAi mediated knock-down of a regulative Ca^{2+} binding protein (CAS) located in the thylakoid membrane of *C. reinhardtii* led to low abundance of the light-harvesting complex –component LHCSR3 (Petroutsos et al., 2011) and also negatively affected the efficiency of the carbon concentrating mechanism under CO_2 deplete conditions (Wang et al., 2016b).

1.7.2 Ca^{2+} signalling in red algae

Besides *C. reinhardtii*, Ca^{2+} signalling was only sparsely investigated in other archaeplastidans. In *Phorphyra yedoensis*, a multicellular rhodophyte, presence of Ca^{2+} was necessary for F-actin movement during monospore development (Li et al., 2009). Ca^{2+} may also mediate auxin-dependent development of thalli-branches in the red seaweed *Gracilaria lichenoides* as electrophysiologically inferred Ca^{2+} fluxes across the plasmamembrane suggest (Wang et al., 2016c).

1.7.3 Ca^{2+} signalling in brown algae

Brown algae, a major group within the stramenopiles, have contributed much to our understanding of fundamental mechanisms in Ca^{2+} signalling such as intracellular Ca^{2+} gradients and Ca^{2+} waves (Brownlee and Taylor, 1992; Coelho et al., 2002). Ca^{2+} plays an important role in polarity of embryo, zygote and rhizoid cell development in the multicellular brown algae *Fucus* and *Pelvetia* (Brownlee and Wood, 1986; Kropf, 1992; Pu and Robinson, 1998). Moreover, osmotic shock-induced and dose-dependent Ca^{2+} waves

were observed to initiate at rhizoid apices and then to propagate to distal regions within the cell (Taylor et al., 1996). The propagation is facilitated by IP_3R-mediated release of Ca^{2+} from intracellular stores similarly to animal cells (Goddard et al., 2000; Taylor et al., 1996).

1.7.4 Ca^{2+} signalling in Oomycetes

Oomycetes are not algae, but represent a major non-photosynthetic group within the stramenopiles. Certain members are important due to their parasitic and saprophytic lifestyles which can present substantial problems in fisheries and agriculture (Zheng and Mackrill, 2016). Ca^{2+} channel blockers negatively affect unidirectional growth of oomycete pseudo-hyphae in marine *Achlya bisexualis and Saprolegnia ferax* but not in terrestrial *Neurospora crassa* (Lew, 1999; Morris et al., 2011). Cold shock triggers zoosporogenesis and zoospore release and is known to induce cytosolic Ca^{2+} elevations important for cytokinesis in *Phytophthora cinnamomi* (Jackson and Hardham, 1996). Furthermore, Ca^{2+} also plays a role in zoospore motility in *Pythium aphanidermatum, P. catenulatum* and *P. dissotocum* (Donaldson and Deacon, 1993), oosporogenesis in *Lagenidium giganteum* (Kerwin and Washino, 1986), and chemotaxis in *Phytophthora sojae* (Hua et al., 2008). The underlying Ca^{2+} channels for these responses are not known, but oomycetes have an expanded array of conserved Polycystic Kidney Disease-RyR Domain Channels which likely play a key role in oomycete biology (Zheng and Mackrill, 2016).

1.7.5 Ca^{2+} signalling in diatoms

Ca^{2+} signalling in diatoms has enjoyed increased attention in the recent years. The pattern of Ca^{2+} being conserved in unicellular motility also applies to diatoms. Ca^{2+} channels located at the plasmamembrane are likely important for the gliding-based locomotion in the pennate diatom *Amphora coffeaformis* as experiments with Ca^{2+} channel blockers including La^{3+}, D-600 and ruthenium red suggest (Cooksey and Cooksey, 1980). Moreover, cytosolic Ca^{2+} elevations visualised with the Ca^{2+} sensitive fluorescent dye Calcium Crimson coincided with directional changes during gliding in *Navicula perminuta* (McLachlan et al., 2012). The cytoskeleton is directly involved in gliding motility as demonstrated by substances which

negatively affect cytoskeleton flexibility and movement (Poulsen et al., 1999). A potential involvement of Ca^{2+} is given here too, since actin/myosin interaction is a Ca^{2+} dependent process in many organisms (Hepler, 2016; Li et al., 2015).

Besides motility, diatoms also utilise Ca^{2+} in environmental monitoring. A culture of *P. tricornutum* cells expressing the luminescent Ca^{2+} reporter Aequorin showed Ca^{2+} elevations in response to hypo-osmotic shock, mechanical stimulation, re-introduction of Fe into Fe depleted cultures and diatom-derived reactive aldehyde (2*E*,4*E/Z*)-decadienal (DD) (Falciatore et al., 2000; Vardi et al., 2006). The latter response to DD received further attention and is thought to represent a stress surveillance system during diatom blooms as DD is predominantly released into the environment by dead diatoms. The dose of extracellular DD influences the shape of a cytosolic Ca^{2+} signature driven by an unknown Ca^{2+} channel, affecting overall nitric oxide (NO) production of a cytosolic Ca^{2+} dependent nitric oxide (NO)-synthase. Relatively low cytosolic NO levels then either arrest cell growth or initiate the apoptosis program after meeting a certain threshold (Vardi et al., 2006).

The capacity for signalling between cells along a diatom chain has not been explored in much detail, but remains an area for further study. In the chain-forming diatom *Pleurosira laevis* the chloroplast is reported to relocate towards the cell centre in response to mechanical or electrical stimulation. This response is Ca^{2+} dependent, and was also observed in cells part of a chain not stimulated directly, suggesting that cell-to-cell communication within a diatom chain is possible (Makita & Shihira Ishikawa, 1997). The centric chain-forming diatom *Chaetoceros decipiens* is proposed to have overlapping membranes within sibling cells (Li et al., 2017), potentially forming junctions through which second messengers such as Ca^{2+} or Ca^{2+} mobilising agents may be exchanged. The microdomain between membrane and frustule shared in these chains may also act as a signal pathway, similar to the apoplastic pathway of plant cells – the latter being shown to be involved in stomata activity (Han et al., 2003). Ion channels are also proposed to allow long-range electric cell-to-cell communication between bacteria residing in biofilms, resulting in biofilm-wide oscillations in membrane potential (Prindle et al., 2018), though this was not investigated for diatoms or the diatom-phycosphere.

P. tricornutum cells expressing the fluorescent Ca^{2+} reporter RGECO confirmed the hypo-osmotic shock response (Helliwell et al., 2019; Helliwell et al., 2020b) and furthermore

showed cytosolic Ca^{2+} elevations in response to re-introduction of various phosphate-compounds into P-starved cells (Helliwell et al., 2020a). Aforementioned EukCat channels are the only ion channels more closely investigated in diatoms and were proven to be predominantly permeable to Ca^{2+}. Moreover, knock-out of the EukCat1 channel in *P. tricornutum* cells resulted in decreased gliding motility and decreased sensibility to plasmamembrane depolarisation (Helliwell et al., 2019)

Most studies were carried out on pennate diatoms. Besides the *P. laevis* chloroplast relocation response (Makita & Shihira Ishikawa, 1997), the role of Ca^{2+} signalling in centric diatoms was not investigated.

1.8 Summary

Ca^{2+} is a versatile and highly conserved intracellular 2nd messenger in all eukaryotes. Besides motility, relatively little is known about the role and underlying components of Ca^{2+} signalling in microalgae. This study aims to increase our understanding on Ca^{2+} signalling in diatoms using imaging techniques and genetic and bioinformatics tools, and will try to address following questions:

- Are there specific Ca^{2+} signatures to specific physiologically relevant stimuli?
- Can analysis of spatiotemporal Ca^{2+} responses to specific stimuli provide further information on the underlying mechanisms of Ca^{2+} signalling in diatoms?
- Can a more detailed bioinformatic analysis tell us more about the evolution and roles of particular Ca^{2+} channels in diatoms?
- Can the findings from pennate diatoms be translated to centric diatoms which include many of the more globally abundant species in the oceans?
- Can we identify specific ion channels that may underlie particular Ca^{2+} signalling responses?

This work will present attempts to expand the arsenal of Ca^{2+} biosensor-expressing microalgae (Chapter 2), investigate spatiotemporal characteristics of Ca^{2+} elevations in response to immediate and gradual hypo-osmotic shocks (Chapter 3), investigate the role and distribution of Two-pore channels in diatoms, a potential functional alternative to RyR- and IP_3R facilitating Ca^{2+} release from internal Ca^{2+} stores (Chapter 4) and will present cold shock as novel inducer of cytosolic Ca^{2+} elevations (Chapter 5).

Chapter 2 Tool development

ABSTRACT

Within microalgae, Ca^{2+} biosensors are only established in the widespread, yet ecologically less important diatom *P. tricornutum*. Broadening the selection of algal lineages containing Ca^{2+} biosensors would be a great resource to explore the role and evolution of Ca^{2+} dependent perception mechanisms beyond plants and animals. We therefore aim to introduce Ca^{2+} biosensors into additional key protists: *T. pseudonana*, a silicifying diatom significantly contributing to nutrient cycling in the oceans, and *C. reinhardtii*, a green alga and one of the best characterised protists.

2.1 Introduction

2.1.1 Visualising cytosolic Ca^{2+} elevations in a cell

A direct way of characterising Ca^{2+} signalling is to visualise changes in Ca^{2+} within a cell. This can be achieved with either Ca^{2+} sensitive fluorescent dyes or genetically encoded Ca^{2+} sensitive biosensors.

Dyes have the potential advantage of simple incorporation into a cell. Dyes may be loaded into cells as an acetoxymethyl (AM) ester (Tsien et al., 1984), though after cleavage of the ester the active anionic form may be actively transported into organelles by endomembrane anionic transporters, leading to an unintended accumulation of dye in those cellular compartments. Additionally, the esterases required to activate AM dyes may be either not present (Paredes et al., 2008) or may be present in disadvantegaous places such as plant cell walls or extracellular place (Kuchitsu et al., 2002). Therefore, AM esters mainly see application in animal cell lines as they present problems when applied on plants and algae.

Dextran-conjugated dyes cannot cross membranes and eliminate problems associated with compartmentalization. However, this makes their introduction into the cells much harder and requires microinjection or biolistics prior each experiment (Bothwell et al., 2006). These are stressful procedures for cells which possibly affect the recorded data.

Fluorescent dyes were applied on *C. reinhardtii* (Braun and Hegemann, 1999) but application on other algal lineages was prevented by aforementioned problems. Genetically encoded Ca^{2+} biosensors may eliminate those problems.

2.1.2 Advantages and mode of action of genetically encoded Ca^{2+} biosensors

Genetically encoded Ca^{2+} biosensors require far more preliminary work but, if successful, provide a stably transformed strain in which each single cell is reliably suitable for experiments. This vastly increases data acquisition and data quality since stressful treatments prior the experiments are circumvented.

Ca^{2+} biosensors are essentially artificial protein chimeras in which light emission is increased or changed in wavelength by binding of Ca^{2+}. The light emission can be based either on bioluminescence or fluorescence.

In the bioluminescent reporter Aequorin, Ca^{2+} binding to three EF-hands results in a conformational change of apoaequorin, allowing it to oxidize the substrate coelenterazine to excited coelenteramide (Mithöfer and Mazars, 2002). Coelenteramide emits blue light as it reverts to ground-state which can be calibrated as a Ca^{2+} elevation. As the emitted light is not very bright, use of aequorin in most cases only allows monitoring of Ca^{2+} elevations in a population of cells or in tissues rather than individual cells. In addition, as it is a based on an irreversible chemical reaction, secondary products such as CO_2 and O_2 and continuous addition of the substrate coelenterazine to the medium might affect the target cell's homeostasis and behaviour (Mithöfer and Mazars, 2002). These features have encouraged the development of alternatives.

Fluorescence based biosensors are generally brighter than ones based on luminescence, allowing recording of single cell Ca^{2+} elevations. However, the requirement of excitation of a particular wavelength can present problems if the target shows auto-fluorescence, e.g. as it is the case with chlorophyll in chloroplasts. Two subclasses of fluorescence based Ca^{2+} biosensors exist:

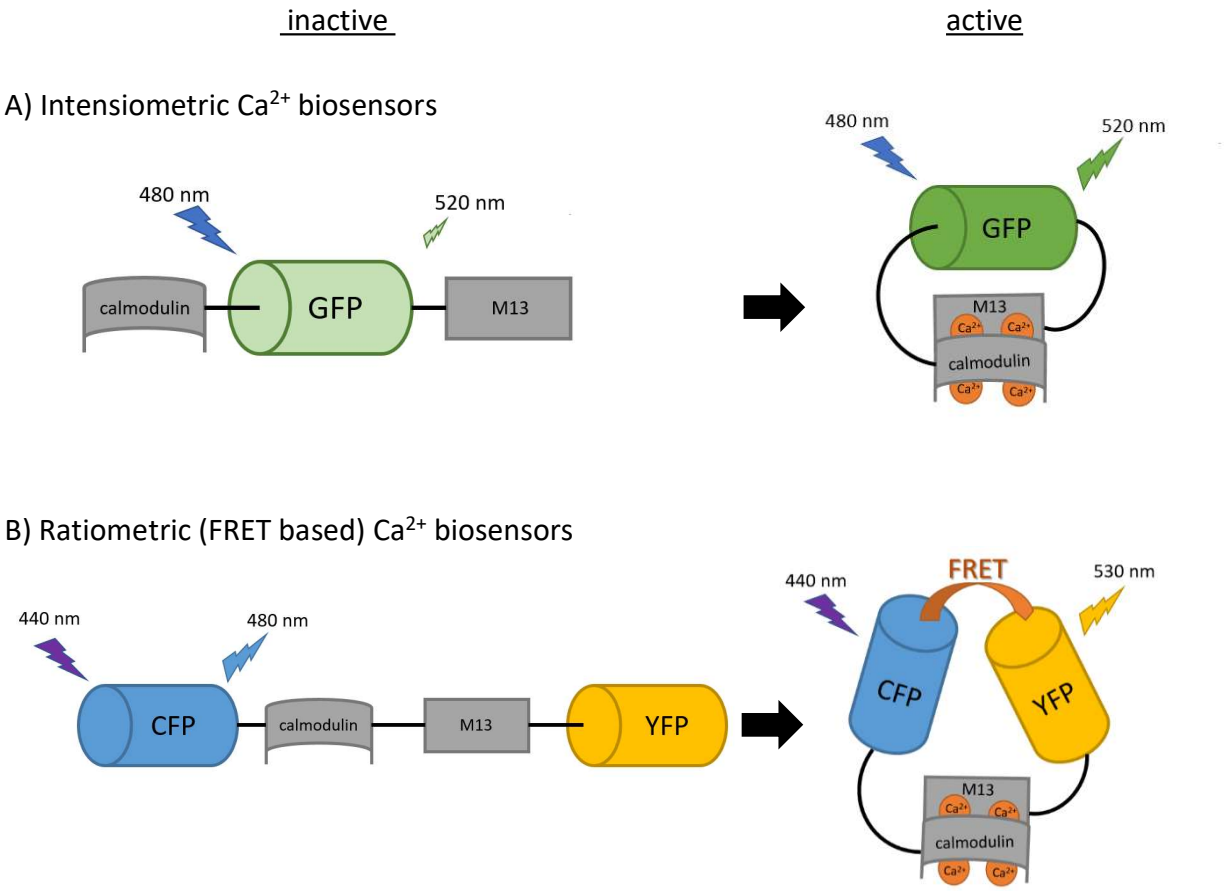

Figure 2.1: Schematics of major fluorescent Ca^{2+} biosensor classes

In both cases, Ca^{2+} binding to calmodulin results binding of the calmodulin with M13, which eventually leads to conformation change. This conformation change either increases fluorescence (A) or shifts the fluorescence to another wavelength (B).

The simpler of the two are called intensiometric Ca^{2+} biosensors and contain a single fluorescent protein (such as GFP), a Ca^{2+} -binding calmodulin at the N-terminus and a calmodulin-binding region (M13) at the C-terminus (Fig. 2.1 A; Examples: gCaMP3, gCaMP-6f, gCaMP6f-RS06, gGECO and gGECO). Ca^{2+} binding to calmodulin leads to an interaction with the N- and C-termini and this conformational change subsequently causes an increase in light emission (Miyawaki et al., 1997; Zhao et al., 2011).

Ratiomentric measurements of Ca^{2+} may be facilitated by using a combination of Ca^{2+}-dependent and Ca^{2+}-independent fluorescent proteins of different wavelengths. This allows the Ca^{2+} dependent fluorescence to be normalised to the fluorescence of the non-

Ca^{2+} sensitive fluorescent protein which is useful to correct changes in dye concentration due to shifts in cell geometry and volume. A more sophisticated subclass of ratiometric Ca^{2+} biosensors utilise Förster resonance energy transfer (FRET) (Fig. 2.1 B). Within a single protein, a pair of fluorophores are in close proximity to each other (1-10 nm, examples: CameleonY3.6 or Twitch3). The donor fluorophore's emission wavelength overlaps with the excitation wavelength of the acceptor chromophore. Ca^{2+} binding results in a conformational change, reducing their physical separation and allowing these two components to exchange energy. This results in a change of colour of the biosensor rather than just intensity, allowing ratiometric measurements (Zhang et al., 2019).

In general, single fluorophore sensors are brighter (have higher quantum yields) than double fluorophore ones but show less photostability and are more sensitive to pH (Nakai et al., 2001; Pologruto et al., 2004; Reiff et al., 2005).

In a separate project, the intensiometric Ca^{2+} biosensor rGECO was established in the pennate diatom *P. tricornutum* and managed to confirm the outlined advantages of genetically encoded and fluorescent Ca^{2+} biosensors (Helliwell et al., 2019). Therefore, fluorescence based Ca^{2+} biosensors were chosen to be introduced into *T. pseudonana* and *C. reinhardtii*, respectively.

2.1.3 The model green alga *C. reinhardtii*

C. reinhardtii is a unicellular freshwater- and soil inhabiting green alga of about 10 µm in diameter. The major morphological characteristics of the wild type are a cell wall made of hydroxyproline-rich glycoproteins, a central pyrenoid surrounded by a cup-shaped single chloroplast and a light-sensitive eyespot close to its two flagella. It is able to grow photoautotrophically, heterotrophically (when organic carbon is available) or mixotrophically. Due to its ease of cultivation (generation time ~8h), *C. reinhardtii* has received much interest from the scientific community. As model organism for cell motility (Huang, 1986; Mitchell, 2001), reproduction (Goodenough et al., 2007; Sekimoto, 2017), sensing (Bickerton et al., 2016; Irihimovitch and Yehudai-Resheff, 2008; Suarez et al., 2013), photosynthesis (Minagawa and Tokutsu, 2015; Rochaix, 1995) and evolution (Ratcliff et al., 2013) it combines powerful genetics with the availability of unique genetic and genomic

resources (Li et al., 2016). This makes *C. reinhardtii* one of the best characterised protists. Additionally, it received considerable attention concerning biotechnological applications (Brodie et al., 2017; Mackinder, 2018).

C. reinhardtii has also provided many insights into Ca^{2+} signalling which were described in Chapter 1.7.1. Briefly, Ca^{2+} elevations in flagella or close to the flagella basal bodies are important for regulation of gliding motility (Collingridge et al., 2013), deflagellation (Lohret et al., 1998), mating (Huang et al., 2007) and control of flagella length (Edel and Kudla, 2015; Liang and Pan, 2013). In contrast, the role of cytosolic Ca^{2+} elevations is less understood, and the only detailed study of cytosolic Ca^{2+} relates to its role in the acid-induced deflagellation response (Wheeler and Brownlee, 2008). However, *C. reinhardtii* has a selection of classes of channels typically located at the plasma membrane of other cell types (e.g. Ca_V, TRP, MscS, see Chapter 1), suggesting that cytosolic Ca^{2+} is involved in other cellular processes (Verret et al., 2010). This knowledge gap is aimed to be addressed using cytosolic Ca^{2+} biosensors in *C. reinhardtii*.

2.1.4 The model diatom *Thalassiosira pseudonana*

T. pseudonana is a highly successful unicellular, marine centric diatom. It plays a significant role in gross photosynthetic carbon fixation in the oceans (Armbrust et al., 2004). A reason for its success may be its unique combination of metabolic processes including genes for the urea cycle, iron uptake and photosynthesis (Armbrust et al., 2004). As a diatom, *T. pseudonana's* cell body is surrounded by two halves of a special cell wall, the frustule made of silica (Sumper and Brunner, 2008).

No studies of Ca^{2+} signalling have been reported in centric diatoms. *T. pseudonana* has genes coding for a single Ca_V-like channel, a Two-pore channel and homologues of the bacterial $BacNa_V$ single domain cation channel named EukCats (Helliwell et al., 2019; Verret et al., 2010) The functions of these channels in *T. pseudonana* are currently unknown.

To investigate Ca^{2+} signalling in centric diatoms we aimed to introduce Ca^{2+}-biosensors in *T. pseudonana*. Plasmids containing biosensors under control of the established FCP-promoter were introduced into *T. pseudonana* using biolistics as previously described (Hopes et al., 2016; Poulsen et al., 2006)

2.2 Methods

2.2.1 *C. reinhardtii* strains and growth conditions

Attempts to introduce Ca^{2+} biosensors into *C. reinhardtii* were performed using the cell wall deficient strain CC-4533, which is the haploid progeny from a cross between 4A- and D66+ (Li et al., 2016), and the strain UVM11, which is the result of an attempt to create a sub-strain with reliable transgene expression (Neupert et al., 2009). All strains were grown in Tris-acetate-phosphate medium (TAP, see (Gorman and Levine, 1965)). TAP plates contained 1.5 % of bacterial grade agar and 50 µg / mL of ampicillin to reduce chances of bacterial contamination. For transformant-selection plates, 8-20 µg/mL Paromomycin or 10-20 µg / mL Zeocin were added. Standard growth conditions were 23° C and 16/8 h light/dark rhythm. Cell density was monitored using Beckman Coulter Z2 (inspected cell size was 4-12 µm).

2.2.2 *T. pseudonana* strains and growth conditions

T. pseudonana strain CCMP1335) was kindly donated by Thomas Mock (University of East
417 Anglia, UK) and cultured in f/2 medium (Guillard, 1975) using pre-filtered and autoclaved seawater from the coastal station L4 in Plymouth. Standard growth conditions were 18° C with 16/8 h light-dark cycle. Growth on plates was achieved by f/2 medium using 50% seawater and 0.8% bacterial grade agar.

Colonies obtained in collaboration with Thomas Mock's lab (University of East Anglia) CCMP 1335 were grown on Aquil-medium using 50% salts and 100% of nutrients and trace elements (Price et al., 1988). Reduced salinity is considered to enhance selection efficiency of nourseothricin and to counteract hyperosmotic stress due to evaporation of H_2O. In both media systems, 100 µg / mL nourseothricin was added for selection of transformed cells.

To isolate fluorescent cells from a non-fluorescent population, fluorescence based cell sorting was performed by Tracy Beachem, Mike Allen lab, Plymouth Marine Laboratory. Depending whether green or red fluorescent proteins were used for transformation, 10000

of the top 1% "greenest" (λex = 520 nm) or "reddest" (λex = 692 nm) cells of a 30 mL culture were isolated, grown and then examined for increased homogeneity.

2.2.3 Designing plasmids encoding Ca^{2+} biosensors for *C. reinhardtii* and *T. pseudonana*

To introduce Ca^{2+} biosensors into *C. reinhardtii* and *T. pseudonana*, a selection of different constructs was chosen presented in Tab. 2.1, aiming to gain flexibility (i.e. utilised wavelengths, intensio- vs. ratiometric sensors, target cell compatibility, varying sensitivities).

Table 2.1: Features and origin of employed Ca^{2+} biosensors.

An asterix indicates ratiometric biosensors, whereas no asterix indicates intensiometric biosensors. An X in the second column indicates whether a construct was designed for the respective host organism.

Ca^{2+} biosensor	***C. reinhardtii/ T. pseudonana***	**Excitation** (nm)	**Emission** (nm)	**Fluorescent Protein**	**source**
Cameleon YC3.6*	X / X	400	480/520	CFP/YFP	Miyawaki 1997
gGECO	X / X	480	520	GFP	Zhao 2013
rGECO	X / X	560	600	mApple	Zhao 2013
gCaMP6f	X / X	480	520	GFP	Chen 2014
gCaMP6F-RS06	X / -	480	520	GFP	Badura 2014
rCaMP2	X / -	560	600	mApple	Akerboom 2013
Twitch3*	X / -	400	480/520	CFP/YFP	Thestrup 2014

2.2.3.1 Plasmids for *C. reinhardtii*

Two major sets of constructs containing Ca^{2+} biosensors were used presented in Tab. 2.2.

Table 2.2: Plasmids for C. reinhardtii.

Overview of plasmid templates and the respective C. reinhardtii specific Ca^{2+} biosensors they contain. pLM005 constructs were done by genscript whereas pCHlamy4 constructs were cloned manually using pLM005 constructs as template. Venus is a YFP derivate used as control.

Plasmid backbone	**Biosensor**		
pLM005	gCaMP6f	Twitch3	rGECO
	gCaMP6f-RS06	Cameleon	gGECO
	rCaMP2	Venus	
pChlamy4	rGECO	gGECO	Venus

The first one is based on the plasmid backbone pLM005 conferring paromomycin resistance (Atkinson et al., 2016). *De novo* synthesised and codon optimised genes for biosensors (rGECO, gGECO, gCaMP6f, gCaMP6fRS06, rCaMP2, Twitch3 and Cameleon (YC3.6)) were inserted by genscript (https://www.genscript.com/) into the pLM005 plasmid using EcoRI and BglII as insertion sites, putting the insert under control of the photosystem I subunit promoter *PsaD* (Fischer and Rochaix, 2001). Received plasmids were verified using restriction digest (PstI) and sequencing (5' flanking primer CAAGCCAGGGTTAGGTGTTG; 3' flanking primer AACCGTGAGCAGCTGGAG).

The second construct is based on the GeneArt *Chlamydomonas* protein expression vector pChlamy_4 (Rasala et al., 2012). It uses a chimeric heat-shock protein 70 promoter (*HSP70A*) and a ribulose 1,5 bisphosphate carboxylase subunit- promoter (*rbcS2*) for consecutive expression. rGECO, gGECO and Venus genes were amplified using verified pLM005-based constructs as template (r/gGECO 5' AAAGAATTCATGGTGGACAGCAGC, rGECO 3' AAAGGATCCCTTGGCGGTCATCATC, gGECO 3' AAAGGATCCGGTCATCATCTGCACG, Venus 5' GGCGAATTCATGGTGAGCAAGGGC, Venus 3' GGCGGATCCCTTGTCGTCATCGTCC). Amplicons were cloned into the pChlamy_4 vector using EcoRI and BamHI restriction sites introduced by the primers. Final constructs were verified using restriction digest (PstI +

HindIII) and sequencing (pChlamy flank_For TGTCCACGAACTTCCGGG, insert rGECO_Rev CCCTTCTTGATCTCGCTCT, insert gGECO_Rev ATGTACACGTTCTCCAGGCT, Venus_Rev CACGCTGAACTTGTGGCC).

2.2.3.2 Plasmids for *T. pseudonana*

The project started with having a pTp-FCP:GFP and a pTp-FCP:NAT (addgene: pICH47732) plasmid in the inventory (Hopes et al., 2016; Poulsen et al., 2006). FCP specifies the promoter and terminator *LHCF9* from the fucoxanthin-chlorophyll binding protein; GFP is green fluorescent protein; NAT is encoding a protein for nourseotricine resistance. GFP expression using this promoter has been reported before (Groger et al., 2016; Poulsen et al., 2006). The vector template was the consecutive expression vector pTpFCP which was furthermore based on the vector pBluescript II SK+ (Poulsen et al., 2006).

Genscript (genscript.com) was consulted to replace the GFP within the pTp-FCP:GFP plasmid with codon optimised versions of four different *de novo* synthesised Ca^{2+} Biosensors - namely gGECO, rGECO, Chameleon and gCamp6f - using the restriction sites SphI and NotI. Received plasmids were cloned in *E. coli* and verified with restriction digest (EcoRV and NotI) as well as PCR using the 5' flanking primer AGTAACGTATCTTCCCCCTCG and 3' target primers ATCTGGCAAGAGCACAGGTC (gCaMP6f), TAGATCCTCCGGTTCCTCCC (g+rGECO), ACGGGTCTTGTAGTTTCCGT (Cameleon), GGCGACCTCGATGTCCTC (NAT-resistance) and TCTTGTAGTTGCCGTCGTCC (GFP).

Since nourseothricin resistance needed for selection of transformant *T. pseudonana* is not located on the same vector as the biosensors, co-transformation of resistance and biosensor was necessary.

2.2.4 Transformation protocols

2.2.4.1 Transformation of *C. reinhardtii* with Ca^{2+} biosensors using electroporation

Prior to electroporation, pLM005 plasmids containing genes for Ca^{2+} biosensors were linearised using EcoRV digest (100-4000 ng DNA, 20 µL total volume of digestion mix), followed by enzyme inactivation (65° C, 20 min). pChlamy_4 -based plasmids were linearised using ScaI digest. $3x10^6$ - $1x10^8$ *C. reinhardtii* cells were suspended in 250 µL TAP + 40 mM sucrose, transferred into one electroporation cuvette (4 mm width) and incubated for 5 min at 16° C. Afterwards, the DNA linearisation mix was added to the cuvette, the contents quickly mixed and immediately electroporated (800 V, 25 µF, exponential protocol; Biorad genepulser xcell (bio-rad.com)). The cuvette mixture was then transferred into 10 mL of TAP + 40 mM sucrose and left overnight for recovery (standard growth conditions). Cells were then spread on one or multiple TAP-plates containing appropriate selection marker. Colonies appear after one week.

Screening for mutants

Colonies were transferred into a 96 well plate and either screened for fluorescence under a microscope (mApple: ex. 541-551nm, em. 565-605nm; GFP: ex. 450-490 nm, em. 500-550 nm) or were screened using colony PCR.

2.2.4.2 Transformation of *T. pseudonana* with Ca^{2+} biosensors using biolistics

The method is based on Hopes et al. (2016). In brief, genetic transformation is realised by microparticle bombardment followed by selection of transformants using nourseothricin.

50 µL of tungsten microcarriers (60 mg/ µL) are washed with water and subsequently combined with 4 µg of plasmid DNA (biosensor and NAT resistance gene, respectively), 50 µL $CaCl_2$ 2.5 M and 20 µL 0.1 M spermidine while mixing. The particles were then pelleted using a centrifuge (10000 rpm, 15 s) and washed with 250 µL 100% ethanol. An additional pelleting step was followed by resuspension of the tungsten particles in 60 µL 100% ethanol. 15 µL of this suspension was then distributed on four macrocarrier discs each (= 1 µg of DNA) and set to dry.

Around 5x 10^7 *T. pseudonana* cells harvested in exponential growth phase were collected onto a 47 mm/ 1.2 µm filter paper from isopore using a vacuum pump. The filter paper was then placed on the centre of a 50 % salinity aquil-medium plate containing 1.5 % agar without antibiotics and set to incubate for 30 minutes.

Biolistic loading was done with a 1350 psi rupture disk and 7 cm of distance. Cells were gently rinsed from the filter paper in 25 mL of ½ salinity aquil-medium, followed by a 24 h recovery phase under standard growth conditions. Cells were then spread on 2-3 selection plates (½ salinity aquil-medium 0,8 % agar + 100 µg/mL nourseothricin). A thin layer of cells was important to make sure that each cell in contact with the selective surface of the plate. Otherwise, “islands” of false positives will occur on more densely occupied areas.

Dark-brown colonies appearing after 2-3 weeks were relocated into a 96-well plate containing 50% salinity aquil-medium and NTC-concentrations between 50-150 ng/µL. The general attempt was to try to compromise between upholding a certain degree of selective pressure without stressing the cells too much – the latter making screening for fluorescent cells unreliable.

2.3 Results

2.3.1 Results involving *C. reinhardtii*

The manual insertion of rGECO, gGECO and Venus genes into the pChlamy_4 vector was positive, yet it was noteworthy that dephosphorylation of 5'-ends (CIP treatment) of the pChlamy_4 vector prior to ligation was necessary which is usually not needed for cloning of sticky ends.

A

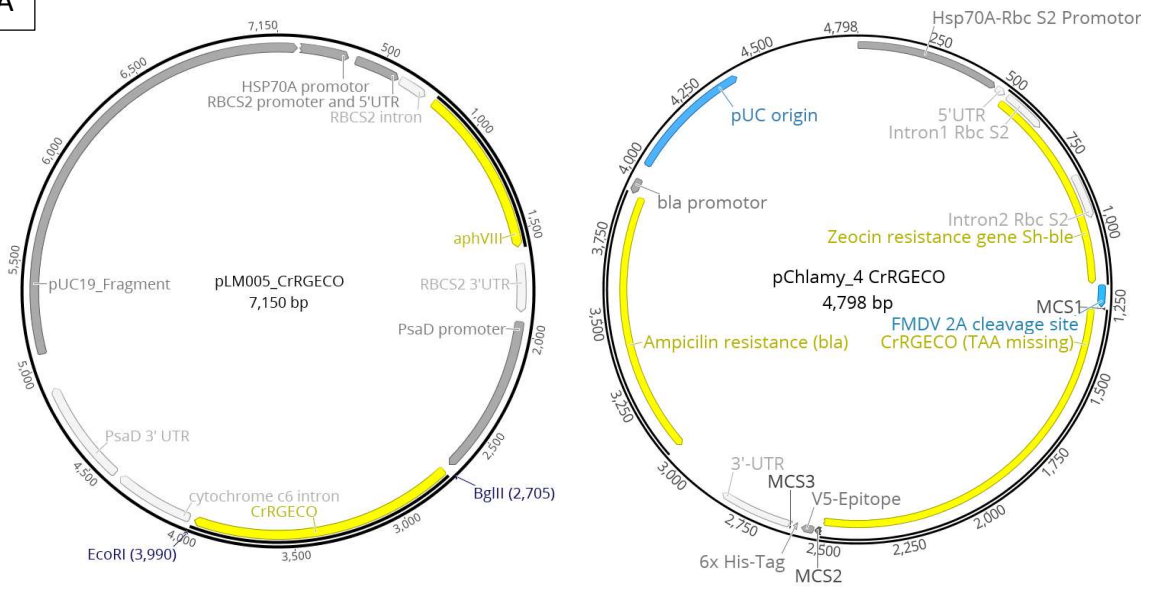

B

A. Expression unit of the pLM005 vector:

B. Expression unit of the pChlamy4 vector:

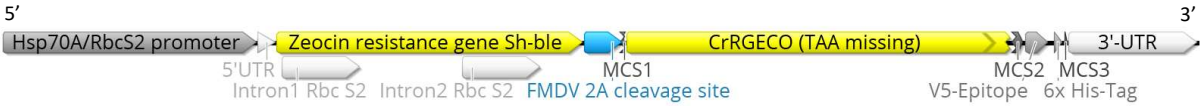

Figure 2.2: novel constructs containing Ca^{2+} biosensor genes for *C. reinhardtii* transformation

A) Exemplary plasmid maps showing the pLM005_rGECO vector (left) and the pChlamy_rGECO vector (right). plM005: aphVIII = paromomycin resistance gene controlled by heat-shock protein 70 promoter (*HSP70A*) and a ribulose 1,5 bisphosphate carboxylase subunit- promoter (*RBCS2*). rGECO is controlled by the promoter of a photosystem I protein D (*PsaD*). The pUC19-Fragment is part of the pUC19 backbone vector containing ampicillin for selection in *E. coli*. pChlamy (right): the expression cassette is under control of the chimeric HSP70A-RbcS2 Promoter. Respective genes for zeocin resistance (sh-ble) and Ca^{2+} biosensor are in the same open reading frame connected with the FMDV2A linker. When translated, the linker cleaves itself, releasing the biosensor protein and enabling bleomycin protein to neutralise zeocin 1:1. **B)** Schematic showing the expression units of the pLM005 and pChlamy4 plasmids with an exemplary rGECO insert in more detail. All schematics were made with geneious 10.0.

Transformation of *C. reinhardtii* with both control vectors pLM005_Venus and pChlamy4_Venus *via* electroporation yielded colonies with fluorescent cells. pChlamy4_Venus produced fewer colonies than pLM005_Venus (1 vs. 42 colonies, respectively) although more copies were used per transformation due to a smaller size of the pChlamy4 vector (4789 vs. 7150 bp, respectively). Of these, 1 pChlamy and 3 pLM005 derived colonies showed Venus fluorescence, making pChlamy less effective but more efficient than pLM005.

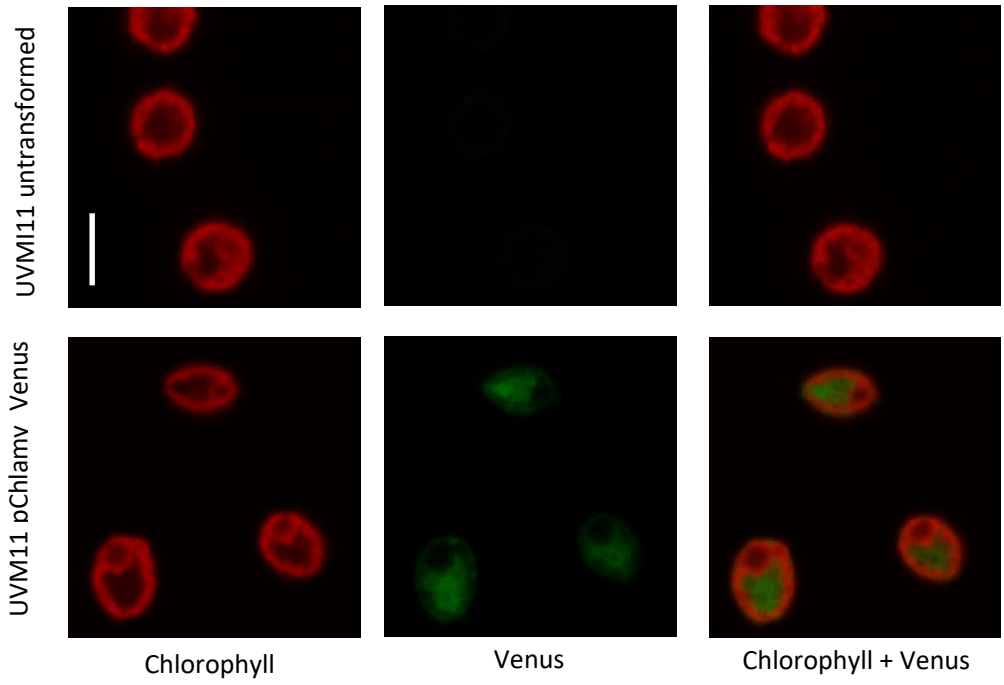

Figure 2.3 Images of transformed *C. reinhardtii*

A) Epifluorescence images of UVM11 cells transformed with pChlamy4_Venus. Chlorophyll, showing the cup shaped chloroplast and the pyrenoid. II = Venus fluorescence located in the cytosol. III = overlay. Scale bar approximately represents 10 µm.

Constructs containing Ca^{2+} biosensors also led to colonies (especially for pLM005), yet fluorescence at respective wavelengths was not observed. For example, pLM005_rGECO applied on the UVM11 strain yielded 81 colonies when 100 ng DNA / transformation was used and ~500 colonies when 300 ng / transformation was used. Of these, 36 colonies were screened for fluorescence with negative results. These relatively high numbers of colonies were rarely achieved though. For numerous transformation attempts which resulted in no

colonies a mistake in collectively shared TAP medium recipe was responsible (phosphate buffer saline instead phosphate buffer was used). A single transformation attempt with a different electroporator (NEPA21, NEPA Gene Co.) also led to non-fluorescent colonies. Notably, pChlamy based constructs which link Ca^{2+} biosensors with the resistance gene never yielded colonies with the exception of a single false positive (rGECO).

Table 2.3 Overview of transformation attempts in C. reinhardtii

List of constructs used for transformation of C. reinhardtii (strain CC4533 and UVM11). Number of different transformation attempts (transf.), total achieved colonies (col.) and fluorescent colonies related to screened ones (fluo/test) are listed. Transformation protocols were in process of adjustments, contributing to the large variety in results. Asterix' indicate that colonies formed but died 11 days afterwards on the plate.

		CC4533			UVM11		
Plasmid	Biosensor	transf.	col.	fluo/test	transf.	col.	fluo/test
pLM005	rGECO	3	13	0/13	4	>1152	0/36
	gGECO	4	13	0/13	5	>1049	0/36
	gCaMP6f	1	10	0/10	-	-	-
	gCaMP6f-RS06	1	11	0/11	-	-	-
	rCaMP2	1	14	0/14	-	-	-
	Twitch3	-	-	-	4	>1102	0/24
	Cameleon	-	-	-	1	12	0/24
	Venus	2	0	0	4	51	5/14
pChlamy4	rGECO	3	0	-	4	1	0/1
	gGECO	3	0	-	2	0	-
	Venus	5	0	-	3	11	4/7*
	empty Pl.	-	-	-	3	38	-*

Resistant yet non-fluorescent colonies raise the question whether false positives were screened. Several colony PCRs were conducted which showed that Ca^{2+} biosensor genes can be found in gDNA extractions of *C. reinhardtii*, indicating that transformation is successful.

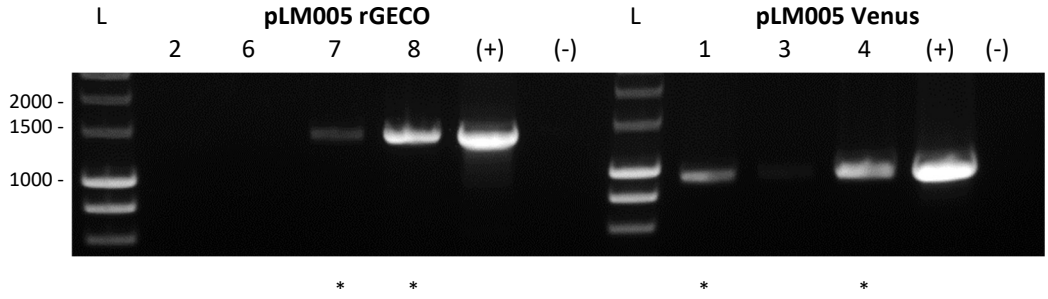

Figure 2.4 PCR on transformed *C. reinhardtii* colonies

Results of a colony PCR on *C. reinhardtii* colonies (numbers 2-8) transformed with pLM005_rGECO and pLM005_Venus, respectively. Bands of expected size (rGECO: 1477 bp; Venus: 899 bp) were able to be amplified. In the positive controls (+) the respective plasmids used for transformation were used as template. Samples with an asterix were chosen for sequencing which returned positive results, showing successful transformation of *C. reinhardtii* with Ca^{2+} biosensors. Similar results were achieved with gGECO and Twitch3.

2.3.2 Results involving *T. pseudonana*

Plasmids containing different Ca^{2+} biosensors (gGECO, rGECO) were transformed into *T. pseudonana* by biolistics. For rGECO transformants, 14 of 71 colonies (20%) had evidence for biosensor presence according PCR, whereas 3 of those showed fluorescence with confocal microscopy (TpR24, TpR61, TpR71). Fluorescence screening for positive rGECO tranformants required inclusion of chlorophyll fluorescence as indicator for live cells since dead cells showed high fluorescence at the same wavelength as rGECO. For gGECO transformants, 12 of 76 colonies (16%) were positive according PCR, 3 of those being fluorescent (TpG1, TpG10, TpG71).

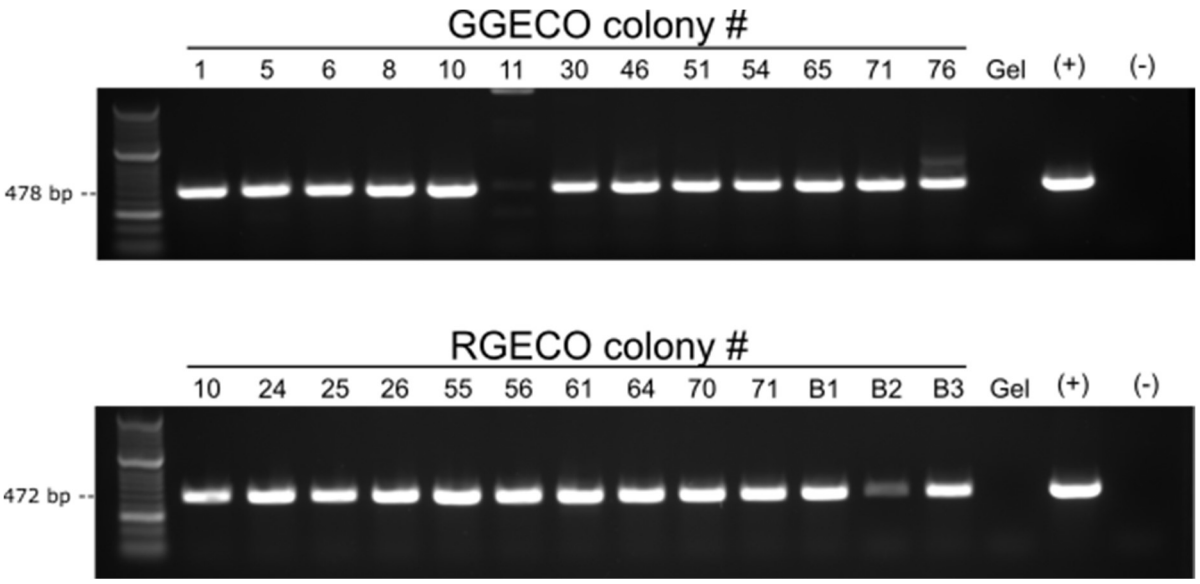

Figure 2.5 PCR on transformed *T. pseudonana* colonies.

From ~80 colonies achieved, 12 colonies showed genetic evidence for gGECO and 13 colonies showed evidence for rGECO, respectively. Primers used started in the promoter region and ended in the 5' area of the biosensor gene. The positive control (+) is the respective plasmid used for biolistic loading. The negative controls include superficially scraped agar from the colony-plate as template to exclude carryover of remnant plasmid DNA from the transformation mix (Gel) as well as a PCR sample with dH_2O as "template" (-).

However, within a population of a positive colony, only 1-10 % of cells show fluorescence at respective wavelengths of GFP, gGECO or rGECO. Of those, the level of baseline fluorescence varied between cells. Some showed very high levels of fluorescence even in unstimulated state, some showed low baseline fluorescence which increased when stimulated (similar to rGECO in *P. tricornutum*), some were "silent" whose presence of biosensor only became obvious when stimulated, yet most cells (estimated 90-99%) did not show any biosensor-related fluorescence. Neither novel colonies obtained through re-streaking of partially positive populations nor cell sorting of TpR71, TpR24, TpG1, and TpG10 resulted in a population with a more homogenous baseline fluorescence.

Four months after acquisition of fluorescent cell lines, biosensor fluorescence was no longer observed in cells taken from plate or liquid culture, yet colony PCR still yielded positive results (not shown).

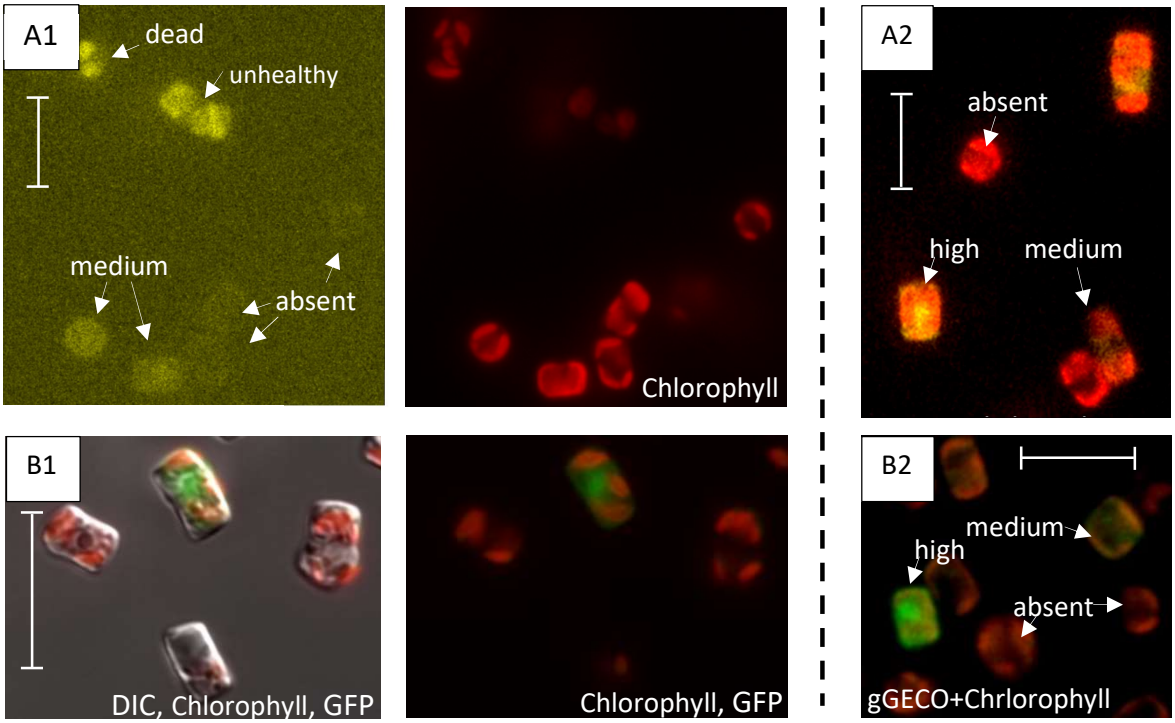

Figure 2.6 Transgene expression in *T. pseudonana* is heterogeneous within a population.

A1) False colour epifluorescent images showing presence or absence of rGECO baseline fluorescence in TpR61. Dead cells appear as false positives, yet are identifiable through their missing chlorophyll fluorescence. **A2)** A similar pattern is present in TpR24. **B1)** *T. p*. transformed with GFP. Left an overlay of DIC, chlorophyll and GFP, right without DIC. **B2)** A similar pattern is present in TpG1 (image taken on confocal microscope). In all images various baseline levels of fluorescence are shown, ranging from high, medium to absent fluorescence. The scales represent 10 µm.

Nonetheless, rGECO transformants of *T. pseudonana* displayed rapid transient increases in fluorescence in response to short-term hypo-osmotic stress, indicating the expression of a functional rGECO reporter.

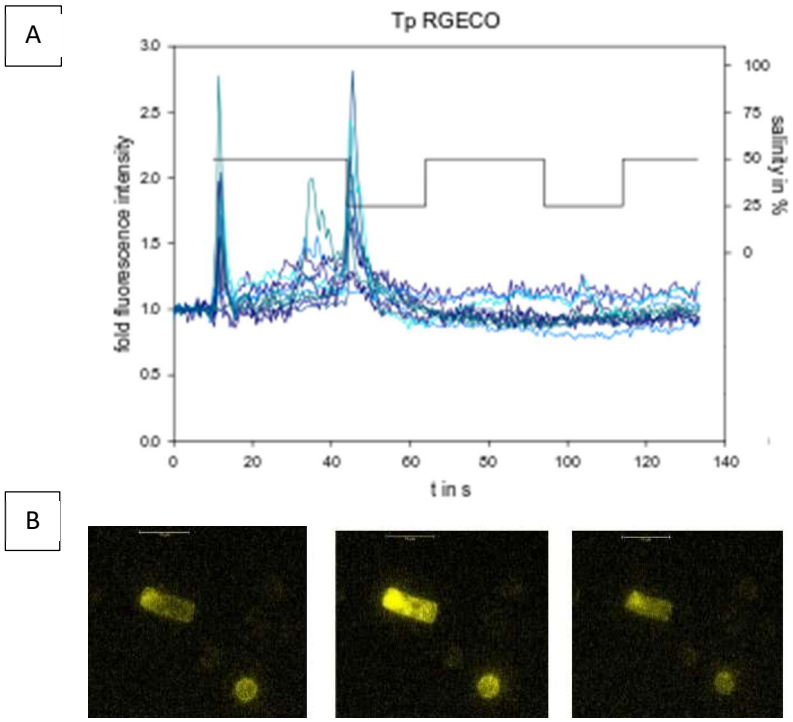

Figure 2.7 Hypo-osmotic shock induces Ca^{2+} elevations in *T. pseudonana*

A) Representative fluorescence traces of 11 TpR10 cells in response to hypo-osmotic shocks (50 % to 25 % salinity f/2 medium, black line). At 10 s perfusion of 50% salinity f/2 medium starts, provoking a single Ca^{2+} elevation caused by the flow and likely unrelated to hypo-osmotic shock. At 45 s a hypo-osmotic shock is applied leading to another single Ca^{2+} elevation. Overall fluorescence is rather weak, leading to a noisy baseline. Strain TpG1 yielded similar results, though gGECO fluorescence overlapped with chlorophyll autofluorescence. **B)** False colour images of total fluorescence TpR1 cells before, during and after Ca^{2+} elevations in fluorescent cells. However, most cells within the population remain silent.

The resting state fluorescence of *T. pseudonana* was of lower magnitude than that observed with *P. tricornutum* which leads to higher noise. The amplitude of hypo-osmotically-induced fluorescence increase was also lower that that observed with *P. tricornutum* (max. 3.0-fold fluorescence increase compared to 8-14 fold fluorescence increase in *P. tricornutum* as shown in Chapter 3 and 4.

However, in addition to hypo-osmotic shock, this strain was used to successfully monitor Ca^{2+} elevations in response to cold shock (Chapter 5) and by K. Helliwell et al. (MBA Plymouth) to monitor signalling in response to phosphate limitation (Helliwell et al., 2020a)

2.4 Discussion

2.4.1 Transformation and construct design was successful in *C. reinhardtii and T. pseudonana*

The respective established transformation methods proved to be applicable to *C. reinhardtii* (electroporation) and *T. pseudonana* (biolistics, with kind support of Amanda Hopes, Thomas Mock lab, University of East Anglia) as colonies harbouring target genes were achieved in both cases. As Venus or GFP-derived fluorescence was observed in both species, it could be assumed that respective plasmid designs should yield stable Ca^{2+} biosensor expression. This was not the case for *C. reinhardtii* and only partially the case for *T. pseudonana*.

2.4.2 Ca^{2+} biosensor expression is likely silenced in *C. reinhardtii*

In *C. reinhardtii*, non-fluorescent but otherwise positive transformants (colony PCR) were observed. A possible explanation could be silencing of the target gene on the transcriptional or posttranscriptional level. This phenomenon is actually not uncommon for this species and has led to continuous development of new strains, new synthetic promoters and establishment of codon optimisation as standard practice for this host due to elevated GC content and a relatively narrow codon bias (Barahimipour et al., 2015). This gave reason to include the UVM11 strain which has been isolated through genetic screening of strains that efficiently express introduced transgenes (Neupert et al., 2009). Though transformation efficiency (colonies per µg DNA) in the present study was indeed higher in this strain, biosensor fluorescence was not observed.

In terms of applied approaches, there is only limited improvement possible: The applied *Hsp70/RbcS2* chimeric promoter (in pChlamy4) and the *PsaD*-promoter (Fischer and Rochaix, 2001) (in pLM005) are relatively reliable compared to other promoters (Perozeni et al., 2018; Rasala et al., 2012) (Payam Mershahi, Alison Smith lab, Cambridge University, personal communication). Alternatives have been developed recently, but their broader establishment remains to be seen (Scranton et al., 2016). An inducible promoter such as *CYC6* (nickel), *NIT1* (ammonium starvation) or *LIP* (light) might help to better control

putative harmful expression of target genes (Ferrante et al., 2008; Koblenz and Lechtreck, 2005; Park et al., 2013). Electroporation as means of transformation is established for *C. reinhardtii*. In electroporation, variables such as temperature, osmolarity, electric conditions, field strength, time of discharge and DNA concentrations have to be carefully optimised to obtain high transformation efficiencies (León and Fernández, 2007). The NEPA21 electroporator (nepagene.jp) allows to monitor and adjust variables related to the applied current to more favourable values and its use should be prioritised in future transformation attempts.

In a similar project, expression of flagella-localised Ca^{2+} biosensors proved to be successful for strain CC4533 with constructs based on the pLM005 vector (Fort et al., 2020), which proves that translation of Ca^{2+} biosensors in *C. reinhardtii* is possible. However, the fluorescence was not stable for long periods and continuous rescreening for antibiotic resistance on selective plates was required. In the present study, pChlamy constructs which should guarantee target gene expression within a Zeocin resistant colony resulted in no colonies when Ca^{2+} biosensors were involved. Therefore, biosensors might be toxic to *C. reinhardtii* if present in the cytosol too long. The demonstration of short-term functional flagella-located Ca^{2+} biosensors would make posttranslational silencing of cytosolic Ca^{2+} biosensors more likely than transcriptional silencing. To confirm this, checking for target gene mRNA transcripts and translated Ca^{2+} biosensors utilising the His-Tag on the pChlamy4 construct would be options worth pursuing.

However, a perhaps more promising approach would be the introduction of introns into the biosensor-genes. 92 % of all *C. reinhardtii* genes contain introns, most of them of a rather large size compared to other microalgae (98.5 % of introns > 100 bP), resulting in ~8.3 exons per gene and average exon length of 190 bp (Merchant et al., 2007). In comparison, *P. tricornutum* only has ~0.7 exons per gene (Bowler et al., 2008) of much longer length. The pChlamy4-vector already employs artificially introduced introns (intron-1 from native *RbcS2*) for its selection marker gene *Sh-ble*, which was reported to result in enhanced mRNA stability and expression (Rasala et al., 2012). This claim received support as expression of other transgenes were also increased when introns were introduced (Baier et al., 2018). Therefore, introducing *RbcS2* introns into the biosensor's genes might make them more "native" to the host, possibly circumventing the currently discussed intron-

dependent “immune system” of *C. reinhardtii* protecting the cell against viral infections and transposable elements (Baier et al., 2018; Weiner et al., 2018).

2.4.3 Transformation of *T. pseudonana* with Ca^{2+} biosensors

Successful *T. pseudonana* transformation was confirmed by colony PCR and a small set of fluorescent cell lines (rGECO: 20% of colonies showed target gene, 21% of those were fluorescent. gGECO: 16% of colonies showed target gene, 19% of those were fluorescent). Considering that two transformed plasmids were necessary to produce successful results and the results were similar between constructs, transformation efficiency was acceptable. Biosensors work and show that *T. pseudonana* likely utilises Ca^{2+} signalling in order to sense hypo-osmotic stress in its environment in a similar way to *P. tricornutum* (Falciatore et al., 2000; Helliwell et al., 2020b; Chapter 3 and 4). At this stage, the limited data does not allow a more detailed discussion of Ca^{2+} signalling in *T. pseudonana*.

Acquisition of high quality data was hampered by the heterogenous expression of biosensors within a population. Daughter colonies of a partially fluorescent population as well as cultures obtained after cell sorting still showed only limited numbers of fluorescent cells, with significant variation in resting state fluorescence. This is unexpected, as the FCP promoter allows a steady and reliable expression of rGECO in *P. tricornutum* (Helliwell et al., 2019; Chapter 3). It is unclear if either expression of biosensors varies within the same population or whether it is problematic to get a clonal population. Although genetic evidence for biosensors in colonies was still present 4 months after acquisition of positive cell lines, it does not disprove presence of wild-type cells. As a pelagic diatom, growing *T. pseudonana* on plates is not trivial. As false-positives easily occur as soon as too many cells are distributed on a selective plate, it could be possible to assume that non-transformed cells “infiltrate” forming colonies and are protected from selection as they are elevated from the selective plate surface. Continuous growth in liquid culture of positive transformants without selective pressure led to neither resistant nor fluorescent strains. This suggests that continuous but subtle selective pressure may be necessary to apply.

If it were to be assumed that cultures are clonal, a reason for variable fluorescence could be that the biosensor is either suppressed or toxic at a certain cell stage. If suppression is the case, an inducible promoter might help (see vector pTpNR; Poulsen et al., 2006). Varying degrees of transgene expression have been observed for *T. pseudonana* before (Nicole Poulsen, Techn. Uni. Dresden, Germany, personal communication). *T. pseudonana* was successfully transformed with fluorescent proteins (Groger et al., 2016; Poulsen et al., 2006; Tanaka et al., 2014), but none of these were Ca^{2+} biosensors. If toxicity of transgenes is the case, possibly only "weak" individuals with reduced silencing capacities show fluorescence which may eventually lead to cell death. Indeed, in strongly fluorescent cells, chlorophyll auto fluorescence was sometimes reduced (Fig. 2.6 A1). Another scenario would be that only "fit" individuals are able to tolerate harmful effects and can afford to maintain expression. This would mean that the majority of cells is rather unhealthy and improvement of culturing conditions would be necessary to ensure more streamlined expression. Indeed, expression of genes often relies on cell healthiness and age of culture. Admittedly, handling and culture conditions would benefit from improvement. These may include: more regular subculturing to guarantee a reliable balance between selective pressure and healthiness of cells; maintaining selective pressure on stock-strains while work-strains should be grown without selective pressure; the inclusion of monitoring Fv/Fm values to assess fitness; improvement of the vector (avoid double transformation, possibly introduce a self-cleaving peptide as in pChlamy4 vector); picking of single cells to guarantee clonal stains; and a much more detailed preliminary screening of "subtle/healthy" and "harsh/effective" concentrations of antibiotics in liquid and solid media, respectively.

Nonetheless, the major aim of visualising Ca^{2+} signalling in *T. pseudonana* was accomplished. *T. pseudonana* clearly needs more care compared to *P. tricornutum*. Investing more work would be worth the effort though, as it offers the chance to investigate Ca^{2+} signalling in a much more ecologically important diatom than *P. tricornutum*.

Chapter 3 Characterisation of hypo-osmotic shock-induced Ca^{2+} elevations in *P. tricornutum*

ABSTRACT

Phaeodactylum tricornutum is a pennate diatom and an important model organism for diatoms in general. Its major habitats are intertidal environments which often face rapid changes in salinity and osmolarity. It is of vital importance to be able to quickly sense and respond to these changes to prevent cell damage. Ca^{2+} signalling plays a role in osmotic signalling in many eukaryotes including diatoms. A detailed examination of role and kinetics of Ca^{2+} in response to osmotic shock will be presented using a *P. tricornutum* strain expressing a genetically encoded Ca^{2+} biosensor (RGECO1),.

P. tricornutum shows a series of individual Ca^{2+} elevations dependent on external Ca^{2+} in response to a gradual drop in osmolarity. These Ca^{2+} elevations are likely vital for osmoregulation as they ensure survival of a potentially lethal drop in salinity. The frequency of these elevations correspond to the rate of osmolarity change, indicating that a cell continuously monitors shifts in the osmolarity in its environment. While sudden large osmotic treatments give rise to Ca^{2+} elevations throughout the cell, more subtle osmotic treatments give rise to increased numbers of cells exhibiting Ca^{2+} elevations that are localised to the cell apices, indicating that the apex is the most osmotically sensitive area in fusiform cells. Oval *P. tricornutum* cells show an overall lower Ca^{2+} signalling activity compared to fusiform cells

P. tricornutum therefore likely utilizes Ca^{2+} elevations with distinct spatial and temporal properties to relay information of the magnitude of hypo-osmotic shocks across the cell.

3.1 Introduction

3.1.1 Habitats of microalgae and dynamics in osmolarity

Diatoms are important primary producers that form the basis of the biome in marine habitats; including estuarine areas (Underwood et al., 1998). The intertidal and estuarine zones and rock pools can be subject to rapid and/ or gradual fluctuations in osmolarity (J C Lewin and Guillard, 1963; Kirst, 1990), dictated by river flow, tides or rainfall. This can lead to local changes in salinity ranging from 0% to >100% seawater which requires protective measures to be taken by the local communities to survive (Kirst, 1990; Underwood et al., 1998). Another example for osmotic stress being an important environmental factor in oceanic systems are polar regions, in which microalgae inhabit the brine-filled cavities of sea ice and are subject to hypo-osmotic stress when the ice melts (Kirst 1989, Campbell 2019). This shows that osmotic stress also can be encountered by organisms not accustomed to coastal areas.

Hypo-osmotic stress is based on osmosis, which is the tendency of a solvent (water in biological systems) to move from a solution of low osmolality to one of high osmolality across a selectively permeable membrane. In a cell, the direction and tendency of water movement is strongly influenced by the electrolyte content of intra- and extracellular fluids. In hypo-osmotic conditions, the relatively high osmotic pressure and negative water potential of internal fluids favours inflow of water into the cell. Depending on the severity of water inflow, this can either lead to a minor osmotic imbalance or to a threatening increase in cell volume, potentially leading to bursting (Balzano et al., 2010; Kirst, 1990; Paasche, 1973; Sarno et al., 2007).

3.1.2 Acclimation to hypo-osmotic stress in diatoms and other organisms

The cell therefore maintains osmotic balance through osmoregulation. This involves either accumulation or excretion of osmotically active substances to mirror the exterior osmotic pressure (= osmoconformers, e.g. diatoms) or to maintain a constant internal osmolarity (= osmoregulators, e.g. bony fish) (Yancey, 2005). Inorganic osmotically active solutes include ions such as K^+, Na^+, or Cl^-, whereas organic solutes may include carbohydrates (e.g. trehalose), polyols (e.g. glycerol, sorbitol), amino acids (e.g. glycine, proline), methylamines (e.g. glycine betaine) and methylsulfonium solutes (e.g. dimethylsulfoniopropionate; DMSP) or urea (Garza-Sánchez et al., 2009; Kinne, 1993; Yancey, 2005).

In animals, specialised organs such as gills in salt water fish or kidneys in vertebrates may maintain osmotic balance (Yancey, 2005). Plants can regulate water loss and uptake via stomata and root cells and can modulate solute content on a cellular level through the vacuole (Chen and Jiang, 2010).

In diatoms, cells exposed to hyper-osmotic stress were shown to accumulate K^+ ions, organic osmolytes such as proline, glycine betaine and DMSP or cyclitols such as cyclohexanetetrol (CHT) to prevent water loss (Dickson and Kirst, 1987; Garza-Sánchez et al., 2009; Kirst, 1990). The preferred osmoprotectants may differ between the diatom species, with proline, glycine and DMSP being primarily used in *P. tricornutum* and *F. cylindrus* (the latter having less glycine), and CHT being primarily used by *Nitzschia ovalis* (Dickson and Kirst, 1987; Garza-Sánchez et al., 2009; Kirst, 1990; Schobert, 1980). In response to hypo-osmotic stress, proline was shown to be secreted in *P. tricornutum* within one hour (Schobert, 1980).

In addition to the osmolyte-based means of osmoregulation in microalgae, changes in morphology were also suggested to increase tolerance to a specific osmotic condition. *Skeletonema* species were shown to alter morphology and chain length in response to osmotic stress (Balzano et al., 2010; Paasche, 1973; Sarno et al., 2007). Moreover, liquid cultures of the pleiomophic diatom *P. tricornutum* were shown to be dominated by the benthic oval form under hypo-osmotic conditions (de Martino et al., 2011). The oval morphotype differs from the pelagic fusiform and triradiate morphotypes in their stronger slilicified cell wall, relatively small vacuoles, lower surface to volume ratio, enhanced lipid

content and higher excretion of extracellular polysaccharides (EPS) (de Martino et al., 2011; Francius et al., 2008), features which may increase the resilience to hypo-osmotic stress.

Although the physiological and morphological consequences of hypo-osmotic stress on diatoms were described, little is known about how these responses are regulated. Moreover, much more rapid means for osmoregulation is needed to prevent cell bursting in response to rapid osmotic changes.

3.1.3 The role of Ca^{2+} signalling in acclimation to new osmotic conditions

Ca^{2+} was shown to be involved in osmotic stress related signalling in a range of eukaryotes (Bickerton et al., 2016; Cessna et al., 1998; Nakayama et al., 2012; Takahashi et al., 1997) including diatoms (Falciatore et al., 2000). How and when osmotic stress-induced Ca^{2+} signalling occurs may differ dependent on respective eukaryotic lineages. In *C. reinhardtii*, hypo- but not hyper-osmotic stress resulted in intracellular Ca^{2+} elevations and loss of flagella (Bickerton et al., 2016; Quarmby, 1996) whereas land plants and the brown alga *Fucus* showed Ca^{2+} elevations in response to both hypo- and hyper-osmotic stress (Cessna et al., 1998; Coelho et al., 2002; Goddard et al., 2000; Takahashi et al., 1997; Taylor et al., 1996) In some species (*Fucus*, yeast), the ability to generate Ca^{2+} elevations was crucial for cell survival in osmotically stressfull conditions (Goddard et al., 2000; Nakayama et al., 2012). Differences in respective Ca^{2+} responses may reflect different mechanisms to address osmotic stress depending on cell environment (fresh/salt water, soil, …) or cell physiologies (i.e. uni- or multicellularity, motility, presence of cell walls, and more).

3.1.4 *P. tricornutum* – a model diatom inhabiting coastal areas

The pennate diatom *P. tricornutum* inhabits estuarine and tidal rock pools, and has been isolated from habitats in the UK, USA, Canada, Finland, Micronesia and the Yellow Sea (de Martino et al., 2007).

In comparison to other diatoms, *P. tricornutum* is rather atypical: It has a pleiomorphic appearance (fusiform, oval or triradiate) and only poorly silicified frustules, allowing it to grow without silicic acids if necessary (Lewin et al., 1958).

Whereas centric diatoms occasionally need to reproduce sexually given that frustules tend to shrink with each subsequent generation (MacDonald, 1869; Mann, 1993; Pfitzer, 1871), *P. tricornutum* likely reproduces completely asexually, and no reduction in frustule size is observed (Rastogi et al., 2019). A further distinction is that centric diatoms may generate flagellated male gametes, whereas *P. tricornutum* and other pennate diatoms do not have flagella in any life stage (Mann, 1993).

Despite its oddities, *P. tricornutum* is an established model organism for phytoplankton and diatom research, with a sequenced genome (Bowler et al., 2008) and means for genetic transformation (Apt et al., 1996). Consequently, *P. tricornutum* has also provided insight into Ca^{2+} signalling in diatoms.

3.1.5 Ca^{2+} signalling in *P. tricornutum*

Hypo-osmotic stress induced Ca^{2+} elevations in a *P. tricornutum* culture in a dose-dependent manner, visualised using the bioluminescent Ca^{2+} reporter aequorin (Falciatore et al., 2000). However, aequorin does not allow examination of these Ca^{2+} elevations on a subcellular level, meaning that the dose-dependent response may be based on either increased amplitudes in individual cells or a larger percentage of responding cells. It remains also unknown whether this single Ca^{2+} elevation would also occur in response to slower, more gradual drops in osmolarity, which are likely more prevalent in nature compared to strong, immediate hypo-osmotic shocks. Additionally, the benthic oval morphotype of *P. tricornutum* was proposed as a more resilient version of the fusiform cells since oval cells dominate cultures when stressful conditions such as low salinity were

applied (de Martino et al., 2011; de Martino et al., 2007). If that is the case, this oval cell resilience may be reflected in lowered Ca^{2+} signalling activity in response to hypo-osmotic shock.

This study is part of a collaborative work with K. Helliwell (MBA Plymouth) who generated a *P. tricornutum* strain expressing the fluorescence based Ca^{2+} biosensor RGECO named PtR1 (Helliwell et al., 2019). K. Helliwell showed the nature of Ca^{2+} signalling in response to rapid hypo-osmotic shocks of different magnitude (Helliwell et al., 2020b). This study will focus on how *P. tricornutum* responds to a more gradual hypo-osmotic shift and will include the oval morphotype (Helliwell et al., 2020b).

3.2 Methods

3.2.1 *P. tricornutum* cultivation and strains

P. tricornutum strain WT670 (alternatively: CCAP 1055/1) originated from the Culture Collection of Algae & Protozoa (https://www.ccap.ac.uk/) and was genetically transformed by Katherine Helliwell (MBA Plymouth) to express the RGECO1 fluorescence based Ca^{2+} biosensor, resulting in the PtR1 strain. PtR1 was cultivated in unshaken 40 mL transparent plastic culture flasks containing 30 mL liquid medium. Growth conditions were 18 °C ambient temperature and illumination of 40-60 µmol $\cdot$ m^{-2} $\cdot$ s^{-1} (Sylvania Luxline Plus 148 F58W/865, Massachusetts, USA) with 16/8 h light-dark cycle.

Long-term cultures were maintained in 100% pre-filtered and autoclaved seawater with added f/2 supplements (Guillard, 1975; J C Lewin and Guillard, 1963); the latter modified by the addition of 100 mM $Na_2SiO_3 \cdot 5H_2O$ and the exclusion of vitamins. Experiments were performed using artificial seawater (ASW; 450 mM NaCl, 30 mM $MgCl_2$, 16 mM $MgSO_4$, 8 mM KCl, 10 mM $CaCl_2$, 2 mM $NaHCO_3$, 97 µM H_3BO_3; pH 8.0 and 20 mM HEPES). Replacement of Ca^{2+} with 200 µM EGTA resulted in Ca^{2+}-free ASW medium.

When used for experiments, PtR1 cells were acclimated to ASW for at least 10 days including one sub-culturing step.

3.2.2 Epifluorescence imaging in *P. tricornutum*

Microscope dishes with 35 mm diameter glass coverslip bases (In Vitro Scientific, Sunnyvale, CA, USA) were coated with poly-L-lysine (Sigma-Aldrich, http://www.sigmaaldrich.com/) to promote cell adhesion to the glass surface. After removing excess poly-L-lysine, 500 µL of cell culture was added and left to settle for 5-30 minutes.

Two microscope setups were used: rapid hypo-osmotic shock experiments were performed on a Nikon Eclipse Ti microscope (Nikon, Japan), whereas all other experiments in this thesis were done on a LEICA DMi8 microscope (Leica, Germany).

The Nikon microscope setup included a 40×1.30 oil immersion objective; a Rhod 530-555 nm excitation and 575-630 nm emission filters (RGECO), a Photometrics Evolve EM-CCD camera (Photometrics, USA) and NIS-Elements AR 3.1 software (Nikon, Japan) (Helliwell et al. 2019, Helliwell et al. 2020b).

The LEICA inverted microscope setup included a 63x 1.4NA oil immersion objective, a 541-551 nm excitation and 565-605 nm emission filter (RGECO), a Hamamatsu ORCA-Flash 4.0 C11440 CMOS camera (Hamamatsu Phototonics, Japan) and Leica application suite X-software v.3.3.0 (Leica, Germany).

In both setups, time resolution was 3.33 frames per second.

Cells were continuously perfused with ASW throughout the recording timeframe *via* a gravity driven perfusion system, and excess liquid in the dish was continuously removed using a vacuum pump. ASW used for perfusion did not contain f/2 supplements, as certain nutrients where shown to induce Ca^{2+} elevations in *P. tricornutum* (Falciatore et al., 2000; Helliwell et al., 2020a). To generate immediate hypo-osmotic shocks, perfusion was switched from ASW to ASW diluted with H_2O. A linear hypo-osmotic transition was generated with a gradient mixer in which ASW 100% was mixed with either dH_2O or ASW 75% before being administered to the perfusion system. The rate of this linear transition was dependent on the applied volumes.

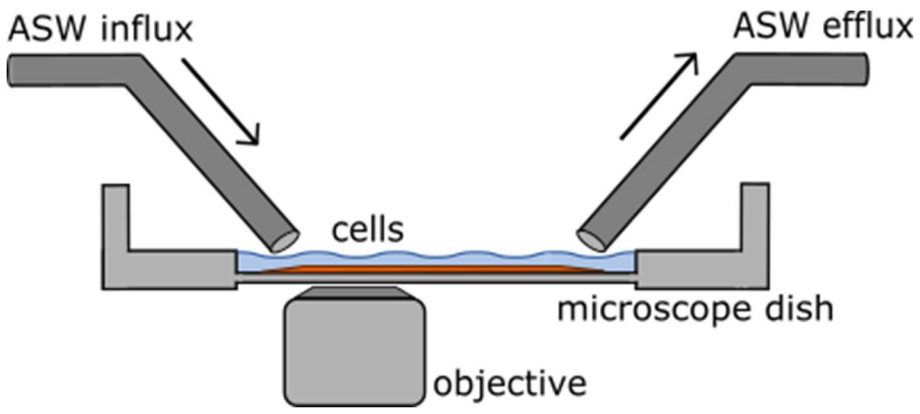

Figure 3.1 : Schematic of the perfusion system on microscope.

500 µL of PtR1 liquid culture in early exponential growth phase was evenly distributed on Poly-L lysine coated glass bottom microscope dishes. PtR1 fluorescence was recorded in cells in close proximity to the influx tube opening.

3.2.3 Processing of imaging data

The mean fluorescence intensity of individual cells in the recorded microscope videos was determined using a region of interest (ROI) engulfing the approximate whole cell area. In case of minor lateral shifts of the visual plane throughout the recording, this ROI was slightly increased. For major lateral shifts, several sets of ROIs at different time-points were used whose values were later merged into one trace.

To visualise traces of cytosolic Ca^{2+}, the fold change in fluorescence (F/F_0) throughout time was determined for each cell. Background fluorescence was subtracted from all F values and then the F_0 value for each cell was calculated from the mean of the initial 16 frames representing resting state fluorescence. Graphs were then generated with Sigmaplot v14.0 (https://systatsoftware.com/) and processed with Inkscape v0.92 (https://www.inkscape.org).

Peaks in a fluorescence trace were defined as F/F_0 values > 1.5 and values larger than four preceding frames and four following frames, respectively.

The area of a Ca^{2+} elevation represents the sum of F/F_0 values within a 30 s interval. Only F/F_0 values > 1.5 were included, and all values were subtracted by 1 to generate a base value of 0 representing periods of no signalling activity.

The percentage of surviving cells was determined by visual assessment of the structural integrity of cells during the hypo-osmotic shocks. Loss of structural integrity hereby describes obvious leaking or bursting of cells or bursting of internal organelles. Cells may have also showed extensive change in size and distribution of organelles, however, these were counted as intact as long as no obvious internal burst was observed.

3.2.4 Generation of kymographs

Kymographs representing the spatial position of cytosolic Ca^{2+} elevations over time were generated in ImageJ v1.51k (http://imagej.nih.gov). Each image within a recording was divided by a rolling median image of 30 frames to produce a pseudo-coloured ratio image for the respective timepoint (Bickerton et al., 2016).

3.3 Results

The *P. tricornutum* RGECO cell line (= PtR1) established by Helliwell et al. (2019) allows the dynamics of cytosolic Ca^{2+} elevations to be monitored in single cells using live-cell epifluorescence imaging. RGECO is an intensiometric biosensor based on the fluorescent protein mApple (See Chapter 2).

3.3.1 PtR1 response to repeated hypo-osmotic shocks

PtR1 cells show Ca^{2+} elevations in response to a single hypo-osmotic shock (Helliwell et al., 2019; Helliwell et al., 2020a). To get an understanding of the cell's ability to respond to a repeated stimulus, perfusion of PtR1 cells with ASW was interrupted four times with ASW of lowered osmolarity.

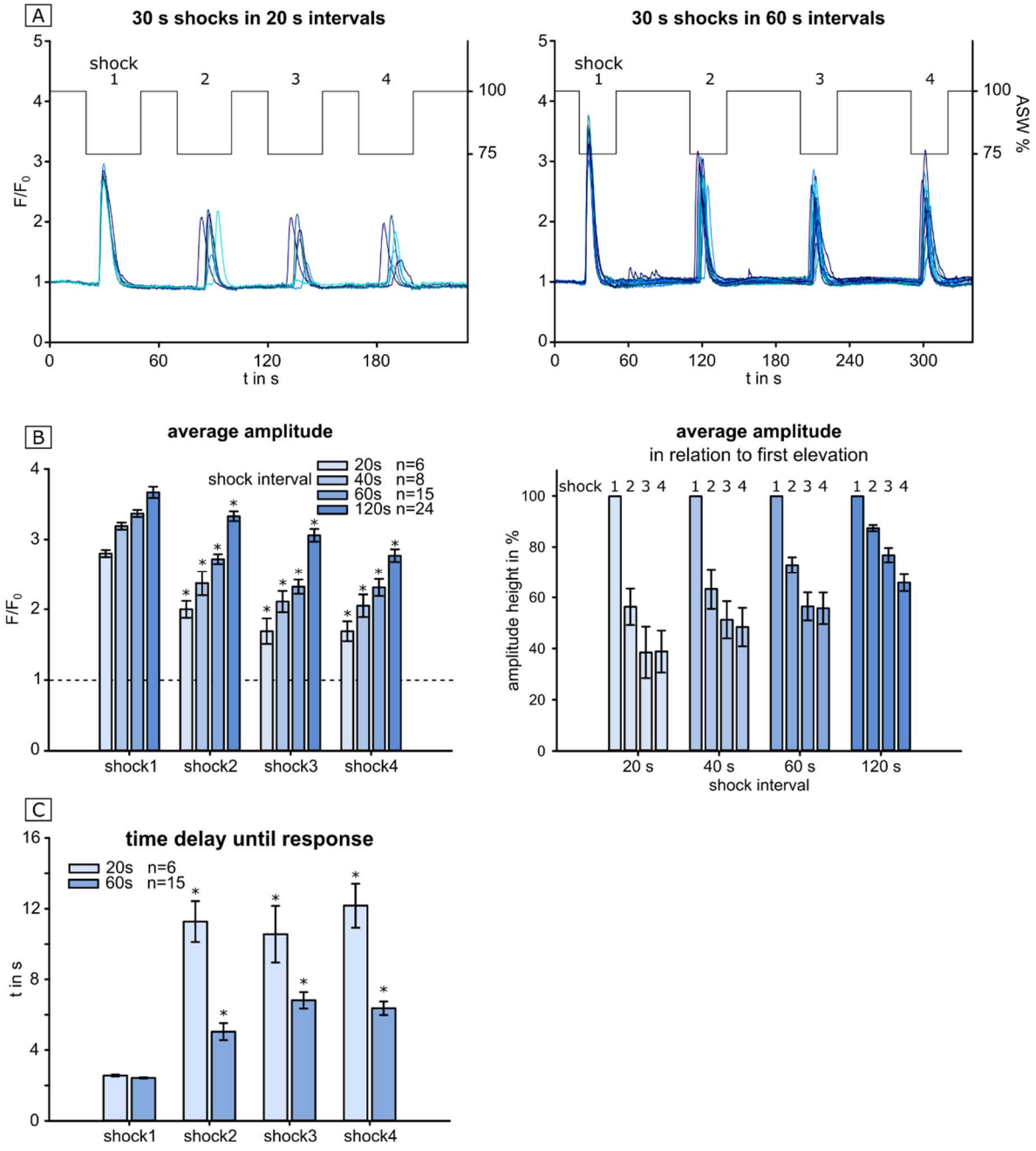

Figure: 3.2 Hypo-osmotic shocks cause transient $[Ca^{2+}]_{cyt}$ elevations in PtR1.

A). Traces of PtR1 fluorescence show single rapid Ca^{2+} elevations (blue traces) in response to four subsequent hypo-osmotic shocks (100% ASW to 75% ASW for 30 s; black trace) applied in different intervals (20, 40, 60 or 120 s). Total number of observed cells were 6, 8, 15 and 24, respectively (two repeated experiments per condition with similar results). **B)** Mean amplitudes of Ca^{2+} elevations from same experiments (SEM). The first response differs in amplitude between the treatments, indicating an unknown variable. The amplitude data is reshown with subsequent Ca^{2+} elevations normalised to the first one (B right). **C)** Time delay until the onset ($F/F_0 > 1.3$) of a Ca^{2+} elevation after shock application for the 20 s and 60 s interval experiment. The data were acquired on the Nikon Ti microscope. Asterisks represent significantly different values in relation to the shock1 value per interval, respectively.

Cells were given four hypo-osmotic shocks in rapid succession with varying intervals between each shock. A single rapid transient Ca^{2+} elevation can be observed for each shock applied in most of the cells. The amplitudes of these Ca^{2+} elevations significantly decreased with successive hypo-osmotic shocks for all intervals, (two-way repeated measures ANOVA with Bonferroni post-hoc test: $P<0.005$) with the exception for shock3 and shock 4 ($P = 0.606$) (Fig. 3.2). The amplitudes also significantly varied in dependence on interval duration (two-way repeated measures ANOVA $P<0.005$) (Fig.3.2 B). More specifically, for the 20 s and 40 s interval, shock 2-3 amplitudes were significantly different from the shock 1 amplitudes (Bonferroni post-hoc test $P<0.01$), but were not significantly different from each other ($P>0.05$). With longer intervals, the amplitudes of subsequent shocks also got significantly different from each other ($P<0.015$), with exception of shock 3 and 4 in the 60 s interval ($P = 0.912$).

Cells responded within 3 s to the first shock and the lag in response time increased to more than 10 s with relatively short intervals of 20 s between the successive shocks. In comparison, the lag in response time for successive shocks was lower (5-7 s) when the interval between those shocks was longer (60 s). The response time of cells was also significantly affected by the interval and number of successive shocks (two-way repeated measures ANOVA $P<0.001$ for both factors overall), but no significant difference was found in the response time for shock 1 (Bonferroni post-hoc test $P>0.005$). More specifically for the 20 s interval, all subsequent shock response-times were significantly different from shock 1 ($P<0.001$ for all response times), but not significantly different from each other ($P>0.621$). Conversely, with a longer interval (60 s), the following response times were not only significantly different from shock 1, but also between each other ($P<0.012$), with exception of the last response time at shock 4, which only was significantly different from the response time for shock1 ($P>0.001$).

Overall, the data indicate that larger shocks translate to larger Ca^{2+} elevations and successive shocks lead to attenuation and increased delay of responses.

3.3.2 Hypo-osmotic shock delivered as a gradual decrease in salinity

In order to investigate Ca^{2+} responses to osmotic changes that may be more representative of changes occurring in the natural environment, hypo-osmotic treatments were delivered as a more gradual, linear shift.

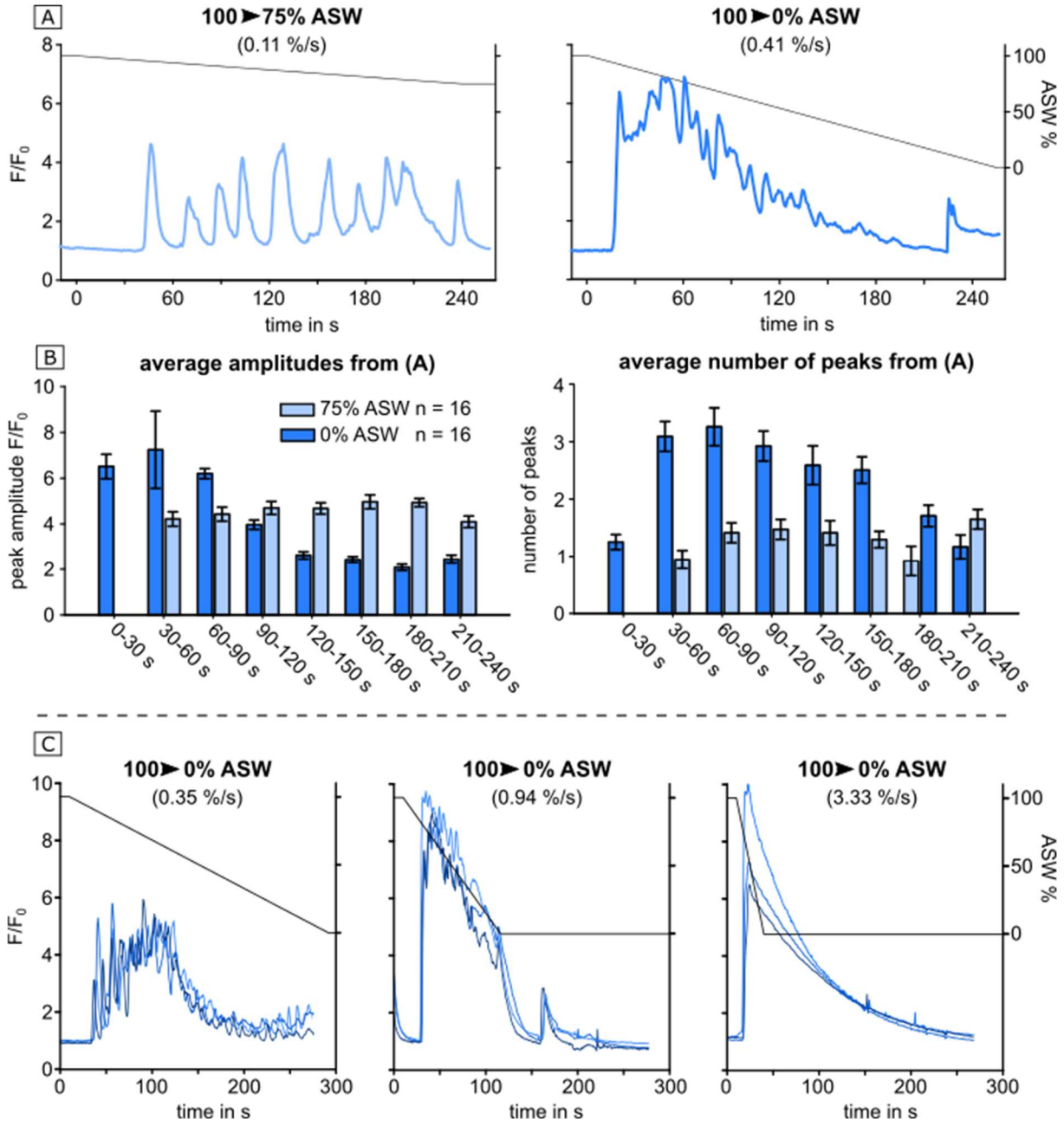

Figure 3.3: Gradual decrease in osmolarity causes repetitive $[Ca^{2+}]_{cyt}$ elevations in PtR1.

A) Normalised fluorescence trace of a representative PtR1 cell in response to a hypo-osmotic gradient from 100% to 75% ASW (left) and from 100% ASW to 0% ASW (100% fresh water, right). Approximate calculated rates of ASW % drop per s in parentheses. All experiments were done in

triplicate with similar results, but data were not merged due to slight differences in ASW % change rate. **B**) Mean (SEM) peak amplitude (left) and number of peaks (right) within 30 s time intervals of 16 individual cells per gradient treatments shown in (A). **C)** Three representative PtR1 fluorescence traces in response to a hypo-osmotic gradient from 100% ASW to 100% fresh water at three different velocities.

When PtR1 cells were exposed to a steady decrease in salinity from 100% ASW to 75% ASW over 4 minutes, they showed multiple, repetitive cytosolic Ca^{2+} elevations (Fig. 3.3 A left). Individual Ca^{2+} elevations continued for the duration of the treatment at a relatively uniform intensity (3-5 fold increase) and number (Fig. 3.3 C), suggesting that a linear gradient in osmolarity/salinity content is continuously triggering the underlying mechanisms of hypo-osmotic stress perception.

When cells were exposed to a more severe and faster gradual drop in osmolarity from 100% ASW to 100% fresh water, individual Ca^{2+} elevations were more difficult to detect as cytosolic Ca^{2+} did not return to resting state levels (Fig. 3.3 A right). A brief spike in Ca^{2+} at the end of the fluorescence trace represents bursting of the cell (Fig. 3.3 A right), though most cells were able to maintain structural integrity for the observed time frame (2 of 13 cells burst; = ~15%). In contrast to the more subtle gradient, the amplitude and number of Ca^{2+} elevations per 30 s interval attenuated over time (Fig. 3.3 B). This may indicate that the ability to generate Ca^{2+} elevations is reduced, possibly due to the depletion of intracellular Ca^{2+} stores or habituation of Ca^{2+} channels.

The Ca^{2+} elevations reflected the rate of change and duration of the hypo-osmotic transitions, as individual elevations became less distinct until they appeared as a single large Ca^{2+} elevation exceptionally long duration (Fig. 3.3 C). *P. tricornutum* is able to survive transition from 100% ASW to freshwater when the transition is not too rapid: A gradual change rate of approximately 3 %/s was lethal for 11 % of cells (n = 18, Fig. 3.3 C right), whereas a nearly immediate change rate of 33 %/s was lethal for 70 % of cells (n = 12, not shown).

3.3.2.1 Spatiotemporal characteristics of osmotic shock-induced Ca^{2+} elevations

In contrast to strong immediate hypo-osmotic shocks which may oversaturate osmotic shock perception leading to strong RGECO signals engulfing the whole cell, Ca^{2+} elevations in response to more subtle hypo-osmotic shifts were less intense and revealed more detail of their spatiotemporal characteristics.

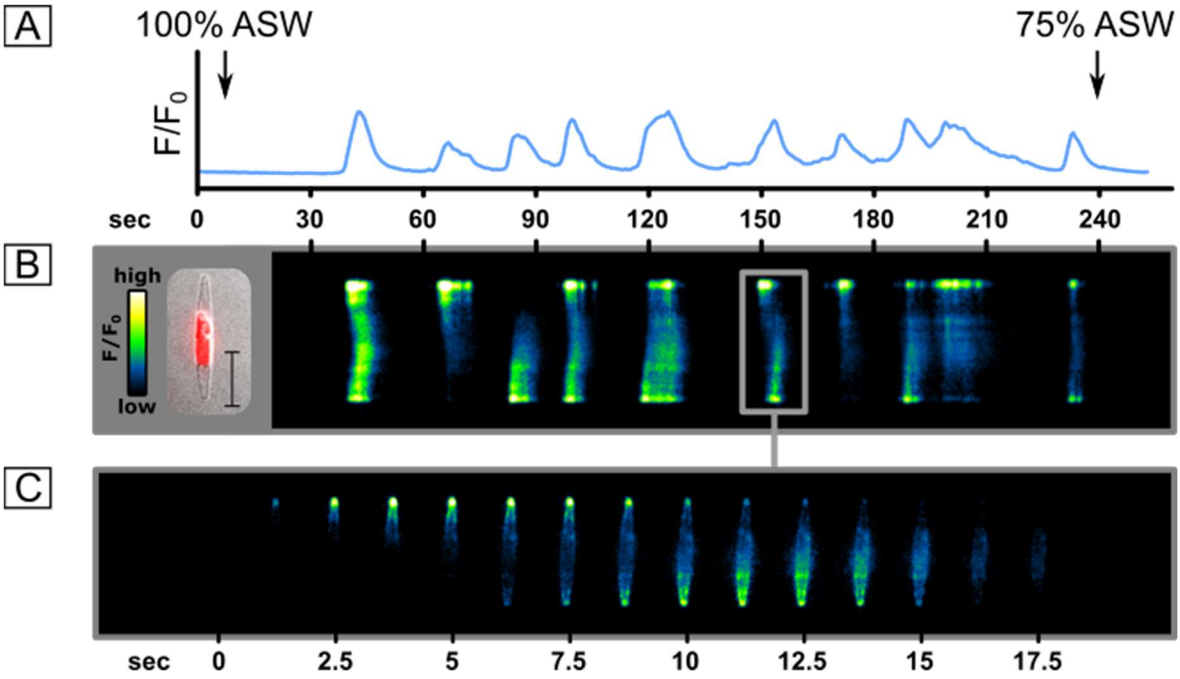

Figure 3.4: Gradual hypo-osmotic shock induces Ca^{2+} elevations protruding from the cell apex

A) Multiple individual Ca^{2+} elevations of a single PtR1 cell in response to a gradual hypo-osmotic shock (arrows, same cell as in Fig. 3.3). **B)** False colour kymograph of the same cell during the same treatment. A DIC image of the cell is shown as reference with chlorophyll auto-fluorescence shown red (grey box, scale bar = 10 µm). **C)** Spatiotemporal details of one exemplary Ca^{2+} elevation visualised as a time-course with t = 1.25 s marking the initiation of that response.

The example fluorescence trace originates from Fig. 3.3 A and shows Ca^{2+} elevations in response to a relatively slow gradual salinity change rate (Fig. 3.4 A). The corresponding kymograph demonstrates that hypo-osmotic-induced Ca^{2+} elevations tended to form at the apex of cells independently and either propagated to the centre of the cell or remained localised (Fig. 3.4 B). Localised Ca^{2+} elevations are represented as lower amplitudes in the fluorescence trace (Fig. 3.4 A). The apex of cells also showed rapid, scintillating Ca^{2+}

elevations which added shoulders or minor bumps in the fluorescence trace of a larger Ca^{2+} elevation (e.g. t = 70 s in Fig.3.4 A and B), indicating that dynamics of Ca^{2+} elevations are slightly simplified in fluorescence traces. Whereas the trace suggested ten individual Ca^{2+} elevations in this experiment, the “upper” tip of the cell showed more than 20 individual Ca^{2+} “sparks” during that time.

The time-course of an individual Ca^{2+} elevation demonstrates independent initiation of two Ca^{2+} elevations at respective apices (Fig. 3.4 C), which then propagated towards the centre of the cell, again appearing as a single Ca^{2+} elevation in the fluorescence trace (Fig. 3.4A t = 150 s).

3.3.2.2 Effect of depleted external Ca^{2+} on osmotic shock response

External Ca^{2+} is required for the generation of single hypo-osmotic shock-induced Ca^{2+} elevations and hypo-osmotic-induced Ca^{2+} signalling is important for cell survival during strong hypo-osmotic shocks (Helliwell et al., 2020b). Experiments were conducted to test whether external Ca^{2+} is required for Ca^{2+} elevations and cell survival in response to more gradual osmotic treatments.

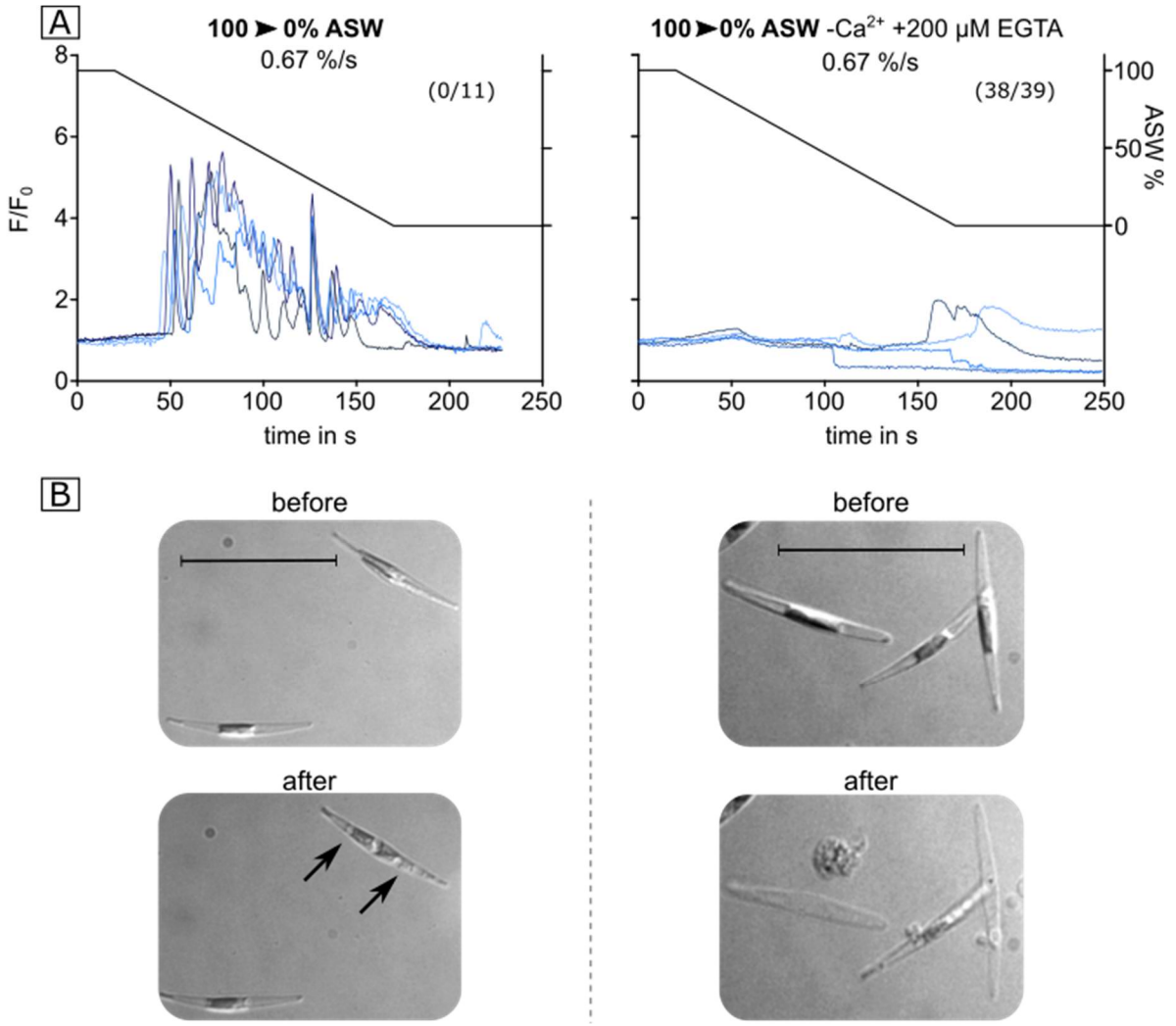

Figure 3.5: External Ca^{2+} is essential for osmoregulation

A) Four representative traces of PtR1 fluorescence cells exposed to a gradual hypo-osmotic shock to dH_2O (100 % to 0% ASW) with an approximate change rate of 0.67 %/s. ASW either contained (left graph, one experiment) or did not contain Ca^{2+} (right graph, 3 independent experiments). The number of cells that burst in relation to total number of cells is shown in parentheses. **B)** DIC images of exemplary cells before and after respective osmotic treatments. Cells are more likely to burst in Ca^{2+} replete shocks. Cells which do not burst may shock rearrangement of internal organelles (arrows). Scale bars represent 30 µm.

With external Ca^{2+}, rapid repetitive Ca^{2+} elevations are observed as described before (Fig. 3.5 A left). Cells showed no obvious damage to cell integrity, although most cells demonstrated internal rearrangement of organelles likely reflecting changes in vacuolar volume (Fig. 3.5 B left).

In contrast, a gradual hypo-osmotic shock of ASW -Ca^{2+} +200 µM EGTA towards dH_2O +200 µM EGTA led to a complete inhibition of Ca^{2+} elevations (Fig. 3.5 A right). The absence of external Ca^{2+} greatly increases the lethality of the treatment since 38 of 39 cells lost structural integrity or burst in the observed timeframe (Fig. 3.5 B right).

Both EGTA and low external Ca^{2+} are proposed to increase membrane permeability (Virk and Clealand, 1990, Webb and Bohr, 1978). EGTA chelates predominantly Ca^{2+} and as such may disturb homeostasis of divalent cations in the cytosol if it enters the cell through a destabilised membrane. As such, it could inhibit membrane repair processes, and it is possible that EGTA increases cell mortality in the experiments above. However, it is unlikely to be mainly responsible for the cell rupture, as K^+ efflux was not increased but decreased under -Ca^{2+} +200 µM EGTA hypo-osmotic shocks (Helliwell et al, 2020b).

3.3.2.3 Ca^{2+} elevations in the oval morphotype

P. tricornutum is known to exhibit three different morphotypes (fusiform, triradiate and oval), depending on environmental conditions (de Martino et al., 2011). The fusiform and triradiate forms are pelagic, whereas the oval form is mostly found in benthic biofilms and is also shown to dominate *P. tricornutum* cultures grown at low salinity (De Martino et al., 2011). Therefore, oval cells may respond to osmotic stress differently. Oval cells were occasionally present in experiments presented above and their signalling activity is now more closely investigated and compared to fusiform cells.

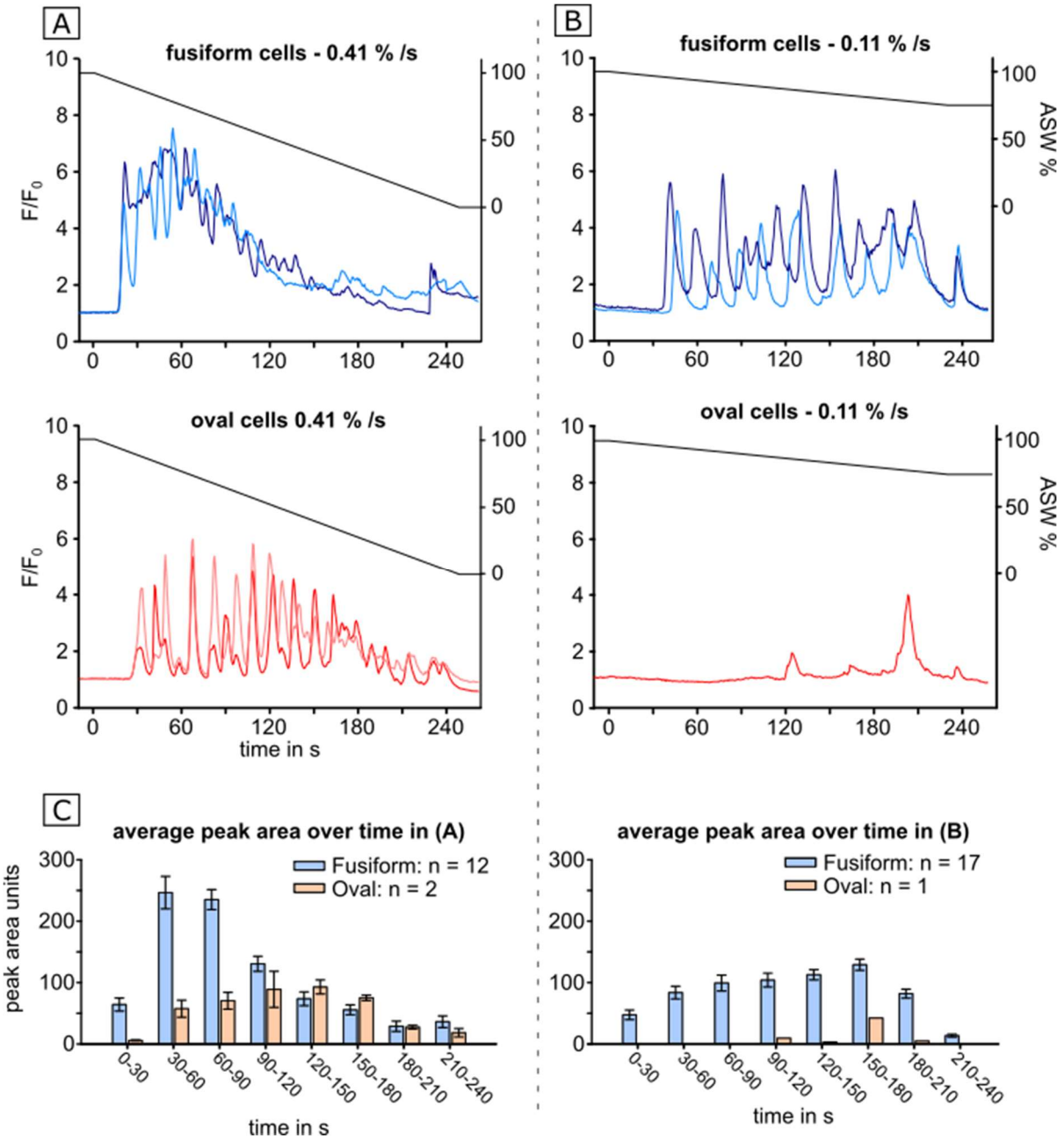

Figure 3.6: Benthic oval morphotype exhibits reduced sensitivity to hypo-osmotic stress.

A) Representative traces of PtR1 fluorescence of two fusiform (blue) and two oval (red) cells from the same dish in response to a gradual hypo-osmotic shock towards 0% ASW (100% dH_2O) **B)** Representative traces of PtR1 fluorescence of two fusiform (blue) and one oval (red) cell from the same dish in response to a hypo-osmotic gradient towards 75% ASW (25% dH_2O). **C)** Mean area of cytosolic Ca^{2+} traces per 30 s time interval for oval and fusiform cells in experiment A and B, respectively (SEM). The area of the trace is a function of both amplitude and number of Ca^{2+} elevations. The fusiform and oval cells used in all experiments originated from the same culture.

In a hypo-osmotic gradient towards fresh water, fusiform cells exhibited a series of rapid converging Ca^{2+} elevations and cytosolic Ca^{2+} did not return to resting state levels throughout the first three quarters of the treatment (Fig. 3.6 A top). In contrast, Ca^{2+} elevations in oval cells remained distinct, allowing cytosolic Ca^{2+} to return to resting state levels throughout the treatment (Fig. 3.6 A bottom). This pattern is further visualised when the peak area of respective fusiform and oval cell fluorescence traces are compared (Fig. 3.6 C left).

The onset of Ca^{2+} elevations of fusiform cells occurred highly uniformly at 18.9 ± 0.6 s after gradient start (approximate 92 % ASW) and were most pronounced at the early stages of the treatment with strong attenuation towards the end of the treatment. In contrast, the Ca^{2+} elevations of the two oval cells were generated later (27.9 ± 0.3 s; approximate 88.5 % ASW) and were most pronounced at the middle stages of the treatment with relatively subtle attenuation towards the end of the treatment.

When applying a less severe hypo-osmotic gradient towards diluted 75% ASW, multiple, independent Ca^{2+} elevations with no clear sign of attenuation occurred in fusiform cells for the duration of the treatment (Fig. 3.6 B top). In contrast, the oval cell responded only four times and three of those elevations were relatively weak (Fig. 3.6 B bottom). This is further visualised when the area of respective fusiform and oval cell fluorescence traces were compared (Fig. 3.6 C right).

The first response in fusiform cells occurred less uniformly at 46.1 ± 3.7 s after gradient start, however, the approximate ASW concentration (95 %) was similar to the more severe treatment. In contrast, the first and weak response in the single oval cell occurred at 121.2 s at approximately 88.6 % ASW.

Twelve additional oval cells distributed among six additional experiments with different gradient velocities also showed a lower number of Ca^{2+} elevations compared fusiform cells, respectively (Helliwell et al., 2020b). These data suggest that the benthic oval morphotype is less sensitive to hypo-osmotic stress compared to planktonic fusiform cells.

3.4 Discussion

This study shows that a gradual hypo-osmotic shock initiates a series of small and quickly reoccurring Ca^{2+} elevations at the apex of fusiform *P. tricornutum* cells which may propagate towards the cell centre and are dependent on external Ca^{2+}. The more subtle drop in osmolarity achieved by the gradient mixer generate overall less intense Ca^{2+} elevations which are better suited for analysis of the underlying mechanisms and may resemble more natural conditions compared to immediate hypo-osmotic shocks performed in many other studies (Apostol et al., 2009; Bickerton et al., 2016; Cessna et al., 1998; Coelho et al., 2002; Falciatore et al., 2000).

3.4.1 Cells continuously respond to a steady decrease of osmolarity

In contrast to an immediate hypo-osmotic shock, a gradual hypo-osmotic shock led to multiple Ca^{2+} elevations. A series of single Ca^{2+} elevations is prevalent at relatively subtle gradual shocks of slow change rate in osmolarity, which merge into overlapping large Ca^{2+} elevations at stronger and faster gradients. These overlapping Ca^{2+} elevations prevent the cytosolic Ca^{2+} concentration to reach resting state levels, but it is not clear whether this is due to a higher number of triggered channels, a longer duration of channel opening, or due to exhausted Ca^{2+} efflux capacities. With faster drops in osmolarity, the opening of channels becomes eventually more synchronised and may lead to a single large Ca^{2+} elevation observed in response to an immediate hypo-osmotic shock.

This shows the limits in the time responsiveness of the RGECO biosensor and imaging setup, but also indicates that the underlying sensing and propagation mechanisms can be very fast if the stimulus intensity allows it.

3.4.2 Underlying mechanisms

3.4.2.1 Putative responsible Ca^{2+} channels

Hypo-osmotic stress manifests in influx of H_2O into the cell body which results in cell expansion (Lucké and McCutcheon, 1932). The cell expansion increases membrane tension, which may result in activation of mechanosensitive Ca^{2+} channels (Bialecka-Fornal et al., 2015; Haswell et al., 2011; Kurusu et al., 2012; Nakayama et al., 2012). Thus, ion channels which are sensitive to mechanical stress are main candidates for Ca^{2+} dependent perception of hypo-osmotic stress in various organisms.

The *P. tricornutum* genome contains seven distinct genes encoding mechanosensitive channels (Verret et al., 2010). Mechanosensitive channels can be involved in osmotic signalling pathways as shown in animal and fungal cells (Hoffmann et al., 2009). In addition, the *P. tricornutum* genome also contains at least six "hyperosmolality-induced Ca^{2+} increase channels (OSCA), a family of mechanosensitive channels involved in osmo-sensing in *Arabidopsis thaliana* (Murthy et al., 2018; Yuan et al., 2014). A third option includes mechanosensitive transient receptor potential channels (TRPs) which were shown to be involved in hypo-osmotic shock response in animals (Hoffmann et al., 2009). *P. tricornutum* has four TRP channels (Verret et al., 2010), two of which have ankyrin repeats at the N-terminus (see Chapter 5). These repeats are suggested to be in contact with sub-membrane structures such as the cytoskeletal acto-mysoin cortex or organelles in animal cells (Gaudet, 2008; Li et al., 2011). Upon cell expansion, these repeats are proposed to function as molecular springs which invoke TRP opening when the relative position of channel and sub-membrane structures changes (Gaudet, 2008).

Although the identity and number of channels important for osmo-sensing in *P. tricornutum* remains unknown, the necessity of external Ca^{2+} for the Ca^{2+} response strongly suggest that Ca^{2+} channels at the plasma membrane play a key role in their initiation for both immediate and gradual hypo-osmotic shocks (Helliwell et al., 2020b).

3.4.2.2 The cell apex as the initiation point for the intracellular Ca^{2+} wave

The apical regions of fusiform *P. tricornutum* cells may represent the main sensors for hypo-osmotic stress. At relatively subtle gradients, rapid repetitive Ca^{2+} elevations (1/s for 4-5 s) may be observed in the apical cytosol. These local Ca^{2+} elevations may result from a higher local concentration of osmo-sensing Ca^{2+} channels. Alternatively, hypo-osmotic-induced cell expansion may have the largest effect on membrane tension in that area, invoking a stronger mechanic stimulus on local channels compared to the rest of the cell body. Both options may apply: cells may tightly regulate the distribution of ion channels in the membrane through distinct micro-domains such as lipid rafts and caveoles, and changes in membrane tension within these micro-domains are proposed to affect activity of mechanosensitive channels more than global change (Bavi et al., 2016; Echarri and Del Pozo, 2015; Huang et al., 2013; Pristerá and Okuse, 2011). A better understanding of the apical architecture (membrane, organelle, cytoskeleton) in *P. tricornutum* is needed to make a profound statement.

3.4.2.3 Propagation of the Ca^{2+} wave

More subtle gradual hypo-osmotic shocks led to propagating Ca^{2+} waves. It is not entirely clear whether strong shocks may simply accelerate the underlying signal propagation mechanisms, leading to a saturation of the signalling system, or whether they enforce additional recruitment of faster components.

However, we propose that these rapid elevations of Ca^{2+} at the apical region in response to subtle drops in osmolarity only propagate further when a local threshold in apical cytosolic Ca^{2+} is met. Once this applies, the Ca^{2+} wave may reach the centre of the cell where it is then decoded by Ca^{2+}-binding proteins.

It remains unclear which components facilitate the propagation of the Ca^{2+} signal throughout the cell. The attenuation of Ca^{2+} elevations which is observed in subsequent immediate hypo-osmotic shocks may indicate exhausted intra-organellar Ca^{2+} stores (vacuole, ER). In plants cells, the vacuole is the largest Ca^{2+} store and is a vital component in plant Ca^{2+} signalling (Schonknecht, 2013). Although less well understood, the *P. tricornutum* vacuole may also be able to support Ca^{2+} signalling events through Ca^{2+} release

channels (Cessna et al., 1998; Choi et al., 2014; Schonknecht, 2013). Since *P. tricornutum* lacks the IP_3R Ca^{2+} release channels found in green algae and animals, putative alternatives in *P. tricornutum* may include CNGCs or TPCs (Verret et al., 2010). However, it is also possible that plasma membrane channels contribute to signal propagation, though these channels may be less abundant compared to the apical area and/ or less sensitive due to reduced effect of local hypo-osmotic stress-induced membrane tension.

3.4.2.4 Decoding the Ca^{2+} wave / cell response

This study showed that *P. tricornutum* cells may tolerate drops in seawater salinity to freshwater levels with ~90% of cells successfully maintaining structural integrity if these drops are applied over a time course of a few minutes instead of a few seconds. This is not only a demonstration of the sturdiness of *P. tricornutum* in response to hypo-osmotic shock, but it also may indicate that organisms in coastal areas may indeed experience and survive such severe osmotic fluctuations in nature (J C Lewin and Guillard, 1963; Kirst, 1990). A similar observation was made in the bacterium *E. coli*, with higher survivability when a hypo-osmotic shock to 0 M NaCl was applied over several minutes, however, intracellular Ca^{2+} was not monitored (Bialecka-Fornal et al., 2015)

The definite mechanisms through which Ca^{2+} signalling is connected to hypo-osmotic stress acclimation *in P. tricornutum* has been investigated in independent studies. K^+ efflux helps to prevent water influx in a range of eukaryotes (Dickson and Kirst, 1987; Hendil and Hoffmann, 1974) and K^+ efflux also has been measured in *P. tricornutum* shortly after hypo-osmotic shock with a microelectrode (Helliwell et al., 2020b). The presence of four K^+ channels with Ca^{2+}-binding EF-hand domains in *P. tricornutum* may support a direct connection between hypo-osmotic-induced Ca^{2+} elevations and K^+ efflux.

Furthermore, global cytosolic Ca^{2+} elevation in response to a strong immediate hypo-osmotic shock were followed by a Ca^{2+} elevation in the nucleus (Helliwell et al., 2020b). The increase in nuclear Ca^{2+} levels may activate Ca^{2+} dependent transcription factors and induce expression of genes related to hypo-osmotic stress, such as components of metabolic pathways involved in the production or release of organic osmolytes (Wehner et al., 2003). However, it may also be the case that both Ca^{2+} signalling pathways are decoupled and

affect different aspects of hypo-osmotic stress acclimation dependent on the severity of the hypo-osmotic shock (Bootman et al., 2009; Stael et al., 2012). Indeed, decoupling of hypo-osmotic induced cytosolic and nuclear Ca^{2+} elevations was reported for *A. thaliana* root cells (Huang et al., 2017) and *Fucus* embryos (Goddard et al., 2000). In the latter, cytosolic Ca^{2+} elevations regulate cell volume whereas nuclear Ca^{2+} elevations regulate cell cycle.

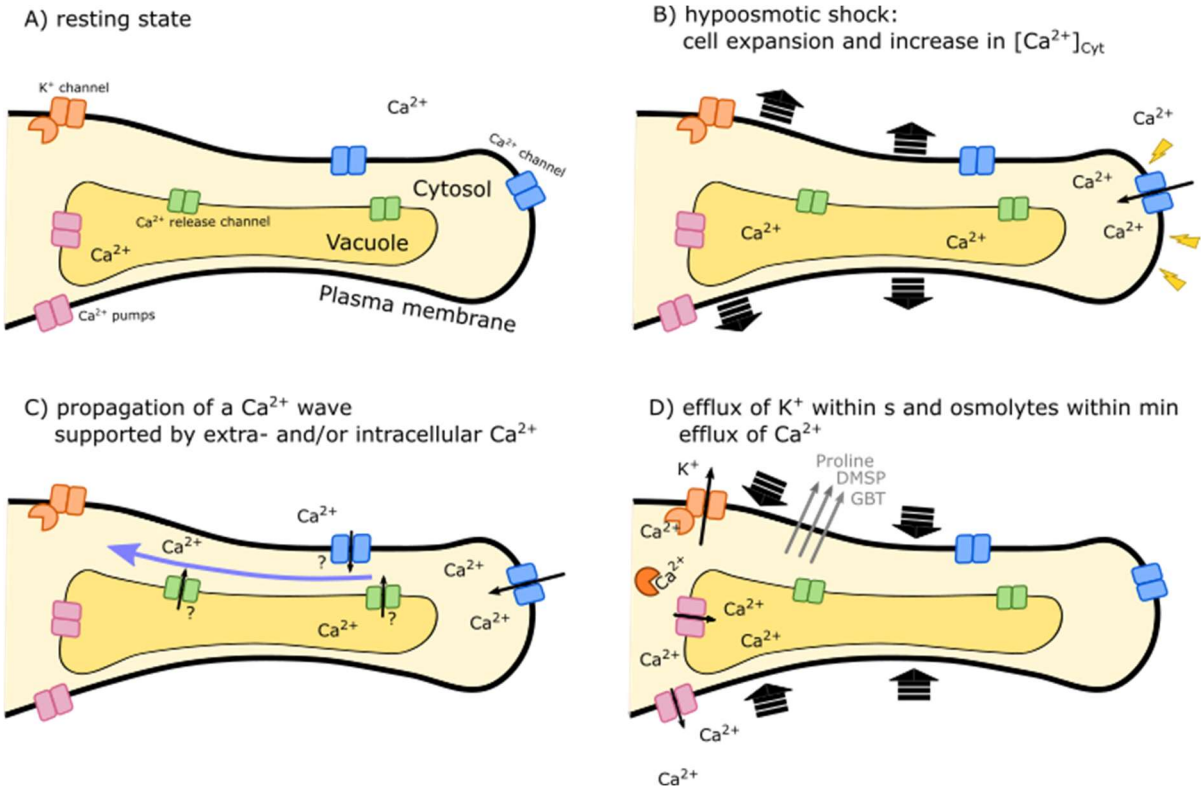

Figure 3.7: Schematic of the hypo-osmotic shock-induced Ca^{2+} response in *P. tricornutum*.

A) Section of a *P. tricornutum* cell in resting state with most of transporters and ion channels involved in the hypo-osmotic shock response inactive. **B)** Upon hypo-osmotic shock, H_2O enters the cell and the cell expands (large black arrows). The apex of cells is the starting point of the Ca^{2+} elevation, possibly due to relatively high impact of cell expansion on membrane tension at this area or relatively high amount of responsive Ca^{2+} channels. **C)** If the stimulus is strong enough, the local Ca^{2+} elevation becomes a global one as a Ca^{2+} wave proceeds from the tip towards the centre of the cell. This Ca^{2+} wave may be fuelled by internal or external Ca^{2+} sources. **D)** The cytosolic Ca^{2+} is actively transported out of the cell by Ca^{2+} pumps and/or Ca^{2+}/H^+ antiporters. The kinetics and localisation of the Ca^{2+} elevation may be decoded by Ca^{2+} binding proteins. K^+ efflux through Ca^{2+} binding K^+ channels may represent a short-term response, osmolyte efflux a mid-term response (Proline, glycine betaine (GBT), or dimethylsulfoniopropionate (DMSP)) and gene-expression / morphotype transition a long-term response.

3.4.3 Oval cells are less sensitive to hypo-osmotic stress

In this study, oval cells elicited fewer and weaker Ca^{2+} elevations in response to gradual hypo-osmotic shocks compared to fusiform cells. The oval morphotype is known to dominate *P. tricornutum* populations under long term hypo-saline conditions (de Martino et al., 2011; de Martino et al., 2007; Ovide et al., 2018). Therefore, oval cell may adopt a different strategy for tolerating hypo-osmotic stress through the presence of a silicified and more rigid cell wall able to tolerate increases in cell turgor. The higher threshold for generating Ca^{2+} elevations may be possibly related to the lack of distinct cell apices, i.e. the more spherical shape may be better suited to resisting cell expansion than the elongated fusiform cells, which may reduce mechano-stimulation of putative Ca^{2+} channels in those regions of the cell.

3.4.4 Conclusion and outlook

This study manifests earlier observation that hypo-osmotic shock-induced Ca^{2+} elevations have a regulative role in the osmoregulation of the euryhaline diatom *P. tricornutum* (Falciatore et al., 2000). In contrast to immediate hypo-osmotic shock treatments, the application of more gradual hypo-osmotic treatments revealed that the osmotic environment is continuously monitored in *P. tricornutum.* This implies a complex underlying signalling system including localised Ca^{2+} elevations and checks for signal propagation; concepts which may play a role in signal decoding. The underlying channels for initiation of the Ca^{2+} elevation are not known but were narrowed down to the plasma membrane of the cell apex. Successful localisation of putative channels to that area may help to identify potential knock-out or knock-down candidates. Data presented in this study also shows that the less sensitive oval morphotype likely has adopted a different strategy for tolerating hypo-osmotic stress, e.g. by a more sturdy shape and higher silification or by reducing the reliance on Ca^{2+} signalling and possible consequent advantages saving costs associated with replenishing solutes lost during the osmotic response.

Chapter 4 Characterisation of Two-pore channels in *P. tricornutum*

ABSTRACT

Two pore channels (TPC) are a major class of ion channels present in both plants and animals. In plants they are responsible for the slow vacuole current and have been linked to propagation of Ca^{2+} waves in root cells in response to salt stress. In animal cells, they are proposed to release Ca^{2+} from endo- and lysosomes. This study aims to investigate the function and distribution of TPCs in diatoms using phylogenetic analysis and physiological studies in *P. tricornutum*.

Bioinformatic searches revealed that all sequenced diatoms have a TPC1 channel similar those found in plants and animals. In addition, TPC1-genes were found in transcriptomes of many more diatoms including centric and pennate lineages, suggesting a broad distribution. The ion selective motif of diatom TPC1 resembles that of animal TPCs, suggesting similar ion selectivity. Moreover, diatom TPC1 also has two EF-hand domains between the two ion transport domains, a feature typical for plant TPCs which suggests Ca^{2+} -dependent activity. Genetic knockout of *TPC1* in *P. tricornutum* suggests that TPC1 is not involved in the hypo-osmotic induced Ca^{2+} response or growth at different salinities.

Most diatoms also possess a novel and unique alternative form of TPC, which is named diatom-TPC-like (dTPCL) in this study. dTPCL has a unique ion selective motif that is not found in other TPCs, suggesting that it has a specialised role within diatoms. It was successfully localised to the vacuole membrane, indicating a role in ion release.

In conclusion, TPC channels are widespread in diatoms and include a novel class of TPC-like channels not found in other eukaryotes.

4.1 Introduction

4.1 Introduction to two-pore channels

Two-pore cation channels (TPCs) are a ubiquitous class of ion channels located in membranes of intracellular organelles such as endosomes and vacuoles and are proposed to assist in the formation and propagation of cytosolic Ca^{2+} elevations through Ca^{2+} release (Furuichi et al., 2001; Hedrich et al., 2018; Ishibashi et al., 2000). TPCs are also present in diatoms, with two genes coding for a TPC in the *P. tricornutum* genome (Verret et al., 2010). The function of TPCs in diatoms is not known, and it is not clear how closely related the two TPCs in *P. tricornutum* are.

4.1.1 Structure and origin of two pore channels

Being part of the cationic pore-forming loop (P-loop) channels, TPCs share a similar structure with other voltage dependent cation channels (VDCC's) such as $BacNa_V$ or four domain Ca^{2+} or Na^+ channels (Ca_V, Na_V). The assembled final channel of all these channels has four shaker-type ion transport domains (Guo et al., 2016; Rietdorf et al., 2011). In the $BacNa_V$ or CatSper channels, the respective gene encodes a single ion transport domain, and the resultant protein is assembled in to a tetramer to form a functional ion channel (Guo et al., 2016). In TPCs, one gene encodes two of these ion transport domains, which assemble as a dimer to form a functional channel. Genes for Ca_V or Na_V encode proteins that already contain all four ion transport domains needed for a functional channel (MacKinnon, 1995), see Fig. 4.1.

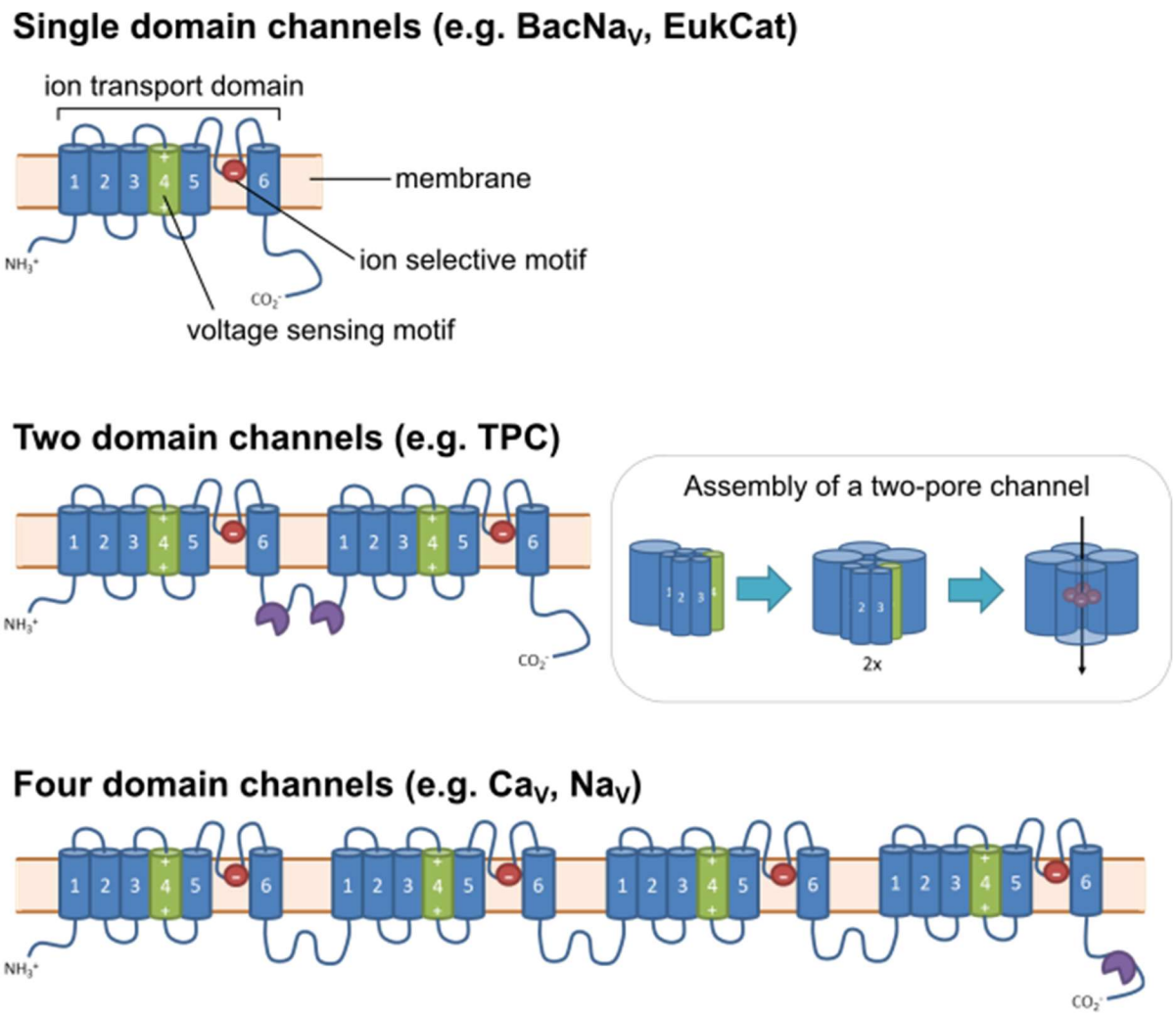

Figure 4.1: Architecture of shaker-type cation channels

Schematic secondary structures of the gene products of several classes of voltage gated cation channels. The gene product of single domain channels contains one ion transport domain consisting of six transmembrane helices (blue), a voltage sensing motif characterised by a series of positively charged amino acid residues (green) and the ion selective motif located in the loop between the 5th and 6th transmembrane segment (red). For single domain channels, four gene products are needed to produce a final tetrameric ion channel. Two domain channels such as TPCs have two ion transport domains, which assemble as a dimer to form a final channel (grey box, right). Four domain channels such as Ca_V or Na_V have all components needed to form a final channel. Some classes of channels have cytosolic Ca^{2+} binding EF-hand domains such as Plant TPCs, animal TPC2 or some animal and green algal Ca_V channels (violet).

In all these types of channels, the shaker-type ion transport domain comprises six transmembrane α-helices. Between the 5th and 6th transmembrane helix the ion-selectivity filter is located in a small loop (MacKinnon, 1995; Wu et al., 2016). The 4th transmembrane segment contains a series of positively charged amino acid residues such as arginines or lysines which confer voltage sensitivity.

TPCs are proposed to originate from a gene duplication event of a voltage gated single domain channel (Rahman et al., 2014). No prokaryotes show homologs of TPCs, and its presence in animals, plants and other eukaryotes suggest that this gene duplication event occurred at an early stage of eukaryotic development (Hedrich et al., 2018).

4.1.2 Function of two pore channels in animals

TPCs in animals (aTPCs) were originally discovered in a cDNA library of rat-kidney cells (Ishibashi et al., 2000). In animals three different subtypes of TPC are known, labelled as TPC1, TPC2 and TPC3 (Zhu et al., 2010).

aTPCs are mostly involved in the release of ions from intracellular organelles, and as such, are likely important for maintenance of ion gradients, Ca^{2+} release, pH control and Ca^{2+} dependent vesicle trafficking (Hedrich et al., 2018; Kintzer and Stroud, 2018). aTPC1 and aTPC3 were found in endo-lysosomes which have an acidic lumen, and aTPC2 was found in lysosomes which have a less acidic lumen in comparison (Calcraft et al., 2009).

The mode of action and ion selectivity are still matter of investigation. aTPC1 seems to be predominantly voltage gated, but luminal pH, the concentration of luminal and cytosolic Ca^{2+} levels, and the endosomal regulators phosphatidylinositol 3,5-bisphosphate ($PI(3,5)P_2$) and nicotinic acid adenine dinucleotide phosphate (NAADP) were also shown to affect channel activity (Cang et al., 2014; Lagostena et al., 2017; Pitt et al., 2014; Rybalchenko et al., 2012; Wang et al., 2012). aTPC2 is not voltage sensitive, but $PI(3,5)P_2$ and potentially NAADP regulate this channel (Calcraft et al., 2009). aTPC3 is not present in humans and its localisation may depend on species. Plasma-membrane localised aTPC3 in fish and frogs are voltage gated Na^+ channels, whereas endolysosome localised aTPC3 in rat and chicken may represent NAADP dependent Ca^{2+} channels (Calcraft et al., 2009; Cang et al., 2014; Kintzer and Stroud, 2018). Among the known negative regulators of aTPCs are rapamycin

"mTor" (Cang et al., 2013) kinases including c-jun-N-terminal kinase and p38 kinase (Jha et al., 2014), Mg^{2+} (Jha et al., 2014) and Ca^{2+} and Na^{+} channel inhibitors (Ca^{2+} = nifedipine, isradipine, verapamil, diltiazem; Na^{+} = lidocaine, bupivacaine) (Cang et al., 2014; Rahman et al., 2014).

In addition to proposed roles as NAADP-activated Ca^{2+} release channels or $PI(3,5)P_2$ activated Na^{+} channels, aTPCs were also shown to conduct K^{+} and H^{+} under certain conditions (Marchant and Patel, 2013; Morgan and Galione, 2014), (Pitt et al., 2010; Pitt et al., 2014). It is proposed that function and ion selectivity of aTPCs may depend on tissue, the presence of currently poorly understood auxiliary subunits (Moran et al., 2015) and the cumulative presence and/or absence of aforementioned positive and negative regulators (Hedrich et al., 2018). Moreover, evidence for heterodimer formation, e.g. an ion transport domain tetramer made of an aTPC1 and aTPC2 gene product, has been presented (Rietdorf et al., 2011). All this may further broaden their functional spectrum, possibly explaining their initially contradictive functional analysis in the past.

Given their broad functional spectrum, aTPC dysfunction is linked to a range of different human diseases associated with thermogenesis (Lear et al., 2014), cytokinesis (Horton et al., 2015), smooth muscle contraction (Tugba Durlu-Kandilci et al., 2010), autophagy (Pereira et al., 2011), nutrient sensing (Cang et al., 2014), exocytosis (Davis et al., 2012) and more, making them a vital target for pathophysiological research.

4.1.3 Function of two pore channels in plants

Shortly after their discovery in animals, homologs of TPCs were also found in plants (pTPC) and were initially described as Ca^{2+} channels localised at the plasma membrane in *A. thaliana*, rice, wheat and tobacco (Furuichi et al., 2001; Kadota et al., 2004; Kurusu et al., 2004; Wang et al., 2005). Later, pTPCs were described as Ca^{2+} release channels located at plant vacuole membranes instead and were presented to be the channels responsible for the characteristic "slow vacuolar current" (Carter et al., 2004; Peiter et al., 2005; Ranf et al., 2007). Most plants have only one pTPC gene, but 2 pTPCs found in the genome of tobacco implies that exceptions exist (Kadota et al., 2004).

Plant TPCs differ from animal TPCs in that they have a different ion selective motif and two EF-hand domains in between their two ion transport domains. The EF-hand domains are thought to modulate the positioning of the voltage-sensing motif upon binding of Ca^{2+} (Guo et al., 2016; Hedrich et al., 2018) and therefore impact channel activity. The hypothesis of pTPCs being the major plant vacuolar Ca^{2+} dependent Ca^{2+} release channel therefore inspired many experiments (Wang et al., 2005; Ward and Schroeder, 1994).

Several experiments suggest that pTPC1 assists the propagation of Ca^{2+} waves. Propagation of Ca^{2+} waves throughout the endoderm of *A. thaliana* seedling root cells in response to NaCl stress was reduced in a TPC1 knock-out strain (Choi et al., 2017; Choi et al., 2014). In contrast to the wild type, an *A. thaliana* TPC1 knock out strain expressing Aequorin showed no wounding-induced Ca^{2+} waves (Kiep et al., 2015). Notably, an *A. thaliana* TPC1 knockout strain expressing a brighter GCamP3 Ca^{2+} biosensor showed only attenuated wounding-induced Ca^{2+} wave instead (Vincent et al., 2017), highlighting the need of sensitive Ca^{2+} reporters. This Ca^{2+} wave was stronger in the *fou2* mutant which expresses a gain-of-function TPC1 channel (Vincent et al., 2017). Vincent et al. presented a response pathway including two GLR channels and initiators and TPC1 as propagators of a Ca^{2+} wave. Like aTPCs, high luminal Ca^{2+} is shown to inhibit pTPC1 activity (Beyhl et al., 2009; Lenglet et al., 2017).

pTPCs were also associated with other Ca^{2+} dependent activities including germination, stomatal movement (Peiter et al., 2005) and in ROS-based cell-cell communication (Choi et al., 2017; Evans et al., 2016; Kurusu et al., 2012; Kurusu et al., 2015). However, it is not clear for most experiments whether pTPC is directly involved in Ca^{2+} release or is rather indirectly involved through changing the membrane potential, affecting the activity of other cation channels.

In contrast, a series of definitive experiments determined that TPC was not involved in Ca^{2+} dependent pathogen defence pathways in *A. thaliana*, rise of Ca^{2+}_{cyt} in response to oxidative stress, and Ca^{2+} signalling in response to cold shock, sucrose, elicitors or salicylic acid (Ranf et al., 2007).

Although the idea of pTPCs acting as Ca^{2+} release channels received support, pTPCs are not highly selective channels (Pottosin et al., 2001), implying a much more versatile physiological function. The current idea is that pTPCs are like aTPCs in that they are highly

regulated and adaptive ion channels which can shuttle K^+, Ca^{2+} or Na^+ either exclusively or together in dependence of the combination of currently present positive and negative regulators and cellular ion distribution (Hedrich et al., 2018).

pTPCs have been evaluated in heterologous systems to determine their ion selectivity: Residue substitutions in the ion selectivity filter motif of the *A. thaliana* TPC channel from MGN to the human TPC2 counterpart VNN converted the rather non- selective *A. thaliana* –TPC channel into an animal TPC2-like Na^+ selective channel (Guo et al., 2017). Combined with recent success in protein crystallisation (Patel et al., 2016), these findings will also help to understand the molecular mechanisms of TPC ion gating in metazoa.

4.1.4 Two pore channels in algae and diatoms

An initial search for TPCs in algal genomes revealed that despite the ubiquitous presence of TPCs in embryophytes, no TPCs were present in green algae (Verret et al., 2010). Red algae also have no known TPC equivalent (Verret et al., 2010). However, TPCs were present in many chromalveolates, including oomycetes, ciliates and diatoms (Verret et al., 2010).

The role of TPCs has not been investigated in any of these algal lineages. The underlying channels of Ca^{2+} signalling in algae are largely unknown (See Chapter 1; (Falciatore et al., 2000; Taylor, 2009; Vardi et al., 2006; Verret et al., 2010; Wheeler and Brownlee, 2008). In diatoms, the only functionally characterised Ca^{2+} conducting channel so far is the novel one-domain bacterial-like EukCat channel (Helliwell et al., 2019). Although TPCs are unlikely to be highly specific Ca^{2+} channels, the presence of propagating hypo-osmotic shock induced Ca^{2+} waves in *P. tricornutum* (Chapter 3) and the absence of clear homologues of conventional Ca^{2+}-release channels such as IP_3R or RyR led us to examine whether TPCs could contribute to cytosolic Ca^{2+} elevations in diatoms.

Therefore, the distribution of TPCs in diatoms and the localisation and function of TPC channels in the model diatom *P. tricornutum*, with a particular focus on their putative assisting role in Ca^{2+} signalling, will be presented.

4.2 Methods

4.2.1 Cultivation and strains

P. tricornutum was cultivated in unshaken plastic culture flasks in 30 mL f/2 medium or ASW as described in chapter 3.2.1. Following strains were used throughout the study: *P. tricornutum* WT670 (alternatively: CCAP 1055/1) (PtWt), *P. tricornutum* transformed with the RGECO Ca^{2+} biosensor (PtR1), and two TPC1 knock out mutant lines of PtR1 (*tpc1-1* and *tpc1-2*).

4.2.2 The origin and verification of PtR1 tpc1 knock out strains.

The two putative knock-out mutant strains were generated in PtR1 by Sam Coffin and Katherine Helliwell (MBA Plymouth) to allow investigation of Ca^{2+} signalling. PtR1 was transformed with three plasmids: one pks_diaCas9:sgRNA1 plasmid, one pks_diaCas9:sgRNA2 plasmid, and one pCLS16604_pNAT plasmid conferring resistance to Nourseotricine. The administration of two plasmids with one sgRNA each led to deletion of a gene fragment in the tpc1 gene, simplifying screening of mutants shown in unrelated studies (Helliwell et al., 2019).

As a result, *tpc1-1* had a biallelic 680 bp deletion and *tpc1-2* a biallelic 662 bp deletion which removed parts of the second EF-hand motif and the second ion transport domain. The sgRNA target sequences used to generate these mutants were GATTGATCAAGAAACCGTCA and GTTGATTGGTATCATCTCAG. The deletions in both mutant strains led to a frameshift in the open reading frame, increasing the likelihood of disrupted function of the gene products.

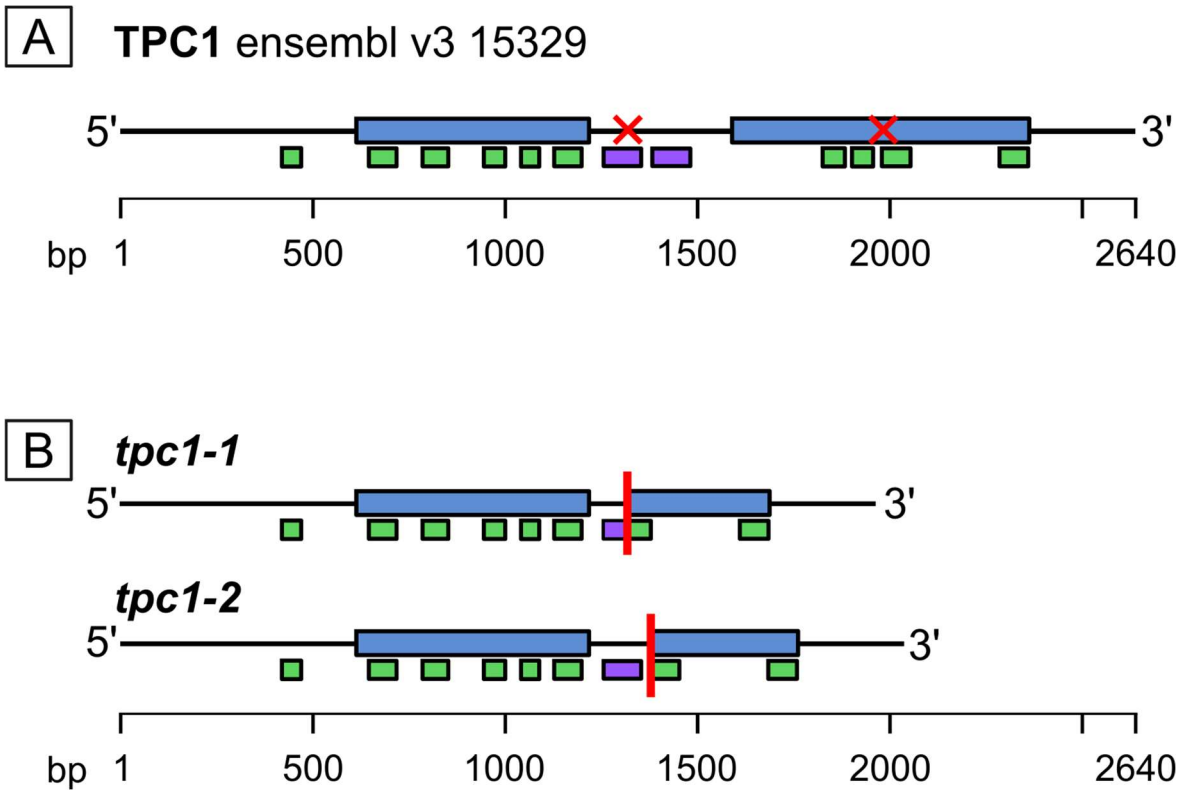

Figure 4.2: Features of the *P. tricornutum* TPC1 gene.

Schematics of the intron-less *P. tricornutum* TPC1 gene showing ion transport domains (blue), successfully identified transmembrane helices (green) and EF hand domains (violet). Annotations were done with Interpro. **A)** Gene model of wildtype TPC1 showing binding sites of sgRNAs (red crosses) used to introduce a deletion in the target gene (K. Helliwell, MBA Plymouth). **B)** Modified gene models of the two generated PtR1 *tpc1* knockout strains screened and sequenced by S. Coffin (MBA Plymouth) showing a 680 bp deletion in *tpc1-1* and a 662 bp deletion in *tpc1-2*. Both mutant lines show removal of an EF hand domain and half of the second ion transport domain (red bars) which also introduced a frameshift.

To guarantee that *tpc1* strains were clonal, the nature of the mutation in *TPC1* was verified in this study by amplifying the locus at which Cas9 was directed for deletion using the primers KEH 208 F (TGCTCGTCAAAATGCTTCCC) and KEH 209 R (CTGAAAACGACTACTGGGCG), resulting in a 1253 bp fragment in the WT and an estimated 590 bp fragment for the two mutants given a successful deletion of a 663 bp fragment. For this, the Phire™ plant direct PCR Kit from Thermo Scientific™ (thermofisher.com) was used for lysis of cells. Cell lysate was used in a Phire™ PCR kit using the manufacturer's protocol for leafs with exclusion of the grinding step of the tissue. The PCR product was not sequenced, as this was done previously by S. Coffin.

4.2.3 Bioinformatics analysis of diatom TPC1 and TPCL channels

P. tricornutum TPC1 and TPCL sequences identified previously (Verret et al., 2010) were obtained from the Phatr2 genome publicly available at https://mycocosm.jgi.doe.gov/Phatr2/Phatr2.home.html (Bowler et al., 2008). Throughout the study, a revised Ensembl v3 genome was published and TPC gene models were checked again (https://protists.ensembl.org/Phaeodactylum_tricornutum/Info/Index, respectively, (Yang et al., 2018)). Both assemblies suggest absence of introns in both TPCs. The revised ensemble v3 gene model for TPCL 1654 which showed a longer N-terminus compared to the Phatr2 JGI TPCL 1654 gene model was rejected because of a stop codon in that N-terminal attachment and a rarely used TGG as start codon. For TPC1, the revised Phatr3_J15329 sequence was selected for this study. Sequence similarity searches using the TPC and TPCL sequences as query were performed using BlastP algorithm on the genomic NCBI-"reference proteins" database (ncbi.nlm.nih.gov) and genomic JGI database (https://genome.jgi.doe.gov/portal/) and the Marine Microbial Eukaryote transcriptomic database MMETSP (Keeling et al., 2014). Obtained sequences were annotated using the browser based Interpro annotation algorithm to get information on number of ion transport domains (PF00520), presence of EF hands (PF00036, PF13405, PF13499, PF13202) or respective completeness of the gene models.

Protein sequence alignments of TPCs were performed in Geneious v.10 (geneious.com, (Kearse et al., 2012) using ClustalW algorithm and BLOSUM cost matrix. Phylogenetic trees were generated with MEGA7 (Kumar et al., 2016) using maximum likelihood as statistical method with 100 bootstrap replications, Poisson as substitution model and Nearest-Neighbour-Interchange as heuristic method. Residues appearing in less than 85% of aligned sequences in the alignment were omitted.

4.2.4 Growth curve

Culture flasks containing 30 mL ASW medium with 100, 50 and 25 % salinity respectively were inoculated with *P. tricornutum* strains in exponential growth phase at matching cell densities leading to an initial cell concentration of ~50000 cells/mL at day 0. All strains were acclimated to respective salinity for several days before inoculation. Three biological replicates were used per salinity condition and strain. Cells were then grown under standard light and temperature conditions (chapter 3.2.1). Cell growth was monitored using a LUNA-FLTM dual fluorescence cell counter (Logoes biosystems, www.logosbio.com) with following settings: brightfield modus, noise reduction 5, roundness 30 %, size range 3-20 µm. The relatively large size range was chosen since the apparatus predominantly seems to identify the less opaque regions of the cell centre and mostly neglects the more translucent apices of the cell. The specific growth rate and generation time was calculated using following formulae:

$$k = \frac{\ln(c2) - \ln(c1)}{t2 - t} \qquad \mu = \frac{k}{\ln(2)}$$

k = specific growth rate

c1/2 = cell concentration in million cells per mL at start/end of exponential growth phase

t1/2 = timepoint of start/end of exponential growth phase in days

μ = generation time (duplications per day)

4.2.5 Statistical analysis

Unless indicated otherwise, imaging experiments were repeated three times with different cultures on different days, respectively. Individual cells within a single imaging experiment were treated as a biological replicate, meaning that an experiment with 16 cells may contain up to 16 biological replicates for analysis. Data of replicate experiments with identical experimental procedure was pooled into one dataset, whose variation is shown as SEM-error bars in graphs, and compared with datasets of other treatments. For number of responding cells, each replicate experiment contributes a single %-value, which means that statistical analysis was not done when number of replicate experiments was below 3.

Normal distribution of respective datasets was tested using Shapiro-Wilk's normality test. When passed, statistical analysis of datasets with two groups were done with Student's t-test, and when not passed with Mann-Whitney's rank sum test. Statistical analysis of datasets with more than two groups were done with Brown-Forsythe's Equal Variance Test followed by Tukey's test for pairwise comparison when the normality test was positive. When the normality test was negative, Kruskal-Wallis' One Way Analysis of Variance on Ranks was used instead. All statistical tests were performed with Sigmaplot v14.0.3.192 (Systat software Inc.)

4.2.6 Assessing survival and cell motility on plates

Agar plates containing 30 mL solid ASW medium (ASW + F/2 nutrients +0.8% agar + 20 mM HEPES pH 8.0) were prepared with varying salt concentrations (0 %, 10 %, 25 %, 50 %, 100 %, 125 %). PtWt, PtR1, *tpc1-1* and *tpc1-2* cultures grown in ASW 100 % in early exponential growth phase were serially diluted in ASW 100 % (no nutrients) meaning cells were not acclimatised to respective NaCl contents in the solid medium plates when applied. This also meant that some NaCl was carried over to ASW 0% NaCl plates, leading to a low concentration of 3% NaCl in ASW. Plates were inoculated with spots of 50 µL of diluted cultures containing 100000, 50000, 5000, 500, and 50 cells, respectively. The plates incubated at 18 °C, 16:8 L:D cycle and at ~40µmol·m^{-2}·s^{-1} for14 days. Afterwards, pictures of the plates were taken, and initial spot area and migration area of the cells were measured using Image J. The fold area increase of the 50000 cell-spots was determined by dividing the migration spot area by the initial spot area.

4.2.7 Ca^{2+} signalling experiments with *tpc1* mutants

The *tpc1* strains were based on the PtR1 strain which allows monitoring of cytosolic Ca^{2+} elevations with epifluorescent microscopy. For hypo-osmotic shock experiments the procedures for data acquisition and data processing were as described in Chapter 3.2.2.

Depolarisation shock medium was standard ASW but with 100 mM instead of 8 mM KCl. NaCl was adjusted to 110% standard concentration to ensure no hypo-osmotic signalling

component overrides the depolarisation response. PtR1 and *tpc1* cells incubated approximately 10 min on the dish prior the perfusion experiment. A dish was perfused for 45 s with ASW, then perfusion was switched to depolarisation medium for 1:45 min.

4.2.8 Localisation of TPC1 and TPCL in *P. tricornutum*

P. tricornutum TPC1 (Phatr3_J15329) and TPCL (phatr2_1654) genes were amplified with exclusion of the stop codon using the proof-reading Phusion polymerase (Thermo Scientific) and following primers:

PtTPC1_For ATGGACACAGCTCACGCTTC PtTPC1_Rev ATCGTCCGTCGGCGTCA

PtTPCL_For ATGAGCTCGCCACGCC PtTPCL_Rev ATTTGCGACGGGAGCAGC

5’ phosphate was added to gel-purified amplicon DNA using polynucleotide kinase according to the manufacturer’s instructions (New England Biolabs, www.neb.international.com). The PhaTI_Venus vector was cut using the *StuI* blunt cutting restriction enzyme and 5’ ends were dephosphorylated using Calf Intestinal Alkaline Phosphatase (New England Biolabls) according to manufacturer’s instructions. The phosphorylated amplicons and dephosphorylated backbone vectors were ligated in a ratio of 1:1 and 1:3 (TPCL) and 1:3 and 1:6 (TPC1) and transformed into chemically competent *E. coli* (strain TOP10, Invitrogen / Thermo Scientific) according to manufacturer’s instructions. Colonies emerged after 16 h at 37 °C. Colonies putatively containing TPCL and TPC1 localisation constructs were picked and presence of plasmid was screened using cells as DNA template in a PCR reaction aimed to amplify 5’ region of the amplicon insertion and the 3’end of the amplicon (colony PCR; Primers: KP326_For TCACGGTCTTCTTCGAGTCC and respective Rev-Primer of the TPC insert) or were screened for fluorescence.

In the final PhaTI_TPC1_Venus and PhaTI_TPCL_Venus plasmids, the respective TPC sequence is inserted in frame with Venus to generate a C-terminal Venus fusion protein. The PhaTI_TPC1_Venus and PhaTI_TPCL_Venus plasmids were introduced into *P. tricornutum* via biolistics using the transformation protocol presented in Chapter 2 XY. 1.25 µg DNA was used per shot for TPCL and TPC1, respectively. Cells were grown on 50% seawater supplemented with f/2 trace element selection plates containing 75 µg/mL Zeocin.

Fluorescent colonies were imaged using confocal microscopy (inverted Zeiss LSM510) with LASER SHARP software and a Plan Neofluar 40x oil objective. Cells were excited with a 488 nm argon/krypton laser and emission was detected between 500-530 nm for Venus and 650-710 nm for chlorophyll.

4.2.9 Staining of *P. tricornutum* vacuole membranes with MDY-64

To stain the vacuole membrane of *P. tricornutum*, the yeast vacuole membrane Marker MDY-64 was used (Thermo Fisher). 0.1 µL of 10 mM MDY-64 in 100 % DMSO was added to 2 mL of *P. tricornutum* ASW liquid culture and after a gentle mix cells were checked for green fluorescence on a Leica DMI8 as described in Chapter 2.

4.2.10 Generation of *P. tricornutum* TPCL knockouts

To knock out the TPCL channel, a CRISPR-Cas9 mediated deletion in its genomic coding sequence using two separate single guide RNAs (sgRNAs) was attempted as described in Hopes et al. (2016). This approach simplifies screening for mutants via colony PCR as a deletion- based band shift represents a biallelic knock out.

A list of potential sgRNAs with NGG PAMs to knock out TPCL were generated using PHYTOCRISPEX web tool (BMC Bioinformatics http://www.phytocrispex.biologie.ens.fr/CRISP-Ex/ (Rastogi et al., 2016)). Since no introns are predicted for TPCL, all sgRNAs could potentially be used. The list of sgRNA candidates was checked for off-target sites with RGEN (http://www.rgenome.net/cas-offinder), and remaining candidates were checked for on-target activity with GPP sgRNA Designer (http://portals.broadinstitute.org/gpp/public/analysis-tools/sgrna-design).

Three sgRNAs were selected to knock out TPCL in this study. The previously established knock out protocol in this lab utilised the CRISPR-Cas9 vector developed by (Nymark et al., 2016) containing one sgRNA insertion site and one gene for Cas9 protein which requires the introduction of three separate plasmids (sgRNA1, sgRNA2, resistance) to generate a deletion based knockout (Helliwell et al., 2019). In this study a modified sgRNA:Cas9 vector was designed similar to the *T. pseudonana* Cas9:sgRNA1:sgRNA2 knockout vector presented in (Hopes et al., 2017), aiming to reduce the number of plasmids and to increase transformation efficiency in *P. tricornutum*.

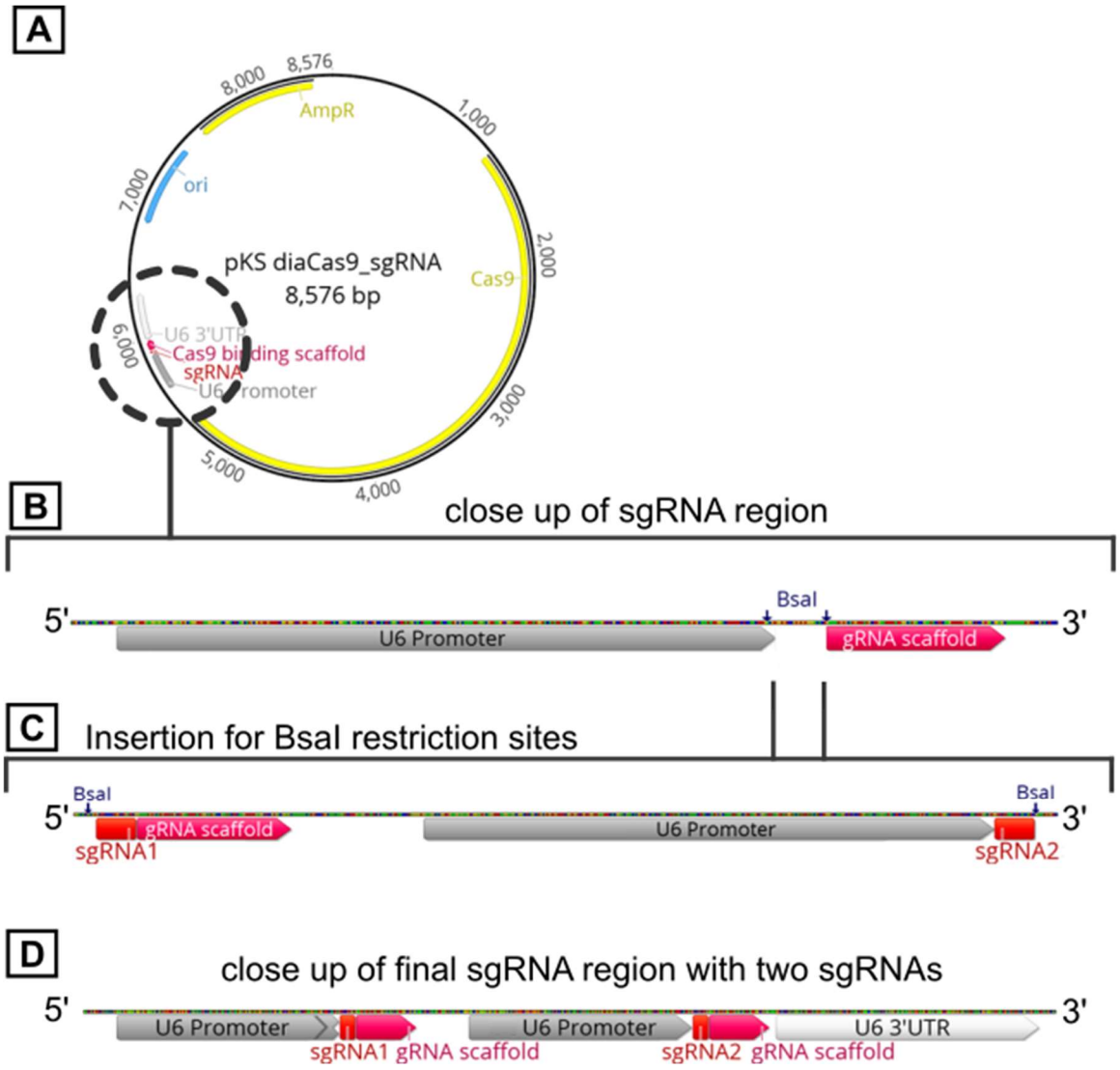

Figure 4.3: Schematics showing the approach to enhance the CRISPR-Cas9 cosntruct for *P. tricornutum.*

A) plasmid map of pKS diaCas9_sgRNA with close up **(B)** of the insertion site of sgRNA oligos using BsaI overhangs. **C)** A short (483 bp) DNA fragment was synthesised (Genscript) to allow tandem expression of two sgRNAs. This could be used as template in a PCR using primers with customised overhangs to introduce specific sgRNAs and BsaI restriction sites. These could then be inserted into the pKS diaCas9_sgRNA plasmid using BsaI, resulting in tandem U6Promoter:sgRNA:gRNAscaffold:terminator cassettes in the final plasmid – similar to the *T. pseudonana* transformation vector presented in Hopes 2016 **(D)**. Figures were generated using Geneious program.

The final pKS_diaCas9:sgRNA1:sgRNA2 plasmid was then co-transformed with the pHaT1:Blast plasmid conferring Blasticidin resistance (Buck et al., 2018) into PtR1 cells as described for *T. pseudonana* cells in Chapter 2. In contrast to the *T. pseudonana* transformation, *P. tricornutum* cells were spread directly on the shooting plate and were not collected on a filter paper. Selection plates contained 50% seawater f/2 + 4 µg/mL Blasticidin. Primers to screen for successful CRISPR-Cas9 mediated deletion in the TPCL gene were TPCL_792_F CTACGATGGAACCGGAGTCG, TPCL_1013_R TTGGTAAAGCGGAGTCGTCC and TPCL_2888_R GCAAGCTCGTGCCAATCATT.

4.2.11 Electrophysiological investigation of TPC1 and TPCL

Genscript was consulted to *de novo* synthesise human-codon optimised coding sequences of *P. tricornutum* TPC1 and TPCL sequences. These were then cloned by genscript into the pcDNA3.1-EGFP vector using HindIII and BamHI restriction sites as described in Helliwell et al. (2019). The procedure of HEK cell transfection is also described in Helliwell et al. (2019). The conditions at which electrophysiological experiments were conducted were as described in Guo et al. (2017).

4.3 Results

4.3.1 Bioinformatic analysis of diatom TPC1 and TPCL

4.3.1.1 Features of TPC- and TPCL in *P. tricornutum*

Previous analysis of the ion channel inventory of diatoms revealed that *P. tricornutum* has two distinct TPCs (Verret et al., 2010; Wheeler and Brownlee, 2008), which are referred to as TPC1 and TPCL in this study. Table 4.1 shows general features of the two gene models.

Table 4.1: Overview of features for the P. tricornutum TPC1 and TPCL channels.

Protein name	Gene model ID	Gene locus	gene length	EF-hands	Signalpeptide
PtTPC1	Phatr3_J15329	chr_19	2640 bp	✓	
PtTPCL	Phatr2_1654	unmapped	3726 bp		✓

The PtTPCL sequence originates from an assembled scaffold that was neither able to be mapped to finished chromosomes nor assigned to organelles (Bowler et al., 2008). In contrast to the TPC1 channel, no signatures of Ca^{2+} binding EF-hand motifs were detected by Interpro in TPCL.

4.3.1.2 Features and distribution of TPC- and TPCL in other sequenced diatoms

Complete genomes are available for five diatoms. These were screened for the presence of voltage-gated ion channels, i.e. TPC1, TPCL, Ca_V and EukCat channels.

Table 4.2: List of putative voltage-gated Ca^{2+} channels within the five completely sequences model diatoms.

Note: data for EukCat and Ca_V was taken from Helliwell et al. (2019).

Type	Species	4d-Ca_V	2d-TPC1	2d-TPCL	1d-EukCat
multipolar centric	*Thalassiosira pseudonana* CCMP1335	1	1	-	3
multipolar centric	*Thalassiosira oceanica* CCMP1005	1	1	-	1
raphid pennate	*Pseudo-Nitzschia multiseries* CLN-47	-	1	1	2
raphid pennate	*Fragilariopsis cylindrus* CCMP 1102	-	1	2	2
raphid pennate	*Phaeodactylum tricornutum* CCAP 1055/1	-	1	1	3

Within the given sequences, four-domain Ca_V channels are restricted to multipolar centric diatoms. One copy of the TPC1 gene is present in each diatom, whereas TPCL is not present in the *Thalassiosira* group. Most listed diatoms have several genes for EukCat channels. *F. cylindrus* has multiple allelic variants of the TPCL gene which can be found on scaffold 5 (ID 185443) and 50 (ID 253779), respectively. The table suggests a pattern of the presence of TPCL when the diatom is a pennate and/or when 4d Ca_V channels are absent. To test whether this distribution continues more widely, the MMETSP transcriptome database (Keeling et al., 2014) was consulted for the presence of TPCL homologs in further diatom species and in other eukaryotes.

4.3.1.3 Features and distribution of TPC- and TPCL in other organisms

TPCL was found in many diatoms, including centric species such as *Corethron pennatum, Ditylum brightwelli*, *Proboscia alata*, *Leptocylindrus danicus* and more, showing that TPCL presence is not restricted to pennate diatoms. Moreover, Ca_V channels are also present in the four aforementioned diatoms, showing that TPCL and Ca_V may coexist at least in centric diatoms. Most diatoms appear to have a single TPCL sequence, but two distinct TPCL sequences found in *Pseudo-nitzschia arenyensis* suggest that exceptions may exist.

Annotating the diatom TPCL sequences for functional domains revealed that most TPCL sequences lack EF-hands, but the *Chaetoceros* GSL56 and *Proboscia alata* TPCL sequences contained a single calcium binding EF-hand domain between the ion transport domains. The diatom TPC1 sequences were slightly shorter than TPCL sequences (TPC1 635 ± 52

residues (n = 4) vs. TPCL 896 ± n = 102 residues (n = 19)), however, TPCL sequences are based on transcriptomic data and for both TPCL and TPC1 many gene models of different lengths may exist, so this data should be regarded with caution.

Homologs of *P.t.* TPC1 were found in other stramenopiles (oomycetes, pelagophytes and brown algae), other algae including haptophytes, rhodophytes and dinoflagellates, and plants. Most of these sequences had two EF-hand domains similar to plant TPC1.

Homologs of *P.t.* TPCL were found diatoms, the stramenopile *Nannochloropsis gaditana*, and opisthokonts including metazoans and choanoflagellates. As TPCL was not found in other eukaryote genomes, the search was broadened on the transcriptome based MMETSP database which mostly returned diatom sequences. The few non-diatom stramenopiles included *Rhizochromulina marina, Phaeomonas parva* and *Heterosigma akashiwo.* The relationship of diatom TPCL and TPC1 was further investigated through phylogenetic inference.

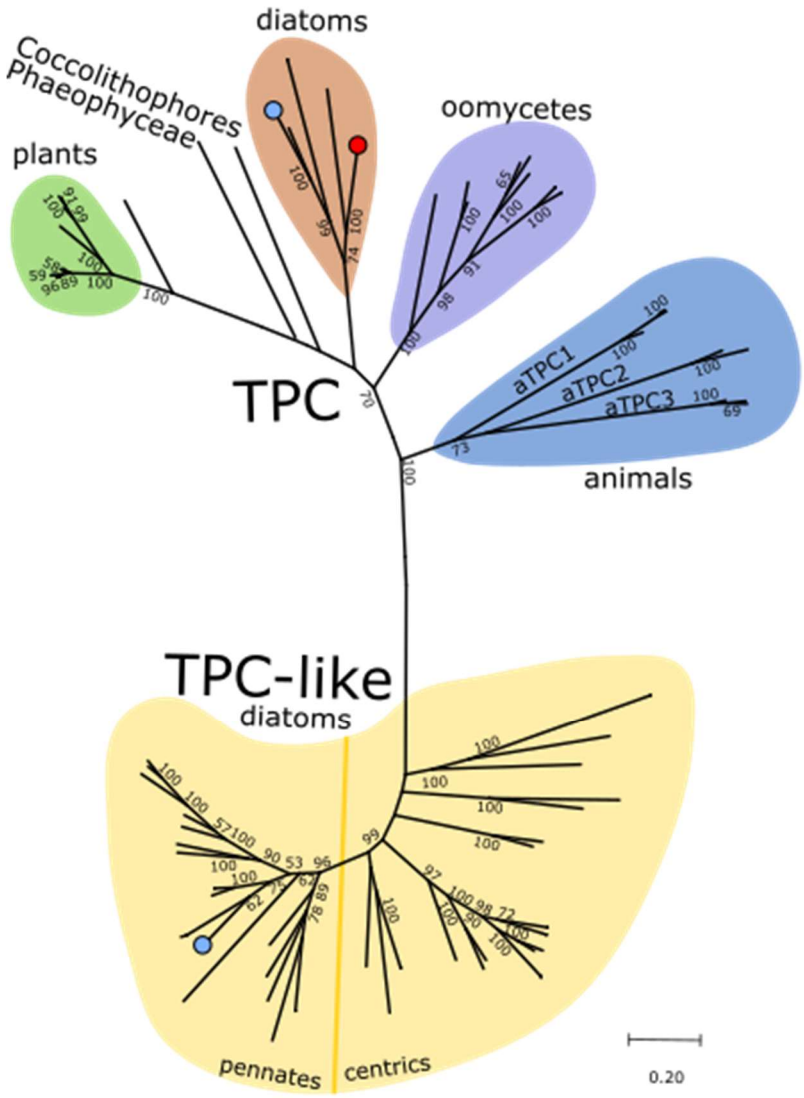

Figure 4.4: Diatoms have two distinct TPC, one of which with no clear homologs within other organisms.

Phylogenetic tree made from a sequence alignment containing the two classes of diatom TPCs in relation to TPCs of other major groups of organisms. Blue dots represent *P. tricornutum*, the red dot *T. pseudonana*. The tree was made in MEGA7 using maximum likelihood method with 100 bootstraps, Poisson correction model and 85% deletion threshold. Only bootstrap values >50 are shown.

The phylogenetic tree shows that TPC and TPCL form two distinct clades (Fig. 4.4). *P.t.* TPC1 is loosely associated with land plant and oomycete TPCs, whereas TPCL has no clear homologs within the tested groups. The relatively long branch on which TPCL is located suggests the channel was subject to more amino acid substitutions per site compared to the other groups. The three distinct TPC subclasses in animals (aTPC1, aTPC2, aTPC3) are also resolved in the tree. The few putative TPCL sequences found in non-diatom stramenopiles were truncated and performed poorly in the alignment, suggesting that these are different channels, and were not included in the final tree. The two TPCL sequences with a single EF-hand are found in different lineages within the centric diatoms, suggesting that it is not an isolated phenomenon.

4.3.1.4 The second ion selective motif in TPC and TPCL

The architecture of the TPC pore suggests that merely the 2nd ion selective motif of TPCs confers ion selectivity (Guo et al., 2017; Schulze et al., 2011). Within the sequence alignment underlying Fig. 4.4 the amino acid residues located within the ion selective motif of the second ion transport domain were compared to allow extrapolation whether these channels differ in their ion selectivity.

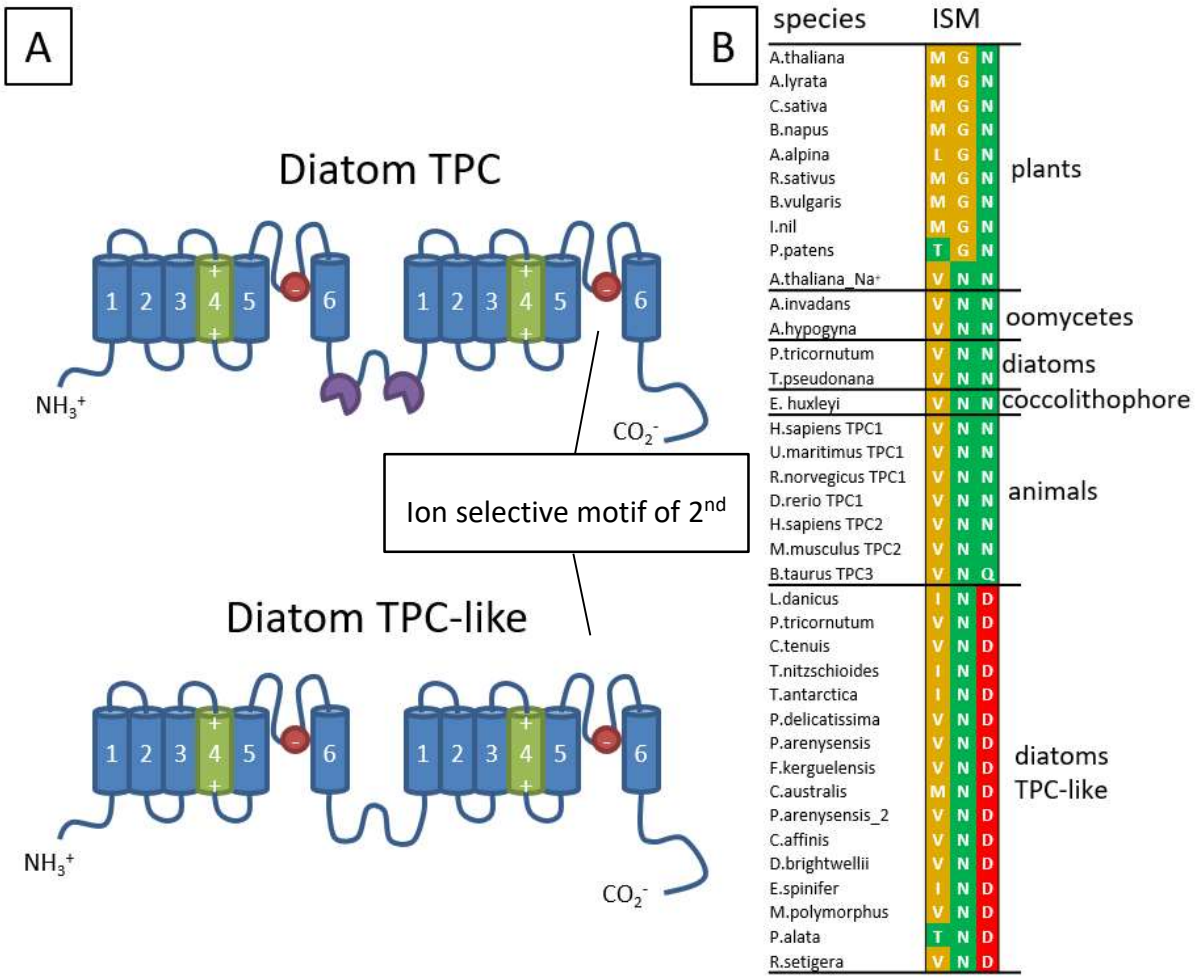

Figure 4.5: TPCL has a novel ion selective motif exhibiting negatively charged amino acid residues. **A)** Schematics of the secondary structure of TPC1 and TPCL in diatoms. Each ion transport domain is composed of 6 transmembrane segments. The 4th segments contains the voltage sensing motif composed of positively charged amino acid residues (green) and a pore loop containing the ion selective motif between the 5th and 6th transmembrane segment (red). **B)** Excerpt of the alignment used for phylogenetic analysis showing amino acid residues of the ion selective motif. The Na^+ selective mutant of *A. thaliana*-TPC1 is included. Green = polar- uncharged, Yellow = non-polar, red = negatively charged amino acid residues.

The diatom TPC ion selective motifs are identical with the ones found in oomycetes and metazoans (VNN; associated with Na^+ selectivity), while plants show characteristic amino acid substitutions (MGN; associated with non-selectivity) (Guo et al., 2016; Guo et al., 2017). In contrast, diatom TPCL exhibits a novel ion selectivity motif in which the last asparagine residue in VNN is replaced by a negatively charged aspartic acid residue (VND). In some cases, the valine residue was replaced by an isoleucine residue (*T. nitzschoides, T. antarctica, L. danicus;* IND), a threonine residue (*P. alata;* TND) or a methionine residue (*C. australis;* MND) – however, the latter two amino acids were highly conserved (-ND). This suggests that TPCL channels have a different ion selectivity compared to other TPCs.

4.3.1.5 Addressing the origin of TPCL

The current understanding of the evolution of shaker-type channels is that duplication events led to doubling the number of ion transport domains within a gene, leading to channels with one domain ($BacNa_V$, CatSper, EukCat, K^+), two domains (TPCs) or four domains (Na_V, Ca_V) in a single gene. To test whether TPCL evolved from independent duplication of a single domain channel or through specialisation of an ancestral TPC, a wider phylogenetic analysis was performed.

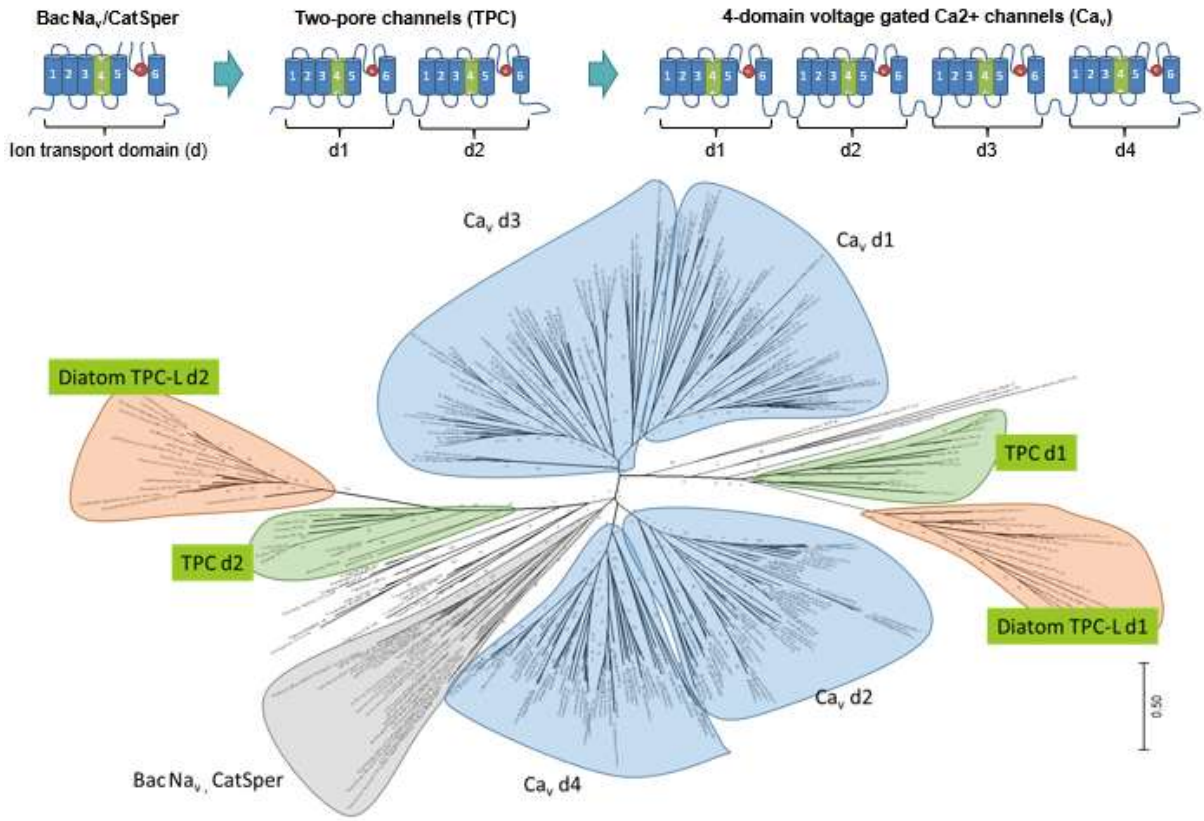

Figure 4.6: TPCL is likely a specialisation of an ancestral TPC.

Schematic images of the secondary structure of ion channels containing one, two or four ion transport domains per gene. The transmembrane domains are numbered 1-6, the ion transport motif is shown as a red dot, the voltage sensing motif is in the 4th transmembrane helix (green). **B)** Phylogenetic tree made from an alignment of ion transport domains of single-domain channels (bacterial BacNa$_V$, animal CatSper and haptophyte and diatom EukCat channels), two-domain channels (plant, animal, oomycete and diatom TPCs and diatom TPCL) and four domain channels (plant, animal, chlorophyte, rhodophyte, choanoflagellate and diatom Ca$_V$ and fungal 4-domain Ca^{2+} channels).

In the presented phylogenetic tree of voltage-gated ion channels (Fig. 4.6), the two ion transport domains (d1 and d2) of TPC form two distinct phylogenetic clades, with domains d1 and d2 of TPCL located within each respective TPC clade. Although the bootstrap values for the nodes at with the TPCL domains separate from the TPC1 branch are low (d1 = 8, d2 = 19), this result supports an origin for TPCL from TPC, rather than an independent duplication of a single domain channel.

As a sidenote, the tree managed to reproduce the currently accepted scenario in which 4d voltage gated channels resulted from the duplication of a 2d channel, since the 4d domains domains 1 and 3 and domains 2 and 4 are more similar, respectively.

4.3.2 Localisation of TPC1 and TPCL in *P. tricornutum*

The cellular localisation of a channel is required to understand its cellular function. PtWt cells were transformed with plasmids designed to constitutively express TPC1 and TPC-L genes tagged with the fluorescent protein Venus at respective C-termini. Transformation of PtWt with pPhaT1_TPC1:Venus and pPhaT1_TPCL:Venus yielded following results:

Table 4.3: Number of Zeocin resistant P. tricornutum colonies generated after transformation of presented plasmid constructs for TPC localisation

Construct name	colonies	screened	fluorescent
pPhaT1_TPCL:Venus 7	5	5	3
pPhaT1_TPCL:Venus 8	1	1	0
pPhaT1_TPCL:Venus 10	12	11	1
pPhaT1_TPC1:Venus 1	0	0	0
pPhaT1_TPC1:Venus 3	0	0	0

Four out of 18 antibiotic-resistant colonies exhibited fluorescence (= 22.2 %; Table 4.3). Three attempts to introduce TPC1:Venus constructs into *P. tricornutum* were performed, with the former two showing a high number of false positive colonies. In the third attempt a new charge of selection marker Zeocin was used which resulted in no colonies for shot and non-shot PtWt cells (Table 4.3).

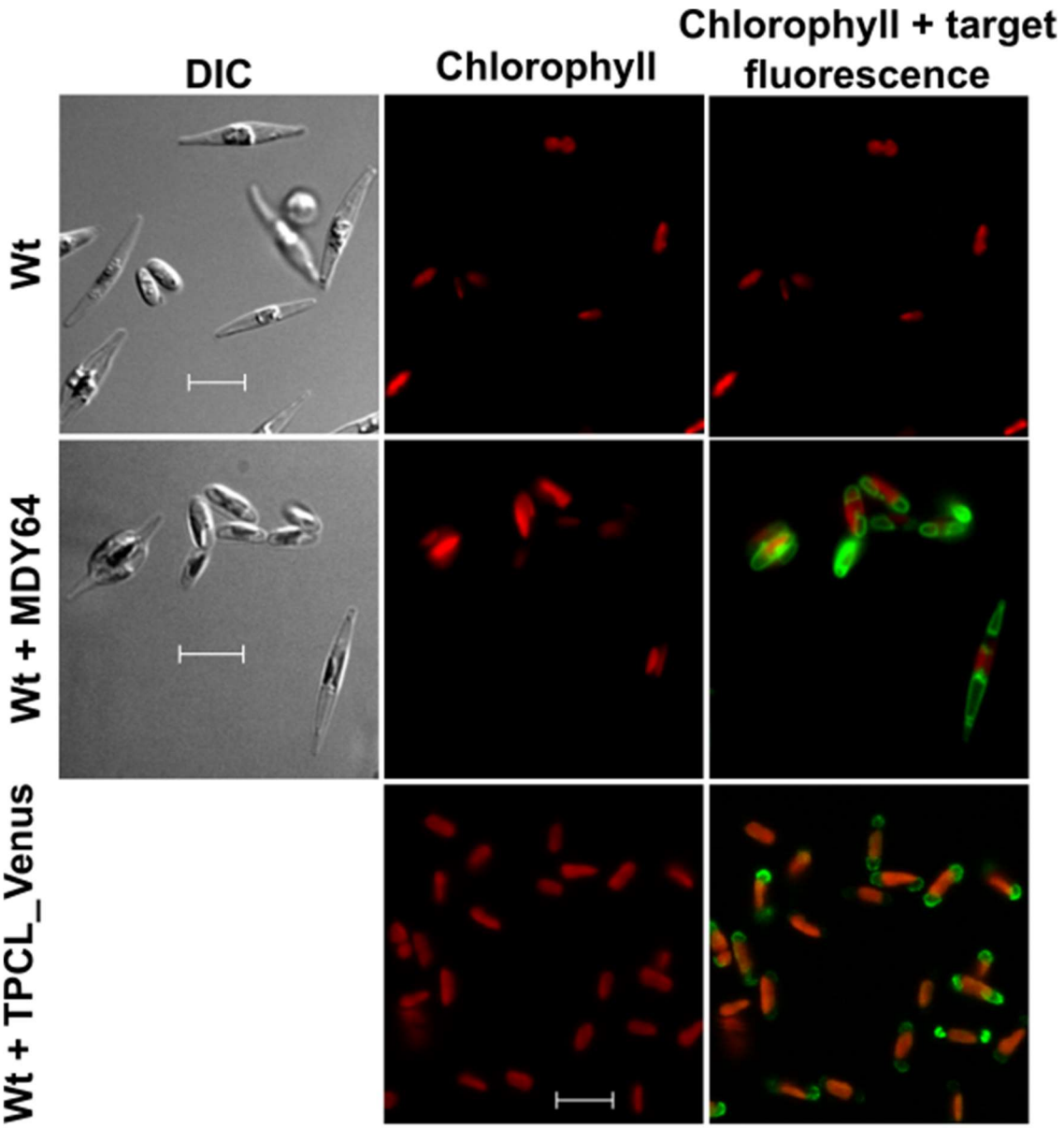

Figure 4.7: TPCL likely localises to the vacuole membrane.

Epifluorescent and confocal microscopy images of *P. tricornutum* cells. Images include oval and fusiform *P. tricornutum* wild type cells (Wt), Wt cells treated with MDY-64 vacuole membrane stain, or Wt cells transformed with pPhaT1_TPCL:Venus plasmid. DIC, chlorophyll autofluorescence (red) and target fluorescence (green) are shown. Scale bars represent 10 µm. Images of Wt and MDY-64 treated cells are widefield epifluorescent images (Leica DMi8), whereas images of TPCL-Venus transformants are confocal images (Zeiss LSM510).

P. tricornutum wild type cells show no green fluorescence (emission 520 nm) when illuminated with light of a wavelength corresponding with GFP fluorescence excitation (470 nm, Fig. 6.7). When treated with the MBY-64 vacuolar membrane stain, two distinct fluorescent regions can be seen per cell, corresponding to the vacuolar membranes. When transformed with TPCL-Venus fusions, oval cells showed similar fluorescence patterns compared to oval cells treated with the membrane stain, indicating that TPCL localises to the vacuole membrane. Curiously, mostly oval cells were present in the three positively transformed strains and continued to dominate respective populations for at least 8 months of liquid culturing.

4.3.3 Characterisation of TPC1 in *P. tricornutum*

4.3.3.1 Verification of the *tpc1* mutants

In a previous study, Katherine Helliwell (MBA Plymouth, UK) created two CRISPR-Cas9 mediated *TPC1* knock-out strains called A3 and E3. The gene editing strategy using two guide RNAs resulted in large deletions (c. 600 bases) in the *TPC1* gene, making it unlikely that a functional protein would be produced. First, the authenticity of PtR1 *tpc1* knock out strains named *tpc1-1* and *tpc1-2* was verified using PCR.

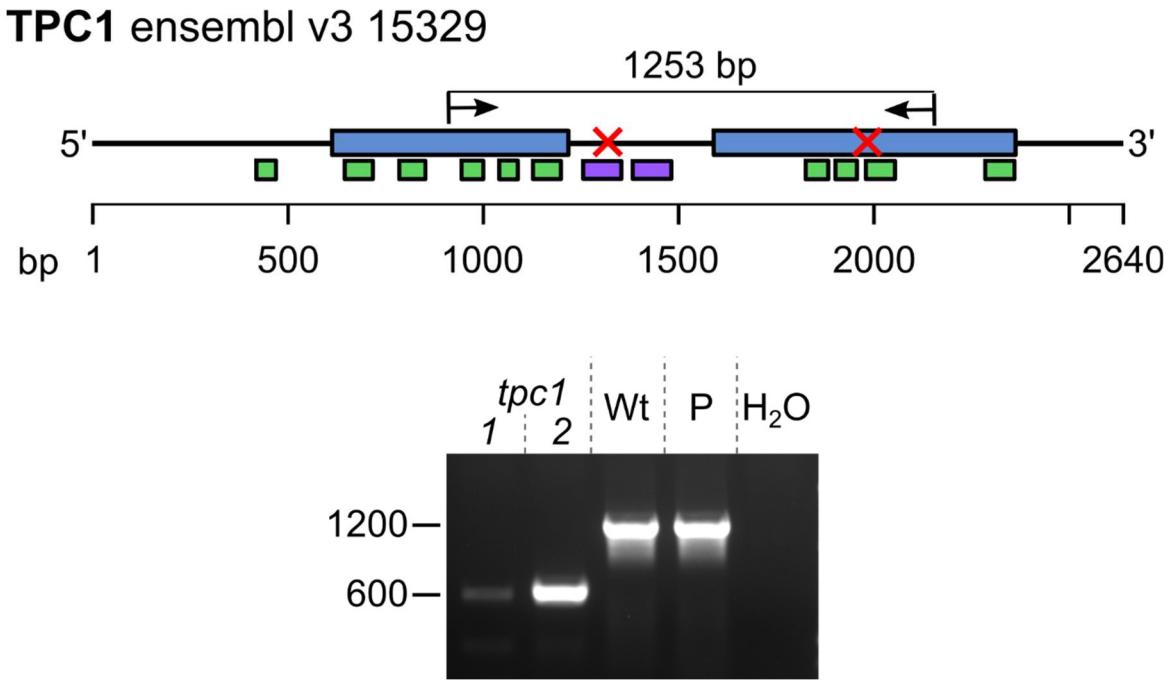

Figure 4.8: Verification of the TPC1 mutant.

Schematics of the *P. tricornutum* TPC1 secondary structure, based on work done by K. Helliwell and S. Coffin (MBA Plymouth). Blue bars represent ion transport domains, violet boxes represent EF-hand domains and green boxes represent transmembrane domains (Interpro), whereas red crosses indicate cutting sites for the CRISPR-Cas9 enzyme. Arrows indicate binding sites for screening primers, with an expected 1253 bp amplicon in wild type TPC1. Below an image of an agarose gel is shown containing PCR results to verify the mutants for this study. Genomic template DNA from *tpc1-1* and *tpc1-2* cells led to a single smaller amplicon compared to template DNA of PtR1 (Wt) and DNA of TPC1:Venus localisation plasmid (P), indicating a biallelic *tpc1* mutation.

Having verified their identity, the *tpc1* knock-out strains were used in a series of experiments to examine their physiology and potential role for TPC1 in Ca^{2+} signalling processes.

4.3.3.2 Growth performance of *tpc1*

To examine the putative role in signalling or ionic homeostasis in response to changing salinity, the growth rate of *tpc1* and wild type cells was determined in a range of NaCl, nitrate and phosphate concentrations.

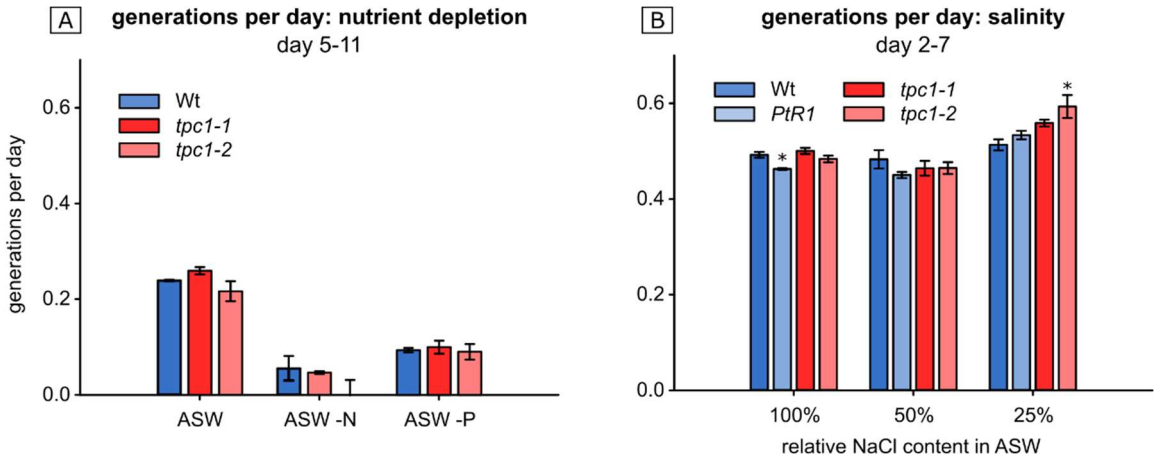

Figure 4.9: Growth rate of *tpc1* in relation to nutrient availability and NaCl content.

A) Generations per day of Wt and *tpc1* strains in phosphate and nitrate deplete conditions. Two biological replicates per condition. **B)** Generations per day of *tpc1* strains in hypo-saline conditions. Cultures presented were inoculated by cells which were acclimated to respective saline conditions. Error bars represent SEM with three biological replicates per condition. Asterisks represent significant differences in relation to the Wt. The salinity-growth experiment was repeated two additional times with three replicates per condition, which did not reproduce obtained significant relationship shown in B). Different growth rates and examination time-points prevented pooling of data.

No significant difference in growth rate between the mutants and the wild type were observed in nitrate and phosphate replete conditions and all strains showed very limited to no growth in these conditions (Fig. 4.9 A).

Wild type, PtR1 and *tpc1* cells were able to grow in all tested salinity conditions (Fig. 4.9B). PtR1 had a significantly lower growth rate at 100% ASW NaCl content compared to Wt and *tpc1-1* cells (Equal variance Brown Forsythe's test $P = 0.005$, Tukey test $P < 0.05$), and *tpc1-2* had a significantly higher growth rate at 25% ASW NaCl content compared to Wt (Equal variance Brown Forsythe's test $P = 0.022$, Tukey test $P < 0.05$). These results were not

reproduced in two additional growth curves (not shown), suggesting that growth of *tpc1-2* is not significantly different from wild type cells under low salinity conditions.

4.3.3.3 Growth and motility of TPC1 depleted cells on solid medium

When grown on solid medium, *P. tricornutum* predominantly transitions into the oval morphotype, which is known for its capability to glide on surfaces (de Martino et al., 2011; Helliwell et al., 2019). External Ca^{2+} is evidently necessary for gliding in some diatoms (cite (Collingridge et al., 2013; Cooksey and Cooksey, 1980; McLachlan et al., 2012). To determine whether knockout of TPC1 may influence the ability of *P. tricornutum* to grow on solid medium, the ability to transition into the oval morphotype, the ability to sense environmental osmotic/saline conditions in the oval morphotype, or the ability to glide on surfaces, PtWt, *tpc1-1* and *tpc1-2* cells were grown on ASW+Agar 1.5% plates with varying NaCl content. Growth and motility was determined after two weeks.

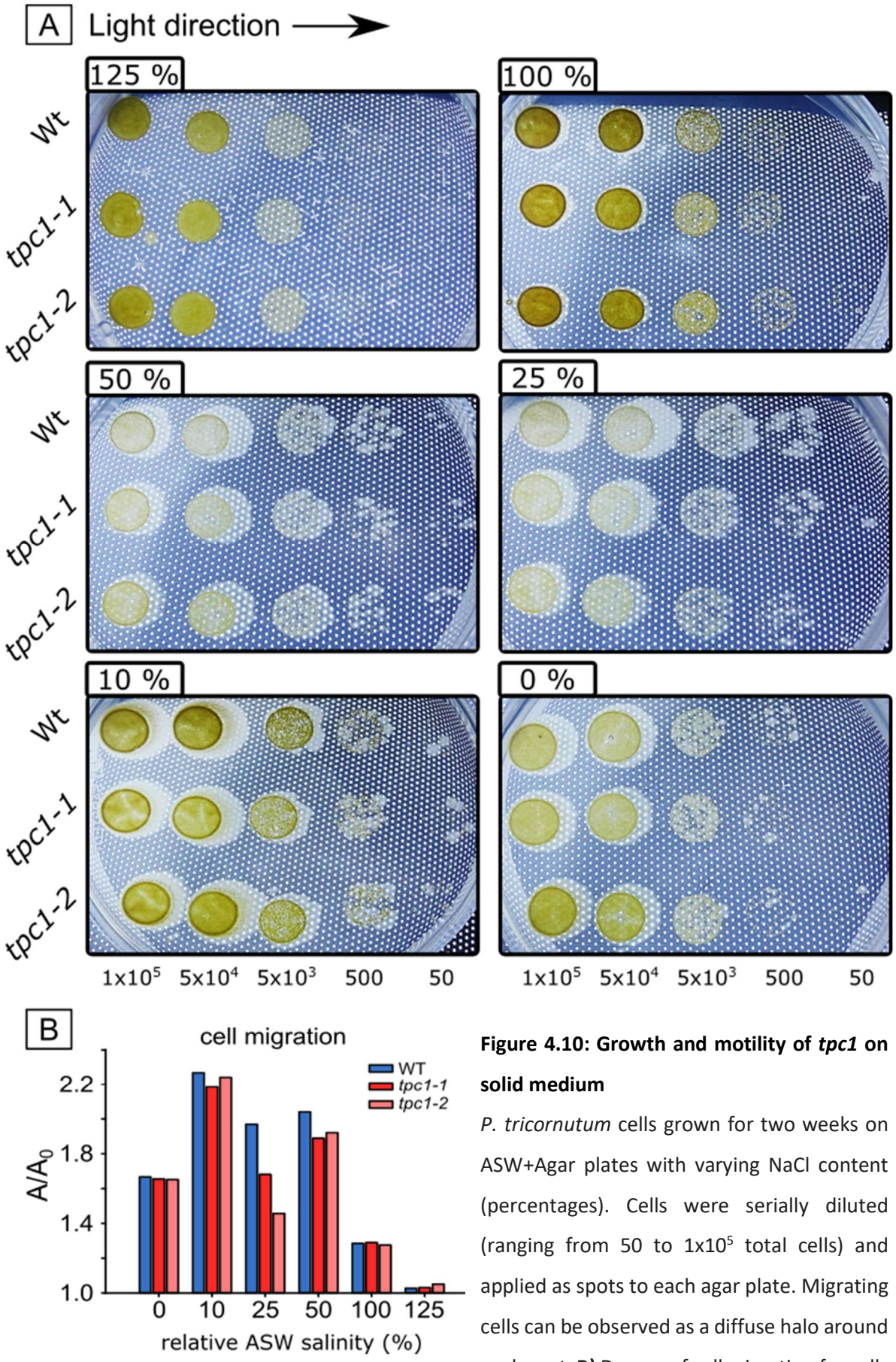

Figure 4.10: Growth and motility of *tpc1* on solid medium

P. tricornutum cells grown for two weeks on ASW+Agar plates with varying NaCl content (percentages). Cells were serially diluted (ranging from 50 to $1x10^5$ total cells) and applied as spots to each agar plate. Migrating cells can be observed as a diffuse halo around each spot. **B)** Degree of cell migration for cells spotted at a density $5x10^4$ cells, measured as the fold increase of total area.

No difference was observed in growth between Wt and *tpc1* cells for the tested conditions; including the plate with 0 % NaCl content in the medium (Fig. 4.10 A).

After two weeks, a diffuse area of cells can also be observed expanding beyond the dimensions of the initial spot. This expansion is due to gliding motility of oval cells and occurred mostly in a direction opposite of the light source. The increased area of cell coverage can be used as a measure of cell motility (Fig. 4.10 B). Firstly, there is a trend on increasing motility with decreasing salinity in all strains with the exception of 0% salinity. Secondly, there are no consistent differences in motility in *tpc1* strains relative to Wt. Although lower motility in both *tpc1* mutants was observed at 25%, this was not observed at other salinities, indicating that *tpc1* mutants did not have a large defect in motility.

4.3.3.4 Ca^{2+} signalling in *tpc1* mutants

4.3.3.4.1 Ca^{2+} elevations in tpc1 mutants in response to periodic hypo-osmotic shocks

The TPC1 channel in plants is proposed to be involved in the propagation of ROS-assisted Ca^{2+} elevations in *A. thaliana* roots in response to salt stress (Choi et al., 2014; Evans et al., 2016). To examine whether *P. tricornutum* TPC1 channel also assists signal propagation or formation of Ca^{2+} elevations, we applied two stimuli that result in cytosolic Ca^{2+} elevations in diatoms, namely hypo-osmotic shock and membrane depolarisation.

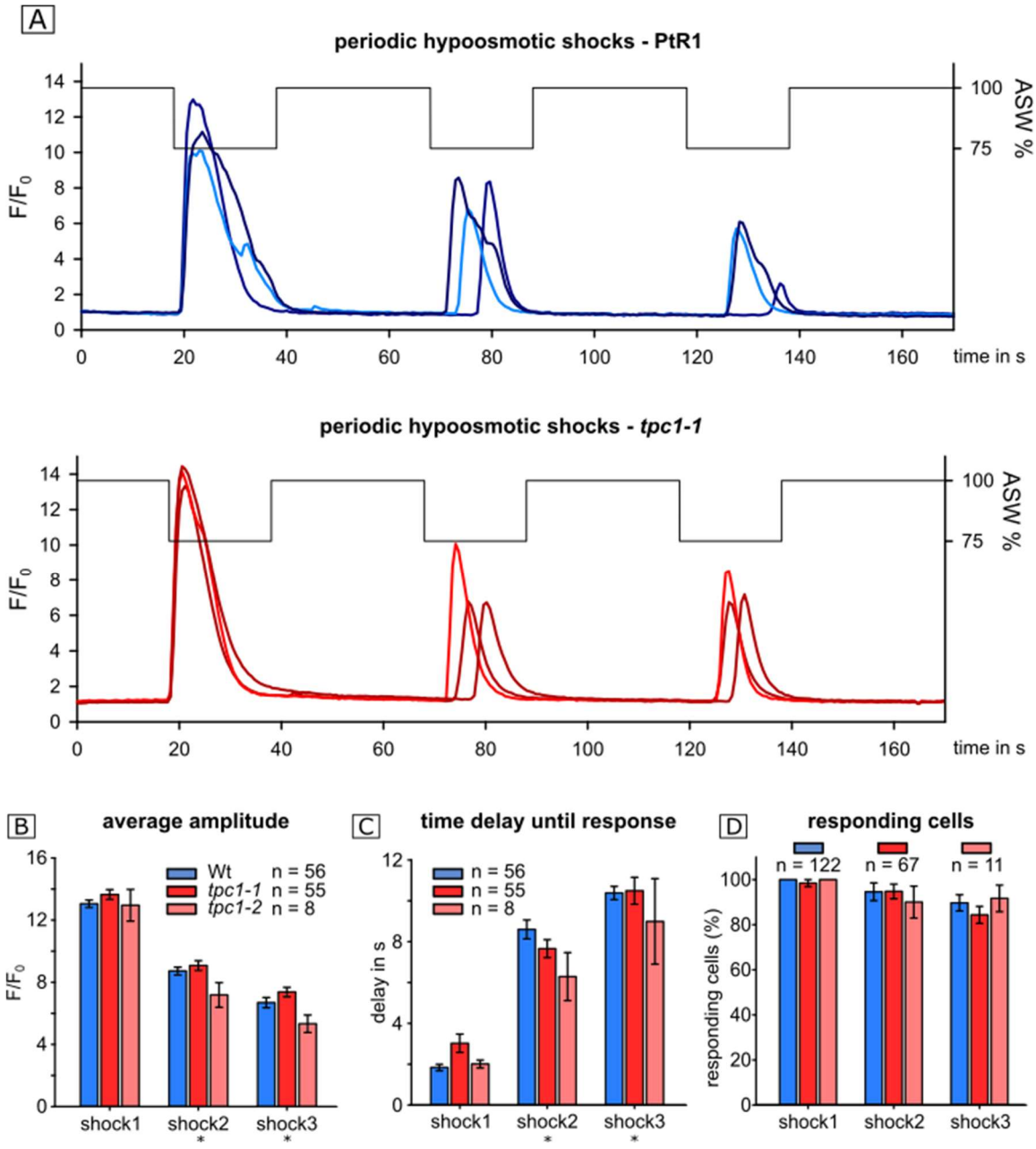

Figure 4.11: The *tpc1* knock out mutants show hypo-osmotic shock induced Ca^{2+} elevations similar to PtR1.

A) Three representative traces of RGECO fluorescence of PtR1 and *tpc1-1* cells in response to three subsequent hypo-osmotic shocks (ASW diluted with H_2O) throughout time ($t_{interval}$ = 30 s). In total, four independent experiments with PtR1, four with *tpc1-1* and two with *tpc1-2* cells were performed with similar results. **B)** Amplitudes of Ca^{2+} elevations recorded in response to each of the three subsequent hypo-osmotic shocks for all replicate experiments mentioned in (A). **C)** Time difference between arrival of diluted ASW in the dish and recorded onset of Ca^{2+} elevation for all replicate experiments mentioned in A (threshold $F/F_0 > 1.5$). **D)** Percentage of cells responding to each hypo-osmotic shock in relation to total number of cells visible in the recorded field of view.

Similar to results presented in Chapter 3, application of a series of hypo-osmotic shocks to PtR1 cells resulted in Ca^{2+} elevations in response to each shock, with attenuation in amplitude and slower response time towards the latter shocks (Fig. 4.11A).

There was a significant influence of the shock-succession on amplitudes (two way repeated measures ANOVA $P < 0.001$) for Wt and the *tpc1* strains (Bonferroni post-hoc test $P<0.001$ for each strain), but no significant influence for strain on amplitude was found (two way repeated measures ANOVA $P = 0.040$) (Fig. 4.11 B).

The response time significantly increased with shock-succession for all strains (two way repeated measures ANOVA $P<0.001$, Bonferroni post-hoc test $P<0.001$ for each strain), but again no significant differences between strains were found (two way repeated measures ANOVA $P = 0.124$) Fig. 4.11 C).

In the Wt strain, the percentage of responding cells lowers with each shock from 100 to 90 %. A similar pattern is observed for tpc1-1 (98 to 84 %) and tpc1-2 (100 to 92 %).

These data indicate that the TPC1 channel in *P. tricornutum* is not involved in generating cytosolic Ca^{2+} elevations in response to rapid hypo-osmotic shock.

4.3.3.4.2 Ca^{2+} elevations in *tpc1* mutants in response to a gradual hypo-osmotic shock

P. tricornutum TPC1 has two EF-hand domains, suggesting that this channel may be activated by cytosolic Ca^{2+} elevations and may assist in propagation of Ca^{2+} waves. To test this, a hypo-osmotic shock was applied to PtR1 and *tpc1* cells in a linear gradient shown to elicit Ca^{2+} waves in Chapter 3.

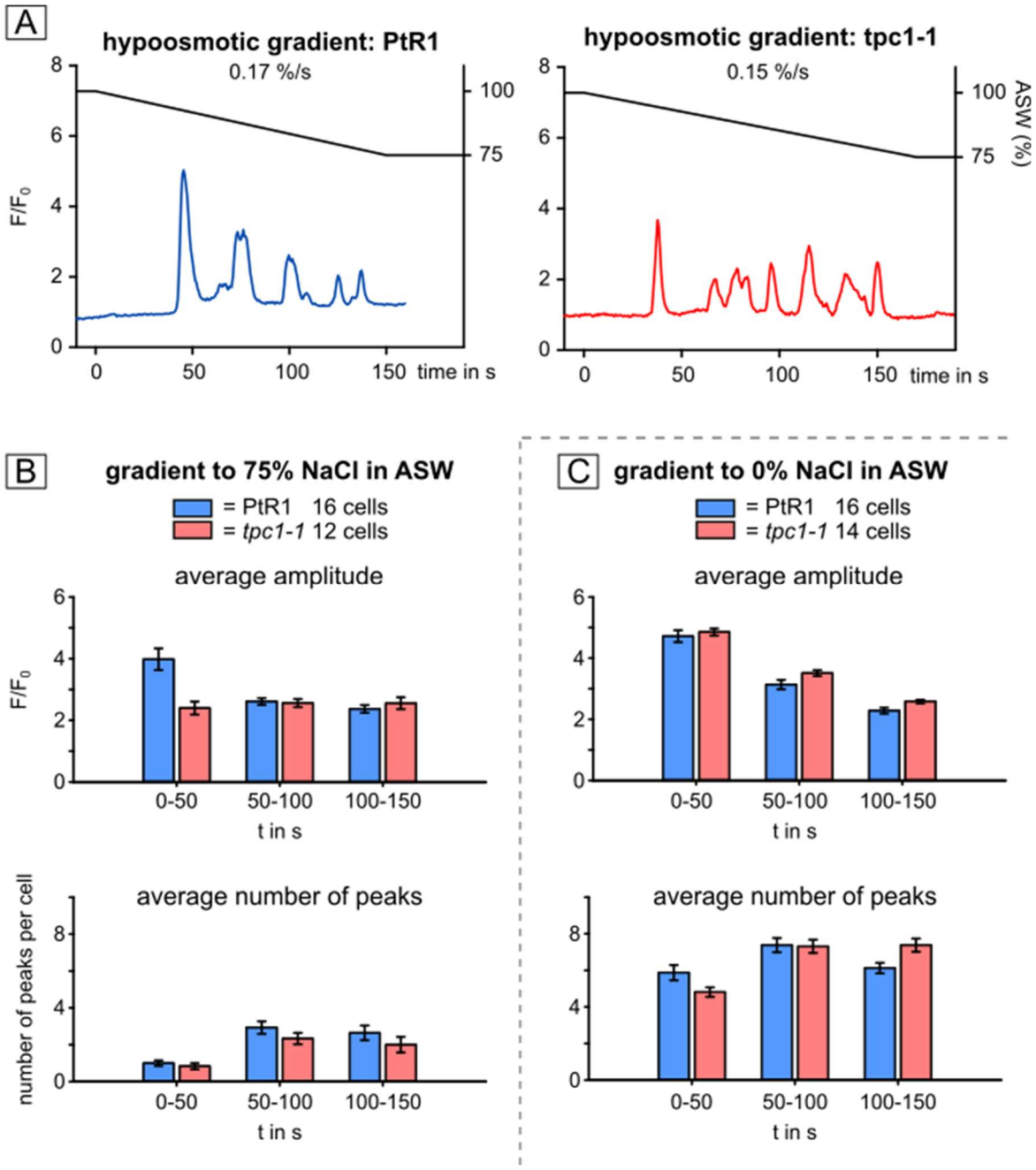

Figure 4.12: The *tpc1* knock-out mutants show linear hypo-osmotic gradient-induced Ca2+ elevations similar to PtR1.

A) One representative trace of RGECO fluorescence of 54 PtR1 and 50 *tpc1-1* cells in response to a hypo-osmotic linear gradient towards ASW diluted with H_2O for a final ASW concentration of 75 %. Included is an approximate calculated change rate in ASW concentration per second. Experiment was repeated three times per strain and treatment with similar results, but slight differences in gradient change rate prevented pooling of data. **B)** Mean amplitudes and number of Ca^{2+} elevations recorded within time intervals of 50 s duration for the treatment shown in (A) **C)** Mean amplitude and number of Ca^{2+} elevations for PtR1 and *tpc1-1* cells in response to a linear gradient to 0% ASW (freshwater) from a single experiment. Two additional experiments yielded similar results.

Both PtR1 and *tpc1* cells showed multiple Ca^{2+} elevations for the duration of the linear hypo-osmotic gradient. Due to technical difficulties in generating identical gradients, the gradient was slightly steeper for PtR1 cells compared to the *tpc1* treatment. This likely contributed to a relatively large initial Ca^{2+} elevation in PtR1 compared to *tpc1* cells (Fig. B 0-50 s interval). Besides this, no differences in amplitudes and number of Ca^{2+} elevations within 50 s time intervals were observed between PtR1 and *tpc1*.

In a more severe and potentially more lethal hypo-osmotic gradient to 0% ASW (freshwater), again no striking difference in the average amplitude and number of peaks was observed between PtR1 and *tpc1-1* cells. Furthermore, no striking increase in cell bursting in *tpc1-1* was observed (2% of PtR1 cells burst (n = 47); 4% of *tpc1-1* cells burst (n = 41)). Taken together, this indicates that TPC1 is not critically involved in propagation or amplification of hypo-osmotic induced Ca^{2+} elevations and that the Ca^{2+} elevations in *tpc1* cells are still able to be translated into protective mechanisms against hypo-osmotic stress.

In order to investigate a putative disturbance in the spatial distribution and propagation of Ca^{2+} elevations in *tpc1*, the signalling patterns of two representative cells within the data presented in Fig. 4.12 A were visualised in a kymograph.

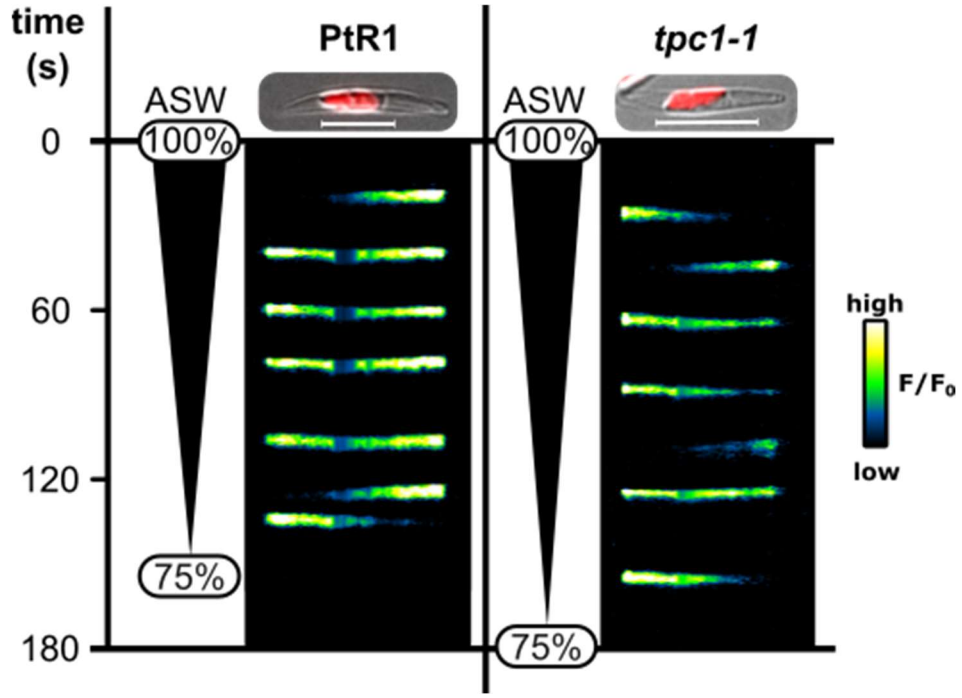

Figure 4.13: *tpc1* cells are still able to exhibit Ca^{2+} waves.

False-colour kymographs showing Ca^{2+} elevations of representative PtR1 and *tpc1-1* cells in response to hypo-osmotic shock applied in a linear gradient. DIC images of the cells are shown with red-indicated chlorophyll autofluorescence and a scale bar of 10 µm. To the left is a timescale (s), triangles represent the approximate gradient for each cell (100 % to 75 % ASW +25 % H_2O), to the right is the fluorescence legend.

As described in Chapter 3, PtR1 cells exhibit Ca^{2+} elevations initiating at respective apices that propagate towards the centre of the cell. Many Ca^{2+} elevations initiated in both apices simultaneously but some were also observed to be restricted to a single apex only. In the representative *tpc1* cell shown, Ca^{2+} elevations also initiated at the cell apices and propagated towards the cell centre, again indicating that TPC1 is not critically involved in the formation and propagation of hypo-osmotic shock induced Ca^{2+} elevations.

4.3.3.4.3 Ca^{2+} elevations in *tpc1* mutants in response to depolarisation of the plasmamembrane

The presence of positively charged amino acid residues in or close to conserved positions of the voltage sensing motif within the 4th transmembrane domain of each pore-containing subunit suggest that TPC1 is sensitive to membrane depolarisation. To test whether TPC1 may be activated by changes in plasmamembrane voltage and/or cytosolic Ca^{2+} elevations, the plasma-membrane of PtR1 and *tpc1* cells was depolarised through perfusion with 100 mM K^+ ASW and Ca^{2+} signalling activity was monitored (Helliwell et al., 2019). Salinity in the K^+ depolarisation treatment was increased slightly (NaCl 110 %) to prevent the highly sensitive hypo-osmotic Ca^{2+} signalling responses from interfering with the depolarisation response. Hyper-osmotic treatment does not result in cytosolic Ca^{2+} elevations

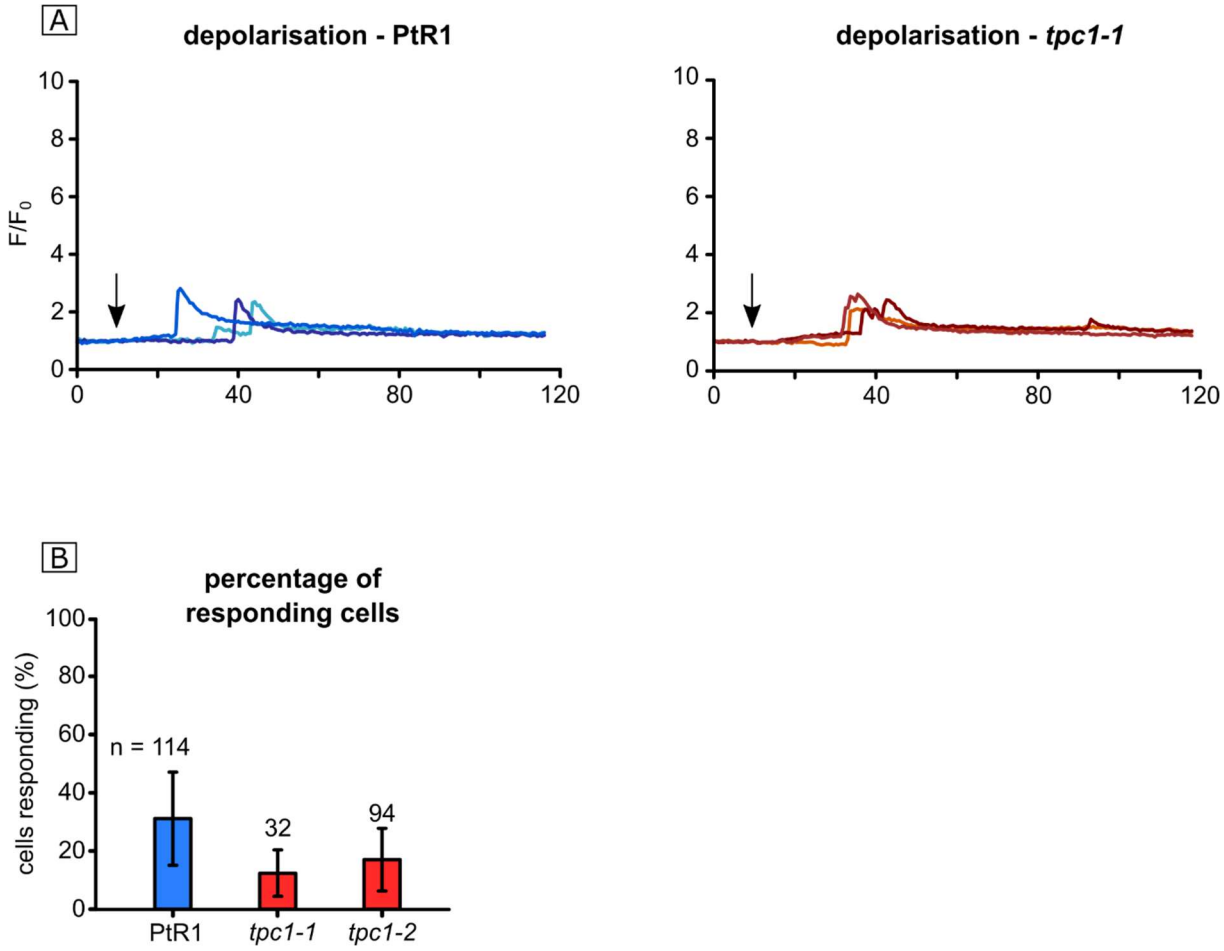

Figure 4.14: Response of PtR1, *tpc1-1* and *tpc1-2* to induced membrane depolarization.

A) Representative traces of RGECO fluorescence from three *Pt*R1 and *tpc1-1* cells in response to ASW 110% NaCl +100 mM K^+ at t = 10 s (arrow). **B)** Percentage of cells responding to depolarisation. Three replicate experiments were done for each strain. Error bars represent SEM.

K^+ treatment led to cytosolic Ca^{2+} elevations in 31 % of PtR1 cells. A similar response was seen in *tpc1* cells (*tpc1-1* = 12 %; tpc1-2 = 17 %) and the percentage of responding *tpc1* cells was not significantly different from the wild type (One-way ANOVA P = 0.533). This indicates that the ability to respond to membrane depolarization is not completely abolished in *tpc1*. However, the number of wild type cells responding to the depolarization treatment is relatively low in comparison to Helliwell et al. (2019) who reported 94 % of PtR1 cells responding to this treatment.

4.3.3.4.4 Ca^{2+} elevations in *tpc1* mutants in response to cold shock

Cold shock also induces Ca^{2+} elevations in PtR1 cells. The cold shock response in *tpc1* mutants will be presented in Chapter 5 Fig. 5.12.

4.3.3.5 Generating TPCL knock-out mutants

To allow a complete analysis of TPC and TPCL in *P. tricornutum*, attempts were also made to knock-out TPCL. A novel cloning strategy was devised, using a pKS_diaCas9:sgRNA1:sgRNA2 plasmid with two distinct sgRNA expression cassettes instead of one, aiming to increase transformation efficiency through lowering the number of plasmid integration events required for successful transformation.

Two plasmids were designed for editing TPCL. One had two sgRNAs targeted to the 5' end of the gene, aiming to introduce a small deletion (approx. 40 bp) and a potential frameshift (pKS_diaCas9_sgRNA:A+B), the other plasmid had two sgRNAs designed to introduce a much larger deletion (approx.. 2kb) within the gene (pKS_diaCas9_sgRNA:A+C). Plasmids were co-transformed into the PtR1 strains alongside plasmid pPhaT1_Blast which confers resistance to Blasticidine (Buck et al., 2018). Four transformations were conducted with these plasmids, but three exhibited problems with the selection using Blasticidine.

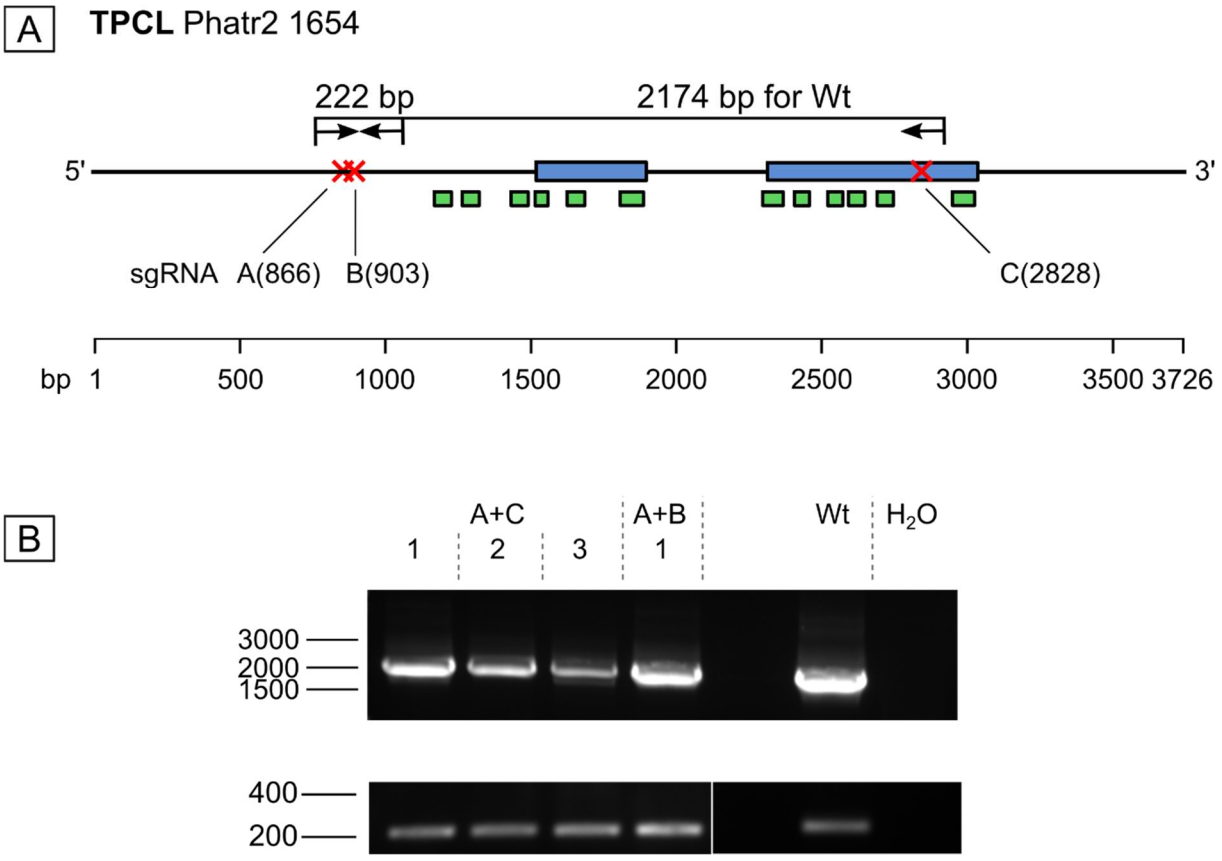

Figure 4.15: Generated resistant colonies did not contain a TPCL knock-out.

A) Schematic of the TPCL gene showing key features identified by Interpro (ion transport domain: blue, transmembrane helices: green) and position of CRISPR-Cas9 cutting sites (red) according to selected sgRNAs (sgRNA A = GCAACCCCAAGACAGTAACG, score 0.80; B = GCCACGCAGCACAAGACGCG, score 0.65; C = GAACAATTTCAACTCCTACC, score 0.69). Primer pairs flanking respective sgRNA combinations A+B and A+C are indicated by arrows. **B)** Images of agarose gels showing results of a colony PCR on colonies achieved with pKS_diaCas9_sgRNA:A+C (top) and pKS_diaCas9_sgRNA:A+B (bottom), respectively. All amplicons are of similar size compared to the Wt-amplicon.

Three colonies were generated with pKS_diaCas9_sgRNA:A+C, and one colony was generated with pKS_diaCas9_sgRNA:A+B. All four colonies were screened by PCR for deletions with both primer pairs (Fig. 4.15 B). None of the four colonies showed a deletion in the TPCL gene. However, the gene editing approach developed here using plasmids containing tandem sgRNAs was subsequently used successfully to knock out a range of other genes in *P. tricornutum* (Katherine Helliwell, personal communication).

4.3.4 Electrophysiological characterisation of diatom TPC channels

To compare the ion selectivity between the TPC1 and TPCL channel, codon-optimised genes were cloned into the pcDNA3.1 vector as a GFP fusion for heterologous expression in human embryonic kidney cells for whole-cell patch clamp experiments. Working in collaboration with Abdul Chachri (MBA Plymouth), HEK cells transfected with TPC1 or TPCL channels exhibited no GFP fluorescence and no heterologous currents. Therefore, expression and/or localisation of TPC channels to the plasma membrane was not achieved.

4.4 Discussion

Ca^{2+} signalling is evidently of great importance for the perception and/or deduction of environmental stimuli in diatoms (see Chapter 3; Vardi et al., 2006; Falciatore et al., 2000; Helliwell et al., 2019). However, apart from the novel class of EukCat channels, very little is known about which particular ion channels in diatoms are involved in the formulation of these Ca^{2+} elevations (Helliwell et al., 2019). This study summarises the current state of characterisation of TPCs in diatoms, a channel family with proposed involvement in Ca^{2+} signalling in animals and plants (Hedrich et al., 2018; Zhu et al., 2010).

4.4.1 TPC1 channels in diatoms

This study examined the role of TPC1 using two biallelic mutants with large deletions in *TPC1*. However, no clear phenotype was identified for these two mutants in this study.

4.4.1.1 *tpc1* shows no defect in growth and oval cell motility

The presented data showed no defect in growth in normal conditions nor in response to changes in salinity or nutrient availability.

When grown on plates, the oval morphotype of *P. tricornutum* is known glide on the surface using its raphe as slide in combination with a lubricant made of extra polymeric substances and adhesive compounds (Cohn and Disparti, 1994; Willis et al., 2013). No defect in *tpc1* motility was observed, unlike the EukCatA1 mutants which are involved in depolarisation-induced Ca^{2+} signalling (Helliwell et al., 2019). Surface motility and speed is shown to be dependent on presence of extracellular Ca^{2+} in the diatoms *P. tricornutum* and *Navicula perminuta*, whereas blue-light induced negative phototaxis is shown to be dependent on intracellular Ca^{2+} release in *Navicula perminuta* (Cooksey and Cooksey, 1980; McLachlan et al., 2012). Assuming these mechanisms also apply to *P. tricornutum*, the presented data suggest that TPC1 is not critically involved in light induced oval cell motility.

Interestingly, negative phototaxis did not occur at higher salinities in all strains, suggesting that oval cell's motility or the ability to transition in into the oval morphotype is dictated by environmental salinity content (de Martino et al., 2011; Ovide et al., 2018).

4.4.1.2 *tpc1* shows no defect in Ca^{2+} signalling

Data presented in this study suggest that TPC1 is not involved in the generation of cytosolic Ca^{2+} elevations in response to hypo-osmotic shock, and is also not essential to guarantee propagation of hypo-osmotic Ca^{2+} waves.

The *tpc1* mutants showed no clear defect in depolarisation induced Ca^{2+} signalling. However, the depolarisation response only occurred in a relatively small percentage of PtR1 cells, which differs greatly from results presented in Helliwell et al. (2019). Differences in the experimental set up may have contributed to these contrasting results. In this study, the intensity of a depolarisation-induced Ca^{2+} elevation increased when the cells were incubated for longer periods on the microscope dish prior the perfusion experiment. In addition, a relatively small time period between initiation of perfusion and initiation of depolarisation treatment was used in this study (40 seconds), whereas Helliwell et al. (2019) used a delay of several minutes prior to applying the depolarisation treatment. Giving the cells more time to acclimate to the perfusion may help to improve their ability to respond to depolarization.

Taken together, the function of TPC1 was not determined in this study, as there was not a strong defect in growth, motility or in Ca^{2+} signalling in response to a variety of stimuli. In order to predict the function of TPC1, the priority should be to determine its localisation and ion selectivity.

4.4.1.3 Bioinformatics analysis suggest dTPC1 to be a Na^+ selective channel at the vacuole membrane

Even though the function of TPC1 in *P. tricornutum* was not determined, this study proves that TPC1 is a widely distributed class of ion channels in diatoms, indicating a conserved role. All five completely sequenced diatoms have a representative of TPC1, and all of those contain an ion selective filter in the 2nd ion transport domain akin to TPCs in animals (VNN). This suggests that diatom TPC1 is a predominantly Na^+ conductive channel, but Ca^{2+}, H^+ and K^+ ions may also pass (Patel, 2015; Pitt et al., 2010; Pitt et al., 2014). It is proposed that animal TPC2 are Ca^{2+} release channels when activated through the mammalian Ca^{2+} messenger NAADP, Na^+ release channels when activated through $PI(3,5)P_2$ or membrane depolarisation, or Ca^{2+}, N^+ and H^+ channels when all aforementioned positive regulators apply (Marchant and Patel, 2013; Patel, 2015). No direct homolog of the NAADP forming enzyme Cd38 (*H. sapiens* BAA18966.1) was found in *P. tricornutum*, indicating that a different Ca^{2+} mobilising mechanism may be in place.

Animal and plant TPCs localise mostly to intracellular organelles with relatively acidic lumina, namely endo/lysosomes and vacuoles (Calcraft et al., 2009; Hedrich et al., 2018; Shen et al., 2013). Diatom TPC1 which has animal (ion selective motif) and plant (EF hands) features, may be no exception. In *A. thaliana* TPC1, an N-terminal di-leucine motif mediates trafficking of TPCs to the vacuole membrane (Larisch et al., 2012). Notably, an N-terminal di-leucine motif might be present at least for *P. tricornutum* and *F. cylindrus* TPC1 (*P.t.* ID 15329; motif RLAILL; *F.c.* ID 237602; motif ESSPLL), suggesting that some diatom TPC1s may also be located at the tonoplast.

The most prominent indicators for diatom TPC1 function remain its EF hands. Diatom TPC1, plant TPCs and animal TPC2 share the feature of two Ca^{2+} binding EF-hand domains in a cytoplasmic loop between the ion transport domains. This contributes to the idea that Ca^{2+} -dependent activation is a conserved feature of this channel class which has been lost in animal TPC1 and TPC3 (Hedrich et al., 2018). In plants, only the second EF-hand domain was shown to promote channel opening by reducing voltage activation towards hyper-polarising potentials (Schulze et al., 2011), whereas EF1 is suggested to maintain structure (Guo et al., 2016; Kintzer and Stroud, 2018). It is unclear whether EF-hands in dTPC1 exactly

mirror this, but it strongly suggests that cytosolic Ca^{2+} levels may also impact dTPC1 channel activity.

Among the putative extrapolated roles of TPC1 in diatoms may therefore be ion signalling and - if present in internal organelles - Ca^{2+} dependent vesicle fusion and fission (Patel, 2015; Ruas et al., 2010).

4.4.2 A novel Two-pore channel: TPCL in diatoms

In addition to the "conventional" diatom TPC1, this study presents the identification of a novel subclass of TPCs named TPCL. It is known for several years that *P. tricornutum* possesses two TPCs (Verret et al., 2010), but from the limited sequences available it was not clear whether this was simply another TPC channel or a distinct class of channel.

TPCL shares the basic structure of conventional two-pore channels as annotations suggest presence of two distinct ion transport domains. Phylogenetic analysis suggests that TPCL is not a result of a novel gene duplication of a single-domain ion channel but rather shares a common ancestor with conventional TPCs. The apparent restriction of TPCL to diatoms indicates that the emergence of this channel class may have coincided with the development of diatoms. However, no representatives of TPCL were found in two of the five fully sequenced diatoms: the multipolar centrics *Thalassiosira pseudonana* and *Thalassiosira oceanica*. Considering that other multipolar centrics do have TPCL representatives, loss of TPCL may have occurred in the *Thalassiosira* lineage relatively recently. As TPCL may be less well conserved in diatoms than the ubiquitous dTPC1, the evolutionary history and function of TPCL in diatoms may therefore be more complex than it seems.

4.4.2.1 The diatom vacuolar channel TPCL possesses a non-canonical ion selective motif

The ion selectivity of a channel is generally determined by charge and size of amino acid residues at the narrowest point(s) in the pore, which imparts selectivity through structural interactions with passing ions or their hydration shells (Roux, 2017). The non-selective *A. thaliana* TPC1 channel was rendered Na^+ selective when its ion selective motif (MGN) was substituted with the animal-TPC motif (VNN), highlighting the sensitivity of selectivity when crucial amino acid residues are replaced (Guo et al., 2017). Therefore, the substitution in the 3rd position of the TPCL ion selective motif in the second ion transport domain from a neutral asparagine residue towards a negatively charged aspartic acid residue likely alters ion selectivity. Negatively charged residues are considered to favour cation selectivity (Hedrich et al., 2018) and dominate the ion selective filters in predominantly Ca^{2+} and, to some extent, Na^+ selective ion channels (Zagotta, 2006). It may therefore be possible that TPCL is a predominantly Ca^{2+} selective ion channel – a potential novelty for the TPC channel family.

Data presented in this study suggest that TPCL is located at the vacuole membrane. Simultaneous labelling with a plasma membrane dye would be needed to fully support this conclusion. No di-leucine motifs were found in the TPCL sequences of the five sequenced Diatoms, suggesting that a different targeting mechanism may be in place. A single EF-hand domain was identified in 2 out of 35 TPCL sequences but it is unclear if those are of structural or sensory function. It is also unclear whether these are remnants of the EF-hand containing TPC ancestor (Hedrich et al., 2018) or a novel re-introduction.

4.4.3 TPC1 and TPCL await electrophysiological examination

Analysis of ion selective motifs of channels can provide hints for ion selectivity, but only electrophysiological analysis of channels is able to provide evidence. In this study, attempts to heterologously express PtTPC1 and PtTPCL in HEK cells were not successful due to low expression.

Plant TPC1 channels have been successfully investigated in HEK cells due to fortunate “mistargeting” of these channels to the periplasmic membrane. It was suggested that

elevated Ca^{2+} in the pipette solution triggered vesicle fusion and increased the number of channels on the plasma membrane (Guo et al., 2017). This adjustment did not increase expression in this study.

Heterologous expression of a non-host protein may be impaired by altered transcription and translation efficiency, erratic protein folding, erratic application of post-translational modifications or product toxicity (Bernaudat et al., 2011; Gomes et al., 2016). Other algae channels such as H^+- or EukCat channels have been successfully expressed in HEK cells before (Helliwell et al., 2019; Taylor et al., 2011). However, TPC1 and TPCL are larger proteins in comparison (i.e. *E. huxleyi* H^+-Channel ID 631975 = 339 aa; *P. tricornutum* EukCatA ID 43878 = 470 aa*, P. tricornutum* TPC1 = 880 aa), and the GFPs attached to the C-termini of the TPC1 and TPCL sequences may also present problems for the formation of the final channel tetramer.

HEK cells are not mandatory for electrophysiological experiments. Plant vacuoles were successfully used to investigate native and exogenuous ion channels (Festa et al., 2016), and vacuoles of particularly large diatoms such as *Coscinodiscus* (2 mm) may present a tempting alternative.

Chapter 5 Ca^{2+} signalling responses in *P. tricornutum* in response to cold shock

ABSTRACT

Diatoms are a group of highly successful photosynthetic microalgae which inhabit a range of diverse habitats including coastal and benthic areas. These areas may be subject to rapid shifts in temperature, e.g. through wind, rain, sun radiation or tides. Temperature is a highly important abiotic stress factor determining molecular dynamics and biophysical properties of proteins and membranes, and as such affects all metabolic processes associated with them. The effect of long-term low temperature on diatom physiology has been investigated previously, but little is known on how diatoms sense changes in temperature to initiate acclimation.

In this study, cytosolic Ca^{2+} elevations coinciding with a rapid decrease in temperature were characterised in two diatom species expressing the fluorescent Ca^{2+} reporter RGECO: the benthic diatom *P. tricornutum* and the pelagic diatom *T. pseudonana*. These cold-induced Ca^{2+} elevations correlate with speed and magnitude of temperature drop, which strongly suggests a role for Ca^{2+} in temperature perception in diatoms. This opens the door towards a better understanding on how diatoms sense and respond to changes in temperature while also providing a new perspective on the evolution of temperature perception pathways in general.

5.1 Introduction

5.1.1 Temperature shifts in marine habitats

Diatoms are an extremely successful group of photosynthetic microalgae. They are estimated to account for 40% of marine primary production (Armbrust, 2009; Falkowski et al., 2004; Field et al., 1998) and significantly contribute to biogeochemical cycling (Bowler et al., 2009; Nelson et al., 1995; Weber and Deutsch, 2012). As such, diatoms can be found in freshwater, diverse marine habitats, terrestrial soils or polar ice formations (Antonelli et al., 2017; Lomas et al., 2019; Malviyaa et al., 2016), and are particularly important species in highly productive coastal ecosystems of higher latitudes (Malviyaa et al., 2016). Some pennate diatoms, such as *P. tricornutum,* thrive within pools of mid- and upper- zones of rocky shores and are highly important primary producers in mudflats of estuarine intertidal regions (Underwood et al., 1998; Virta et al., 2019).

Coastal regions can be subject to rapid shifts in temperature perceived as cold shock for intertidal diatoms. On a warm day, water temperature in rock pools or mud may elevate whereas an incoming tide could cause a very rapid, near instantaneous decrease (Howland et al., 2000; Zimmerman and Kremer, 1984). In July 2019, the water in a 10 cm deep pond in the rocky shore of Looe (Cornwall, UK) exhibited tide- and daytime driven temperature extremities (14 °C → 32 °C → 13.9 °C in one day), each interrupted by periods of a baseline temperature (15-16 °C) when high-tide ocean covered the pond (H. Parry-Wilson, Mieszkowska lab, MBA Plymouth, unpublished), demonstrating that coastal microorganisms may face a large range in temperature.

The frequency of rapid temperature shifts in coastal areas is likely to increase in the future: Since air temperature tends to rise more quickly over land than over sea, global warming will lead to increasing gradients in temperature and atmospheric pressure between terrestrial and oceanic areas, encouraging extreme weather events in the coastal intersection (Harley et al., 2006).

Sudden changes in temperature (= shock) have generally a more severe impact on the cell than slow ones, and can pose potential danger for cell survival if the temperature change occurs rapidly and strongly enough. This may be of increased importance for poikilothermic and relatively immobile species such as diatoms.

Thus, diatoms and other microalgae need to protect themselves from harmful temperature effects which depend on the direction of temperature change.

5.1.2 Effects of high temperature on cell physiology

Elevated temperatures generally increase molecular dynamics and metabolic efficiency, but can lead to denaturation and aggregation of proteins if critical a threshold is met (Parag et al., 1987). This may result in disturbance in intracellular transport through collapse of the cytoskeleton (Parrotta et al., 2015; Toivola et al., 2010), lowered metabolic efficiency through lowered enzymatic stability and shifted reaction equilibria (Robinson, 2015), and increased ROS generation through damaged components of the photosynthetic and respiratory apparatus (Crafts-Brandner and Salvucci, 2004; Hasanuzzaman et al., 2013; Mathur et al., 2014). Furthermore, enhanced membrane permeability can lead to shifts in intracellular pH and affect homeostasis (Babsky et al., 2005; Drummond et al., 1986).

5.1.3 Effects of low temperature on cells

In contrast to heat, cold reduces molecular dynamics. The physiological consequences can be broadly categorised as follows:

I) Low temperature leads to decreased enzymatic turnover rates caused by decreased water viscosity (Podolsky, 1994) and increased activation energy as described by the Arrhenius equation (Georlette et al., 2004; Kingston-Smith et al., 1997). Cells indirectly counteract this by an increased number of enzymes which usually manifests in an overexpressed protein translation machinery (Broeze et al., 1978; Cavicchioli et al., 2000; Fraser et al., 2002; Guy et al., 1992).

II) Increased biomembrane rigidity with reduced temperature affects membrane integrity, transport, cell division and membrane protein function (de Mendoza et al., 1983; Murata and Los, 1997; Steponkus, 1984). It is known that bacteria, archaea, plants and animals may counteract this effect by desaturation and shortening of phospholipid chains to ensure membrane fluidity (Cavicchioli et al., 2000; de Mendoza et al., 1983; Murray et al., 2007; Popov et al., 2017).

III) As a consequence of I) and II), ROS are generated in mitochondria (Purvis et al., 1995) and particularly chloroplasts (Gollan et al., 2017; Liu et al., 2018; Ruban et al., 2012) due to excess electron transport in relation to reduced utilisation of electrons in catabolic or anabolic metabolism. ROS damage membranes and degrade proteins (Apel and Hirt, 2004) but can be controlled directly by release of ROS-scavengers (Sharma et al., 2012) and indirectly by decrease of metabolism in these organelles (Yuan et al., 2018).

IV) Low temperature affects secondary and tertiary structure of proteins and mRNA (Owttrim, 2006; Privalov, 1990; Tsai et al., 2002) which furthermore impacts transcription, translation, replication, nucleoid packing and mRNA folding. Cells may maintain these structures by protein chaperones, RNA-helicases and RNA-binding “cold-shock” proteins, respectively (Melencion et al., 2017; Owttrim, 2006).

V) The photosynthetic capacity is reduced as a result of aforementioned effects (mainly I, II and III), potentially leading to photodamage (Hodgson et al., 1987; Liu et al., 2018; Somerville, 1995; Sonoike, 1999). Low temperatures amplify or mimic light-stress (Foyer, 2018), e.g. through reduction in LHCSII mobility, thus preventing photosystem state transition (Nellaepalli et al., 2012), reduction in PSII repair rate (Murata et al., 2007) and increase in non-photochemical quenching (Georgieva and Yordanov, 1994; Jahns and Holzwarth, 2012)

5.1.4 Effects of low temperature on diatoms and other microalgae

Currently available data on low temperature stress on microalgae focuses on their ability to acclimate to long-term cold stress rather than short-term responses to cold shock. Diatoms dominate primary productivity in polar regions and show key adaptions in physiology (Lyon and Mock, 2014).

A canonical correspondence analysis (statistical method to determine relationship between a collective of species and their environment, allowing to rank environmental variables in importance) of marine eukaryotic phytoplankton meta-transcriptomes from polar, temperate and tropical zones revealed that surface temperature accounts for 28.3% of metabolic variability, which is close to values obtained for other highly relevant factors such as nutrients (nitrate 31.7%, phosphate 34.9%) and light (30.17%) (Toseland et al., 2013). Moreover, transcripts linked with protein translation had the highest positive correlation score with low temperature in this study (Toseland et al., 2013), and were found to be significantly affected by a temperature difference of 4 °C in another study focusing on Antarctic phytoplankton (Pearson et al., 2015). Further evidence for cold induced increase in protein, RNA and ribosomes synthesis was found in the open ocean diatom *T. pseudonana* and polar diatom *F. cylindrus* when expression was compared between two temperatures (*T.p.*: 4-11 °C vs. 20-27 °C: *F.c.*: -2 °C vs. 10 °C) (Toseland et al., 2013). Notably, this increase in translation did not completely counteract reduced protein production rates in *T. pseudonana*, since expression of inducible GFP at 11 °C was still reduced by almost a third compared to 20 °C (Toseland et al., 2013). The arctic bloom-forming diatom *Thalassiosira gravida* endures prolonged irradiance at 0-5 °C through strong sustained non-photochemical quenching and increased pigment levels (Lacour et al., 2018)

Low temperature also triggered transition of the pelagic fusiform to the benthic oval morphotype in the pennate diatom *P. tricornutum* (de Martino et al., 2011). Oval cells derived from low-temperature and hyposaline growth conditions exhibited similar EST expression profiles with emphasis on signalling, cell homeostasis and lipid metabolism pathways, indicating an overlap in how these two stresses are experienced by *P. tricornutm* (de Martino et al., 2011). These findings together indicate that in response to low temperature, microalgae prioritise protein translation while scaling down photosynthesis.

5.1.5 Temperature sensing mechanisms

In order to orchestrate responses to cold stress or cold shock, a sensory system for temperature needs to be present to initiate and prioritise mitigation mechanisms.

Molecular thermo-sensing describes the mechanism in which sensory nucleic acids, proteins and membranes experience structural changes during shifts in temperature (Klinkert and Narberhaus, 2009; Sengupta and Garrity, 2013). Temperature-sensitive ion channels such as heat sensitive anoctamin Cl^- channels (Cho and Oh, 2013), heat sensitive members of the K^+ conducting K_{2p} channel family (Lamas et al., 2019; Schneider et al., 2014) and heat- and cold sensitive members of Ca^{2+} - and Na^+ - conducting TRP-channels translate temperature induced changes in membrane rigidity into ion fluxes (Clapham, 2003).

Many more channels were shown to respond to spontaneous changes in membrane tension, curvature, and rigidity, potentially making almost any channel slightly thermo-sensitive (Calabrese et al., 2002; Gu et al., 2001; Laitko and Morris, 2004; Lundbæk et al., 2005; Morris and Juranka, 2007).

Although the details of sensory mechanisms in plants and animals are still not fully understood, many cold shock events are associated with cytosolic Ca^{2+} elevations. In animal dorsal root neurons, a temperature decrease of 10 °C resulted influx of external Ca^{2+} into the cytosol (Suto and Gotoh, 1999), thought to depolarise the neuron membrane and modulate AP fire rates (Adair, 1999). In plant cells, cold induces Ca^{2+} elevations which confer cold tolerance through downstream responses (Guo et al., 2018).

5.1.5.1 Animals

TRPM8 (M = melastatin) and TRPA1 (A = ankyrin) channels in the tips of animal sensory neurons are vital for sensing temperature drops and chilling-related pain in animals (Clapham, 2003). In contrast to heat sensitive TRPs (Singh et al., 2019), the molecular mechanism underlying chilling sensitivity of these channels is still being investigated (Brauchi et al., 2004; Liu and Rohacs, 2020; Xu et al., 2020; Yin et al., 2018). It is clear that low temperature increases the open probability of the channels and creates an inward cationic current carried by Ca^{2+} and /or Na^+ ions which is inversely proportional to absolute

temperature (Voets et al., 2004). This locally depolarises the membrane of neuron tips and triggers action potentials which propagate to the brain. Just as other TRPs, TRPM8 is polymodal and can also be triggered by ligands such as menthol or icilin (Patapoutian et al., 2003).

5.1.5.2 Plants

In plants, cold stress perception likely incorporates a complicated cross-talk of photosynthesis-dependent and -independent signalling pathways, involving signalling agents such as ROS (Suzuki and Mittler, 2006), the chloroplast PQ-pool (Huner et al., 1998; Karpinski et al., 1999), NO (Sehrawat et al., 2013), plant hormones (Liu et al., 2020) and Ca^{2+} (Liu et al., 2019). The ICE-CBF-Cor pathway is understood in most detail, in which a putatively cold sensitive ion channel is responsible for a Ca^{2+} dependent phosphorylation cascade affecting inducers of C-repeat-binding transcription factors (CBF) (Knight and Knight, 2012). These further regulate the expression of cold-responsive genes (COR genes) which are crucial for cold-acclimation in plants (Knight and Knight, 2012; Liu et al., 2019). The identity of the main cold inducible Ca^{2+} channel in plants is still unknown, but mechanosensitive channels were proposed for this role (Liu et al., 2019).

5.1.5.3 Diatoms

It is not known how diatoms predominantly sense, initiate and prioritize mechanisms to address the problems caused by cold shock. It is conceivable that a plant-like battery of independent signalling systems involving the redox-state of the chloroplast and ion fluxes at the plasma membrane co-exist. With four TRP- and seven MS-channels, the cosmopolitan benthic diatom *P. tricornutum* possesses prime candidates for temperature sensitive Ca^{2+} channels (Verret et al., 2010). Ca^{2+} signalling has already been shown to be vital in sensing and responding to hypo-osmotic stress (Falciatore et al., 2000; Helliwell et al., 2019; Helliwell at al., unpublished; Chapter 3) and sensing of phosphate (Helliwell et al., 2020a) and iron (Allen et al., 2008; Falciatore et al., 2000).

We therefore aim to examine the role of Ca^{2+} signalling in chilling stress perception, attempt to address the involvement of underlying ion channel(s) in *P. tricornutum* through a combination of genetically-encoded biosensors, gene manipulations, imaging and growth rate measurements.

5.2 Methods

5.2.1 Cultivation of *P. tricornutum* strains

The *P. tricornutum* strains used in this study were *P. tricornutum* wild-type (PtWT) based on CCAP 1055/1 from the Culture Collection of Algae and Protozoa (SAMS limited, Scottish Marine Institute, Oban, UK), *P. tricornutum* transformed with the RGECO Ca^{2+} biosensor (PtR1), the two PtR1-*tpc1* knock-out strains presented in Chapter 4 (*tpc1-1* and *tpc1-2*) and three PtR1-*eukcata1* knock-out strains (*eukcata1-1, eukcata1-2, eukcata1-3;* Helliwell et al., 2019). All mutant strains were provided by Katherine Helliwell, MBA Plymouth.

The *T. pseudonana* strain expressing RGECO biosensor was generated in Chapter 2.

Growth conditions and recipes for ASW ($\pm Ca^{2+}$) are described in Chapter 3.2.1. Growth temperature regimes different from standard conditions are indicated if applicable.

5.2.2 Imaging of cold shock responses.

5.2.2.1 Application of temperature shocks to *P. tricornutum* cells on a microscope setup

Microscope dishes containing *P. tricornutum* strains were prepared as described in Chapter 3.2.2. The Leica microscope setup used to monitor PtR1 RGECO fluorescence is also described in Chapter 3.2.2. ASW perfusion medium (with no nutrient supplements) was applied to the cells in the microscope dish using a gravity-driven perfusion system described in Chapter 3.2.2. Bottles containing ASW were warmed to 40 °C using a water bath, cooled to 0 °C using watered ice or left at room temperature and then were freshly introduced to the perfusion system for each single experiment. The tubing system used to administer cold ASW to the cells was insulated with cotton wool.

To apply a cold shock to the dish, perfusion of warm ASW or ASW of room temperature was switched to cold ASW. The perfusion system and heat radiation of the microscope buffered the input temperatures of warm and cold ASW to approximately 30-33 °C to 7-10 °C in the dish, respectively. In most experiments, this maximised temperature drop was applied which was considered to be within the physiological range of temperatures likely

to be experienced by a benthic intertidal diatom (H. Parry-Wilson, Mieczkova lab Marine Biological association of the UK, unpublished, see Introduction)

Standard perfusion flow speed was 16 mL min^{-1} but this was altered with a valve to administer temperature shocks with slower temperature drop rates. To administer shorter temperature drops, the perfusion of cold ASW was completely interrupted.

5.2.2.2 Recording of temperature within the microscope setup

The temperature within the dish was recorded in close proximity to the dish outflow with the optical temperature sensor TPR430 connected to FSO2-4 using the Pyro Oxygen Logger software 3.315 (pyroscience.com) and a time resolution of one datapoint per second. The temperature difference for each second in relation to the respective precedent second was determined, and the largest temperature drop within a second represents the temperature drop rates shown in this study.

5.2.2.3 Pretreatment of PtR1 cells with ruthenium red for cold shock experiments

Ruthenium red (RRed; stock 10 mM in H_2O) was added to a tube containing 500 µL of PtR1 culture to achieve final RRed concentration of 10 or 5 µM. The contents were gently mixed and 500 µL was applied to a microscope dish as described and set to incubate for 5-10 min at room temperature. RRed was not added to ASW used for perfusion.

5.2.2.4 Perfusion of PtR1 cells with ASW containing menthol and / or DMSO

10 mL of 100% DMSO was used as solvent for a 1 M menthol (SIGMA) stock solution. From this, ASW with 100 µM, 200 µM and 1 mM menthol was made, giving a maximum final DMSO concentration of 0.1%. In a separate experiment, DMSO was added to ASW to a final concentration of up to 5%. PtR1 cells were then perfused with ASW +DMSO ± menthol and fluorescence was recorded as described.

5.2.2.5 Cold shock test on cold acclimated cells

A PtR1 culture in early exponential growth phase (ASW medium) was used to inoculate two culture flasks with 30 mL ASW. One of these was further cultivated at 18 °C, the other was cultivated at 4°C. Both had 16:8 light/dark cycle with an illumination of ~60 µmol·m^{-2}·s^{-1} for 4 days. Samples of these cultures were then prepared for microscopy. Microscope dishes were prepared as described in Chapter 3.2.2 but the dishes containing cold grown cells were placed at 4 °C to set and were cooled during transport to the microscope. Then, a cold shock experiment was performed which included perfusion of warm ASW for 1 min to prepare the cells for cold shock as described in 5.2.2.1.

5.2.2.6 Processing of fluorescence and temperature recordings

The procedure of processing fluorescence recordings and the determination amplitude and time delay of responses is described in Chapter 3.2.3. The duration of a Ca^{2+} elevation was defined as the peak width measured at half maximal amplitude. All error bars shown represent standard error of the mean.

5.2.3 Statistical analysis

Statistical analysis was performed as described in Chapter 4.2.5.

5.2.4 Growth curves of PtWT after cold shock using ASW with or without Ca^{2+}

A growth curve was performed using cells that experienced a cold shock with and without external Ca^{2+} to inhibit Ca^{2+} signalling. 90 mL of PtWT cells in early exponential phase grown in 18 °C ASW were distributed into two falcon tubes and centrifuged (1000 g, 6 min). The two pellets were re-suspended in 25 mL -Ca^{2+} ASW (0 mM $CaCl_2$, +200 µM EGTA) and 25 mL standard ASW, respectively. 10 mL of each washed culture (= 25 x 10^6 cells) were distributed into two falcon tubes each and the cells were centrifuged again. A shock treatment followed by quickly adding 20 mL of different types of ASW: Pellets washed with

-Ca^{2+} were shocked with 4 °C -Ca^{2+} ASW or 22 °C -Ca^{2+} ASW. Pellets washed with +Ca^{2+} ASW were shocked with 4 °C +Ca^{2+} ASW or 22 °C +Ca^{2+} ASW. Cold shocked samples were immediately placed on ice after resuspension. To restore external Ca^{2+} contentration, 10 mL of 20 mM Ca^{2+} ASW of matching temperature was added to -Ca^{2+} samples after 5-10 min, whereas +Ca^{2+} samples received ASW of matching temperature with standard Ca^{2+} content (10 mM).

Two mL of each treated culture were then added to 30 mL of 4 °C or 22 °C ASW (triplicates), leading to a starting population of 7 x 10^5 cells/mL. Two separate growth curve experiments were prepared this way, one at 4 °C and the other at 18 °C ambient temperature with identical illumination regimes (16/8 h of ~60 µE m^{-2} s^{-1}).

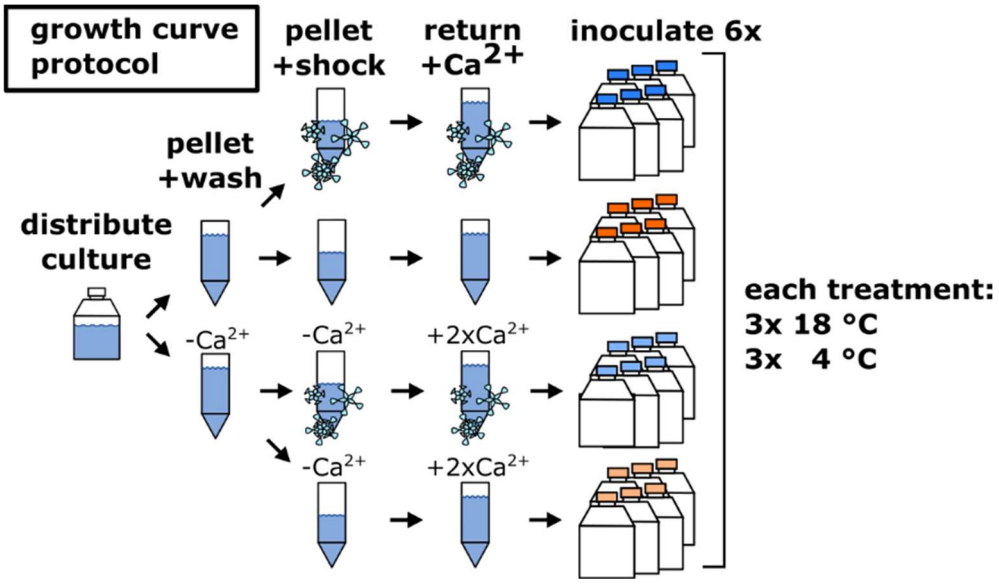

Figure 5.1: Schematic of the growth curve protocol.

A culture was divided and wither cold shocked or not cold shocked with ASW ± Ca^{2+}. –Ca^{2+} = ASW – Ca^{2+} +200 µM EGTA, snowflakes indicate 2 °C cold shock treatment. Blue colour variations represent samples with an applied cold shock, orange colour variations represent room temperature controls. High intensity colours represent +Ca^{2+} treatments, whereas faint colours represent -Ca^{2+} treatments.

Photosynthetic efficiency (Fv/Fm) was monitored during the procedure to check for cell viability after $-Ca^{2+}$ treatments and/or cold shock treatments through PAM fluometry. One 1.5 mL aliquot was taken prior the first centrifugation step and one aliquot was taken 5 min after respective treatment application ($\pm Ca^{2+}$ cold shock and respective room temperature controls). These aliquots were transferred into a measuring cuvette, wrapped in aluminium foil and dark-adapted for 20 min at respective treatment temperatures. Fv/Fm ratios were measured using AquaPen-C (Photon Systems Instruments, https://psi.cz/).

Generation time was calculated as described in Chapter 4.2.4.

5.2.5 Phylogenetic analysis of diatom TRP channels.

Reference sequences of several human TRP channels (TRPP1-3, TRPV1-6, TRPM1-8, TRPA1, TRPC1-7), human TRP-like Polycystin Cation channels (TRPP2-3), insect TRPN1 and TRPA1 (*D. melanogaster*) and two distinct yeast TRPY (*R. tuloroides, M. pulcherrima*) were obtained from the NCBI protein sequence database (https://www.ncbi.nlm.nih.gov). The human TRPM8 sequence was used as query to detect TRP homologs in the genomes of *P. tricornutum, F. cylindrus, F. solaris, T. oceanica* and *P. nitzschia multiseries* available at the JGI protein database (https://mycocosm.jgi.doe.gov/). Accession numbers of sequences are listed in supplement appendix B.

Sequences were annotated with Interpro (https://www.ebi.ac.uk/interpro/) and ion transport domains (Pfam ID = PF00520) used to build a multiple sequence alignment, avoiding the highly variable N- and C-termini of many TRP channels. The sequences were aligned using the ClustalW algorithm with the BLOSUM cost matrix in Geneious v10.0.8 software (https://www.geneious.com). The phylogenetic tree was generated using MEGA7 (Kumar et al., 2016) with maximum likelihood method (100 bootstraps) based on the Poisson correction model. Positions with less than 85% site coverage were eliminated leading to a total of 178 tested positions.

5.3 Results

5.3.1 Short term cold shock results in a single cytosolic Ca^{2+} elevation

To test if diatoms employ Ca^{2+} signalling for sensing temperature, ASW of different temperatures was perfused over cells of the PtR1 strain expressing RGECO (Helliwell 2019) in a live-cell epifluorescence imaging setup.

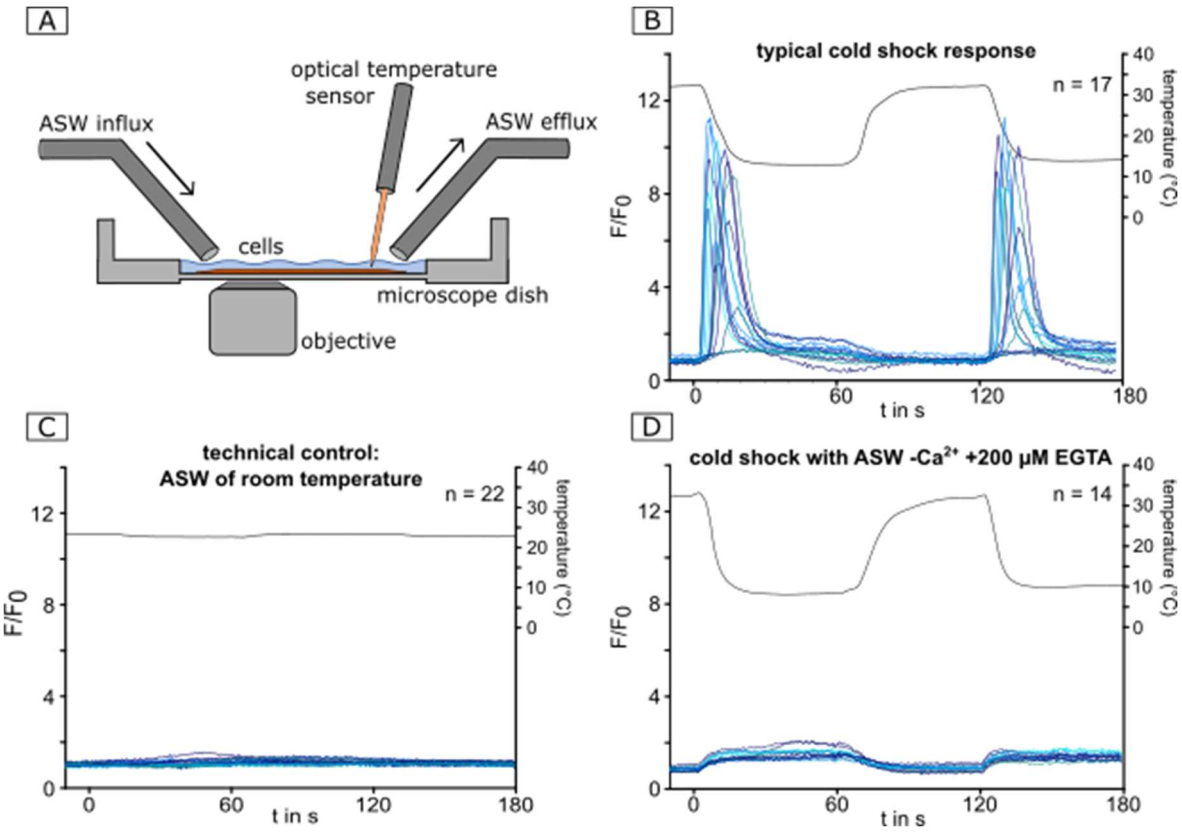

Figure 5.2: Cold shock causes a single cytosolic Ca^{2+} elevation and requires extracellular Ca^{2+}.
A) Schematic of experimental setup to observe Ca^{2+} elevations in PtR1 cells caused by changes in temperature **B)** Successive perfusion of PtR1 cells with ASW at 33 °C and 14 °C. Blue lines represent traces of relative R-GECO fluorescence in 17 representative cells. The black line represents the recorded temperature in the dish as a function of time. **C)** Experimental set up as in (B) but with the two ASW solutions allowed to equilibrate to room temperature. **D)** Perfusion of PtR1 cells in the absence of external Ca^{2+} using warm and cold ASW -Ca^{2+} +200 µM EGTA.

A single transient cytosolic Ca^{2+} elevation was observed in 97 % of cells (n = 63) when a rapid decrease in temperature was applied (Fig. 5.2 B). In contrast, a rapid temperature increase did not elicit an increase in cytosolic Ca^{2+}. Reapplying the same treatment 2 min after the first resulted in a second cold shock response without attenuation, though the number of cells responding was lower (81 %, n = 63; Fig. 5.2 B). The cold induced Ca^{2+} elevation is not an artefact caused by switching of the perfusion system or differences in ASW media as no response was recorded in cells perfused with ASW allowed to equilibrate to room temperature (Fig. 5.2 C).

To test whether the cold shock response requires external Ca^{2+}, the experiment was repeated with Ca^{2+}-free ASW Ca^{2+} containing 200 µM EGTA. This successfully abolished the large cold-induced Ca^{2+} elevation (Fig. 5.2 D). Notably, a minor increase in baseline fluorescence correlated with low temperature. As fluorescence emission from fluorescent proteins exhibits a degree of temperature dependence, it was assumed that this is likely due to temperature-dependent changes in R-GECO fluorescence and was not analysed further (Ohkura et al., 2012).

5.3.2 The characteristics of Ca^{2+} elevations relate to the degree of cold shock

Ca^{2+} elevations induced in response to a stimulus may present in a graded manner whereby Ca^{2+} elevations are proportional to stimulus strength or in an “all or nothing” manner, where Ca^{2+} elevations are of similar magnitude as long as a threshold is met. To test this, the magnitude of the PtR1 cold shock response in relation to duration and magnitude of cold shock was examined. Cells were perfused with warm ASW (34 °C in the dish) and then switched to cold ASW for varying durations (4, 7, 9, and 26 seconds) followed by sealing of the perfusion valve. In this setup, change in duration of cold shock also affected the maximum rate of temperature decrease.

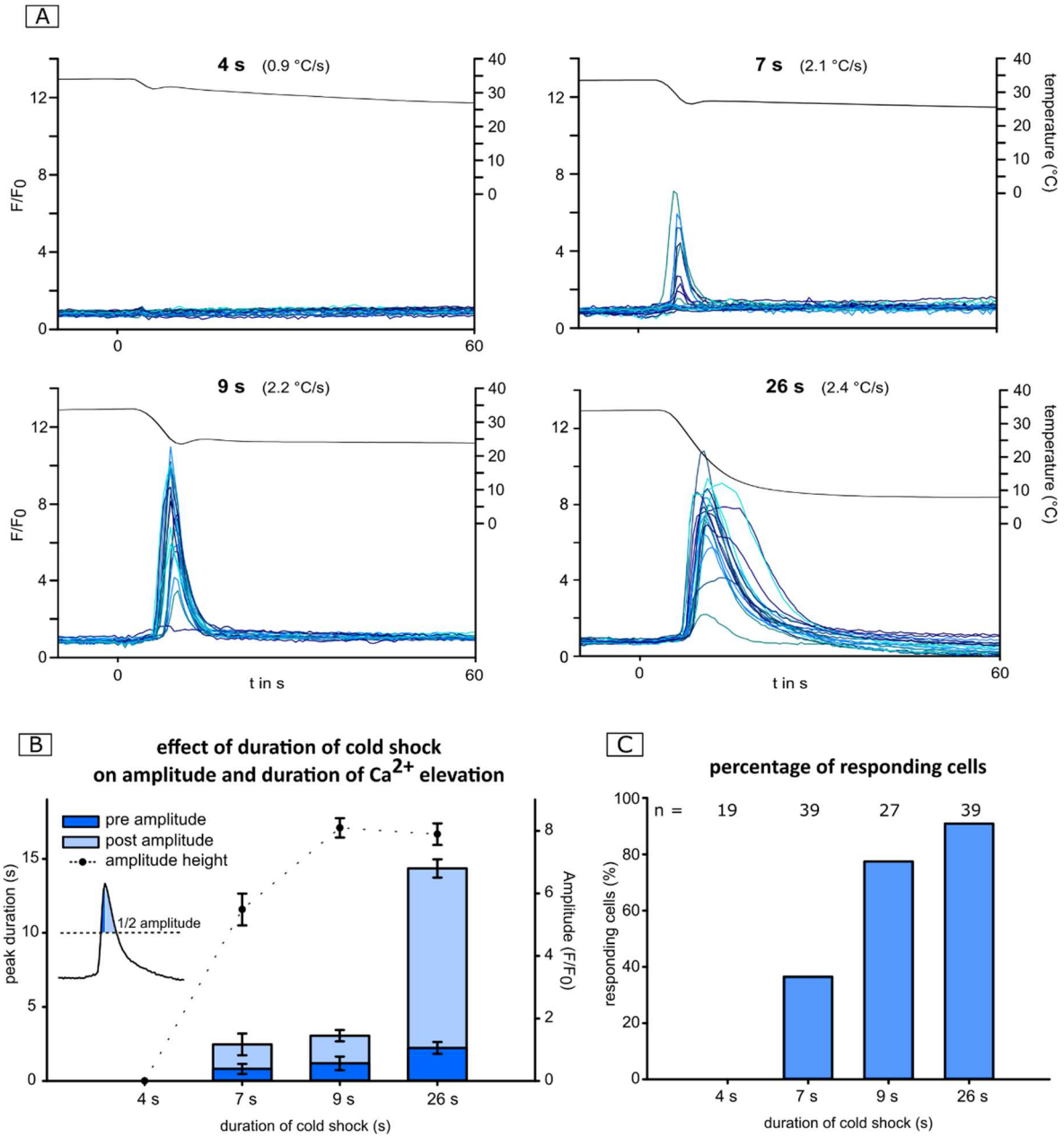

Figure 5.3: Cold-shock induced Ca^{2+} elevations correlate with duration of cold shock.

A) Four representative experiments showing 20 traces of PtR1 $[Ca^{2+}]_{cyt}$ when exposed to increasing durations of cold shock starting at t = 0. Data for 4, 7, 9 and 26 s of cold shock duration were compiled from 2, 3, 2 and 1 individual experiments, respectively. The maximum rate of temperature drop (ΔT/s) is shown in brackets. **B)** Duration of Ca^{2+} elevations shown as full width at half maximum amplitude in relation of the duration of cold stimulus. The duration is divided into a pre- and post-amplitude component (dark and bright blue, respectively). The average amplitude (dashed line) of responding cells in relation of the duration of cold stimulus is also shown. **C)** Pooled total numbers of cells within each treatment group (n) and the percentage of those which showed cooling-induced Ca^{2+} elevations**.**

No Ca^{2+} elevations were recorded in response to a very brief cold shock with relatively slow maximum temperature drop rate (Fig. 5.3 A 4s). Note that the temperature in the dish continued to decrease slowly towards room temperature, which also did not evoke a Ca^{2+} elevation.

When magnitude and rate of temperature drop increased, cells showed Ca^{2+} elevations. The duration of the Ca^{2+} elevation increased significantly with cold shocks of larger magnitude (One-way ANOVA on ranks $P>0.001$ for both pre- and post amplitude elevation-duration) (Fig. 5.3 B). More precisely, the only non-significant difference in response-duration was observed between the pre-amplitude component for the 7 s and 9 s cold shock (Dunn's post-hoc test $P = 0.451$) (Fig. 5.3 B).

The amplitude also increased significantly with larger cold shock magnitude (one way ANOVA on ranks $P <0.001$), but did not increase further with cold shocks longer than 9 s (Dunn's pairwise comparison $P = 1.000$ for 9 s vs 26 s amplitude, $P<0.011$ for all other comparisons) (Fig. 5.3 B). Although a cold shock of 26 or 9 s duration evoked a Ca^{2+} elevation of similar amplitude, the duration of the Ca^{2+} elevation, in particular the post-amplitude component, was greatly increased with longer shock duration (Fig. 5.3 B).

The percentage of responding cells also correlated positively with longer shock duration (Fig. 5.3 C)

Taken together, the amplitude and duration of the Ca^{2+} elevation is determined by the magnitude of the cold shock.

5.3.3 Ca^{2+} elevations correlate with rate of temperature decrease

To address whether the rate of temperature change influenced Ca^{2+} elevations, PtR1 cells were shocked with cold ASW at three different perfusion rates.

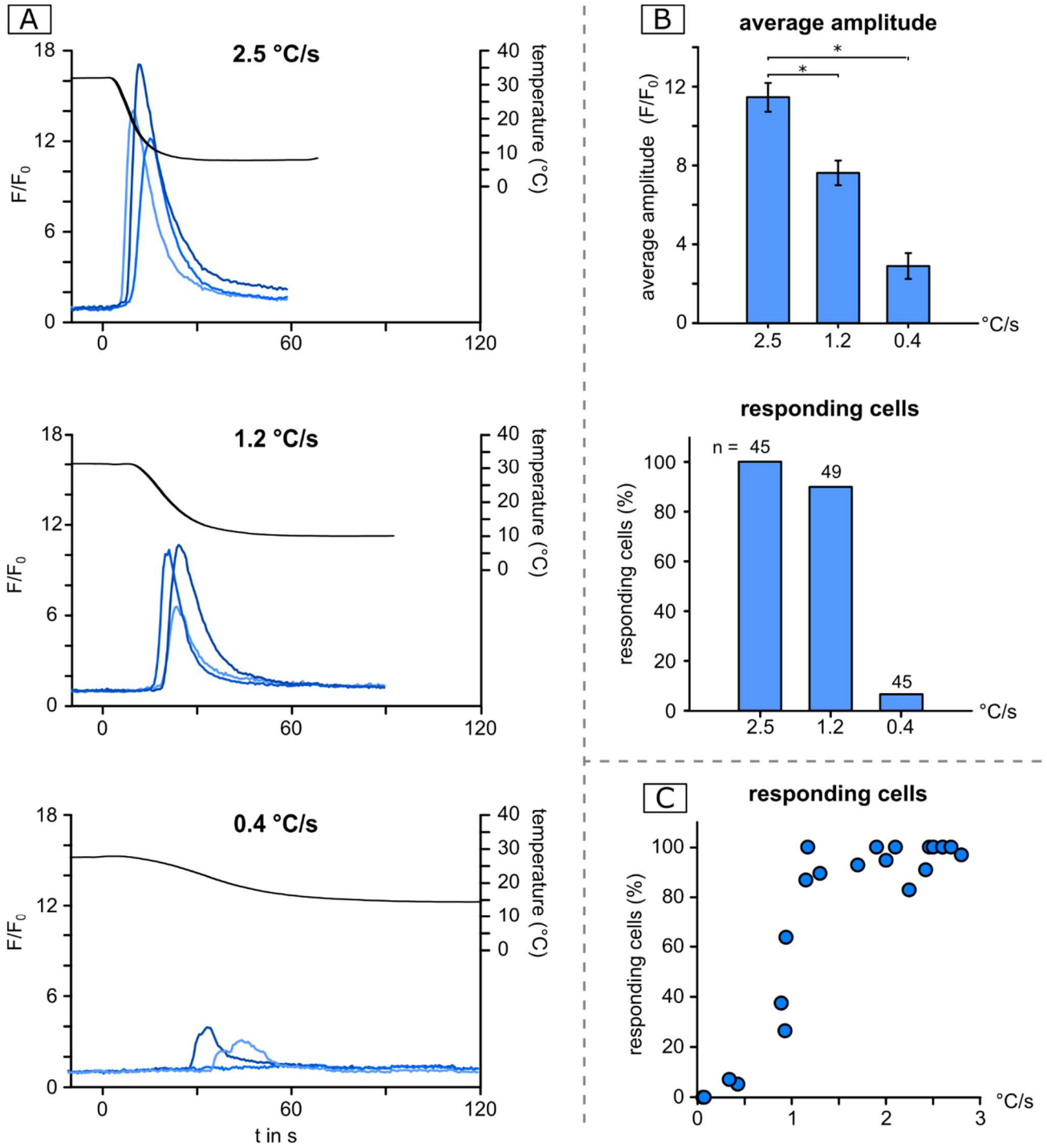

Figure 5.4: Amplitude of Ca^{2+} elevations and ratio of responding cells correlate with speed and magnitude of T-drop.

A) Three representative traces of P.tR1 fluorescence showing cold shock-induced Ca^{2+} elevations in dependence of temperature drop rate. **B)** Average amplitude (SEM) and percentage of responding cells in relation to temperature drop rate. Data compiled from two separate experiments per treatment group **C)** Percentage of responding cells as a function of maximum temperature drop rate in °C/s in 21 separate experiments.

An unavoidable consequence of altering the rate of perfusion for this experiment was that the perfusate slowly equilibrated to room temperature. This led to lower temperature-maxima and higher temperature-minima with slower perfusion speeds, with an absolute temperature decrease of 25, 22 or 13 °C for the 2.5, 1.2 and 0.4 C°/s treatments, respectively (Fig. 5.4 A).

Faster cold shocks and larger total drops in temperature led to more and more pronounced Ca^{2+} elevations (Fig. 5.4 A). The amplitude significantly increases with faster temperature drop rates (One way ANOVA on Ranks P>0.001, Dunn's pairwise comparison P>0.001 for all but 1.2 vs. 0.4 C°, which was found non significant) (Fig. 5.4 B). At a low temperature drop rate of 0.4 °C/s only 2 of 45 cells responded with a weak 3-fold fluorescene intensity.

By assessing a wide range of temperature gradients, a temperature decrease rate of approximately 1 °C/s provokes a response in 50% of cells (Fig. 5.4 C). However, the variable of differences in total temperature decrease still applies and should be borne in mind.

5.3.4 Cold induced Ca^{2+} elevations initiate at the apex of cells

Ca^{2+} elevations induced by hypo-osmotic shock (Chapter 3) initiate at the apex of cells. To test whether this also applies to the cold response, the Ca^{2+} elevations of three representative cells were analysed more closely.

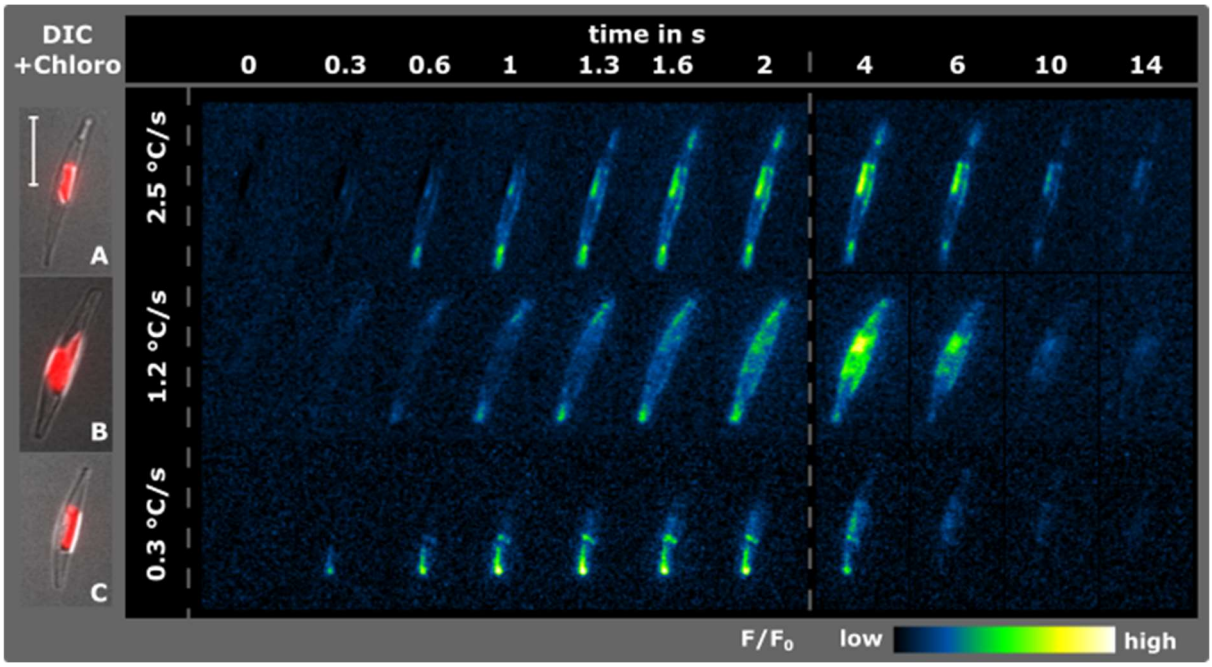

Figure 5.5: Cold shock induced Ca2+ elevations initiate at the apex of cells.

False colour images of three PtR1 cells showing cold induced Ca2+ elevations in response to cold shock of three different temperature gradients. The spectrum of colours represent fold fluorescence increase in relation to resting state fluorescence. t_0 = relative resting state fluorescence (F_0), $t_{0.3}$ = initiation of the Ca^{2+} elevation. DIC images of respective cells with overlay of chlorophyll auto-fluorescence (red) are shown in the left panel. The scale bar represents 10 µm.

Ca^{2+} elevations in response to cold shock initiate at the apex of cells and can form independently from each other (see cell B vs. C). However, with sufficient rate of temperature drop, Ca^{2+} elevations occur more or less simultaneously in both central and peripheral regions (see t = 0.3 - 0.6 s for cell A). Ca^{2+} elevations did not spread across the whole cell when maximum temperature drop rate was relatively slow (cell C vs A and B). Again, the duration and intensity of Ca^{2+} elevations depend of stimulus strength.

5.3.5 PtR1 cold shock response is dependent on temperature change but is more sensitive at lower temperatures

The cold shock response may be may be either triggered by temperature change or by meeting a low threshold temperature. In the latter scenario, the cold shock response may be elicited "retroactively" if the Ca^{2+} signalling is inhibited during the cooling process. To test this, cells were rapidly cooled using ASW $-Ca^{2+}$, then perfused with cold ASW $+Ca^{2+}$, followed by a standard ASW $+Ca^{2+}$ cold shock.

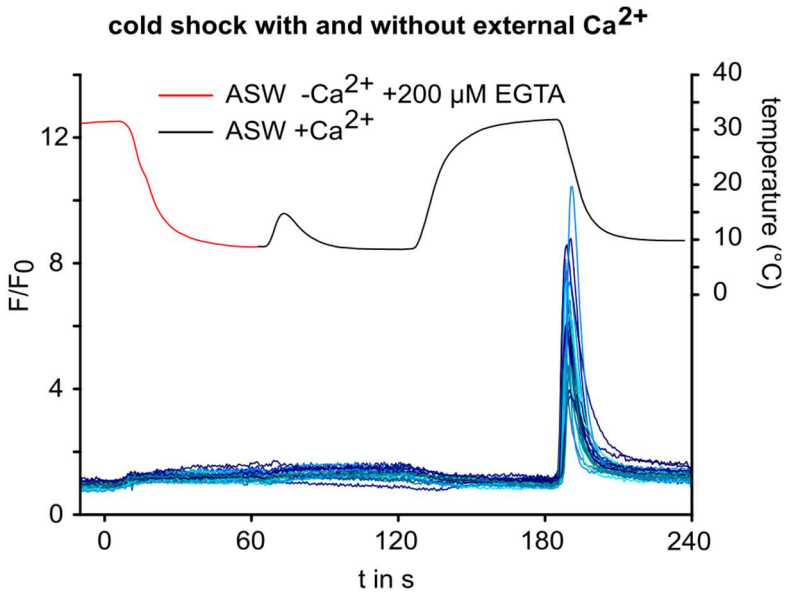

Figure 5.6: PtR1 cold shock response requires change in temperature.

A) 23 representative traces of $[Ca^{2+}]_{cyt}$ of PtRG cells which were subject to a cold shock without external Ca^{2+} (ASW $-Ca^{2+}$ +200 µM EGTA) which was followed by perfusion of cold ASW $+Ca^{2+}$ (black line) and an additional cold shock with external Ca^{2+}. Only the cold shock with external Ca^{2+} resulted in a response. The minor increase in temperature at 70s was caused by the perfusion tubing network giving rise to a slight warming prior to perfusion of the $+Ca^{2+}$ cold medium. Three additional experiments were performed with identical results.

When PtR1 cells were cold shocked without Ca^{2+} in the cold ASW (Fig. 5.6), no Ca^{2+} elevation occurred as previously shown (Fig. 5.2 C). When external Ca^{2+} was reintroduced to the cold shocked cells at the lower temperature, there was still no Ca^{2+} elevation (t = 60 s) (Fig. 5.6). However, a Ca^{2+} elevation did occur if the cells were returned to a higher temperature and subjected to a standard ASW +Ca^{2+} cold shock (t = 120-240 s). This indicates that the responsible Ca^{2+} elevation is triggered by a rapid drop in temperature rather than low absolute temperature.

Although a fast rate of temperature drop is clearly more effective in eliciting strong Ca^{2+} elevations, it could still be possible that the temperature range at which this change occurs plays a role, too. To test this, cells were treated with cold shocks at different starting temperatures (33 °C and 23 °C), aimed to apply a similar total drop in temperature (c. 10°C).

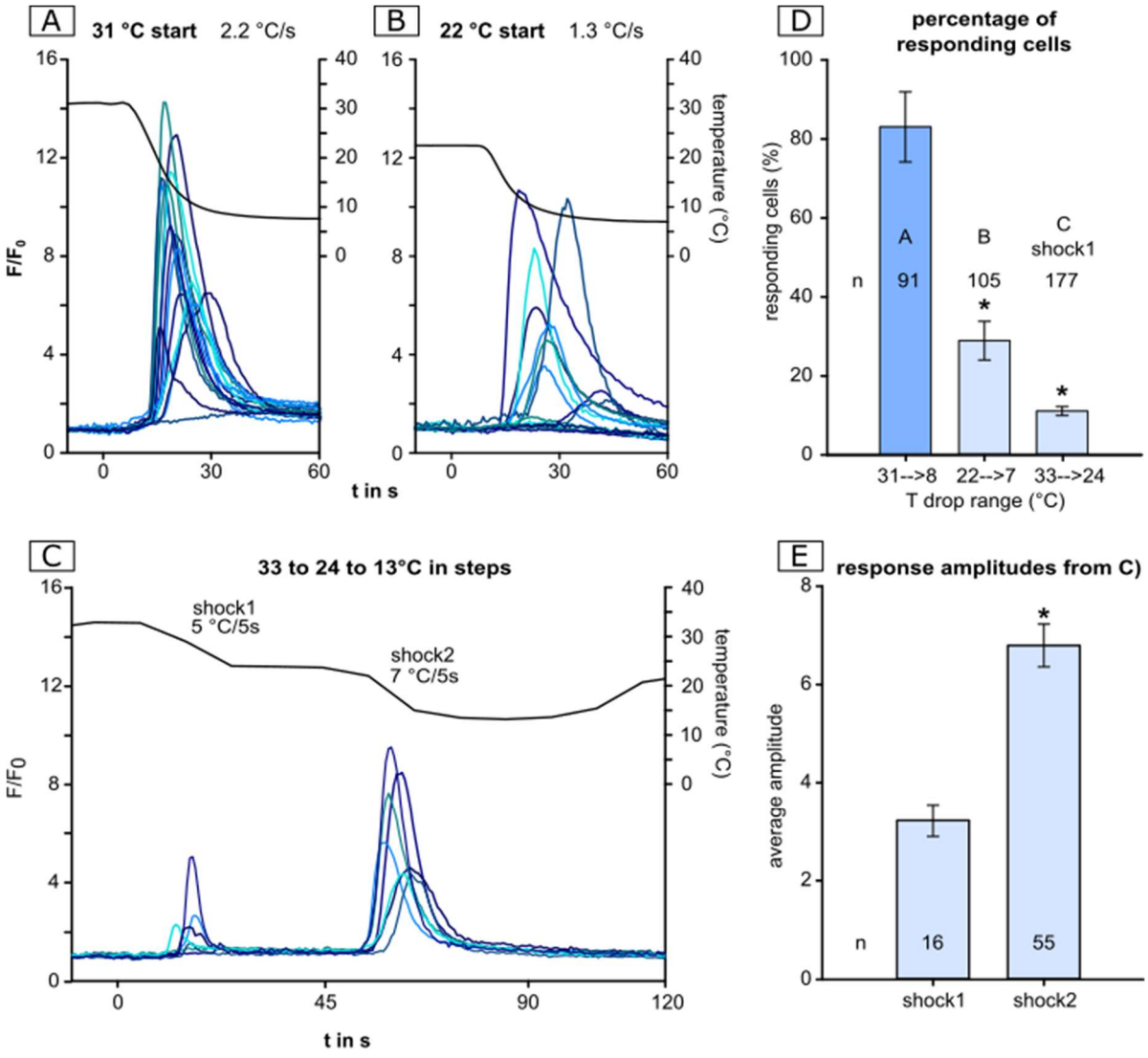

Figure 5.7: PtR1 cold shock response is more sensitive at lower temperature range.

A) 16 representative traces of PtR1 fluorescence in response to a relatively strong cold shock from 31 to 8 °C. **B)** The same treatment but with lower starting temperature of 23 °C. 16 representative traces. **C)** The temperature drop is applied in two steps (shock1: 0-45 s, 33 to 24 °C; shock2: 45-90 s, 24 to 13 °C). 7 representative traces. **D)** Percentage of cells responding to treatment A, B and C shock1 (3, 7 and 2 separate experiments, respectively). **E)** Average amplitude (SEM) of Ca^{2+} elevations of responding cells from experiment (C).

Cells were subjected to cold shock treatments with different starting temperatures (33 or 22°C) but the same ending temperature (7°C) (Fig. 5.7 A). The treatment of the larger temperature drop gave larger Ca^{2+} elevations and caused significantly more cells to respond (Fig 5.7 D, two-way ANOVA with Tukey post-hoc test: $P < 0.001$ compared to both other treatments). However, the maximum temperature change rate was higher in A.

Cells were then subjected to a total temperature drop of 18 °C, separated into two consecutive shocks covering a higher (33-24 °C) and lower (24-15 °C) temperature range, respectively (Fig 5.7 C). The second shock gave Ca^{2+} elevations of higher magnitude (Fig D, two-way ANOVA with Tukey post-hoc test: $P = 0.044$ and a higher percentage of responding cells (shock1 26 ± 5 % vs. shock2 81 ± 3 %; n = 177).

This confirms that the *P. tricornutum* cold shock response is dependent on absolute temperature drop range, but also indicates that the cold shock response is more sensitive at lower temperature ranges.

5.3.6 Absence of external Ca^{2+} during a single cold shock does not impair long term growth at low temperature

Experiments were carried out to determine the potential role of Ca^{2+} elevations in regulating the physiological responses to cold shock. Cells were subjected to a cold shock in the presence or absence of external Ca^{2+} to inhibit cold-induced Ca^{2+} elevations, and long-term growth in the presence of external Ca^{2+} at two contrasting temperatures (4 and 18°C) was then observed.

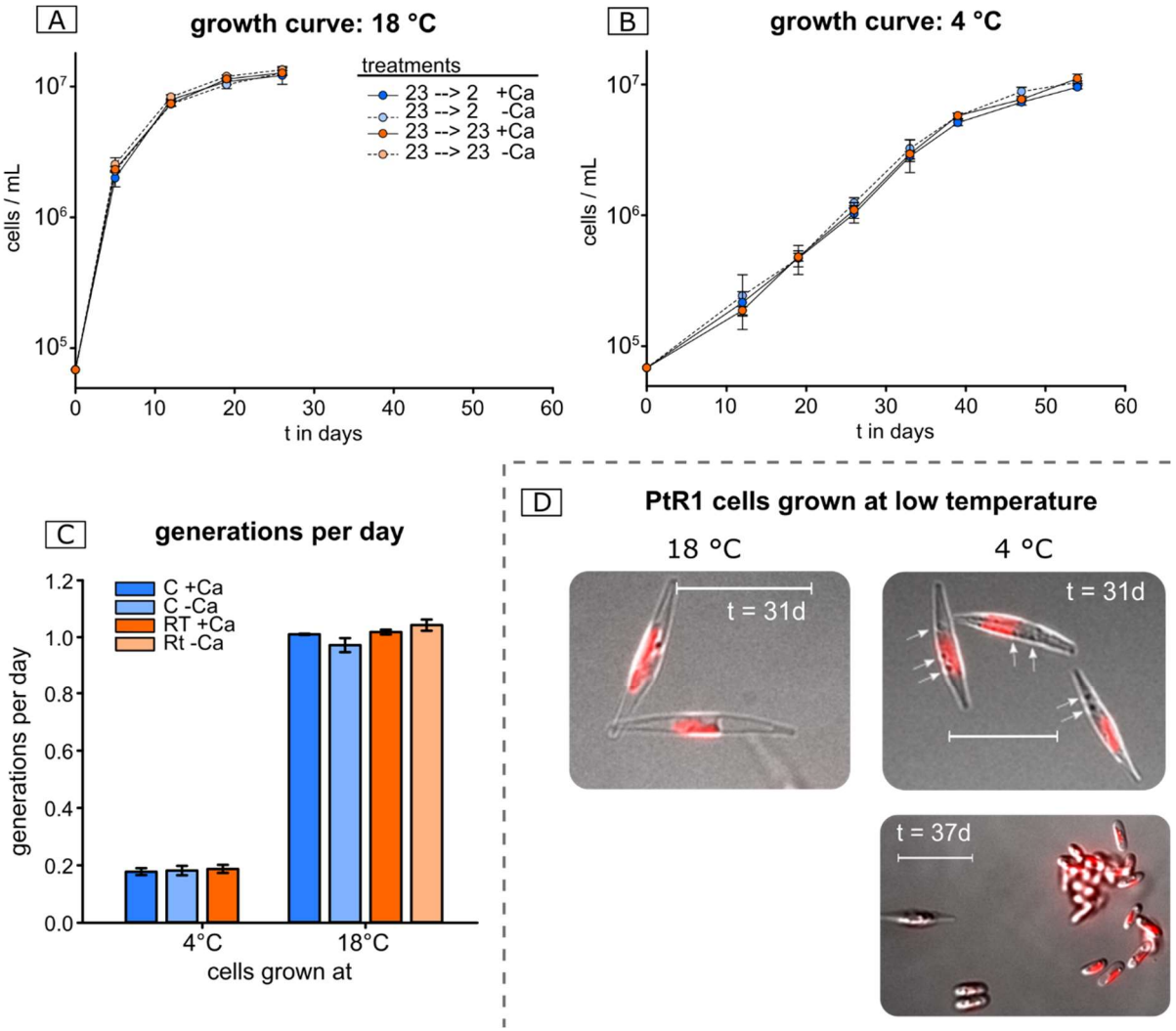

Figure 5.8: Inhibition of cold shock induced Ca^{2+} response does not affect growth at low temperatures.

A and B): Growth curves of PtWT cells grown at 18 or 4 °C ambient temperature. Before the start of the curve, cells were cold shocked with ASW with and without Ca^{2+}. **C)** Growth rate of cultures shown in A and B in relation to ambient temperature. Generations per day was calculated from day 0-5 and 12-33 and for the growth curves at 18 °C and 4 °C, respectively. At 4 °C ambient temperature, a Rt $-Ca^{2+}$ control was not included. **D)** DIC images of PtR1 cells grown at 18 or 4 °C. Red = chlorophyll auto-fluorescence, bar = 20 µm, arrows indicating accumulation of particles.

There was no significant difference in generation time of the -Ca^{2+} treatments compared to the controls when grown at 18 °C ambient temperature (one-way ANOVA P = 0.088) (Fig. 5.8 A and C). When placed in 4 °C ambient temperature, cells survived but grew slower compared to 18 °C (Fig. 5.8 A). However, there was again no significant difference between the generation times between the treatment groups (one-way ANOVA P = 0.839) (Fig. 5.8 C).

Growth at 4 °C ambient temperature for more than 30 days affected the appearance of cells (Fig. 5.8 D). Fusiform cells showed accumulation of particles and abundance of oval cells was increased, indicating that long term growth at low temperature affects cell physiology and may provoke transition into the oval morphotype (de Martino et al., 2011). However, nutrient limitation may also be involved as nutrients were not supplemented for this period.

Neither –Ca^{2+} treatments nor cold shocks affected photosynthetic efficiency. The pre-experiment Fv/Fm ratio of 0.45 stayed between 0.45 – 0.49 within 10 min after shock application irrespective of the treatment.

Taken together, the presented data suggests that impairment of the cold shock induced Ca^{2+} response does not prevent the cells from acclimating to low temperature.

5.3.7 Cold-acclimated cells still respond to cold shock.

Physiological changes in cold-acclimated cells may make them less responsive to cold shock. To test this, PtR1 cells were acclimated to 4 °C or 18 °C ambient temperature for four days and were then treated with a cold shock.

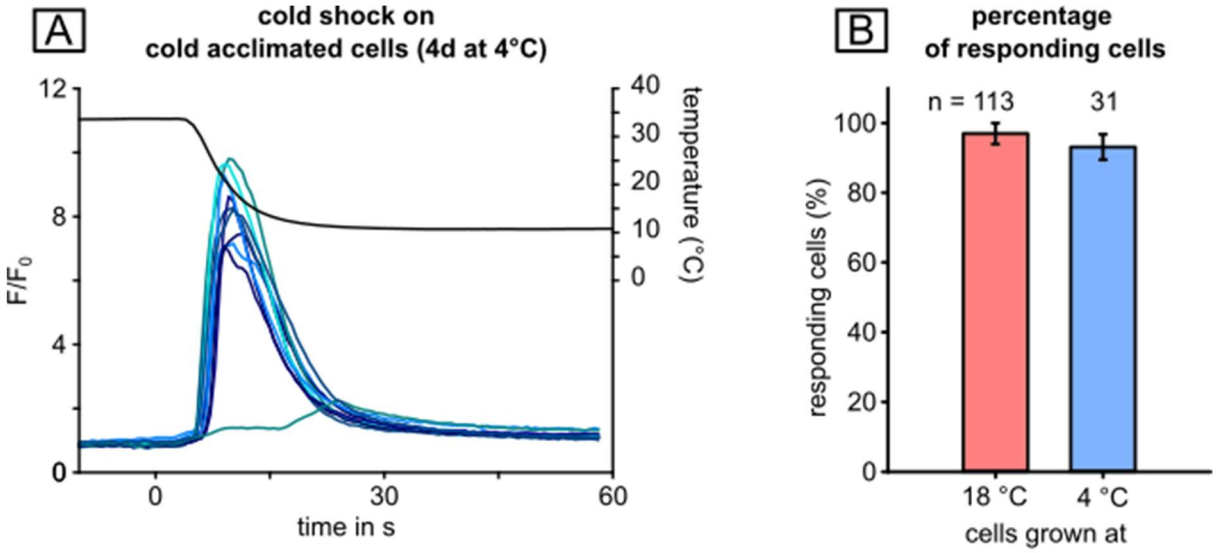

Figure 5.9: Cells acclimatised to 4 °C still exhibit cold shock-induced Ca2+ elevations.
A) Representative fluorescence traces of cold-acclimated PtR1 cells in response to cold shock. Four separate experiments with maximum temperature drop-rates between 2.2 - 3.2 C°/s were performed with similar results. The control culture was grown at 18 °C ambient temperature (two independent experiments). **B)** The percentage of cells at each acclimation temperature responding to a cold shock.

Cold acclimated cells still showed a typical cold shock response coinciding with the drop of temperature in the dish (Fig 5.9 A). There was also no significant difference in the percentage of cells exhibiting a response (Fig. 5.9 B). This suggests that *P. tricornutum* still responds to cold shock regardless of temperature acclimation state.

5.3.8 Identification of the Ca^{2+} channel(s) responsible for the cold shock induced Ca^{2+} response

Ion channels are primarily responsible for the generation of Ca^{2+} elevations in Ca^{2+} signalling processes. In animal systems, transient receptor potential channels (TRP) are known to underlie Ca^{2+} signalling in response to temperature change. TRPs have also been identified in diatoms (Verret et al., 2010), but their relation to other cold sensitive TRP channel classes (TRPM8 and TRPA1) is unknown. To address this, homologs of animal TRP channel sequences were identified in diatoms using the MMETP database and phylogenetically analysed.

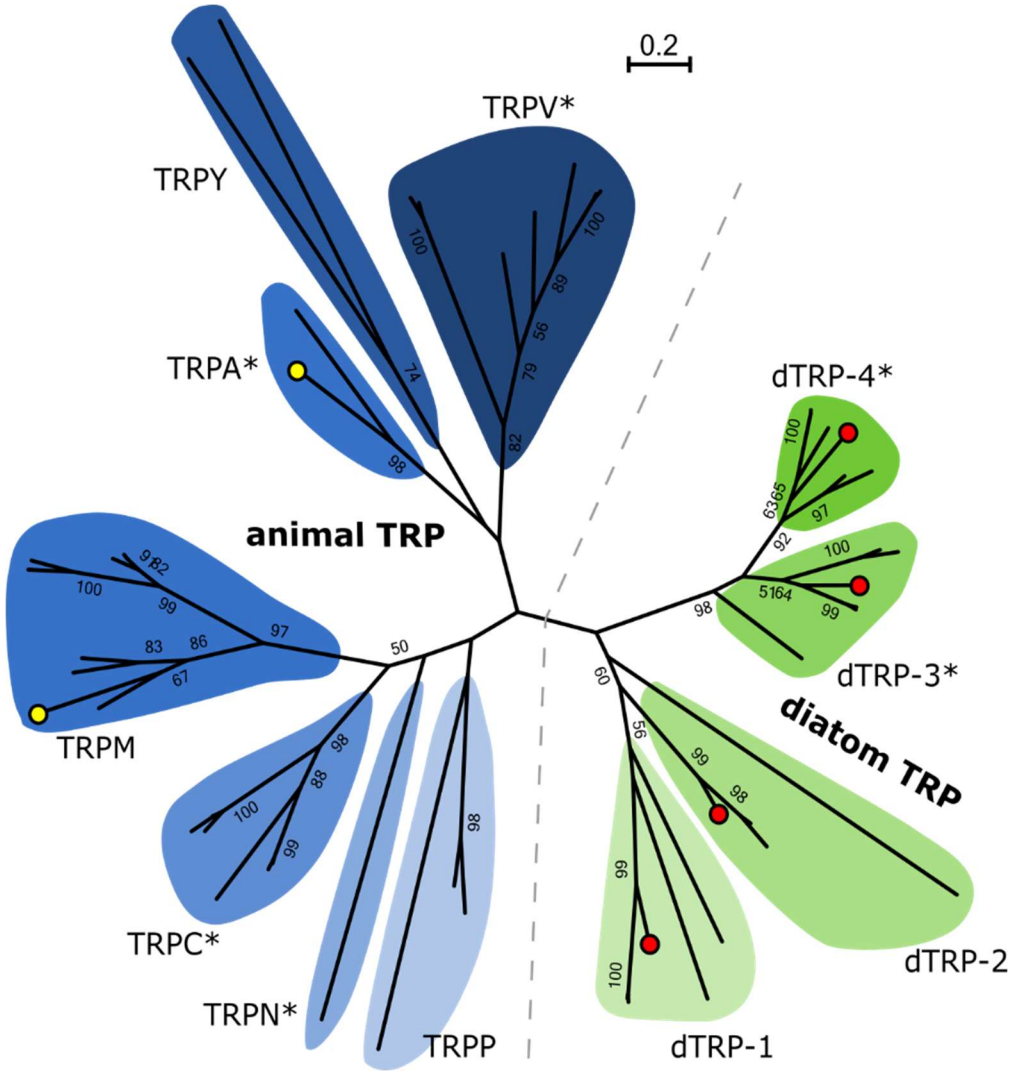

Figure 5.10: Diatom TRP channels are distinct from animal TRP channels.

A) Phylogenetic tree based on the maximum likelihood method (200 bootstraps; only values >50 are shown) generated with MEGA7 comparing the ion transport domains of human TRPs (TRP-P/ -C/ -M/ -A/ -V), insect TRPN1 and TRPA1 (*D.melanogaster*) and yeast TRPY (*R. tuloroides, M. pulcherrima*) with various TRP channel sequences found in diatoms (*F. solaris, T. pseudonana, P. tricornutum, Pseudo Nitschia multiseries, F. cylindrus, T. oceanica*; green). The four TRP channels of *P. tricornutum* are marked with a red dot, human TRPM8 and TRPA1 channels known for cold perception are marked with a yellow dot, clades containing channels with N-terminal ankyrin repeats are marked with an asterix. The scale shows the number of substitutions per site in the sequence.

The phylogenetic tree shows that ion transport domains of yeast/human/insect TRPs and TRP-like channels (TRPP) are all more similar to each other (Fig. 5.10 blue) compared to diatom TRPs (Fig. 5.10 green). Diatom TRPs can be divided into two major clades with two additional subclades each. The channels in diatom clades dTRP-3 and dTRP-4 have N-terminal ankyrin repeats similar to animal TRPA, TRPV, TRPC and TRPN channels. The four *P. tricornutum* TRPs are equally distributed among the four diatom TRP clades which may suggest different functions. Animal TRPM8 and TRPA1 channels are in two relatively distinct clades, suggesting that their cold sensitivity may have arisen independently (Liu & Qin 2011).

Taken together, diatoms do not have clear homologues of the cold sensitive human TRPs but instead have their own subset of distinct TRPs.

The highly variable C- and N-termini were not included in the alignment which made the evolutionary relationship of animal TRP-families slightly differ from literature (Pedersen et al., 2005)

To further investigate the potential role of diatom TRP in the cold shock response, the effect of three different pharmacological agents on generation of cold shock induced Ca^{2+} elevations was investigated: Menthol is a ligand that activates the animal cold sensitive TRPM8 channel (Yin et al., 2018). DMSO is proposed to mimic cold induced membrane rigidification – providing a potential trigger for some TRPs given their mechanosensitivity, including cold sensitive TRPA1 (Liu et al., 2017; Ranade et al., 2015). Ruthenium red (RRed) is a non-selective Ca^{2+} channel blocker shown to affect numerous TRP channels including TRPA1 (Andrade et al., 2008; Christensen et al., 2016; Silva et al., 2015).

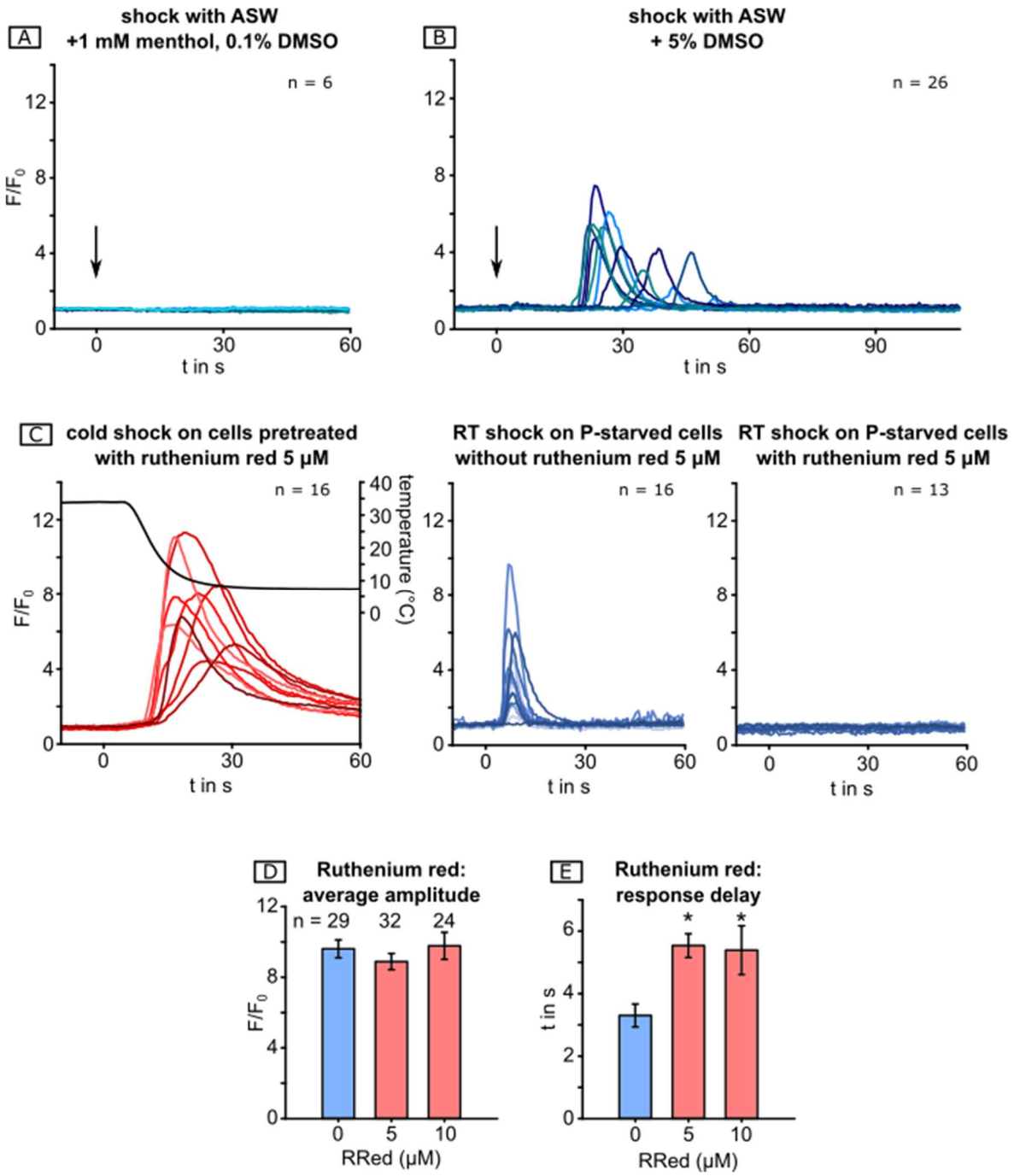

Figure 5.11: Effects of menthol, DMSO and ruthenium red on the PtR1 cold shock response.

A) Six representative traces of PtR1 fluorescence in response to ASW containing 1 mM menthol (+0.1% final DMSO as solvent carrier). An additional experiment with 100 µM menthol yielded identical results. **B)** 25 representative traces of PtR1 fluorescence in response to ASW +5% DMSO **C)** 16 representative fluorescence traces of PtR1 cells pre-treated with ruthenium red (5 µM final, 5 min pre-incubation) in response to cold shock. An experiment with 10 µM RRed was also performed with similar results; both conditions were repeated once. Blue traces show inhibitory effect of Ruthenium Red on the P-repletion response. **D)** Average amplitude (SEM) of responding cells pre-treated with ruthenium red. **E)** Time to onset of response for cells pre-treated with ruthenium red.

The TRPM8 channel agonist menthol did not provoke a Ca^{2+} response in PtR1 (responding cells: 0/23 to ASW +100 µM menthol; 0/18 cells to ASW +1 mM menthol) (Fig. 5.11 A).

Perfusion of PtR1 cells with ASW +5% DMSO did result in Ca^{2+} elevations in 50 % of observed cells (n = 25) (Fig. 5.11 B). Ca^{2+} elevations also occurred in response to ASW +1% DMSO, though the number of responding cells was reduced to 8% (n = 24) (not shown). The osmolarity of ASW diluted with DMSO was not adjusted – a hypo-osmotic shock component to the Ca^{2+} response can therefore not be excluded – however, a hypo-osmotic shock of 1% salinity decrease does not induce Ca^{2+} elevations (Helliwell et al., 2020b).

RRed inhibits Ca^{2+} elevations in phosphate-starved *P. tricornutum* cells in response to phosphate resupply (Fig. 5.11 C, blue traces, (Helliwell et al., 2020a). In contrast, RRed did not inhibit cold-shock induced Ca^{2+} elevations (Fig. 5.11 C, red traces), given that neither the average amplitude (one-way ANOVA P = 0.459) nor percentage of responding cells (one-way ANOVA P = 0.346) was significantly affected (Fig. 5.11 D). This implies that the cold response is based on a different mechanism than the P-sensing response in P-depleted cells. However, the time delay until cells responded to cold shock in RRed treated cells was significantly higher compared to non-treated cells (one-way ANOVA P = <0.001, post-hoc test P = 0.003) (Fig. 5.11 E), indicating that RRed affects an unknown component of the cold response.

A more direct approach to determine the involvement of an ion channel in a cell response are mutant strains with ion channel knock outs. Diatom EukCatA channels are a novel class of voltage-gated Na^+/Ca^{2+} channels that are related to single-domain voltage-gated Na^+ channels in bacteria ($BacNa_V$; Helliwell et al., 2019). TPC1 is a putative vacuolar Ca^{2+} release channel in plant tissues (Peiter et al., 2005; Wang et al., 2005) and is also found in diatoms (see Chapter 4). In PtR1, EukCatA1 and TPC1 were knocked out by K. Helliwell (Helliwell et al., 2019, see Chapter 4), respectively.

Since both $BacNa_V$ channels and plant TPCs have proposed roles in temperature perception (Arrigoni et al., 2016; Lin et al., 2005), the cold shock response of PtR1 *eukcata1* and *tpc1* was investigated.

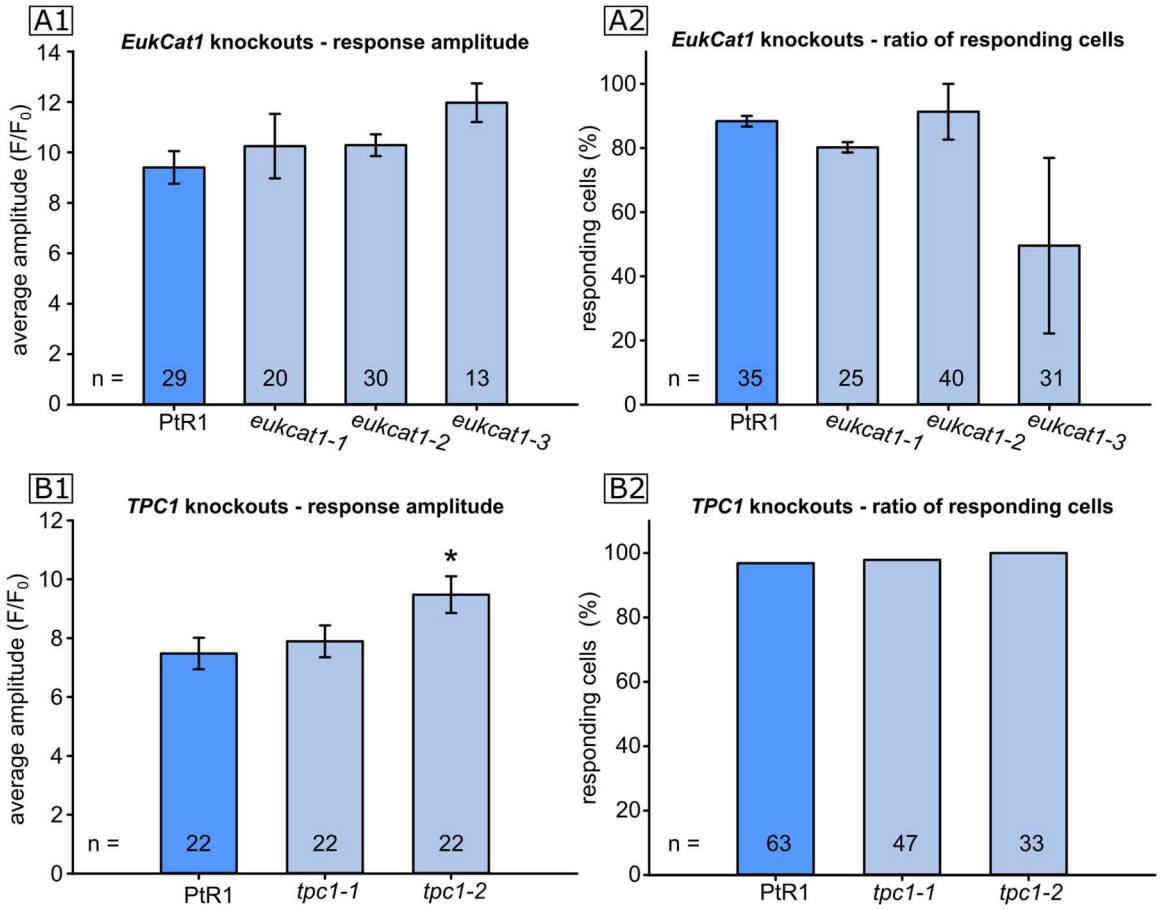

Figure 5.12: Neither TPC1 nor EukCatA1 channels are essential for cold shock response in PtR1. **A)** Average cold shock response amplitudes (SEM) and percentage of responding cells for PtR1 and three PtR1-*eukcata1* strains in response to cold shock (33 → 10 °C). Two independent experiments per strain. **B)** Average cold shock response amplitudes (SEM) and percentage of responding cells for PtR1 and two PtR1-*tpc1* strains in response to cold shock (33 → 10 °C). One independent experiment per strain.

Response amplitudes of *eukcat1* strains were not significantly different compared to PtR1 for all three mutant strains (one-way ANOVA P = 0.966) (Fig. 5.12 A1). The same is applies for the percentage of responding cells (Kruskal Wallis' one-way ANOVA on Ranks P = 0.067) (Fig. 5.12 A2). In one of the two experiments conducted with the *eukcat1-3* strain very few cells showed a cold shock response (22 %) leading to a large margin of error (Fig 5.12 A2 *eukcat1-3*). Since the replicate experiment did not reproduce this (77 % responded), a difference in the cold shock application, e.g. reduced perfusion rate due to a bubble in the perfusion system may be responsible.

The *tpc1-2* strain showed a significantly higher amplitude compared to the PtR1 and *tpc1-1* strain (one-way ANOVA P = 0.037, post hoc test P = 0.047) (Fig. 5.12 B1), while the percentage of responding cells was unaffected (Fig. 5.12 B2). It should be borne in mind that only one replicate experiment was performed on this temperature range for *tpc*. The significantly higher amplitudes of *tpc1-2* were not confirmed in an additional experiment which covered a smaller temperature range (22 → 10 °C, not shown).

Taken together, these results indicate that neither TPC1 nor EukCatA1 channels are essential for initiation of cold shock induced Ca^{2+} elevations.

5.3.9 Assessing potential cross-talk between hypo-osmotic and cold shock induced Ca2+ elevations

Hypo-osmotic and chilling stress can coincide in nature, e.g. an incoming tide affecting a warmed rock pool. In plants, the respective stress perception pathways are suggested to be in cross-talk, meaning that nodes within the signalling cascade of hypo-osmotic stress and cold stress perception may overlap and result in a similar stress response (Rensink et al., 2005).

To test if cold shock-induced Ca^{2+} elevations prime PtR1 for hypo-osmotic shock, cells were treated with a cold shock followed by a severe hypo-osmotic shock which would normally lead to high numbers of cells bursting and cell survival was investigated.

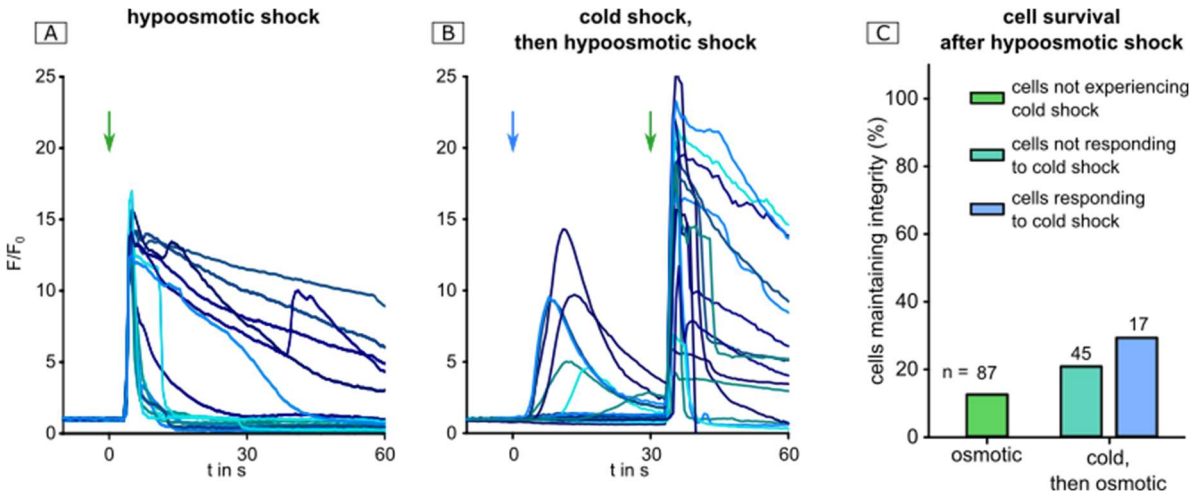

Figure 5.13: The effect of cold shock on hypo-osmotic shock cell survival.

A) 16 representative traces of PtR1 fluorescence in response to a lethal hypo-osmotic shock at t = 0 s (100% H_2O; green arrow). Bursting and leaking cells are represented by slowly decreasing traces of PtR1 fluorescence. The experiment was repeated twice with similar results. **B)** 16 representative traces of PtR1 fluorescence in response to a cold shock (22 to 8 °C; blue arrow) followed by a lethal hypo-osmotic shock at equal low temperature (green arrow). One additional experiment, similar results. **C)** Percentage of cells maintaining structural integrity (no leakage, bursting or collapse of organelles) during hypo-osmotic shock with and without previous cold shock. Cells that experienced prior cold shock are further differentiated into cells which did/did not show cold-induced Ca^{2+} elevations. Data was pooled from two independent experiments per treatment.

As presented in Chapter 3, a sudden and severe hypo-osmotic shock is lethal for *P. tricornutum*. This was confirmed in this experiment, in which a sudden shift towards fresh water caused 90 % of 87 cells to lose structural integrity within the observed timeframe of 2 min (Fig. 5.13 A+C). The traces of cells loosing structural integrity may show a very short Ca^{2+} elevation followed by a steep decrease in case of bursting or may show a gradual decrease in case slow leakage of cell contents. Traces of cells managing to maintain structural integrity also appear as a peak followed by a gradual decrease in fluorescence which may indicate exhausted but recovering Ca^{2+} efflux capacities.

When a relatively subtle cold shock was applied before the hypo-osmotic shock, a Ca^{2+} elevation occurred in 17 out of 62 cells (27 %) (Fig. 5.13 B+C). Those responding cells did not show a significantly higher survival rate compared to cells that did not respond nor experienced a preceding cold shock.

Taken together, the presented data suggest that the chance of surviving a potentially lethal hypo-osmotic shock was not increased for the cells with a preceding cold shock induced Ca^{2+} elevation.

Hypo-osmotic shock is putatively sensed through mechanosensitive Ca^{2+} channels which translate shifts in membrane tension into Ca^{2+} elevations (Chapter 3). Membranes may be the primary sensor for temperature and hypo-osmotic shock in *P. tricornutum*. A measurable cold shock-induced shrinkage or expansion of PtR1 cells would support this hypothesis and may furthermore indicate that both stimuli trigger the same ion channel. Thus, the cell area before, during and after cold shock was measured.

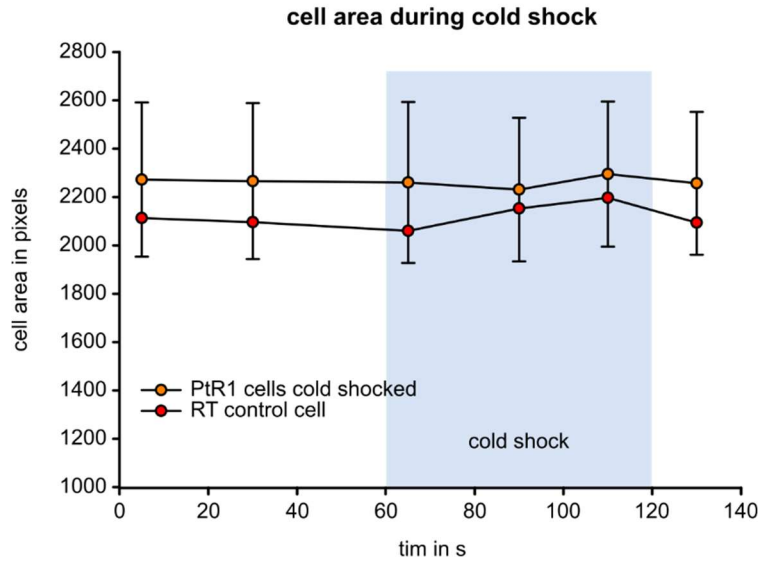

Figure 5.14: Cell area is largely unaffected by cold shock.

Average area of cross-sections of 12 PtR1 cells before, during (blue area) and after a cold shock (orange dots with StDev as error bars, temperature drop 33 to 8 °C, max. 3 °C/s). The red dots show the cell area of a single control cell at 33 °C throughout a similar timeframe. Cell size was determined manually on a DIC recording using ImageJ.

The applied cold shock was relatively fast and strong, which should induce a Ca^{2+} response in a high percentage of cells. However, cell size during cold shock was not affected compared to the pre- and post-cold shock conditions (Fig. 5.14).

To further test the degree of independence of the cold and osmotic Ca^{2+} signals, PtR1 Ca^{2+} elevations were monitored in response to simultaneous cold and osmotic treatments

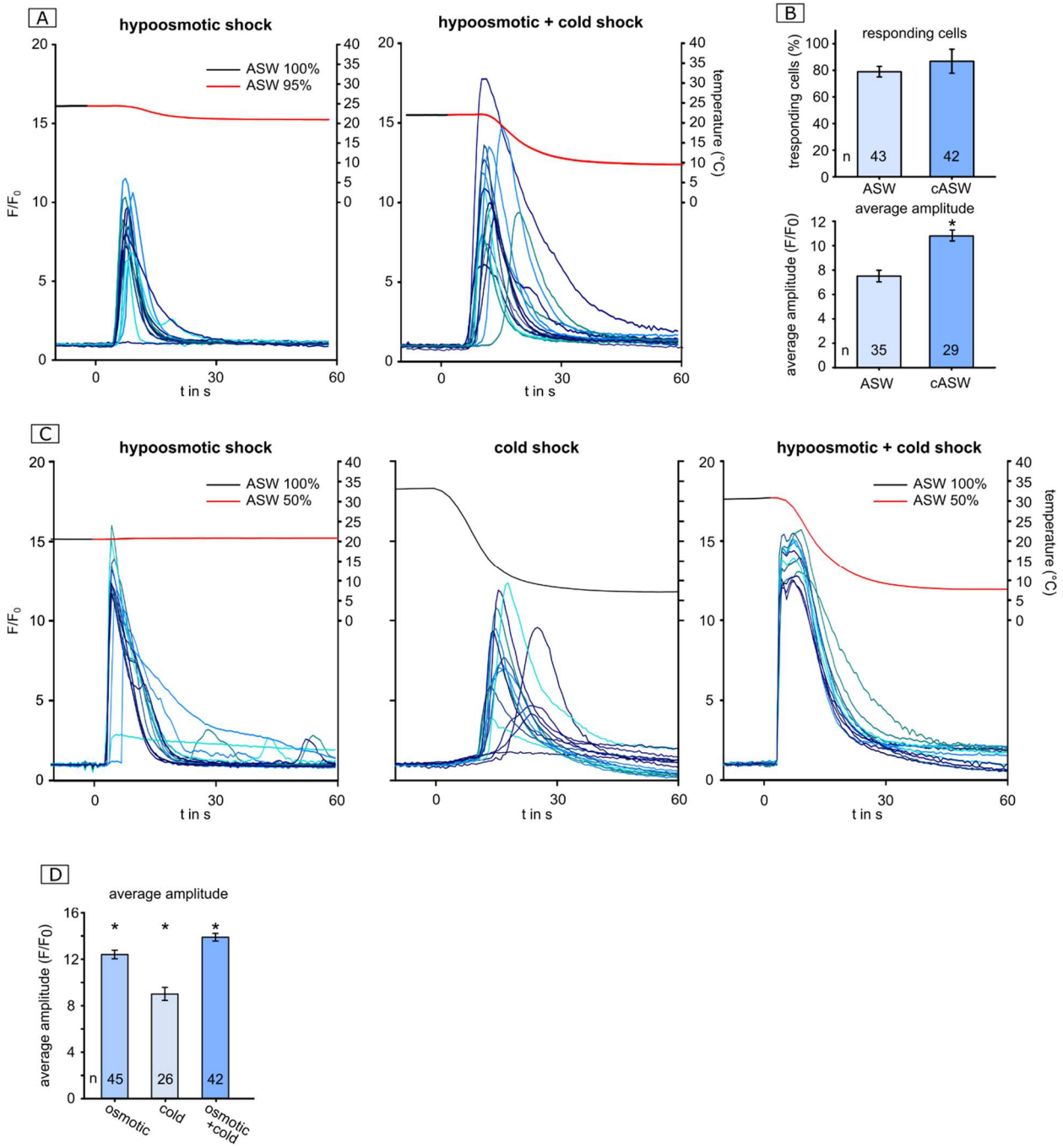

Figure 5.15: Effect of simultaneous cold- and hypo-osmotic shock on Ca^{2+} elevations.

A) 12 representative traces of PtR1 fluorescence in response to a sole hypo-osmotic shock (two additional experiments with similar results) or a simultaneous hypo-osmotic- and cold shock (10 °C drop in T, one additional experiment with similar results). **B)** Percentage of responding cells and the average response amplitude in (A). **C)** Similar procedure as in in (A) but with stronger hypo-osmotic- and cold shocks. 13 representative traces (two additional experiments per treatment). **D)** Average amplitude of responding cells in (C). For biphasic peaks the higher amplitude was chosen.

A subtle hypo-osmotic shock of 5 % drop in salinity resulted in single Ca^{2+} elevations of approximately 20 s duration (Fig. 5.15 A). With simultaneous cold and osmotic shock, the duration of Ca^{2+} elevations was longer and average amplitude and the Ca^{2+} elevation was significantly increased (Student's t-test $P < 0.001$, Fig. 5.15 B). However, the number of responding cells was not affected (Student's t-test $P > 0.05$; Fig. 5.15 B). A stronger hypo-osmotic shock to 50 % ASW resulted in steep Ca^{2+} elevations which all initiated 4 s after perfusion was switched (Fig. 5.15 C left). The elevations had a duration of approximately 20 s. In comparison, a strong cold shock from 34 to 8 °C triggered Ca^{2+} elevations with a less steep slope and with a longer delay of response initiation (≥10 s, Fig. 5.13 C middle). Combination of both shocks led to biphasic Ca^{2+} elevations in 71 % of 42 cells (Fig. 5.13 C right). The first peak was steep and quickly generated similar to the sole hypo-osmotic shock response (Fig. 5.13 C left). The second peak occurred 2.9 ± 0.2 s (SEM) later and was of slightly higher amplitude than the first peak in 24 out of 30 cells. The amplitudes of Ca^{2+} elevations caused by the three different treatments were all significantly different from each other (Fig. 5.13 D, with the cold shock causing the lowest and the combined cold- and hypo-osmotic shock causing the highest Ca^{2+} elevations (Kruskal-Wallis One Way Analysis of Variance on Ranks $P < 0.001$).

Taken together, hypo-osmotic induced Ca^{2+} elevations are influenced in magnitude when a cold shock stimulus is added. A biphasic Ca^{2+} elevation occurs when both shocks are relatively strong.

5.3.10 Cold shock response of *T. pseudonana*

To test whether the cold shock induced Ca^{2+} elevation is a conserved phenomenon in diatoms, *T. pseudonana* cells encoding the RGECO biosensor presented in Chapter 2 were treated with a cold shock.

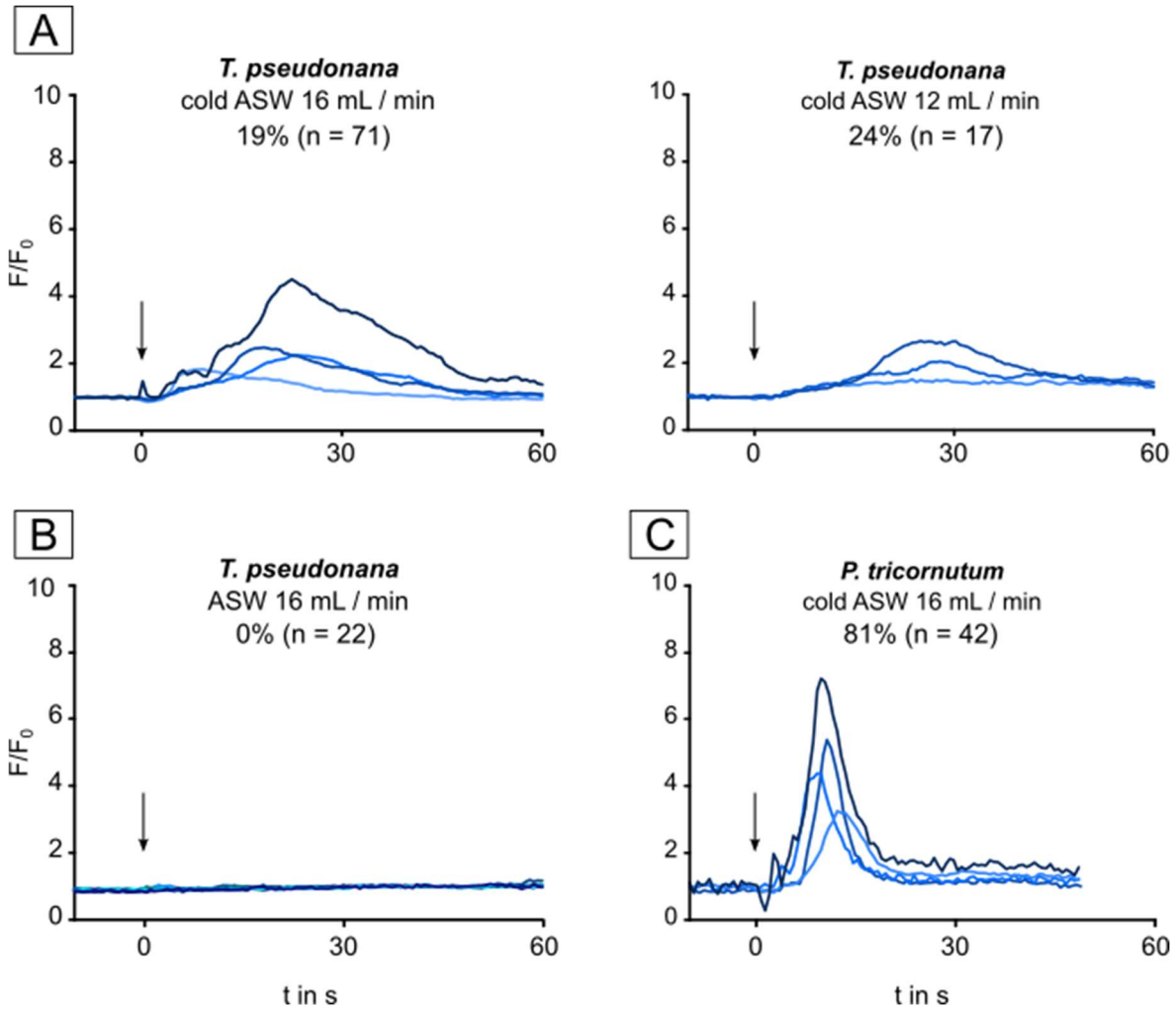

Figure 5.16: *T. pseudonana* also shows cold-induced Ca^{2+} elevations.

A) Four representative traces of *T. pseudonana* cells expressing cytosolic RGECO in response to a cold shock (arrows, 33 → 10 °C) administered at two different velocities. Percentage of responding cells and number of cells in the field of view are also shown. One experiment per condition. B) Treatment control with perfusion of ASW at room temperature. C) *P. tricornutum* cold shock response at a same temperature range for comparison.

T. pseudonana cells also generated cytosolic Ca^{2+} elevations in response to cold shock, and magnitude of these elevations may also depend temperature decrease rate (Fig. 5.16 A). As in P. tricornutum, ASW media equilibrated to room temperatures did not cause Ca^{2+} elevations (Fig. 5.16 B). Compared to *P. tricornutum*, cold induced Ca^{2+} elevations in *T. pseudonana* are less pronounced and less transient, and cells are less responsive to cold shock (19 % vs. 81 %, respectively) (Fig. 5.16 A and C). It should be borne in mind that heterologous expression of RGECO in T. pseudonana is still prevalent as described in Chapter 2. Taken together, these findings suggest that cold shock-induced Ca^{2+} elevations are conserved in diatoms.

5.4 Discussion

5.4.1 Dose dependent Ca^{2+} elevations in response to cold shock imply a regulatory role

This study demonstrates that *P. tricornutum* cells exhibit a single Ca^{2+} elevation in response to cold shock. The amplitude and likelihood of the Ca^{2+} elevation positively correlates with the rate and/or magnitude of temperature change rather than an absolute temperature. A response cannot occur when extracellular Ca^{2+} is absent. In addition, a response cannot be formed "retroactively" when Ca^{2+} is reintroduced to PtR1 after the cold shock is finished, further highlighting the importance of temperature change, rather than absolute temperature to elicit a response. There is a distinct spatial pattern of Ca^{2+} elevations which arise primarily at the cell apices.

However, the role of cold-induced Ca^{2+} elevations in *P. tricornutum* are not yet known, and it cannot be ruled out that the observed response has no physiological role and is rather a physical consequence of Ca^{2+} channel activation or generation of reversible membrane fractures during temperature drops. Since cold-induced Ca^{2+} elevations were also recorded in *T. pseudonana*, indicating that it is a conserved response, and since observed Ca^{2+} elevations in this study bear several parallels to the well-characterised plant cold shock response, a regulative role will be assumed for this discussion.

When comparing presented data with those of higher plant studies, some clear methodological differences need to be borne in mind. These include the use of bioluminescent aequorin as a Ca^{2+} reporter in many plant studies which has different Ca^{2+} binding, Ca^{2+} dissociation and light emission kinetics compared to RGECO, allowing to visualise more subtle Ca^{2+} elevations with a spatial resolution on single-cell scale in this study. Moreover, in plants, responses were generally studied from a mixture of cell types rather than single cells.

1. Like *P. tricornutum*, cold shock in *A. thaliana* root cells also induces a single transient increase in cytosolic Ca^{2+} of less than 30 s in duration (Knight 1999, Kiegle 2000). The magnitude of the cold induced Ca^{2+} elevations in plant roots can differ dependent on cell type (Kiegle et al., 2000). While different morphotypes of *P. tricornutum* may show different patterns of cold shock-induced Ca^{2+} elevations, only the fusiform morphotype was investigated in this study. In contrast to *P. tricornutum*, plants can show more complex Ca^{2+} elevations in response to cold shock than single peaks: Biphasic Ca^{2+} elevations occur at relatively slow temperature drop rates with the second phase having a duration of several minutes (Plieth et al., 1999) and Ca^{2+} oscillations have been observed in guard cells after cold shock (Allen et al., 2000). This indicates that the mechanisms underlying temperature sensing in diatoms may be less complex compared to plants.
2. Like *P. tricornutum*, **c**old shock induced Ca^{2+} elevations in plants are also primarily dependent on temperature drop rate rather than a threshold temperature (Minorsky and Spanswick, 1989; Plieth et al., 1999). However, it has been shown in plants that expression of multiple CBF transcripts in *A. thaliana* and wheat may depend on a temperature threshold rather than temperature change, indicating that mechanisms able to sense a temperature threshold may also be involved (Winfield et al., 2009, 2010; Zarka et al., 2003). It is unclear whether this also applies to *P. tricornutum* as the responses that occur in addition to the Ca^{2+} elevation are unknown.
3. Like *P. tricornutum*, *A. thaliana* root cells were shown to be more sensitive to temperature change at a lower temperature range than compared to a higher temperature when total drop in temperature was identical (Plieth et al., 1999). Plieth speculated that stronger Ca^{2+} elevations at lower temperatures may either represent an increased need for adaptation or were based on chilling-induced inhibition of Ca^{2+} efflux capacities, which may also apply for *P. tricornutum.*
4. Like *P. tricornutum*, external Ca^{2+} is essential to initiate a cold shock response in plants (Knight et al., 1996) which suggests the involvement of ion channels at the plasma membrane in both systems.

A major difference between *P. tricornutum* and plants is that Ca^{2+} elevations in *P. tricornutum* require faster shocks and larger total drops in temperature. *A. thaliana* root cells can respond to a temperature drop of 1 °C given a sufficiently fast temperature drop rate (Plieth et al., 1999), whereas *P. tricornutum* did not respond to a total temperature drop of less than 4.7 °C. Cucumber seedling root cells responded to a relatively small total temperature drop of 5 °C with temperature drop rate of ~0.33 °C/s (Minorsky and Spanswick, 1989), whereas *P. tricornutum* cells showed mostly no response over 9 °C with a slightly faster maximum drop rate of 0.4 °C/s.

A lower temperature drop sensitivity and the ability for reproductive growth at 4 °C may suggest that *P. tricornutum* has a larger temperature tolerance range compared to the investigated annual land plants (*A. thaliana*, tobacco, cucumber, wheat). However, soil and water buffer temperature change, suggesting that *P. tricornutum* simply does not encounter rapid temperature change as often as land plants so a much less sensitive and sophisticated temperature sensing toolkit may be required.

Cold-induced Ca^{2+} elevations in *P. tricornutum* bear some differences to those observed in neurons of homeothermic animals. In these, cold pain is predominantly sensed by nociceptors which are inactive at skin temperature levels and are activated by meeting a noxious cold threshold-temperature (<15 °C) (McKemy, 2018). Conversely, innocuous cooling is sensed by a different type of thermoreceptor whose firing rate increases with lower temperatures, and whose temperature threshold is likely raised through inactivating outward K^+ currents of heat-sensitive K^+ channels (González et al., 2017; McKemy, 2018). However, a similarity to cold induced Ca^{2+} elevations in *P. tricornutum* is that external Ca^{2+} is also necessary to invoke Ca^{2+} elevation in neurons, though here cytosolic Ca^{2+} generates the receptor potential for a subsequent action potential (McKemy, 2018).

5.4.2 The physiological consequence of cold shock-induced Ca^{2+} signalling

The data presented in this study raise questions about the role of the Ca^{2+} response to cold shock. The hypothesis that the cold shock-induced Ca^{2+} elevation is essential for cold acclimation and survival was not proven since inhibiting Ca^{2+} elevations by removing external Ca^{2+} did not affect growth rate of cold-grown cells.

1. The relatively subtle cold shock prior the growth curve may have not been stressful enough to impact growth capacity; regardless of whether external Ca^{2+} was present or absent during the cold shock. Limited support for this was found in the Fv/Fm measurements taken 5 min after application of cold shock ($\pm Ca^{2+}$) which did not differ from pre-experiment values, indicating that the delicate photosynthetic machinery did not experience cold-induced oxidative stress in this timeframe (Liu et al., 2018; Lukatkin, 2002; Ruban et al., 2012).
2. Ca^{2+} signalling may not be the only signalling system for cold shock perception in *P. tricornutum.* Other potential primary temperature sensors may include non-ion channel transmembrane proteins registering cold-induced changes in membranes such as histidine kinase 33 in bacteria (Murata and Los, 2006) or the G-protein regulator COLD1 in plants (Guo et al., 2018; Ma et al., 2015; Manishankar and Kudla, 2015), temperature sensitive phytochromes (Fortunato et al., 2016; Franklin et al., 2007; Qiu et al., 2019; Wang et al., 2019), nucleic acid-based thermometers (Sengupta and Garrity, 2013), or ROS levels (Huner et al., 1998; Miura and Furumoto, 2013). ROS is an important signalling agent and was shown to be involved in cell compartment specific modulation of the Redox network in response to cold shock and contributes to the cold acclimation and recovery program in plants (Dreyer and Dietz, 2018; Moller and Sweetlove, 2010; Suzuki and Mittler, 2006). Considering that most stress responses result in lowered metabolism in plants (Yuan et al., 2018), ROS induced “general” metabolic shutdown and redox modulation could have been sufficient to acclimate *P. tricornutum* to cold in this experiment. Recently, *P. tricornutum* cells expressing fluorescent ROS biosensors were generated, potentially providing much needed insight into cold-induced oxidative stress in diatoms (Mizrachi et al., 2019; van Creveld et al., 2015).

3. The cold shock Ca^{2+} response may be exclusively relevant for short-term responses such as resealing of cold-induced ruptures in the plasma-membrane (Cheng et al., 2015) or adjustments to the photosynthetic machinery that can happen within seconds to minutes (Fujita et al., 1994; Murchie and Ruban, 2020). In plants, the timeframe in which low temperature-induced expression of cold on-regulated genes (COR genes) occurs can also range from minutes to several hours (Thomashow, 1999) which would fall below the time resolution used in the growth curve. Therefore, a function of the fast Ca^{2+} elevations observed in response to cold may be to avoid acute damage, akin to the "emergency" response to osmotic stress (see Chapter 3, Helliwell et al., 2020b). The immediate cell survival after cold shock could be investigated with Sytox dyes in future studies.
4. Incomplete removal of Ca^{2+} following centrifugation and washing steps may result in residual Ca^{2+} in the medium. To minimise cell stress and/or cell loss, pellets were washed only once with ASW -Ca^{2+} +200 µM EGTA before the cold shock treatment. It was not tested if this single washing step sufficiently eliminates Ca^{2+} elevations completely, but it should be assumed that the Ca^{2+} response was limited compared to the controls.

5.4.3 *P. tricornutum* is likely able to acclimate to low temperature

An important finding is that Ca^{2+} elevations still occur in response to cold shock in PtR1 cells grown at 4 °C for four days or three weeks, respectively. Assuming that respective timeframes were sufficient to achieve acclimation, this indicates that Ca^{2+} elevations are not tied to physiological adaptions which cannot be reversed in a few minutes (e.g. lipid composition or osmolyte accumulation) (Nievola et al., 2017; Wehner et al., 2003).

In addition, it may also be that Ca^{2+} responses may occur regardless of acclimation state and are decoded further downstream, depending on the activity or expression of Ca^{2+}-sensitive downstream components. Cross-talk of cold, salt and drought stress in plants is achieved through versatile 2nd messengers such as Ca^{2+}, ROS and inositol phosphates at the signal perception stage and calmodulins, kinases and phosphatases at the signal transduction stage (Huang et al., 2012; Schulz et al., 2013). Since these components are not extrinsic to diatoms, decoding at the signal transduction stage may also apply to the *P.*

tricornutum signalling network. Further work is needed to decipher the meaning of Ca^{2+} elevations in cold acclimated cells. However, there are reasons to think that *P. tricornutum* acclimates to low temperature:

A physiological consequence of cold acclimation in *P. tricornutum* may be transition into the oval morphotype which dominated a liquid culture grown at 4 °C for three weeks in this study. This transition in response to low temperature has been observed before (de Martino et al., 2011; de Martino et al., 2007; Gutenbrunner et al., 1994). When transcriptomes of oval and fusiform cells grown at the same temperature (19 °C) were compared, genes involved in nucleotide and fatty acid synthesis and membrane remodelling were upregulated in oval cells (Ovide et al., 2018). This could contribute to higher resilience to prolonged low temperature stress compared to fusiform cells. However, it remains unclear whether the transition to the oval morphotype in this study occurred exclusively due to low temperature or if other known transition stimuli such as nutrient limitation or lack of stirring were involved (de Martino et al., 2011).

Coincidently, nucleotide and ribosome synthesis were also shown to be upregulated in the diatoms *T. pseudonana* and *F. cylindrus* to compensate cold-induced reduction of transcription and translation efficiency (Toseland et al., 2013). Upregulation of fatty acid synthesis and membrane remodelling proteins such as desaturases aimed to maintain membrane fluidity are also a common response in bacteria, archaea, and plants to cold stress (Cavicchioli et al., 2000; Popov et al., 2017; Russell, 2008). In *Synechocystis,* cold-induced expression of desaturases depends on the extent of the shift in temperature but not on the absolute temperature (Los et al., 1993). In the cyanobacterium *A. nidulans* the onset of phase separation of the cytoplasmic membrane occurs around °14 C in cells grown at 38 °C and 4 °C in cells grown at 28 °C (Ono and Murata, 1981). Monitoring the cold shock response in PtR1 cells of various acclimation states and morphotypes might provide more detail relating to the sensory mechanism.

P. tricornutum may also acclimate to low temperature by altering the sterol content of biomembranes. Absolute sterol content in *P. tricornutum* was increased up to 7-fold when grown at 13 °C compared to 23 °C (Véron et al., 1996). Sterols increase membrane fluidity at low temperatures, extending the temperature range in which membrane-associated biological processes can take place, and are therefore important for low temperature

acclimation in plants and poikilothermic animals (Crockett, 1998; Dufourc, 2008). Sterols are also shown to play a key role in lipid raft formation and to influence ion channel activity, both being mechanisms which are affected by low temperature (Levitan et al., 2010; Xu et al., 2001).

An additional option to maintain DNA translation and transcription efficiency at low temperatures may be cold shock proteins. Cold shock proteins share a characteristic nucleic acid binding domain allowing them to bind to single stranded DNA and RNA and counteract cold-induced negative effects on ribosomal translation and mRNA secondary structure (Keto-Timonen et al., 2016). As such, cold shock proteins were identified to be crucial in successful cold shock acclimation in bacteria and were also found to be upregulated in cold stressed plants (Karlson et al., 2002; Keto-Timonen et al., 2016; Kim et al., 2007; Sasaki and Imai, 2011). *P. tricornutum* has five distinct proteins containing the "cold shock DNA binding" domain (Pfam: PF00313) whose expression was not altered by different light regimes, shifts in CO_2 supply, nutrient starvation, or morphology state (Maheswari et al., 2005). A wider analysis of changes in gene expression and physiology/metabolism under cold stress are needed to understand the potential roles of Ca^{2+} signalling.

5.4.4 Spatiotemporal patterns of cold induced Ca^{2+} elevations indicate involvement of ion channels

As previously established, cold shock induces a single Ca^{2+} elevation in *P. tricornutum* with the duration and amplitude being dependent on stimulus strength. The presented data suggests that the Ca^{2+} elevation is stronger if a similar total temperature drop covers a lower temperature range than a higher one. This would strongly support the presence of a specialised cold sensitive ion channel in *P. tricornutum*, since a stronger response at lower temperatures contrasts with the general observation that low temperature leads to reduced ion flux, higher voltage dependency and lowered channel opening probability as shown for multiple Ca_V, Na_V and K^+ channels (Korogod and Demianenko, 2017; Yang and Zheng, 2014).

In this study, the duration of the post-amplitude component of the Ca^{2+} elevation significantly increases with the duration of temperature drop. This indicates that channel open probability is maintained for a significant time until feedback mechanisms result in channel closure. Furthermore, imaging of the Ca^{2+} elevation indicates that it initiates at the apex of cells but propagates towards the centre only if the temperature drop rate is fast enough to elicit a sufficiently large apical Ca^{2+} elevation. This and the necessity of external Ca^{2+} indicates that a threshold of apical cytosolic Ca^{2+} is necessary for signal propagation. The propagation itself may be either reliant on the same channel responsible for the initial Ca^{2+} elevation if the cold effect on the apex affects the rest of cell in an attenuated way, or may be reliant on different channels which are either based on Ca^{2+} -induced Ca^{2+} release from internal stores or Ca^{2+} dependent channels on the plasma membrane (Wang and Thompson, 1995). Typical animal Ca^{2+} release channels such as IP_3R and RyR-channels are absent in diatoms, suggesting that other types of channels have this role (see Chapter 3 and 4).

5.4.5 Cold shock and osmotic Ca^{2+} signalling. Independent or linked?

It is curious to see similarities in the spatiotemporal patterns of cold- and hypo-osmotic shock induced Ca^{2+} elevations. Hypo-osmotic induced Ca^{2+} responses also initiate at the apex of cells independently, propagate through the cell if apical elevation is large enough, correlate with stimulus strength and are dependent on external Ca^{2+}, and the hypo-osmotic shock response is also not inhibited by the non-selective Ca^{2+} channel blocker ruthenium red (Helliwell et al., 2020b). However, there are some clear differences: Inhibition of the hypo-osmotic shock-induced Ca^{2+} elevation leads to lethal structural damage, whereas present data suggest no increased lethality following inhibition of cold-induced Ca^{2+} elevation (Chapter 3). In contrast to hypo-osmotic shock (Helliwell et al., 2020b), the presented data in this study does not suggest a notable change in cell size during or shortly after cold shock. Data presented in this study show no attenuation of the Ca^{2+} elevation in two successive cold shocks, whereas the opposite was the case for hypo-osmotic shocks. A trial experiment performed in this study using a *P. tricornutum* strain transformed with a K^+ sensitive fluorescent biosensor suggest no K^+ efflux during cold shock, whereas K^+ efflux was observed for hypo-osmotic shock (Helliwell et al., 2020b).

Similarities in spatiotemporal patterns of the cold- and hypo-osmotic induced Ca^{2+} elevations raise the question of whether the Ca^{2+} signature hypothesis applies. Accordingly, both stimuli would result in the same, probably more general cell response (McAinsh and Pittman, 2009; Sanders et al., 2002). Ca^{2+} elevations causing a rather general than specific stress response was proposed to be the case in plants (Seki et al., 2001; Seki et al., 2002), but arguments in favour of high specificity also exist (Kreps et al., 2002; Tattersall et al., 2007). If the Ca^{2+} signature hypothesis does not apply (Scrase-Field and Knight, 2003), *P. tricornutum* may not be able to distinguish cold and hypo-osmotic stress. In this scenario, both stresses may trigger the same primary sensor, such as Redox balance or membrane tension (Ayee and Levitan, 2018; Conrard and Tyteca, 2019; Kurusu et al., 2012).

Although a precursory cold shock may have led to a slightly higher chance of surviving a potentially lethal hypo-osmotic shock, the involvement of Ca^{2+} signalling is not clear as improved survival did not depend on whether cells were responding to the cold shock. However, the applied hypo-osmotic shock of 100% freshwater may have been too lethal and the timeframe of 30 s between these shocks too short to produce a measurable difference.

Ca^{2+} elevations in response to simultaneous cold- and relatively subtle hypo-osmotic shock were larger compared to Ca^{2+} elevation in response to a sole cold shock, indicating that both stimuli may reinforce each other. Although a higher amplitude for combined shocks was also the case if respective shocks were relatively strong, the Ca^{2+} elevations now differed in that they were of a biphasic nature. This suggests that strong cold- and osmotic shock have different underlying mechanisms. However, the second peak which likely represents the cold response occurred earlier when combined with a hypo-osmotic shock.

Taken together, the presented data suggests that cold- and hypo-osmotic shock Ca^{2+} responses are generated via different pathways and that *P. tricornutum* can differentiate cold from hypo-osmotic shock. However, presented data also suggest that the hypo-osmotic response influences the cold response. Further experiments with pharmacological agents may help to dissect the two components of the Ca^{2+} response to combined cold and osmotic treatments in *P. tricornutum*.

In plants, the degree of cold and osmotic stress cross-talk is still investigated but components of each response pathway may interact. OST1 regulates stomatal closure in plants and is involved in freezing tolerance in *A. thaliana* (Ding et al., 2019). Cold stress induced ABA-independent OST1 phosphorylation whereas osmotic stress induced ABA-dependent OST1 phosphorylation, indicating that plants have sophisticated decoding mechanisms (Ding et al., 2018; Merlot et al., 2002). Moreover, osmotic shock activated the DREB2 and CBF4 transcription factors which are normally involved in the ICE-CBF-COR transcriptional cascade of the plant cold shock response (Huang et al., 2012). Homologs of key components of the plant cold shock response such as ICE1, ICE2 or CBF transcription factors are not present in *P. tricornutum*, suggesting a different signal transduction pathway in diatoms.

5.4.6 The cell apices of fusiform *P. tricornutum*: putative antennae for cold and hypo-osmotic shock

In-depth consideration of the underlying mechanisms generating cold and osmotic shock Ca^{2+} responses is not possible since the underlying ion channels are unknown. However, both cold- and hypo-osmotic shock affect bio membranes, a potential primary sensor for both stresses, and both stimuli induce Ca^{2+} elevations at the apices of *P. tricornutum*.

Hypo-osmotic shock causes cell swelling which increases membrane tension, and cold promotes conversion from the liquid-crystalline stage to the gel-crystalline stage which also affects membrane tension, thickness, curvature and rigidity (Ayee and Levitan, 2018; Conrard and Tyteca, 2019; Hjort Ipsen et al., 1987; van Meer et al., 2008). The phase transition of an artificial monolipid vesicle was shown to occur in milliseconds, demonstrating that membranes can react fast enough to act as temperature sensors for rapid temperature shifts (Nagarajan et al., 2012).

However, since phase transition temperature of a membrane is dependent on lipid composition and protein, sterol and water content, and the former three being potentially tightly regulated and localised, cold may affect some areas of the membrane more strongly than others (Popova and Hincha, 2005). The composition of the apical membrane in *P. tricornutum* might provide an environment for increased channel sensitivity to mechanical

change due to increased membrane curvature or specialised lipid rafts or caveoles (Dart, 2010; Poveda et al., 2014), possibly explaining why both cold- and hypo-osmotic shocks initiate there. This receives further support from studies with mechanosensitive channels which suggests that local change in membrane properties have a higher influence of channel activity compared to global change in cell shape (Bavi et al., 2016).

5.4.7 Ion channels in *P. tricornutum* and their putative involvement in the cold shock response:

5.4.7.1 Mechanosensitive channel*s*

Mechanosensitive channels were indeed proposed to be the main cold activated channel in plants (Mori et al., 2018) and are important for hypo-osmotic shock responses (Kung et al., 2010). The *P. tricornutum* genome contains seven different mechanosensitive channels (Verret et al., 2010) which should be prioritised for future experiments as they may underlie both cold- and hyperosmotic shock responses in *P. tricornutum.* Other promising candidates include OSCA channels, piezo channels or TRP channels which are also mechanosensitive and present in P. tricornutum (Murthy et al., 2018; Pedersen et al., 2005; Ridone et al., 2019).

5.4.7.2 Transient Receptor Potential channels

The best characterised Ca^{2+} permeable channels sensitive to low temperature are animal TRPM8 and TRPA1. The presented phylogenetic tree (Fig. 5.10) shows that TRPs in diatoms group into two major clades which are evolutionarily distinct to animal TRPs. This implies that animal and diatom TRPs may have evolved from a common ancestral TRP which further diversified after divergence of respective lineages. Notably, one of the two major diatom TRP clades contains TRPs with a series of ankyrin repeats in the N-terminus.

Although molecular mechanisms underlying TRP channel cold shock activation are not completely understood, it is suggested that ankyrin repeats confer mechanosensitivity that allows animal heat sensitive TRPVs and cold sensitive TRPA1 to sense temperature effects on the membrane (Corey et al., 2004; Yin and Kuebler, 2010). The C-terminus also plays a

role, since replacement of the cold sensitive TRPM8 C-terminus with the C-terminus of heat-sensitive TRPV1 rendered TRPM8 heat sensitive (Brauchi et al., 2006). Furthermore, TRPA1 and TRPM8 also have coiled-coil domains that are implicated in cold-activation and channel assembly (Paulsen et al., 2015; Tsuruda et al., 2006).

In this study RRed was employed to explore TRP channel activity in *P. tricornutum.* RRed is a cationic dye and antagonist for calmodulin (Sasaki et al., 1992) and a range of cation channels (Ca_V: (Cibulsky and Sather, 1999), RyR: (Xu et al., 1999), Piezo1: (Soattin et al., 2016), K_{2P}: (Czirják and Enyedi, 2003)) including many TRPs (Cahusac, 2009). Within cold sensitive TRPs, RRed was reported to block TRPA1 but not TRPM8 (Behrendt et al., 2004; Christensen et al., 2016; Mueller-Tribbensee et al., 2015; Peier et al., 2002), showing that not every TRP channel is affected by it. In this study, RRed treated cells showed a significant delay in the Ca^{2+} response, indicating that an unknown component of the cold induced Ca^{2+} response was affected. The applied concentration of 5-10 µM was in the concentration range of almost complete TRPA1 inhibition in other studies (Peier et al., 2002; Soattin et al., 2016) and also prevented the phosphate induced Ca^{2+} response in phosphate starved PtR1 cells (Helliwell et al., 2020a). This indicates that the cold shock Ca^{2+} response in *P. tricornutum* involves different Ca^{2+} channel(s) than the phosphate response (Helliwell et al., 2020a).

Menthol is known to activate animal TRPM8 channels through interaction with specific conserved sites within the protein sequence ($TRPM8_{human}$: Arg^{842}, Tyr^{745}, Tyr^{1005}, (Yin et al., 2018)). Application of menthol to *P. tricornutum* did not produce any agonistic effects on cytosolic Ca^{2+} levels even though the chosen concentration (100 µM to 1mM) was higher than in TRPM8 patch clamp experiments (50-500 µM (McKemy et al., 2002)). Arg^{842} is likely part of the voltage sensing motif in animal TRP channels and alignments presented in this study suggest diatom TRPs may also be voltage sensitive. However, diatom TRPs have no tyrosine residues in relative position of animal Tyr^{745} which may explain why menthol had no effect on diatom TRP channels.

Notably, DMSO which was used as a solvent for menthol (Chuang et al., 2004) led to Ca^{2+} elevations in *P. tricornutum* when added to perfusion medium in sufficiently high concentration (1-5 %). DMSO also led to cytosolic Ca^{2+} elevations and/or increased COR expression in *Medicago sativa, Brassica napus, Arabidopsis thaliana* and *Ganoderma*

lucidum and was therefore proposed to mimic cooling induced rigidification of biomembranes, contributing to the idea of membranes as primary temperature sensor in plants and fungi (Furuya et al., 2014; Liu et al., 2017; Örvar et al., 2000; Sangwan et al., 2001). However, in animal systems, DMSO increases membrane fluidity and decreases membrane firmness (Best, 2015; Gurtovenko and Anwar, 2007). At higher concentrations of DMSO, membrane bilayers collapse (de Menorval et al., 2012; Notman et al., 2006). Furthermore, it is commonly used as cryoprotectant (Best, 2015), solvent for peptides (Amodeo et al., 1991), cell fusogen (Norwood and Zeigler, 1982) and chemical penetration enhancer (Notman et al., 2007), which may suggest that DMSO-induced Ca^{2+} elevations in *P. tricornutum* and plants may be due to increased membrane permeability rather than rigidification.

5.4.7.3 Two–pore cation channels

TPCs are intracellular channels proposed to be involved in Ca^{2+} release in plants and animals (Chapter 4). PtTPC1 knock-out strains investigated in this study showed no significant difference in the cold shock induced Ca^{2+} elevations. The plant TPC1 antagonist aluminium was reported to block cold shock induced Ca^{2+} elevations in tobacco BY-2 cells (Lin et al., 2005) and two cellular Ca^{2+} pools were shown to contribute to cold induced Ca^{2+} elevations in *A. thaliana* (Knight et al., 1996), suggesting an involvement of plant TPC1 channels in the plant cold shock response. However, neither plant TPC1 and TPC2 knockouts nor TPC1 over-expression did affect cold induced Ca^{2+} elevations in *A. thaliana* (Ranf et al., 2007) which corresponds with results presented in this study. However, the novel diatom TPCL channel shown to localise to the vacuolar membrane may be involved in Ca^{2+} signal propagation in *P. tricornutum* (Chapter 3).

5.4.7.4 EukCat channels

EukCats are a novel class of single domain rapid-depolarization-activated Na^+- and Ca^{2+}-permeable channels found in diatoms and other eukaryotic microalgae (Helliwell et al., 2019). EukCats are structurally similar to prokaryote $BacNa_Vs$ and both classes have a C-terminal cytoplasmic domain that terminates in a four-stranded coiled-coil (Helliwell et al., 2019; Shaya et al., 2014). The "neck" which connects the coiled-coil domain with the main $BacNa_V$ body is shown to undergo transitions from an orderly to disordered state when the channel opens, and the likelihood of this transition is shown to positively correlate with increased temperature in the *Silicibacter pomeroy* channel Na_VSp1 (Arrigoni et al., 2016). The coiled-coil domain in EukCat1 may therefore render it more heat than cold sensitive, explaining the presented data showing no involvement in formation of cold-induced Ca^{2+} elevations.

Interestingly, cold-sensitive TRPA1 and TRPM8 channels also show a cytosolic feature of structural similarity to the neck and coiled-coil domain of $BacNa_Vs$, which was suggested to participate in their temperature sensing (Arrigoni et al., 2016; Tsuruda et al., 2006). If true, the other two EukCats in *P. tricornutum* (Helliwell et al., 2019) may be worth further investigation.

5.4.8 Summary and outlook

This study is the first presentation of conserved cold-induced Ca^{2+} elevations in two distinct diatoms. The graded responses imply a regulatory function but the physiological consequence of these Ca^{2+} elevations was not resolved. The recorded Ca^{2+} elevations have a higher spatiotemporal resolution than those of most plant studies. The apices of fusiform *P. tricornutum* cells may function as mechanical antennae for an unknown cold-sensitive Ca^{2+} channel. Despite spatiotemporal similarities in cold- and hypo-osmotic induced Ca^{2+} elevations, presented data suggests different underlying signalling pathways.

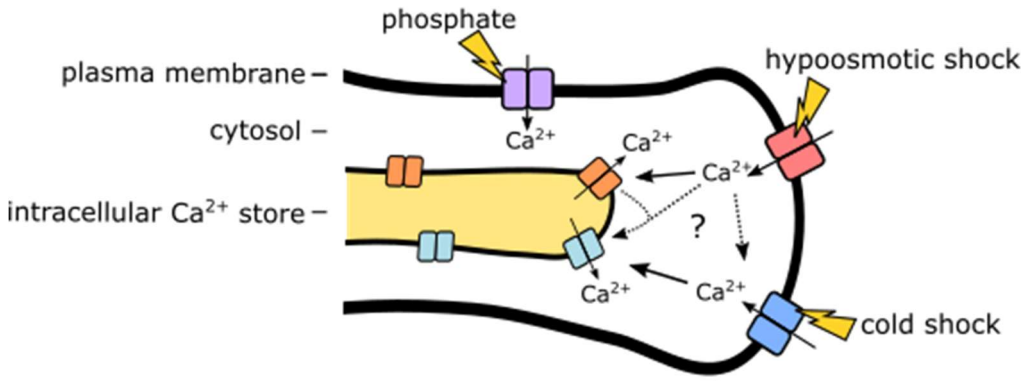

Figure 5.17: Putative mechanism of cold shock-induced Ca^{2+} elevations in *P. tricornutum*

Schematic cross section of a *P. tricornutum* apex presenting three separate Ca^{2+} signalling pathways. The involved channels are unknown, but all depend on channels at the plasmamembrane for initiation. Hypo-osmotic and cold shock likely include separate channels located at the apex, but the hypo-osmotic shock response may influence the cold shock response, and both show Ca^{2+} waves possibly fuelled by intracellular Ca^{2+} release. Phosphate sensing utilises a clearly different pathway including a ruthenium red sensitive Ca^{2+} channel and a more uniform cytosolic Ca^{2+} elevation without a Ca^{2+} wave (Helliwell, unpublished).

Employment of further Ca^{2+} channel antagonists or successful localisation of the seven mechanosensitive channels, four TRP channels and the remaining two EukCat channels in *P. tricornutum* may indicate preferential occurrence at the cell apices and might narrow down potential knock-out candidates. More detailed imaging may help to detect Ca^{2+} signalling events at micro-domain scale in response to sub-saturating stimuli and to dissect stimulus-specific responses. Once the necessity and mechanism of the cold-induced Ca^{2+} response is better understood, the oval morphotype of *P. tricornutum* would be an ideal candidate to investigate acclimation and adaption in parallel

Chapter 6 Summary

The aim of this study was to expand understanding of diatom Ca^{2+} signalling mechanisms in response to abiotic changes in the environment.

The questions presented in Chapter 1 are addressed below.

6.1 Are there specific Ca^{2+} signatures to specific physiologically relevant stimuli?

Hypo-osmotic shock induced Ca^{2+} responses which *P. tricornutum* showed in this study are seen in most eukaryotes that have been examined, indicating that these responses are likely to be universal. However, the mechanisms themselves, including their components, the specificity, the sensitivity or the cost-effectiveness may differ between species.

Abiotic factors play a vital role in the distribution and abundance of natural populations (Parmesan et al., 2005; Parmesan et al., 2006). It is therefore to be expected that phytoplankton living in similar habitats of *P. tricornutum* to encounter similar stresses, and thus to have developed similar effective osmo- and temperature regulation-mechanisms ensuring their survival. Indeed, the multicellular brown alga Fucus also shows transient Ca^{2+} elevations in response to hypo-osmotic shock (Goddard et al., 2000). However, hypo-osmotic shock induced cytosolic Ca^{2+} elevations were also observed in the freshwater green alga *C. reinhardtii* (Bickerton et al., 2016), which shows that employment of Ca^{2+} for hypo-osmotic emergency responses also plays a role in organisms accustomed to hypotonic surroundings. Besides adjustments to the osmotic homeostasis, the shock response may differ between species in how the physiology is adjusted (types of osmolytes) and could include stress avoidance reactions for some species (e.g. burrowing, generation of protective biofilms).

Ca^{2+} signatures examined in this study in response to cold and osmotic stimuli differ from those in response to P-resupply (Helliwell et al., 2020a), implying that Ca^{2+} signatures can be specific in *P. tricornutum*. This study also clearly demonstrates that magnitude, duration and spatio-temporal features of Ca^{2+} signatures in *P. tricornutum* may represent the

duration, strength or change rate of the stimulus, which is common for Ca^{2+}-based sensory systems (Goddard et al., 2000; Minorsky and Spanswick, 1989; Suto and Gotoh, 1999).

Moreover, this study provides the first demonstration of a Ca^{2+} response to cold shock in diatoms, with rate of temperature decrease being more important in determining the properties of the Ca^{2+} response than a threshold temperature - similar to plant systems (Minorsky and Spanswick, 1989; Plieth et al., 1999) and animal innocuous cold thermoreceptors (McKemy, 2018). Sensing rapid temperature change through single Ca^{2+} elevations (diatoms, plants (Kiegle et al., 2000), noxious cold shock in animals (McKemy, 2018)) rather than through modulation of action potential fire rates (innocuous cold shock in animals (McKemy, 2018; Orio et al., 2012)) may be more economic to sustain for single cells while also being more suited for an emergency response. Furthermore, this study provides evidence that the cold- and osmotic Ca^{2+} responses do not share the same pathways. Although not investigated in sufficient detail to draw refined conclusions, it represents the first attempt to characterise Ca^{2+} signalling cross-talk in diatoms. All this is important for understanding the specificity of responses and how they might be decoded.

The spatiotemporal diversity of presented Ca^{2+} elevations also highlights the necessity to consider how a cell will likely encounter a stimulus in nature. *P. tricornutum* would more likely be exposed to gradual shifts in osmolarity as presented in this study than sudden ones presented in previous studies (Helliwell et al., 2019; Helliwell et al., 2020a). Conversely, the cold shocks applied on *P. tricornutum* often covered 20 °C in less than a minute, which is likely to be an exception in the natural environment. Such rapid transitions in temperature and osmolarity and most likely to be experienced in benthic diatoms in inter-tidal regions (e.g. estuaries, rock pools). Other areas that may experience rapid transitions could be sea-ice, e.g. when hyper-saline brine channels are flushed with seawater. In comparison, diatoms in the open ocean are less likely to experience such extreme of salinity and temperature, and transitions will be slower. There may be incidences where heavy rain could influence salinity at the very surface, or when cells move through the thermocline, but the large water volume and relatively frequent turbulences will have a strong buffering effect. Hence, the response mechanisms of diatoms populating the open ocean would be expected to be suited for slower transitions in these parameters, albeit this study showed that *T. pseudonana* is able to respond to rapid osmotic- and cold shock as well. Planktonic

organisms in coastal, near-shore environments may experience fast transitions of salinity and temperature, but probably within minutes rather than seconds.

Diatoms also play an important role in fresh water environments, and it would be interesting to include one of these as model in future experiments. Likewise, it would be interesting to investigate the subjectiveness of chilling stress and cold-induced Ca^{2+} elevations in *Fragilariopsis cylindrus* – an arctic diatom with established means of genetic transformation (Hopes, 2017).

6.2 Can analysis of spatiotemporal Ca^{2+} responses to specific stimuli provide further information on the underlying mechanisms of Ca^{2+} signalling in diatoms?

This study harbours the first characterisation of spatiotemporal characteristics of cytosolic Ca^{2+} elevations in diatoms – or any phytoplankton. Presented data demonstrate localised Ca^{2+} elevations and occurrence of Ca^{2+} waves in *P. tricornutum*, indicating a complex multi-instance- and component signalling system which also indicates development of an intracellular Ca^{2+}-release mechanism independent from canonical IP_3Rs in diatoms. Presented Ca^{2+} signatures in response to temperature and osmotic change differ from those observed in the P-repletion response, which showed no initiation at the apex and no propagating Ca^{2+} waves (Helliwell et al., 2020a). This and the inhibition of the P-response by ruthenium red (Helliwell et al., 2020a) suggests different underlying channels. An earlier study also implied Ca^{2+} elevations induced by mechanical stimulation which would be worth closer examination (Falciatore et al., 2000). Do these Ca^{2+} elevations also initiate at the cell apex?

This study also highlights differences in signalling between the morphotypes of *P. tricornutum,* providing an interesting role model to investigate differences in Ca^{2+} signalling in two genetically identical yet physiologically different isoforms of the same species. It was also recently proposed that the benthic oval morphotype actually represents the more ancient form of *P. tricornutum* and the pelagic form developed relatively recently (Sabir et al., 2018), adding to the justification to investigate oval cells in more detail in future studies.

6.3 Can a more detailed bioinformatic analysis tell us more about the evolution and roles of particular Ca^{2+} channels in diatoms?

In this study, phylogenetic analysis revealed that the second TPC in *P. tricornutum* in fact represents a novel class of diatom-restricted TPC-like proteins with distinct features, which raises new questions about the roles of TPCs in diatoms. However, the role of diatom TPC and TPCL were not resolved. Does TPCL functionally replace a distinct but lost ion channel, or does it have a diatom-specific role given its apparent restriction to diatoms? There are also unresolved questions regarding the presence or absence of entire channel classes within diatoms (e.g. restriction of Ca_V to members of the centric clade, perhaps involved in male gamete motility?) and in diatoms compared to other lineages (e.g. role of TPCL or EukCat2 and EukCat3) (Helliwell et al., 2019; Verret et al., 2010).

The TPCL analysis points out limitations in currently available genome-databanks due to overrepresentation of animal and plant genomes (Chapter 3). The guaranteed increased availability of more and better genomes within stramenopiles or phytoplankton lineages in the future - for example as provided by the Marine Microbial Eukaryote Transcriptome Project (MMETSP) and the Darwin Tree of Life Project - will help to dissect patterns in presence or absence of different kinds of Ca^{2+} channels more clearly. In a broader sense, phylogenetic analysis can point out curiosities worthy of further attention or provide a broader context to the evolutionary role of channels, but it obviously cannot replace functional analysis (Chapter 3).

6.4 Can the findings from pennate diatoms be translated to centric diatoms which include many of the more globally abundant species in the oceans?

This study presents the first data on Ca^{2+} signalling in an oceanic diatom which will increase our understanding of how oceanic diatoms perceive and respond to their environment. Given their ecological importance, the potential value of RGECO1 expressing *T. pseudonana* in understanding nutrient signalling may easily go beyond fundamental research (e.g. implied Ca^{2+} dependent iron sensing and iron-induced centric diatom blooms (Falciatore et al., 2000; Tsuda et al., 2003)). However, it is clear that this system is far less developed compared to *P. tricornutum,* and more work is needed to understand the nature (and significance) of the heterogeneous RGECO1 expression and lower signal intensity in *T. pseudonana*. Nonetheless, *T. pseudonana* has already provided limited but much needed confirmation of the cold- and hypo-osmotic shock response in centric diatoms (Chapter 2 and 5). Fundamental differences in signalling are to be expected however, dictated by their different habitats, reproduction modes or orchestration of pennate diatom gliding.

6.5 Can we identify specific ion channels that may underlie particular Ca^{2+} signalling responses?

This study did not reveal the identity of ion channels underlying any of presented stimuli. However, thanks to the high spatiotemporal resolution of presented Ca^{2+} elevations, we may narrow down potential ion channel candidates once their localisation is known.

Bioinformatic annotation of ion channel sequences may reveal functional domains (EF-hands, ankyrin repeats) which provide interesting targets for genetic manipulation to better understand the molecular mechanism of channel activation or interaction with signal transduction components once the general role of a channel is better understood (Gaudet, 2008; Guo et al., 2016).

Although diatoms (and other microalgae) have a similar diversity in cation channel classes compared to more complex organisms, the number of channels within those classes is relatively low (Verret et al., 2010). The problems of channel redundancy may therefore be less of an issue in diatoms than in plants and could help to extrapolate the role and mode of action of algal ion channels in more complex organisms.

6.6 Future steps and tools to understand Ca^{2+} signalling in diatoms

The immediate following steps for the hypo-osmotic response project would go in three directions. Further understanding of the sensory perception would require the identification of the responsible ion channel through knock-out/down techniques. Moreover, the signal transmission stage is a completely unknown chapter in diatom signalling, which could be approached by identifying involved Ca^{2+} binding messenger proteins. Finally, it is not completely understood what the actual Ca^{2+} elevation are doing besides the K^+ efflux, as there could be many other responses. Once channels and Ca^{2+} binding proteins have been identified, a next step would be to see if these are conserved amongst diatoms and in other algae, and whether their expression and distribution is different in the verious *P. tricornutum* morphotypes.

Further steps for the TPC chapter are clear, as it would strongly benefit of a TPCL knockout and TPC1 localisation to offer a complete picture. As both presented problems, alternative transformation techniques (see 6.6.4) or localisation techniques (antibodies) may be required.

The priority of the cold shock project would be to decipher the physiological role of the cold-induced Ca^{2+} elevations. As there is no increased mortality observed in -Ca2+ cold shocks, the effects are likely less obvious and require further testing. Monitoring ROS production, gene transcription, membrane composition or likelihood of oval cell transition within cold shocked cultures with/without calcium are potential targets to investigate.

Moreover, there are a few technical limitations of this study, which would benefit from being addressed if possible:

6.6.1 Focus on intensiometric Ca^{2+} biosensors is problematic

This study demonstrates the value of fluorescent biosensors to investigate Ca^{2+} elevations in single cells compared to luminescent aequorin. RGECO1 has a relatively high dynamic range (signal ratio from Ca^{2+}-free to Ca^{2+}-bound state), high quantum yield (efficiency of photon absorption vs. emission) and high affinity making it useful for detection of small-scaled Ca^{2+} elevations. However, RGECO1 saturates more easily (Hires et al., 2008), is

sensitive to pH and most importantly does not allow ratiometric measurements, thus making measurements prone to errors related to differences in intracellular distribution and expression levels (Hires et al., 2008; Keinath et al., 2015). Conversely, FRET-based biosensors such as Cameleon are not pH sensitive and allow ratiometric measurements, but have a lower dynamic range and show a lower signal to noise ratio compared to RGECO (Hires et al., 2008). Co-expression of RGECO with another fluorescent protein would allow ratiometric imaging as it was done in plants cells (RGECO + mTurquoise; (Waadt et al., 2017)), or generation of an entirely new strain expressing a ratiometric bionsensor may be necessary to fully characterise Ca^{2+} elevations in diatoms.

A valid argument may be that this study did not address the pH-sensitivity of RGECO1 (Keinath et al., 2015). Intracellular pH shifts occur in concert with Ca^{2+} elevations in plants, likely fuelled by increased activity of CAX antiporters (Behera et al., 2018). This could imply a decrease in pH during Ca^{2+} elevations in *P. tricornutum* or *T. pseudonana*, consequently attenuating RGECO1 fluorescence (Keinath et al., 2015). Obviously, this putative attenuation is more than compensated by the Ca^{2+} response at least *in P. tricornutum*. Moreover, pH effects on presented Ca^{2+} elevations may be relatively negligible at least for hypo-osmotic shock, as no striking shift in pH was observed in a *P. tricornutum* strain expressing the pH biosensor pHluorinin in response to osmotic shock (Glen Wheeler, MBA Plymouth, personal communication).

Lastly, identification and (in)dependence of organelle specific signalling from cytosolic Ca^{2+} elevations is necessary to understand the scope of cytosolic Ca^{2+} elevations (nucleus, chloroplast, mitochondrion). Why not investigate fluxes of other important ions such as Cl^-, K^+ and Na^+, preferably in a single strain utilising different wavelength-reporters?

6.6.2 Electrophysiological characterisation of diatom Ca^{2+} channels is needed

While understanding of Ca^{2+} signalling in potential channel mutants will continue to be very informative, more details of channel selectivity and kinetics will be required to fully understand their functions. Single electrode voltage clamp experiments were done successfully in the large diatom *O. sinensis* (Taylor, 2009), but other established model diatoms are too small, making the employment of heterologous systems necessary (Helliwell et al., 2019). As attempts to express TPC- and TPCL-GFP fusions in HEK cells were not successful in this study, exploration of alternatives may be needed including plant

vacuoles, large diatoms or oocytes, aiming to ensure correct protein folding, channel subunit-assembly or non-inferring of posttranscriptional modifications (Hannig and Makrides, 1998; Mao et al., 2015; Miller and Zhou, 2000; Suttangkakul et al., 2019).

6.6.3 The role of membrane biophysics in ion channel activity – not to be underestimated?

Ca^{2+} elevations at the apical regions of fusiform *P. tricornutum* cells suggest that these may provide an environment for highly sensitive membrane tension-based stimuli perception (cold + osmotic). As many ion channels show a limited degree of mechano-sensitivity (Yoshimura and Sokabe, 2010), it may be necessary to consider localised differences in structure and biophysical properties of membranes to truly understand the mode of action of channels in the native host cell (e.g. effect of lipids (Cordero-Morales and Vasquez, 2018), cholesterol content (Levitan et al., 2010), general membrane thickness and curvature (Bavi et al., 2016) or caveoles (Huang et al., 2013)). Better spatiotemporal resolution in imaging (confocal microscopy, localised Ca^{2+} biosensors with high affinity) may help to dissect micro-domain signalling at the cell apex or vacuole membranes (Clapham, 2007) and may also help to prevent misinterpretation of eventual electrophysiological data on ion channels in heterologous expression systems.

6.6.4 Refinement of genetic tools to improve transformation

In this study, a significant effort was spent on genetic transformation of algae with mixed results for both transformation efficiency and gene expression. Established methods would benefit from further refinement: Complete circumvention of co-transformation would increase transformation efficiency (Hopes et al., 2017), inducible promoters would circumvent potential long-term toxicity of overexpressed ion channels or Cas9 (Adler-Agnon et al., 2018; Chu et al., 2016; Erdene-Ochir et al., 2019), introduction of introns in *C. reinhardtii* transgenes may render them more "authentic" (Baier et al., 2018) and selection would benefit from a more thorough screening of ideal concentrations of antibiotics vs. cell numbers. Notably, the toolkit for transformation in *P. tricornutum* has been expanded, including electroporation (Zhang and Hu, 2014) and recently by bacterial conjugation (Sharma et al., 2018; Slattery et al., 2018). The latter method allows transgenes to remain on (temporary) episomes, circumventing potentially harmful constitutive expression of Cas9, random integration of DNA into the host and should eventually allow non-transgenic mutant lines (Sharma et al., 2018). This method is potentially extremely useful for localisation of ion channels and Ca^{2+} binding proteins as well as investigating double- or triple knockouts.

Due to limited ability to generate mutants in diatoms, this and previous studies have focused on forward genetics (targeted knock-outs) to identify the roles of individual Ca^{2+} channels (Helliwell et al., 2019). As genetic technologies are constantly improving, employment of high through-put reverse genetics involving mutant libraries (e.g. *C. reinhardtii* CLiP librabry, (Li et al., 2016)) may be possible for future studies. In plants, this approach led to the discovery of OSCA1 channels (Yuan et al., 2014).

It is also worth noting that *in vivo* investigation of Ca^{2+} signalling in diatoms is not affected by ethical concerns (genetic editing, drugs, noxious temperatures), an advantage over many animal studies (Saro et al., 2020).

6.6.5 Addressing downstream decoding of Ca^{2+} elevations

P. tricornutum has a wide array of Ca^{2+} binding proteins (calmodulins, calcineurins, a calreticulin, CDPKs) and many proteins with conserved Ca^{2+}-binding domains (approximately 92 proteins with EF, EGF, EGF-like, RTX or C2 domains) as well as 16 proteins with calmodulin-binding IQ-domains. The potential consequences of Ca^{2+} sensing may include Ca^{2+} dependent kinase cascades, transcriptional responses, ion channel activation or merely Ca^{2+} buffering (Clapham, 2007). A better understanding of the transduction stage is necessary to dissect the meaning of diverse Ca^{2+} elevations. While the arsenal of Ca^{2+} binding proteins in diatoms is complex, it is less numerous compared to other multicellular model organisms (Weinl and Kudla, 2009), potentially making their investigation less problematic. A highly promising target could be Ca^{2+}-binding K^+ channels for the osmotic-shock response.

The role of Ca^{2+} efflux proteins in shaping of Ca^{2+} signatures is also often overlooked, and they may prove interesting targets to investigate the influence of temperatures on Ca^{2+} elevations given their temperature dependency (Reuter and Seitz, 1968).

6.7 Summary

In concert with previous studies, this study shows that Ca^{2+} signalling likely plays a key role in the perception of environmental stresses and helps the diatoms to adjust their physiology and cell composition accordingly. Understanding the physiology and underlying signalling pathways of diatoms may help in a number of ways.

Diatoms are one of the most successful photosynthetic organisms on our planet, and understanding why they have been able to occupy some many diverse habitats is key to understanding their ecological success. Moreover, understanding the sensitivity and susceptance to problems (e.g. pH, temperature, osmotics) of signalling pathways helps to predict the scope of tolerance for diatoms to future climatic and nutritional conditions in these habitats. Furthermore, it provides insights in how production of economically interesting metabolites is organised, offering potential levers in the signalling pathway for means of manipulation or to optimise harvest timepoints. These may include stress-response pathways presented in this study, or diurnal and circadian rhythm pathways, or

nutrient sensing pathways. Finally, it expands our understanding in on how evolutionary drivers shaped signalling pathways in general and optimised ion channel properties to physiological requirements in particular, and will add another eukaryotic group to the plant-, animal- and fungus-dominated sources to understand the evolution of Ca^{2+} signalling. The work presented here demonstrates the feasibility of carrying out detailed studies of Ca^{2+} signalling in diatoms to answer some of these questions. Continuing this work will help to understand how the highly relevant but also fascinating diatoms shape our world.

Appendix A Protein Accessions (TPC trees)

List of channel accession numbers used for the alignment in Fig. 4.4 and 4.6

1d channels (BacNav+CatSper)

Thecamonas_trahens_ATCC_50062 tr_A0A0L0DT43
Scyphosphaera_aptseinii_RCC1455_NavBac1_CAMPEP_0119345692_ext
Rhodomonas spec CCMP768_CAMPEP_0191587494
theri_CCMP459_NavBac1_CAMPEP_0185163318_ext
P.tricornutum_54164_NavBac
P.tricornutum_43878_NavBac
P.tricornutum_43828_NavBac
NavRh "Polycystic kindey disease type2 protein"
Mus musculus sp|A2ARP9.2| CatSper
Mus_musculus gi|21314844|ref|NP_647462.1 CatSper
Magnetococcus marinus NavMs WP_011712479.1
jgi|Fracy1|197275|e_gw1.32.95.1
jgi|Fracy1|197260|e_gw1.32.12.1
Homo sapiens sp|Q96P56.2| CatSper
Homo sapiens NP444282.3 CatSper
Gephyrocapsa_oceanica_RCC1303_NavBac3_CAMPEP_0185397670_extb
Gephyrocapsa_oceanica_RCC1303_NavBac1_CAMPEP_0185427228extb
Ehux_379_NavBac1_CAMPEP_0187645740
Coscinodiscus_wailesii_CCMP2513_CAMPEP_0172488904
Chaetoceros_affinis_CAMPEP_0187026534
Bacillus pseudofirmus NavBp
Bacillus halodurans NaChBac
Aureococcus_anophagefferens_NavBac1_62498
Acrobacter butzleri NavAb

4d Ca_V channels

Green algae

V.carteri_0090s0001.1
V.carteri_0066s0019.1
V.carteri_0039s0004.1
V.carteri_0017s0009.1
V.carteri_0011s0076.1
V.carteri_0004s0321.1
O.lacimarius_45407
O.lacimarius_32140
O.lacimarius_28283
O.lacimarius_16877
O.lacimarius_13647
O.lacimarius_7925
M.sp.RCC99_106148
M.sp.RCC99_105920

Red algae

Porphyridium_3690.7
Porphyridium_3431.1
Porphyridium_2284.15
Porphyridium_2051.39

Diatoms

Thalassiosira weissflogii
Thalassiosira rotulaCCMP3096
Thalassiosira pseudonana
Proposcia alata P1-D3
Plasmodiophora brassicae CEP00345.1
Leptocylindrus danicus CCMP1856
Dytillum brightwelli GSO105
Cyclotella meneghiniana CCMP338

M.sp.RCC99_105780

M.sp.RCC99_95305
M.sp.RCC99_84447
M.sp.RCC99_82714
M.sp.RCC99_62568
M.sp.RCC99_61641
M.pusilia_48447
M.pusilia_47192
M.pusilia_32293
M.pusilia_21063
M.pusilia_21004
M.pusilia_60
D.salina_0502s00008.1
D.salina_0502s00006.1
D.salina_0237s00009.1
D.salina_0173s00005.1
D.salina_0044s00007.1
C.reinhardtii_17.g720600.t1.1_Cav1
C.reinhardtii_17.g702850.t1.1_Cav5
C.reinhardtii_16.g667451.t1.1_Cav6a
C.reinhardtii_16.g667350.t1.1_Cav6b
C.reinhardtii_16.g665100.t1.1_Cav3
C.reinhardtii_16.g665050.t1.2_Cav2
C.reinhardtii_12.g532350.t1.1_Cav8
C.reinhardtii_11.g467528.t1.1_Cav4
C.reinhardtii_10.g444850.t1.1_Cav7
C.reinhardtii_07.g333535.t1.1_Cav9

Euglenozoa
T.grayi_XP_009306110.1
T.cruzi_marinkellei_EKF32800.1
L.mexicana_XP_003878633.1
B.saltans_CUG91870.1

Choanoflagellate
S.rosetta_004989719.1

Metazoa
O.anatinus_XP_007654239.1
M.musculus_NP_001035993.1
M.musculus_NP_033912.2
M.musculus_NP_033911.2
H.sapiens_ACH89974.1
D.melanogaster_AAC47406.1
D.melanogaster_AAA81883.1

4d Fungal
S. cerevisiae NP_011733.3 d1
P.camemberti CRL22690.1 d1
C.albicans AAN86029.1 d1
A.niger EHA17962.1 d1

2d channels (TPC)

Diatom TPCL
Staurosira complex CCMP2646 TPC-L MMETSP1361-20130828|48554_1
Pseudo-nitzschia delicatissima B596 MMETSP0327-20121206|4565_1
Phaeodactylum tricornutum TPC-like 1654
Nitzschia sp. RCC80 TPC-L MMETSP0014_2-20120614|29745_1
Leptocylindrus danicus CCMP1856 TPC-L MMETSP1362-20130617|6306_1
Fragilariopsis kerguelensis L26_C5 TPC-L C5-20130909|144829_1
Ditylum brightwellii GSO105 TPC-L GSO105-20130911|5939_1
Dactyliosolen fragilissimus TPC-L MMETSP0580-20130426|22789_1
Cylindrotheca closterium TPC-L MMETSP0017_2-20120614|15281_1
Corethron pennatum TPC-L L29A3-20140214|164528_1
Chaetoceros UNC1202 TPC-L contig_4109_6053_8794
Chaetoceros neogracile TPC-L MMETSP1336-20130426|36466_1
Chaetoceros dichaeta CCMP1751 TPC-L MMETSP1447-20131203|10471_1
Chaetoceros debilis MM31A-1 TPC-L MM31A_1-20140214|8095_1
Amphiprora sp TPC-L D1 20130823|5111_1

TPC
S.diclina TPC EQC40823.1
R.norvegicus TPC1
P.tricornutum TPC
P.patens TPC
M.musculus TPC2
H.sapiens TPC1
E.huxleyi TPC
C.sativa TPC
B.taurus TPC3
B.napus TPC
A.thaliana TPC AAD15312.1
A.invadans TPC ETV92736.1

Appendix B Protein Accessions (TRP tree)

List of TRP channel accession numbers used for the alignment in Fig. 5.10.

TRPY R.toruloides PRQ76274.1
TRPY M.pulcherrima QBM88187.1
TRPV6 H. sapiens sp|Q9H1D0.1
TRPV5 M.musculus sp|P69744.2
TRPV4 H. sapiens sp|Q9HBA0.2
TRPV3 H.sapiens sp|Q8NET8.2
TRPV2 H. sapiens sp|Q9Y5S1.1
TRPV1 H. sapiens sp|Q8NER1.2
TRPP3 H.sapiens NP_057196.2
TRPP2 H.sapiens_XP_011530332.1
TRPP1 H.sapiens_XP_024306069.1
TRPN D.melanogaster NP_523483.2
TRPML3 H. sapiens sp|Q8TDD5.1
TRPML2 H.sapiens sp|Q8IZK6.2
TRPML1 sp|Q9GZU1.1
TRPM8 H.sapiens NP_076985.4
TRPM7 H.sapiens NP_060142.3
TRPM6 H.sapiens NP_001170782.1
TRPM5 H.sapiens AAI43354.1
TRPM4 H.sapiens NP_060106.2
TRPM3 H.sapiens NP_001353076.1
TRPM2 H.sapiens NP_001307280.1
TRPM1 H.sapiens NP_001238953.1
TRPM1 H.sapiens NP_015628.2
TRPC7 H. sapiens sp|Q9HCX4.1
TRPC6 H. sapiens sp|Q9Y210.1
TRPC5 H. sapiens sp|Q9UL62.1
TRPC4 H. sapiens sp|Q9UBN4.1
TRPC3 H. sapiens sp|Q13507.3
TRPC1 H.sapiens CAA61447.1
TRPA1 H.sapiens NP_015628.2
TRPA1 Drosophila virilis ADG84994.1
T.pseudonana |Thaps3|24328
T.pseudonana |Thaps3|23780
T.pseudonana |Thaps3|23027
T.oceanica EJK69360.1
T.oceanica EJK58127.1
T.oceanica EJK46236.1
P.tricornutum |Phatr2|50255
P.tricornutum |Phatr2|49250
P.tricornutum |Phatr2|49054
P.tricornutum |Phatr2|47206
P.nitzschia|Psemu1|253683
P.nitzschia|Psemu1|238255
P.nitzschia|Psemu1|185033
F.solaris GAX28431.1
F.solaris GAX23887.1
F.solaris GAX21636.1
F.solaris GAX19398.1
F.cylindricus Fracy1|237208
F.cylindricus Fracy1|248226

List of References

Adair, R.K. (1999). A model of the detection of warmth and cold by cutaneous sensors through effects on voltage-gated membrane channels. Proceedings of the National Academy of Sciences *96*, 11825.

Adler-Agnon, Z., Leu, S., Zarka, A., Boussiba, S., and Khozin-Goldberg, I. (2018). Novel promoters for constitutive and inducible expression of transgenes in the diatom Phaeodactylum tricornutum under varied nitrate availability. Journal of Applied Phycology *30*, 2763-2772.

Aiyar, P., Schaeme, D., Garcia-Altares, M., Carrasco Flores, D., Dathe, H., Hertweck, C., Sasso, S., and Mittag, M. (2017). Antagonistic bacteria disrupt calcium homeostasis and immobilize algal cells. Nat Commun *8*, 1756.

Ali, R., Ma, W., Lemtiri-Chlieh, F., Tsaltas, D., Leng, Q., von Bodman, S., and Berkowitz, G.A. (2007). Death don't have no mercy and neither does calcium: Arabidopsis CYCLIC NUCLEOTIDE GATED CHANNEL2 and innate immunity. Plant Cell *19*, 1081-1095.

Allen, A.E., LaRoche, J., Maheswari, U., Lommer, M., Schauer, N., Lopez, P.J., Finazzi, G., Fernie, A.R., and Bowler, C. (2008). Whole-cell response of the pennate diatom Phaeodactylum tricornutum to iron starvation. Proceedings of the National Academy of Sciences *105*, 10438.

Allen, G.J., Chu, S.P., Schumacher, K., Shimazaki, C.T., Vafeados, D., Kemper, A., Hawke, S.D., Tallman, G., Tsien, R.Y., Harper, J.F.*, et al.* (2000). Alteration of Stimulus-Specific Guard Cell Calcium Oscillations and Stomatal Closing in Arabidopsis Mutant. Science *289*, 2338.

Allen, G.J., and Schroeder, J.I. (2001). Combining Genetics and Cell Biology to Crack the Code of Plant Cell Calcium Signaling. Sciences STKE *102*, 1-7.

Amodeo, P., Motta, A., Picone, D., Saviano, G., Tancredi, T., and Temussi, P.A. (1991). Viscosity as a conformational sieve. NOE of linear peptides in cryoprotective mixtures. Journal of Magnetic Resonance (1969) *95*, 201-207.

Andrade, E.L., Luiz, A.P., Ferreira, J., and Calixto, J.B. (2008). Pronociceptive response elicited by TRPA1 receptor activation in mice. Neuroscience *152*, 511-520.

Antonelli, M., Wetzel, C.E., Ector, L., Teuling, A.J., and Pfister, L. (2017). On the potential for terrestrial diatom communities and diatom indices to identify anthropic disturbance in soils. Ecological Indicators *75*, 73-81.

Apel, K., and Hirt, H. (2004). Reactive oxygen species: metabolism, oxidative stress, and signal transduction. Annu Rev Plant Biol *55*, 373-399.

Apostol, S., Ursu, D., Lehmann-Horn, F., and Melzer, W. (2009). Local calcium signals induced by hyper-osmotic stress in mammalian skeletal muscle cells. Journal of Muscle Research and Cell Motility *30*, 97-109.

Apt, K.E., Kroth, P.G., and Grossman, A.R. (1996). Stable nuclear transformation of the diatom Phaeodactylum tricornutum. Mol Gen Genet. *252*, 572-579.

Arias-Darraz, L., Cabezas, D., Colenso, C.K., Alegria-Arcos, M., Bravo-Moraga, F., Varas-Concha, I., Almonacid, D.E., Madrid, R., and Brauchi, S. (2015). A transient receptor potential ion channel

in Chlamydomonas shares key features with sensory transduction-associated TRP channels in mammals. Plant Cell *27*, 177-188.

Armbrust, E.V. (2009). The life of diatoms in the world's oceans. Nature *459*, 185-192.

Armbrust, E.V., Berges, J.A., Bowler, C., Green, B.R., Martinez, D., Putnam, N.H., Zhou, S., Allen, A.E., Apt, K.E., Bechner, M.*, et al.* (2004). The Genome of the Diatom Thalassiosira Pseudonana: Ecology, Evolution, and Metabolism. Science *306*, 79-86.

Arrigoni, C., Rohaim, A., Shaya, D., Findeisen, F., Stein, R.A., Nurva, S.R., Mishra, S., McHaourab, H.S., and Minor, D.L., Jr. (2016). Unfolding of a Temperature-Sensitive Domain Controls Voltage-Gated Channel Activation. Cell *164*, 922-936.

Atkinson, N., Feike, D., Mackinder, L.C., Meyer, M.T., Griffiths, H., Jonikas, M.C., Smith, A.M., and McCormick, A.J. (2016). Introducing an algal carbon-concentrating mechanism into higher plants: location and incorporation of key components. Plant Biotechnol J *14*, 1302-1315.

Atri, A., Amundson, J., Clapham, D., and Sneyd, J. (1993). A single-pool model for intracellular calcium oscillations and waves in the Xenopus laevis oocyte. Biophys J *65*, 1727-1739.

Ayee, M.A.A., and Levitan, I. (2018). Membrane Stiffening in Osmotic Swelling: Analysis of Membrane Tension and Elastic Modulus. Curr Top Membr *81*, 97-123.

Babsky, A., Hekmatyar, S.K., Gorski, T., Nelson, D.S., and Bansal, N. (2005). Heat-induced changes in intracellular Na+, pH and bioenergetic status in superfused RIF-1 tumour cells determined by 23Na and 31P magnetic resonance spectroscopy. International Journal of Hyperthermia *21*, 141-158.

Bagur, R., and Hajnóczky, G. (2017). Intracellular Ca(2+) Sensing: Its Role in Calcium Homeostasis and Signaling. Mol Cell *66*, 780-788.

Baier, T., Wichmann, J., Kruse, O., and Lauersen, K.J. (2018). Intron-containing algal transgenes mediate efficient recombinant gene expression in the green microalga Chlamydomonas reinhardtii. Nucleic Acids Res *46*, 6909-6919.

Balzano, S., Sarno, D., and Kooistra, W.H.C.F. (2010). Effects of salinity on the growth rate and morphology of ten Skeletonema strains. Journal of Plankton Research *33*, 937-945.

Barahimipour, R., Strenkert, D., Neupert, J., Schroda, M., Merchant, S.S., and Bock, R. (2015). Dissecting the contributions of GC content and codon usage to gene expression in the model alga Chlamydomonas reinhardtii. Plant J *84*, 704-717.

Bavi, O., Cox, C.D., Vossoughi, M., Naghdabadi, R., Jamali, Y., and Martinac, B. (2016). Influence of Global and Local Membrane Curvature on Mechanosensitive Ion Channels: A Finite Element Approach. Membranes (Basel) *6*.

Behera, S., Xu, Z., Luoni, L., Bonza, M.C., Doccula, F.G., De Michelis, M.I., Morris, R.J., Schwarzländer, M., and Costa, A. (2018). Cellular Ca²⁺ Signals Generate Defined pH Signatures in Plants. The Plant Cell *30*, 2704.

Behrendt, H.J., Germann, T., Gillen, C., Hatt, H., and Jostock, R. (2004). Characterization of the mouse cold-menthol receptor TRPM8 and vanilloid receptor type-1 VR1 using a fluorometric imaging plate reader (FLIPR) assay. Br J Pharmacol *141*, 737-745.

Bernaudat, F., Frelet-Barrand, A., Pochon, N., Dementin, S., Hivin, P., Boutigny, S., Rioux, J.B., Salvi, D., Seigneurin-Berny, D., Richaud, P.*, et al.* (2011). Heterologous expression of membrane proteins: choosing the appropriate host. PLoS One *6*, e29191.

Berridge, M., Lipp, P., and Bootman, M. (1999). Calcium signalling. Current biology *9*, R157-R159.

Bessen, M., Fay, R.B., and Witman, G.B. (1980). Calcium control of waveform in isolated flagellar axonemes of chlamydomonas. Journal of Cell Biology *86*, 446-455.

Best, B.P. (2015). Cryoprotectant Toxicity: Facts, Issues, and Questions. Rejuvenation Res *18*, 422-436.

Beyhl, D., Hörtensteiner, S., Martinoia, E., Farmer, E.E., Fromm, J., Marten, I., and Hedrich, R. (2009). The fou2 mutation in the major vacuolar cation channel TPC1 confers tolerance to inhibitory luminal calcium. The Plant Journal *58*, 715-723.

Bhattacharya, D., and Medlin, L.K. (1998). Algal Phylogeny and the Origin of Land Plants. Plant Physiology *116*, 9.

Bialecka-Fornal, M., Lee, H.J., and Phillips, R. (2015). The Rate of Osmotic Downshock Determines the Survival Probability of Bacterial Mechanosensitive Channel Mutants. Journal of Bacteriology *197*, 231.

Bick, A.G., Calvo, S.E., and Mootha, V.K. (2012). Evolutionary diversity of the mitochondrial calcium uniporter. Science (New York, N.Y.) *336*, 886-886.

Bickerton, P., Sello, S., Brownlee, C., Pittman, J.K., and Wheeler, G.L. (2016). Spatial and temporal specificity of Ca2+ signalling in Chlamydomonas reinhardtii in response to osmotic stress. New Phytol *212*, 920-933.

Blankenship, R.E. (2010). Early evolution of photosynthesis. Plant Physiol *154*, 434-438.

Bootman, M.D., Fearnley, C., Smyrnias, I., MacDonald, F., and Roderick, H.L. (2009). An update on nuclear calcium signalling. Journal of Cell Science *122*, 2337.

Bose, J., Pottosin, II, Shabala, S.S., Palmgren, M.G., and Shabala, S. (2011). Calcium efflux systems in stress signaling and adaptation in plants. Front Plant Sci *2*, 85.

Bothwell, J.H., Brownlee, C., Hetherington, A.M., Ng, C.K., Wheeler, G.L., and McAinsh, M.R. (2006). Biolistic delivery of Ca2+ dyes into plant and algal cells. Plant J *46*, 327-335.

Bowler, C., Allen, A.E., Badger, J.H., Grimwood, J., Jabbari, K., Kuo, A., Maheswari, U., Martens, C., Maumus, F., Otillar, R.P*., et al.* (2008). The Phaeodactylum genome reveals the evolutionary history of diatom genomes. Nature *456*, 239-244.

Bowler, C., Vardi, A., and Allen, A.E. (2009). Oceanographic and Biogeochemical Insights from Diatom Genomes. Annual Review of Marine Science *2*, 333-365.

Brauchi, S., Orio, P., and Latorre, R. (2004). Clues to understanding cold sensation: thermodynamics and electrophysiological analysis of the cold receptor TRPM8. Proc Natl Acad Sci U S A *101*, 15494-15499.

Brauchi, S., Orta, G., Salazar, M., Rosenmann, E., and Latorre, R. (2006). A Hot-Sensing Cold Receptor: C-Terminal Domain Determines Thermosensation in Transient Receptor Potential Channels. The Journal of Neuroscience *26*, 4835.

Braun, F.-J., and Hegemann, P. (1999). Direct measurement of cytosolic calcium and pH in living Chlamydomonas reinhardtii cells. European Journal of Cell Biology *78*, 199-208.

Brawley, S.H., Blouin, N.A., Ficko-Blean, E., Wheeler, G.L., Lohr, M., Goodson, H.V., Jenkins, J.W., Blaby-Haas, C.E., Helliwell, K.E., Chan, C.X*., et al.* (2017). Insights into the red algae and

eukaryotic evolution from the genome of Porphyra umbilicalis (Bangiophyceae, Rhodophyta). Proc Natl Acad Sci U S A *114*, E6361-E6370.

Brodie, J., Chan, C.X., De Clerck, O., Cock, J.M., Coelho, S.M., Gachon, C., Grossman, A.R., Mock, T., Raven, J.A., Smith, A.G.*, et al.* (2017). The Algal Revolution. Trends Plant Sci *22*, 726-738.

Broeze, R.J., Solomon, C.J., and Pope, D.H. (1978). Effects of low temperature on in vivo and in vitro protein synthesis in Escherichia coli and Pseudomonas fluorescens. Journal of bacteriology *134*, 861-874.

Brownlee, C., and Taylor, A.R. (1992). Cytoplasmic calcium, calcium currents and fluxes during fertilization and early development of Fucus serratus. In Progress in Plant Growth Regulation: Proceedings of the 14th International Conference on Plant Growth Substances, Amsterdam, 21–26 July, 1991, C.M. Karssen, L.C. van Loon, and D. Vreugdenhil, eds. (Dordrecht: Springer Netherlands), pp. 651-662.

Brownlee, C., and Wood, J.W. (1986). A gradient of cytoplasmic free calcium a in growing rhizoid cells of Fucus serratus. Nature *320*, 624-626.

Brunet, T., and Arendt, D. (2016). From damage response to action potentials: early evolution of neural and contractile modules in stem eukaryotes. Philos Trans R Soc Lond B Biol Sci *371*, 20150043.

Buck, J.M., Rio Bartulos, C., Gruber, A., and Kroth, P.G. (2018). Blasticidin-S deaminase, a new selection marker for genetic transformation of the diatom Phaeodactylum tricornutum. PeerJ *6*, e5884.

Cahusac, P.M.B. (2009). Effects of transient receptor potential (TRP) channel agonists and antagonists on slowly adapting type II mechanoreceptors in the rat sinus hair follicle. Journal of the Peripheral Nervous System *14*, 300-309.

Calabrese, B., Tabarean, I.V., Juranka, P., and Morris, C.E. (2002). Mechanosensitivity of N-type calcium channel currents. Biophys J *83*, 2560-2574.

Calcraft, P.J., Ruas, M., Pan, Z., Cheng, X., Arredouani, A., Hao, X., Tang, J., Rietdorf, K., Teboul, L., Chuang, K.T.*, et al.* (2009). NAADP mobilizes calcium from acidic organelles through two-pore channels. Nature *459*, 596-600.

Campbell, A.K. (2015). In Intracellular Calcium (Wiley), p. 18.

Campiglio, M., and Flucher, B.E. (2015). The Role of Auxiliary Subunits for the Functional Diversity of Voltage-Gated Calcium Channels. Journal of Cellular Physiology *230*, 2019-2031.

Cang, C., Bekele, B., and Ren, D. (2014). The voltage-gated sodium channel TPC1 confers endolysosomal excitability. Nature Chemical Biology *10*, 463.

Cang, C., Zhou, Y., Navarro, B., Seo, Y.J., Aranda, K., Shi, L., Battaglia-Hsu, S., Nissim, I., Clapham, D.E., and Ren, D. (2013). mTOR regulates lysosomal ATP-sensitive two-pore Na(+) channels to adapt to metabolic state. Cell *152*, 778-790.

Carafoli, E. (2002). Calcium signaling: a tale for all seasons. Proceedings of the National Academy of Sciences of the United States of America *99*, 1115-1122.

Carpaneto, A., Ivashikina, N., Levchenko, V., Krol, E., Jeworutzki, E., Zhu, J.K., and Hedrich, R. (2007). Cold transiently activates calcium-permeable channels in Arabidopsis mesophyll cells. Plant Physiol *143*, 487-494.

Carter, C., Pan, S., Zouhar, J., Avila, E.L., Girke, T., and Raikhel, N.V. (2004). The vegetative vacuole proteome of Arabidopsis thaliana reveals predicted and unexpected proteins. Plant Cell *16*, 3285-3303.

Cavicchioli, R., Thomas, T., and Curmi, P.M.G. (2000). Cold stress response in Archaea. Extremophiles *4*, 321-331.

Cessna, S.G., Chandra, S., and S., L.P. (1998). Hypo-osmotic Shock of Tobacco Cells Stimulates Ca2+ Fluxes Deriving First from External and then Internal Ca2+ Stores. Journal of Biological Chemistry *273*, 27286–27291.

Chen, H., and Jiang, J.-G. (2010). Osmotic adjustment and plant adaptation to environmental changes related to drought and salinity. Environmental Reviews *18*, 309-319.

Cheng, X., Zhang, X., Yu, L., and Xu, H. (2015). Calcium signaling in membrane repair. Semin Cell Dev Biol *45*, 24-31.

Cho, H., and Oh, U. (2013). Anoctamin 1 mediates thermal pain as a heat sensor. Curr Neuropharmacol *11*, 641-651.

Choi, W.G., Miller, G., Wallace, I., Harper, J., Mittler, R., and Gilroy, S. (2017). Orchestrating rapid long-distance signaling in plants with Ca2+ , ROS and electrical signals. Plant J *90*, 698-707.

Choi, W.G., Toyota, M., Kim, S.H., Hilleary, R., and Gilroy, S. (2014). Salt stress-induced Ca2+ waves are associated with rapid, long-distance root-to-shoot signaling in plants. Proc Natl Acad Sci U S A *111*, 6497-6502.

Christensen, A.P., Akyuz, N., and Corey, D.P. (2016). The Outer Pore and Selectivity Filter of TRPA1. PLoS One *11*, e0166167.

Chu, L., Ewe, D., Rio Bartulos, C., Kroth, P.G., and Gruber, A. (2016). Rapid induction of GFP expression by the nitrate reductase promoter in the diatom Phaeodactylum tricornutum. PeerJ *4*, e2344.

Chuang, H.H., Neuhausser, W.M., and Julius, D. (2004). The super-cooling agent icilin reveals a mechanism of coincidence detection by a temperature-sensitive TRP channel. Neuron *43*, 859-869.

Cibulsky, S.M., and Sather, W.A. (1999). Block by Ruthenium Red of Cloned Neuronal Voltage-Gated Calcium Channels. Journal of Pharmacology and Experimental Therapeutics *289*, 1447.

Clapham, D.E. (2003). TRP channels as cellular sensors. Nature *426*, 517-524.

Clapham, D.E. (2007). Calcium Signaling. Cell *131*, 1047-1058.

Cock, J.M., Sterck, L., Rouzé, P., Scornet, D., Allen, A.E., Amoutzias, G., Anthouard, V., Artiguenave, F., Aury, J.-M., Badger, J.H.*, et al.* (2010). The Ectocarpus genome and the independent evolution of multicellularity in brown algae. Nature *465*, 617-621.

Coelho, S.M., Taylor, A.R., Ryan, K.P., Sousa-Pinto, I., Brown, M.T., and Brownlee, C. (2002). Spatiotemporal patterning of reactive oxygen production and Ca(2+) wave propagation in fucus rhizoid cells. Plant Cell *14*, 2369-2381.

Cohn, S.A., and Disparti, N.C. (1994). Environmental factors influencing diatom cell motility. Journal of Phycology *30*, 818-828.

Collingridge, P., Brownlee, C., and Wheeler, G.L. (2013). Compartmentalized calcium signaling in cilia regulates intraflagellar transport. Curr Biol *23*, 2311-2318.

Conrard, L., and Tyteca, D. (2019). Regulation of Membrane Calcium Transport Proteins by the Surrounding Lipid Environment. Biomolecules *9*.

Cooksey, B., and Cooksey, K.E. (1980). Calcium Is Necessary for Motility in the Diatom Amphora coffeaeformis. Plant Physiology *65*, 129-131.

Cordero-Morales, J.F., and Vasquez, V. (2018). How lipids contribute to ion channel function, a fat perspective on direct and indirect interactions. Curr Opin Struct Biol *51*, 92-98.

Corey, D.P., García-Añoveros, J., Holt, J.R., Kwan, K.Y., Lin, S.-Y., Vollrath, M.A., Amalfitano, A., Cheung, E.L.M., Derfler, B.H., Duggan, A*., et al.* (2004). TRPA1 is a candidate for the mechanosensitive transduction channel of vertebrate hair cells. Nature *432*, 723-730.

Crafts-Brandner, S.J., and Salvucci, M.E. (2004). Analyzing the impact of high temperature and CO2 on net photosynthesis: biochemical mechanisms, models and genomics. Field Crops Research *90*, 75-85.

Crockett, E.L. (1998). Cholesterol Function in Plasma Membranes from Ectotherms: Membrane-Specific Roles in Adaptation to Temperature1. American Zoologist *38*, 291-304.

Currey, J.D. (2005). Hierarchies in Biomineral Structures. Science *309*, 253-254.

Czirják, G., and Enyedi, P. (2003). Ruthenium Red Inhibits TASK-3 Potassium Channel by Interconnecting Glutamate 70 of the Two Subunits. Molecular Pharmacology *63*, 646.

Dart, C. (2010). Lipid microdomains and the regulation of ion channel function. J Physiol *588*, 3169-3178.

Davis, L.C., Morgan, A.J., Chen, J.L., Snead, C.M., Bloor-Young, D., Shenderov, E., Stanton-Humphreys, M.N., Conway, S.J., Churchill, G.C., Parrington, J*., et al.* (2012). NAADP activates two-pore channels on T cell cytolytic granules to stimulate exocytosis and killing. Curr Biol *22*, 2331-2337.

de Martino, A., Bartual, A., Willis, A., Meichenin, A., Villazan, B., Maheswari, U., and Bowler, C. (2011). Physiological and molecular evidence that environmental changes elicit morphological interconversion in the model diatom Phaeodactylum tricornutum. Protist *162*, 462-481.

de Martino, A., Meichenin, A., Shi, J., Pan, K., and Bowler, C. (2007). Genetic and phenotypic characterization of Phaeodactylum tricornutum(Bacillariophyceae) accessions. Journal of Phycology *43*, 992-1009.

de Mendoza, D., Klages Ulrich, A., and Cronan, J.E. (1983). Thermal regulation of membrane fluidity in Escherichia coli. Effects of overproduction of beta-ketoacyl-acyl carrier protein synthase I. Journal of Biological Chemistry *258*, 2098-2101.

de Menorval, M.A., Mir, L.M., Fernandez, M.L., and Reigada, R. (2012). Effects of dimethyl sulfoxide in cholesterol-containing lipid membranes: a comparative study of experiments in silico and with cells. PLoS One *7*, e41733.

Dickson, D.M.J., and Kirst, G.O. (1987). Osmotic adjustment in marine eukaryotic algae: The role of inorganic ions, quaternary ammonium, tertiary sulphonium and carbohydrate solutes. New Phytologist *106*, 645-655.

Ding, Y., Jia, Y., Shi, Y., Zhang, X., Song, C., Gong, Z., and Yang, S. (2018). OST1-mediated BTF3L phosphorylation positively regulates CBFs during plant cold responses. The EMBO Journal *37*, e98228.

Ding, Y., Lv, J., Shi, Y., Gao, J., Hua, J., Song, C., Gong, Z., and Yang, S. (2019). EGR2 phosphatase regulates OST1 kinase activity and freezing tolerance in Arabidopsis. The EMBO Journal *38*, e99819.

DiPetrillo, C.G., and Smith, E.F. (2013). Methods for Analysis of Calcium/Calmodulin Signaling in Cilia and Flagella. Methods in Enzymology *524*, 37-57.

Dodd, A.N., Love, J., and Webb, A.A. (2005). The plant clock shows its metal: circadian regulation of cytosolic free Ca(2+). Trends Plant Sci *10*, 15-21.

Donaldson, S.P., and Deacon, J.W. (1993). Changes in motility of Pythium zoospores induced by calcium and calcium-modulating drugs. Mycological Research *97*, 877-883.

Dreyer, A., and Dietz, K.J. (2018). Reactive Oxygen Species and the Redox-Regulatory Network in Cold Stress Acclimation. Antioxidants (Basel) *7*.

Drummond, I.A., McClure, S.A., Poenie, M., Tsien, R.Y., and Steinhardt, R.A. (1986). Large changes in intracellular pH and calcium observed during heat shock are not responsible for the induction of heat shock proteins in Drosophila melanogaster. Mol Cell Biol *6*, 1767-1775.

Dufourc, E.J. (2008). Sterols and membrane dynamics. J Chem Biol *1*, 63-77.

Echarri, A., and Del Pozo, M.A. (2015). Caveolae – mechanosensitive membrane invaginations linked to actin filaments. Journal of Cell Science *128*, 2747.

Edel, K.H., and Kudla, J. (2015). Increasing complexity and versatility: how the calcium signaling toolkit was shaped during plant land colonization. Cell Calcium *57*, 231-246.

Edel, K.H., Marchadier, E., Brownlee, C., Kudla, J., and Hetherington, A.M. (2017). The Evolution of Calcium-Based Signalling in Plants. Curr Biol *27*, R667-R679.

Emery, L., Whelan, S., Hirschi, K.D., and Pittman, J.K. (2012). Protein Phylogenetic Analysis of Ca(2+)/cation Antiporters and Insights into their Evolution in Plants. Front Plant Sci *3*, 1.

Erdene-Ochir, E., Shin, B.-K., Kwon, B., Jung, C., and Pan, C.-H. (2019). Identification and characterisation of the novel endogenous promoter HASP1 and its signal peptide from Phaeodactylum tricornutum. Scientific Reports *9*, 9941.

Ermak, G., and Davies, K.J.A. (2002). Calcium and oxidative stress: from cell signaling to cell death. Molecular Immunology *38*, 713-721.

Evans, M.J., Choi, W.G., Gilroy, S., and Morris, R.J. (2016). A ROS-Assisted Calcium Wave Dependent on the AtRBOHD NADPH Oxidase and TPC1 Cation Channel Propagates the Systemic Response to Salt Stress. Plant Physiol *171*, 1771-1784.

Falciatore, A., d'Alcala, M.R., Croot, P., and Bowler, C. (2000). Perception of Environmental Signals by a Marine Diatom. Science *288*, 2363-2366.

Falkowski, P.G., Barber, R.T., and Smetacek, V. (1998). Biogeochemical Controls and Feedbacks on Ocean Primary Production. Science *281*, 200.

Falkowski, P.G., Katz, M.E., Knoll, A.H., Quigg, A., Raven, J.A., Schofield, O., and Taylor, F.J. (2004). The evolution of modern eukaryotic phytoplankton. Science *305*, 354-360.

Fasano, J.M., Massa, G.D., and Gilroy, S. (2002). Ionic signaling in plant responses to gravity and touch. J Plant Growth Regul. *21*, 71-88.

Ferrante, P., Catalanotti, C., Bonente, G., and Giuliano, G. (2008). An optimized, chemically regulated gene expression system for Chlamydomonas. PLoS One *3*, e3200.

Festa, M., Lagostena, L., and Carpaneto, A. (2016). Using the plant vacuole as a biological system to investigate the functional properties of exogenous channels and transporters. Biochim Biophys Acta *1858*, 607-612.

Field, C.B., Behrenfeld, M.J., Randerson, J.T., and Falkowski, P. (1998). Primary Production of the Biosphere: Integrating Terrestrial and Oceanic Components. Science *281*, 237.

Figueroa-Martinez, F., Nedelcu, A.M., Smith, D.R., and Reyes-Prieto, A. (2015). When the lights go out: the evolutionary fate of free-living colorless green algae. New Phytologist *206*, 972-982.

Fischer, N., and Rochaix, J.-D. (2001). The flanking regions of PsaD drive efficient gene expression in the nucleus of the green alga Chlamydomonas reinhardtii. Mol gen Genomics *265*, 888-894.

Fort, C., Collingridge, P., Brownlee, C., and Wheeler, G. (2020). Flagella Ca2+ elevations regulate pausing of retrograde intraflagellar transport trains in adherent Chlamydomonas flagella. bioRxiv *in peer review*.

Fortunato, A., Jaubert, M., Enomoto, G., Bouly, J.-P., Raniello, R., Thaler, M., Malviya, S., Bernardes, J., Rappaport, F., Gentili, B*., et al.* (2016). Diatom Phytochromes Reveal the Existence of Far-Red-Light-Based Sensing in the Ocean OPEN. The Plant Cell *28*.

Foyer, C.H. (2018). Reactive oxygen species, oxidative signaling and the regulation of photosynthesis. Environmental and Experimental Botany *154*, 134-142.

Francius, G., Tesson, B., Dague, E., Martin-Jézéquel, V., and Dufrêne, Y.F. (2008). Nanostructure and nanomechanics of live Phaeodactylum tricornutum morphotypes. Environmental Microbiology *10*, 1344-1356.

Franklin, K.A., Allen, T., and Whitelam, G.C. (2007). Phytochrome A is an irradiance-dependent red light sensor. The Plant Journal *50*, 108-117.

Fraser, K.P.P., Clarke, A., and Peck, L.S. (2002). Low-temperature protein metabolism: seasonal changes in protein synthesis and RNA dynamics in the Antarctic limpet Nacella concinna Strebel 1908. Journal of Experimental Biology *205*, 3077.

Fujita, Y., Murakami, A., Aizawa, K., and Ohki, K. (1994). Short-term and Long-term Adaptation of the Photosynthetic Apparatus: Homeostatic Properties of Thylakoids. In The Molecular Biology of Cyanobacteria, D.A. Bryant, ed. (Dordrecht: Springer Netherlands), pp. 677-692.

Fujiu, K., Nakayama, Y., Iida, H., Sokabe, M., and Yoshimura, K. (2011). Mechanoreception in motile flagella of Chlamydomonas. Nat Cell Biol *13*, 630-632.

Fujiu, K., Nakayama, Y., Yanagisawa, A., Sokabe, M., and Yoshimura, K. (2009). Chlamydomonas CAV2 encodes a voltage- dependent calcium channel required for the flagellar waveform conversion. Curr Biol *19*, 133-139.

Furuichi, T., Cunningham, K.W., and Muto, S. (2001). A putative two pore channel AtTPC1 mediates Ca(2+) flux in Arabidopsis leaf cells. Plant Cell Physiol. *42*, 900-905.

Furuya, T., Matsuoka, D., and Nanmori, T. (2014). Membrane rigidification functions upstream of the MEKK1-MKK2-MPK4 cascade during cold acclimation in Arabidopsis thaliana. FEBS Lett *588*, 2025-2030.

Garza-Sánchez, F., Chapman, D.J., and Cooper, J.B. (2009). Nitzschia Ovalis(Bacillariophyceae) Mono Lake Strain Accumulates 1,4/2,5 Cyclohexanetetrol in Response to Increased Salinity. Journal of Phycology *45*, 395-403.

Gaudet, R. (2008). A primer on ankyrin repeat function in TRP channels and beyond. Mol Biosyst *4*, 372-379.

Georgieva, K., and Yordanov, I. (1994). Temperature Dependence of Photochemical and Non-Photochemical Fluorescence Quenching in Intact Pea Leaves. Journal of Plant Physiology *144*, 754-759.

Georlette, D., Blaise, V., Collins, T., D'Amico, S., Gratia, E., Hoyoux, A., Marx, J.C., Sonan, G., Feller, G., and Gerday, C. (2004). Some like it cold: biocatalysis at low temperatures. FEMS Microbiology Reviews *28*, 25-42.

Goddard, H., Manison, N.F.H., Tomos, D., and Brownlee, C. (2000). Elemental propagation of calcium signals in response-specific patterns determined by environmental stimulus strength. Proceedings of the National Academy of Sciences *97*, 1932.

Gollan, P.J., Lima-Melo, Y., Tiwari, A., Tikkanen, M., and Aro, E.-M. (2017). Interaction between photosynthetic electron transport and chloroplast sinks triggers protection and signalling important for plant productivity. Philosophical Transactions of the Royal Society B: Biological Sciences *372*, 20160390.

Gomes, A.R., Byregowda, S.M., Veeregowda, B.M., and Balamurugan, V. (2016). An Overview of Heterologous Expression Host Systems for the Production of Recombinant Proteins. Advances in Animal and Veterinary Sciences *4*, 346-356.

González, A., Herrera, G., Ugarte, G., Restrepo, C., Piña, R., Pertusa, M., Orio, P., and Madrid, R. (2017). IKD Current in Cold Transduction and Damage-Triggered Cold Hypersensitivity. In The Plastic Brain, R. von Bernhardi, J. Eugenín, and K.J. Muller, eds. (Cham: Springer International Publishing), pp. 265-277.

Goodenough, U., Lin, H., and Lee, J.-H. (2007). Sex determination in Chlamydomonas, Vol 18.

Goodenough, U.W., Shames, B., Small, L., Saito, T., Crain, R.C., Sanders, M.A., and Salisbury, J.L. (1993). The Role of Calcium in the Chlamydomonas reinhardtii Mating Reaction. J Cell Biol *121*, 365-374.

Gorman, D., and Levine, R. (1965). Cytochrome F and Plastocyanin: their sequence in the photosynthetic electron transport chain of Chlamydomonas reinhardtii. Proc. Natl. Acad. Sci. *54*, 1665-1669.

Grimm, C., Chen, C.-C., Wahl-Schott, C., and Biel, M. (2017). Two-Pore Channels: Catalyzers of Endolysosomal Transport and Function. Frontiers in Pharmacology *8*, 45.

Groger, P., Poulsen, N., Klemm, J., Kroger, N., and Schlierf, M. (2016). Establishing super-resolution imaging for proteins in diatom biosilica. Sci Rep *6*, 36824.

Gu, C.X., Juranka, P.F., and Morris, C.E. (2001). Stretch-activation and stretch-inactivation of Shaker-IR, a voltage-gated K+ channel. Biophys J *80*, 2678-2693.

Guillard, R.L. (1975). Culture of phytoplankton for feeding marine invertebrates. Culture of Marine Invertebrate Animals, 29-60.

Guo, J., Zeng, W., Chen, Q., Lee, C., Chen, L., Yang, Y., Cang, C., Ren, D., and Jiang, Y. (2016). Structure of the voltage-gated two-pore channel TPC1 from Arabidopsis thaliana. Nature *531*, 196-201.

Guo, J., Zeng, W., and Jiang, Y. (2017). Tuning the ion selectivity of two-pore channels. Proc Natl Acad Sci U S A *114*, 1009-1014.

Guo, X., Liu, D., and Chong, K. (2018). Cold signaling in plants: Insights into mechanisms and regulation. Journal of Integrative Plant Biology *60*, 745-756.

Gurtovenko, A.A., and Anwar, J. (2007). Modulating the Structure and Properties of Cell Membranes: The Molecular Mechanism of Action of Dimethyl Sulfoxide. The Journal of Physical Chemistry B *111*, 10453-10460.

Gutenbrunner, S.A., Thalhamer, J., and Schmid, A.-M.M. (1994). Proteinaceous and immunochemical distinctions between the oval and fusiform morphotypes of Phaeodactylum tricornutum (bacillariophyceae). Journal of Phycology *30*, 129-136.

Guy, C.L., Huber, J.L., and Huber, S.C. (1992). Sucrose phosphate synthase and sucrose accumulation at low temperature. Plant physiology *100*, 502-508.

Hannig, G., and Makrides, S.C. (1998). Strategies for optimizing heterologous protein expression in Escherichia coli. Trends in Biotechnology *16*, 54-60.

Harley, C.D.G., Randall Hughes, A., Hultgren, K.M., Miner, B.G., Sorte, C.J.B., Thornber, C.S., Rodriguez, L.F., Tomanek, L., and Williams, S.L. (2006). The impacts of climate change in coastal marine systems. Ecology Letters *9*, 228-241.

Harz, H., and Hegemann, P. (1991). Rhodopsin-regulated calcium currents in Chlamydomonas. Nature *351*, 489 - 491.

Hasanuzzaman, M., Nahar, K., Alam, M.M., Roychowdhury, R., and Fujita, M. (2013). Physiological, biochemical, and molecular mechanisms of heat stress tolerance in plants. International journal of molecular sciences *14*, 9643-9684.

Haswell, E.S., Phillips, R., and Rees, D.C. (2011). Mechanosensitive channels: what can they do and how do they do it? Structure *19*, 1356-1369.

Haworth, A.S., and Brackenbury, W.J. (2019). Emerging roles for multifunctional ion channel auxiliary subunits in cancer. Cell calcium *80*, 125-140.

Hayashi, T., Harada, A., Sakai, T., and Takagi, S. (2006). Ca2+ transient induced by extracellular changes in osmotic pressure in Arabidopsis leaves: differential involvement of cell wall-plasma membrane adhesion. Plant, Cell and Environment *29*, 661-672.

Hedrich, R., Mueller, T.D., Becker, D., and Marten, I. (2018). Structure and Function of TPC1 Vacuole SV Channel Gains Shape. Molecular Plant *11*, 764-775.

Hedrich, R., and Neher, E. (2018). Venus Flytrap: How an Excitable, Carnivorous Plant Works. Trends in Plant Science *23*, 220-234.

Helliwell, K.E., Chrachri, A., Koester, J.A., Wharam, S., Verret, F., Taylor, A.R., Wheeler, G.L., and Brownlee, C. (2019). Alternative Mechanisms for Fast Na(+)/Ca(2+) Signaling in Eukaryotes via a Novel Class of Single-Domain Voltage-Gated Channels. Curr Biol *29*, 1503-1511 e1506.

Helliwell, K.E., Harrison, E., Christie-Oleza, J., Rees, A.P., Downe, J., Aguilo-Ferretjans, M.M., Al-Moosawi, L., Brownlee, C., and Wheeler, G.L. (2020a). A novel Ca2+ signalling pathway co-ordinates environmental phosphorus sensing and nitrogen metabolism in marine diatoms. (bioRxiv).

Helliwell, K.E., Kleiner, F.H., Hardstaff, H., Chrachri, A., Gaikwad, T., Salmon, D., Smirnoff, N., Wheeler, G., and Brownlee, C. (2020b). Spatiotemporal patterns of intracellular Ca2+

signalling enable sophisticated perception of a dynamic osmotic environment in marine diatoms. New Phytol *in revision*.

Hendil, K.B., and Hoffmann, E.K. (1974). Cell volume regulation in ehrlich ascites tumor cells. Journal of Cellular Physiology *84*, 115-125.

Hepler, P.K. (2016). The Cytoskeleton and Its Regulation by Calcium and Protons. Plant Physiol *170*, 3-22.

Hetherington, A.M., and Brownlee, C. (2004). The generation of Ca2+ signals in plants. Annual Review of Plant Biology *55*, 401-427.

Hill-Eubanks, D.C., Werner, M.E., Heppner, T.J., and Nelson, M.T. (2011). Calcium signaling in smooth muscle. Cold Spring Harb Perspect Biol *3*, a004549.

Hires, S.A., Tian, L., and Looger, L.L. (2008). Reporting neural activity with genetically encoded calcium indicators. Brain Cell Biol *36*, 69-86.

Hjort Ipsen, J., Karlström, G., Mourtisen, O.G., Wennerström, H., and Zuckermann, M.J. (1987). Phase equilibria in the phosphatidylcholine-cholesterol system. Biochimica et Biophysica Acta (BBA) - Biomembranes *905*, 162-172.

Hodges, M.E., Wickstead, B., Gull, K., and Langdale, J.A. (2012). The evolution of land plant cilia. New Phytologist *195*, 526-540.

Hodgson, R.A.J., Orr, G.R., and Raison, J.K. (1987). Inhibition of photosynthesis by chilling in the light. Plant Science *49*, 75-79.

Hoffmann, E.K., Lambert, I.H., and Pedersen, S.F. (2009). Physiology of Cell Volume Regulation in Vertebrates. Physiological Reviews *89*, 193-277.

Hopes, A. (2017). Expanding the molecular toolbox in diatoms: developing a transformation system, CRISPR-Cas and Inverse Yeast-1-hybrid. . PhD Thesis, University of East Anglia.

Hopes, A., Nekrasov, V., Belshaw, N., Grouneva, I., Kamoun, S., and Mock, T. (2017). Genome Editing in Diatoms Using CRISPR-Cas to Induce Precise Bi-allelic Deletions. Bio-Protocol *7*.

Hopes, A., Nekrasov, V., Kamoun, S., and Mock, T. (2016). Editing of the urease gene by CRISPR-Cas in the diatom Thalassiosira pseudonana. Plant Methods *12*, 49.

Horton, J.S., Wakano, C.T., Speck, M., and Stokes, A.J. (2015). Two-pore channel 1 interacts with citron kinase, regulating completion of cytokinesis. Channels (Austin) *9*, 21-29.

Howland, R.J.M., Tappin, A.D., Uncles, R.J., Plummer, D.H., and Bloomer, N.J. (2000). Distributions and seasonal variability of pH and alkalinity in the Tweed Estuary, UK. Science of The Total Environment *251-252*, 125-138.

Hua, C., Wang, Y., Zheng, X., Dou, D., Zhang, Z., Govers, F., and Wang, Y. (2008). A Phytophthora sojae G-protein alpha subunit is involved in chemotaxis to soybean isoflavones. Eukaryotic cell *7*, 2133-2140.

Huang, B.P.-H. (1986). Chlamydomonas reinhardtii: A Model System for the Genetic Analysis of Flagellar Structure and Motility. In International Review of Cytology, G.H. Bourne, J.F. Danielli, and K.W. Jeon, eds. (Academic Press), pp. 181-215.

Huang, F., Luo, J., Ning, T., Cao, W., Jin, X., Zhao, H., Wang, Y., and Han, S. (2017). Cytosolic and Nucleosolic Calcium Signaling in Response to Osmotic and Salt Stresses Are Independent of Each Other in Roots of Arabidopsis Seedlings. In Frontiers in Plant Science, p. 1648.

Huang, G.-T., Ma, S.-L., Bai, L.-P., Zhang, L., Ma, H., Jia, P., Liu, J., Zhong, M., and Guo, Z.-F. (2012). Signal transduction during cold, salt, and drought stresses in plants. Molecular Biology Reports *39*, 969-987.

Huang, H., Bae, C., Sachs, F., and Suchyna, T.M. (2013). Caveolae Regulation of Mechanosensitive Channel Function in Myotubes. PLOS ONE *8*, e72894.

Huang, K., Diener, D.R., Mitchell, A., Pazour, G.J., Witman, G.B., and Rosenbaum, J.L. (2007). Function and dynamics of PKD2 in Chlamydomonas reinhardtii flagella. J Cell Biol *179*, 501-514.

Huner, N.P.A., Öquist, G., and Sarhan, F. (1998). Energy balance and acclimation to light and cold. Trends in Plant Science *3*, 224-230.

Irihimovitch, V., and Yehudai-Resheff, S. (2008). Phosphate and sulfur limitation responses in the chloroplast of Chlamydomonas reinhardtii. FEMS Microbiol Lett *283*, 1-8.

Ishibashi, K., Suzuki, M., and Imai, M. (2000). Molecular cloning of a novel form (two-repeat) protein related to voltage-gated sodium and calcium channels. Biochem Biophys Res Commun *270*, 370-376.

J C Lewin, a., and Guillard, R.R.L. (1963). Diatoms. Annual Review of Microbiology *17*, 373-414.

Jackson, S.L., and Hardham, A. (1996). A transient rise in cytoplasmic free calcium is required to induce cytokinesis in zoosporangia of Phytophthora cinnamomi. European journal of cell biology *69 2*, 180-188.

Jahns, P., and Holzwarth, A.R. (2012). The role of the xanthophyll cycle and of lutein in photoprotection of photosystem II. Biochimica et Biophysica Acta (BBA) - Bioenergetics *1817*, 182-193.

Jha, A., Ahuja, M., Patel, S., Brailoiu, E., and Muallem, S. (2014). Convergent regulation of the lysosomal two-pore channel-2 by Mg(2)(+), NAADP, PI(3,5)P(2) and multiple protein kinases. EMBO J *33*, 501-511.

Jimenez-Gonzalez, C., Michelangeli, F., Harper, C.V., Barratt, C.L., and Publicover, S.J. (2006). Calcium signalling in human spermatozoa: a specialized 'toolkit' of channels, transporters and stores. Hum Reprod Update *12*, 253-267.

Kadota, Y., Furuichi, T., Ogasawara, Y., Goh, T., Higashi, K., Muto, S., and Kuchitsu, K. (2004). Identification of putative voltage-dependent Ca2+-permeable channels involved in cryptogein-induced Ca2+ transients and defense responses in tobacco BY-2 cells. Biochem Biophys Res Commun *317*, 823-830.

Kamiya, R., and Witman, G.B. (1984). Submicromolar levels of calcium control the balance of beating between the two flagella in demembranated models of Chlamydomonas. The Journal of cell biology *98*, 97-107.

Karlson, D., Nakaminami, K., Toyomasu, T., and Imai, R. (2002). A Cold-regulated Nucleic Acid-binding Protein of Winter Wheat Shares a Domain with Bacterial Cold Shock Proteins. Journal of Biological Chemistry *277*, 35248-35256.

Karpinski, S., Reynolds, H., Karpinska, B., Wingsle, G., Creissen, G., and Mullineaux, P. (1999). Systemic Signaling and Acclimation in Response to Excess Excitation Energy in Arabidopsis. Science *284*, 654.

Kearse, M., Moir, R., Wilson, A., Stones-Havas, S., Cheung, M., Sturrock, S., Buxton, S., Cooper, A., Markowitz, S., Duran, C.*, et al.* (2012). Geneious Basic: an integrated and extendable desktop software platform for the organization and analysis of sequence data. Bioinformatics *28*, 1647-1649.

Keeling, P.J., Burki, F., Wilcox, H.M., Allam, B., Allen, E.E., Amaral-Zettler, L.A., Armbrust, E.V., Archibald, J.M., Bharti, A.K., Bell, C.J.*, et al.* (2014). The Marine Microbial Eukaryote Transcriptome Sequencing Project (MMETSP): illuminating the functional diversity of eukaryotic life in the oceans through transcriptome sequencing. PLoS Biol *12*, e1001889.

Keinath, N.F., Waadt, R., Brugman, R., Schroeder, J.I., Grossmann, G., Schumacher, K., and Krebs, M. (2015). Live Cell Imaging with R-GECO1 Sheds Light on flg22- and Chitin-Induced Transient [Ca(2+)]cyt Patterns in Arabidopsis. Mol Plant *8*, 1188-1200.

Kerwin, J.L., and Washino, R.K. (1986). Oosporogenesis by Lagenidium giganteum: induction and maturation are regulated by calcium and calmodulin. Canadian Journal of Microbiology *32*, 663-672.

Keto-Timonen, R., Hietala, N., Palonen, E., Hakakorpi, A., Lindström, M., and Korkeala, H. (2016). Cold Shock Proteins: A Minireview with Special Emphasis on Csp-family of Enteropathogenic Yersinia. Front Microbiol *7*, 1151-1151.

Kiegle, E., Moore, C.A., Haseloff, J., Tester, M.A., and Knight, M.R. (2000). Cell-type specific calcium responses to drought, salt and cold in the Arabidopsis root. The Plant Journal *32*, 267-278.

Kiep, V., Vadassery, J., Lattke, J., Maaß, J.-P., Boland, W., Peiter, E., and Mithöfer, A. (2015). Systemic cytosolic Ca2+ elevation is activated upon wounding and herbivory in Arabidopsis. New Phytologist *207*, 996-1004.

Kim, J.S., Park, S.J., Kwak, K.J., Kim, Y.O., Kim, J.Y., Song, J., Jang, B., Jung, C.H., and Kang, H. (2007). Cold shock domain proteins and glycine-rich RNA-binding proteins from Arabidopsis thaliana can promote the cold adaptation process in Escherichia coli. Nucleic Acids Res *35*, 506-516.

Kingston-Smith, A.H., Harbinson, J., Williams, J., and Foyer, C.H. (1997). Effect of Chilling on Carbon Assimilation, Enzyme Activation, and Photosynthetic Electron Transport in the Absence of Photoinhibition in Maize Leaves. Plant Physiology *114*, 1039.

Kinne, R.K.H. (1993). The role of organic osmolytes in osmoregulation: From bacteria to mammals. Journal of Experimental Zoology *263*, 346-355.

Kintzer, A.F., and Stroud, R.M. (2018). On the structure and mechanism of two-pore channels. FEBS J *285*, 233-243.

Kirst, G.O. (1990). Salinity Tolerance of Eukaryotic Marine Algae. Annual Review of Plant Physiology and Plant Molecular Biology *41*, 21-53.

Kleist, T.J., Spencley, A.L., and Luan, S. (2014). Comparative phylogenomics of the CBL-CIPK calcium-decoding network in the moss Physcomitrella, Arabidopsis, and other green lineages. Front Plant Sci *5*, 187.

Klinkert, B., and Narberhaus, F. (2009). Microbial thermosensors. Cellular and Molecular Life Sciences *66*, 2661-2676.

Knight, H., Trewavas, A.J., and Knight, M.R. (1996). Cold calcium signaling in Arabidopsis involves two cellular pools and a change in calcium signature after acclimation. The Plant Cell *8*, 489.

Knight, H., Trewavas, A.J., and Knight, M.R. (1997). Calcium signalling in Arabidopsis thaliana responding to drought and salinity. The plant journal *12*, 1067-1078.

Knight, M.R., and Knight, H. (2012). Low-temperature perception leading to gene expression and cold tolerance in higher plants. New Phytol *195*, 737-751.

Knight, M.R., Smith, S.M., and Trewavas, A.J. (1992). Wind-induced plant motion immediately increases cytosolic calcium. Plant Biology *89*, 4967-4971.

Koblenz, B., and Lechtreck, K.F. (2005). The NIT1 promoter allows inducible and reversible silencing of centrin in Chlamydomonas reinhardtii. Eukaryot Cell *4*, 1959-1962.

Kocot, K.M., Aguilera, F., McDougall, C., Jackson, D.J., and Degnan, B.M. (2016). Sea shell diversity and rapidly evolving secretomes: insights into the evolution of biomineralization. Front Zool *13*, 23.

Korogod, S.M., and Demianenko, L.E. (2017). Temperature Effects on Non-TRP Ion Channels and Neuronal Excitability. Opera Medica et Physiologica *3*, 84-92.

Kreps, J.A., Wu, Y., Chang, H.S., Zhu, T., Wang, X., and Harper, J.F. (2002). Transcriptome changes for Arabidopsis in response to salt, osmotic, and cold stress. Plant Physiol *130*, 2129-2141.

Kropf, D.L. (1992). Establishment and expression of cellular polarity in fucoid zygotes. Microbiol Rev *56*, 316-339.

Kuchitsu, K., Ward, C.W., Allen, G.J., Schelle, I., and Schroeder, J.I. (2002). Loading acetoxymethyl ester fluorescent dyes into the cytoplasm of Arabidopsis and Commelina guard cells. New Phytologist *153*, 527-533.

Kumar, S., Stecher, G., and Tamura, K. (2016). MEGA7: Molecular Evolutionary Genetics Analysis Version 7.0 for Bigger Datasets. Mol Biol Evol *33*, 1870-1874.

Kung, C., Martinac, B., and Sukharev, S. (2010). Mechanosensitive channels in microbes. Annu Rev Microbiol *64*, 313-329.

Kuo, I.Y., and Ehrlich, B.E. (2015). Signaling in muscle contraction. Cold Spring Harb Perspect Biol *7*, a006023.

Kurusu, T., Iida, H., and Kuchitsu, K. (2012). Roles of a putative mechanosensitive plasma membrane Ca2+-permeable channel OsMCA1 in generation of reactive oxygen species and hypo-osmotic signaling in rice. Plant signaling & behavior *7*, 796-798.

Kurusu, T., Kuchitsu, K., and Tada, Y. (2015). Plant signaling networks involving Ca2+ and Rboh/Nox-mediated ROS production under salinity stress. Frontiers in Plant Science *6*.

Kurusu, T., Sakurai, Y., Miyao, A., Hirochika, H., and Kuchitsu, K. (2004). Identification of a putative voltage-gated Ca2+ -permeable channel (OsTPC1) involved in Ca2+ influx and regulation of growth and development in rice. Plant Cell Physiol. *45*, 693-702.

Lacour, T., Larivière, J., Ferland, J., Bruyant, F., Lavaud, J., and Babin, M. (2018). The Role of Sustained Photoprotective Non-photochemical Quenching in Low Temperature and High Light Acclimation in the Bloom-Forming Arctic Diatom Thalassiosira gravida. Frontiers in Marine Science *5*, 354.

Lagostena, L., Festa, M., Pusch, M., and Carpaneto, A. (2017). The human two-pore channel 1 is modulated by cytosolic and luminal calcium. Sci Rep *7*, 43900.

Laitko, U., and Morris, C.E. (2004). Membrane tension accelerates rate-limiting voltage-dependent activation and slow inactivation steps in a Shaker channel. The Journal of general physiology *123*, 135-154.

Lamas, J.A., Rueda-Ruzafa, L., and Herrera-Pérez, S. (2019). Ion Channels and Thermosensitivity: TRP, TREK, or Both? International journal of molecular sciences *20*, 2371.

Lanner, J.T., Georgiou, D.K., Joshi, A.D., and Hamilton, S.L. (2010). Ryanodine receptors: structure, expression, molecular details, and function in calcium release. Cold Spring Harbor perspectives in biology *2*, a003996-a003996.

Larisch, N., Schulze, C., Galione, A., and Dietrich, P. (2012). An N-terminal dileucine motif directs two-pore channels to the tonoplast of plant cells. Traffic *13*, 1012-1022.

Lear, P.V., González-Touceda, D., Porteiro Couto, B., Viaño, P., Guymer, V., Remzova, E., Tunn, R., Chalasani, A., García-Caballero, T., Hargreaves, I.P.*, et al.* (2014). Absence of intracellular ion channels TPC1 and TPC2 leads to mature-onset obesity in male mice, due to impaired lipid availability for thermogenesis in brown adipose tissue. Endocrinology *153*, 975-986.

Lenglet, A., Jaslan, D., Toyota, M., Mueller, M., Muller, T., Schonknecht, G., Marten, I., Gilroy, S., Hedrich, R., and Farmer, E.E. (2017). Control of basal jasmonate signalling and defence through modulation of intracellular cation flux capacity. New Phytol *216*, 1161-1169.

León, R., and Fernández, E. (2007). Nuclear Transformation of Eukaryotic Microalgae. In Transgenic Microalgae as Green Cell Factories, R. León, A. Galván, and E. Fernández, eds. (New York, NY: Springer New York), pp. 1-11.

Levitan, I., Fang, Y., Rosenhouse-Dantsker, A., and Romanenko, V. (2010). Cholesterol and ion channels. Subcell Biochem *51*, 509-549.

Lew, R.R. (1999). Comparative analysis of Ca2+ and H+ flux magnitude and location along growing hyphae of Saprolegnia ferax and Neurospora crassa. European Journal of Cell Biology *78*, 892-902.

Lewin, J.C., Lewin, R.A., and Philpott, D.E. (1958). Observations on Phaeodactylum tricornutum. J. Gen. Mircobiol. *18*, 418-426.

Li, J., Blanchoin, L., and Staiger, C.J. (2015). Signaling to actin stochastic dynamics. Annu Rev Plant Biol *66*, 415-440.

Li, L., Saga, N., and Mikami, K. (2009). Ca2+ influx and phosphoinositide signalling are essential for the establishment and maintenance of cell polarity in monospores from the red alga Porphyra yezoensis. Journal of Experimental Botany *60*, 3477-3489.

Li, M., Yu, Y., and Yang, J. (2011). Structural biology of TRP channels. Adv Exp Med Biol *704*, 1-23.

Li, X., Zhang, R., Patena, W., Gang, S.S., Blum, S.R., Ivanova, N., Yue, R., Robertson, J.M., Lefebvre, P.A., Fitz-Gibbon, S.T.*, et al.* (2016). An Indexed, Mapped Mutant Library Enables Reverse Genetics Studies of Biological Processes in Chlamydomonas reinhardtii. Plant Cell *28*, 367-387.

Liang, Y., and Pan, J. (2013). Regulation of flagellar biogenesis by a calcium dependent protein kinase in Chlamydomonas reinhardtii. PLoS One *8*, e69902.

Lin, C., Yu, Y., Kadono, T., Iwata, M., Umemura, K., Furuichi, T., Kuse, M., Isobe, M., Yamamoto, Y., Matsumoto, H.*, et al.* (2005). Action of aluminum, novel TPC1-type channel inhibitor, against

salicylate-induced and cold-shock-induced calcium influx in tobacco BY-2 cells. Biochemical and Biophysical Research Communications *332*, 823-830.

Liu, L., and Rohacs, T. (2020). Regulation of the cold-sensing TRPM8 channels by phosphoinositides and Gq-coupled receptors. Channels *14*, 79-86.

Liu, T., Jiao, X., Yang, S., Zhang, Z., Ye, X., Li, J., Qi, H., and Hu, X. (2020). Crosstalk between GABA and ALA to improve antioxidation and cell expansion of tomato seedling under cold stress. Environmental and Experimental Botany, 104228.

Liu, X., Zhou, Y., Xiao, J., and Bao, F. (2018). Effects of Chilling on the Structure, Function and Development of Chloroplasts. Frontiers in Plant Science *9*.

Liu, Y., Dang, P., Liu, L., and He, C. (2019). Cold acclimation by the CBF-COR pathway in a changing climate: Lessons from Arabidopsis thaliana. Plant Cell Rep *38*, 511-519.

Liu, Y.N., Zhang, T.J., Lu, X.X., Ma, B.L., Ren, A., Shi, L., Jiang, A.L., Yu, H.S., and Zhao, M.W. (2017). Membrane fluidity is involved in the regulation of heat stress induced secondary metabolism in Ganoderma lucidum. Environ Microbiol *19*, 1653-1668.

Lohret, T.A., McNally, F.J., and Quarmby, L.M. (1998). A Role for Katanin-mediated Axonemal Severing during Chlamydomonas Deflagellation. Mol biol cell *9*, 1195-1207.

Lomas, M.W., Baer, S.E., Acton, S., and Krause, J.W. (2019). Pumped Up by the Cold: Elemental Quotas and Stoichiometry of Cold-Water Diatoms. Frontiers in Marine Science *6*.

Los, D., Horvath, I., Vigh, L., and Murata, N. (1993). The temperature-dependent expression of the desaturase gene desA in Synechocystis PCC6803. FEBS Letters *318*, 57-60.

Lucké, B., and McCutcheon, M. (1932). The living cell as an osmotic system and its permeability to water. Physiological Reviews *12*, 68-139.

Lukatkin, A.S. (2002). Contribution of Oxidative Stress to the Development of Cold-Induced Damage to Leaves of Chilling-Sensitive Plants: 1. Reactive Oxygen Species Formation during Plant Chilling. Russian Journal of Plant Physiology *49*, 622-627.

Lundbæk, J.A., Birn, P., Tape, S.E., Toombes, G.E.S., Søgaard, R., Koeppe, R.E., Gruner, S.M., Hansen, A.J., and Andersen, O.S. (2005). Capsaicin Regulates Voltage-Dependent Sodium Channels by Altering Lipid Bilayer Elasticity. Molecular Pharmacology *68*, 680.

Lyon, B.R., and Mock, T. (2014). Polar Microalgae: New Approaches towards Understanding Adaptations to an Extreme and Changing Environment. Biology (Basel) *3*, 56-80.

Ma, Y., Dai, X., Xu, Y., Luo, W., Zheng, X., Zeng, D., Pan, Y., Lin, X., Liu, H., Zhang, D*., et al.* (2015). COLD1 Confers Chilling Tolerance in Rice. Cell *160*, 1209-1221.

MacDonald, J.D. (1869). On the structure of the Diatomaceous frustule and its genetic cycle. Ann. Mag. mt. Hist. *4*, 1-8.

Mackinder, L., Wheeler, G., Schroeder, D., Riebesell, U., and Brownlee, C. (2010). Molecular Mechanisms Underlying Calcification in Coccolithophores. Geomicrobiology Journal *27*, 585-595.

Mackinder, L.C.M. (2018). The Chlamydomonas CO2 -concentrating mechanism and its potential for engineering photosynthesis in plants. New Phytol *217*, 54-61.

MacKinnon, R. (1995). Pore Loops: An Emerging Theme in Ion Channel Structure Neuron *14*, 889-892.

Maheswari, U., Montsant, A., Goll, J., Krishnasamy, S., Rajyashri, K.R., Patell, V.M., and Bowler, C. (2005). The Diatom EST Database. Nucleic Acids Res *33*, D344-347.

Malviyaa, S., Scalcob, E., Audicc, S., Vincenta, F., Veluchamya, A., Poulaind, J., Wincker, P., Iudiconeb, D., Vargasc, C., Bittnera, L*., et al.* (2016). Insights into global diatom distribution and diversity in the world's ocean. PNAS *113*, E1516-E1525.

Manishankar, P., and Kudla, J. (2015). Cold tolerance encoded in one SNP. Cell *160*, 1045-1046.

Mann, D.G. (1993). Patterns of sexual reproduction in diatoms. In Twelfth International Diatom Symposium, H. van Dam, ed. (Dordrecht, Springer Netherlands), pp. 11-20.

Mao, Y., Yan, R., Li, A., Zhang, Y., Li, J., Du, H., Chen, B., Wei, W., Zhang, Y., Sumners, C*., et al.* (2015). Lentiviral Vectors Mediate Long-Term and High Efficiency Transgene Expression in HEK 293T cells. Int J Med Sci *12*, 407-415.

Marchadier, E., Oates, M.E., Fang, H., Donoghue, P.C., Hetherington, A.M., and Gough, J. (2016). Evolution of the Calcium-Based Intracellular Signaling System. Genome Biol Evol *8*, 2118-2132.

Marchant, J.S., and Patel, S. (2013). Questioning regulation of two-pore channels by NAADP. Messenger (Los Angel) *2*, 113-119.

Marchant, J.S., and Patel, S. (2015). Two-pore channels at the intersection of endolysosomal membrane traffic. Biochem Soc Trans *43*, 434-441.

Mathur, S., Agrawal, D., and Jajoo, A. (2014). Photosynthesis: response to high temperature stress. J Photochem Photobiol B *137*, 116-126.

McAinsh, M.R., and Pittman, J.K. (2009). Shaping the calcium signature. New Phytologist *181*, 275-294.

McGoldrick, L.L., Singh, A.K., Demirkhanyan, L., Lin, T.-Y., Casner, R.G., Zakharian, E., and Sobolevsky, A.I. (2019). Structure of the thermo-sensitive TRP channel TRP1 from the alga Chlamydomonas reinhardtii. Nature Communications *10*, 4180.

McKemy, D.D. (2018). Molecular basis of peripheral innocuous cold sensitivity. Handb Clin Neurol *156*, 57-67.

McKemy, D.D., Neuhausser, W.M., and Julius, D. (2002). Identification of a cold receptor reveals a general role for TRP channels in thermosensation. Nature *416*, 52-58.

McLachlan, D.H., Underwood, G.J.C., Taylor, A.R., and Brownlee, C. (2012). Calcium release from intracellular stores is necessary for the photophobic response in the benthic diatom Navicula Permiuta (Bacillariophyceae). Journal of Phycology *48*, 675-681.

Melencion, S.M.B., Chi, Y.H., Pham, T.T., Paeng, S.K., Wi, S.D., Lee, C., Ryu, S.W., Koo, S.S., and Lee, S.Y. (2017). RNA Chaperone Function of a Universal Stress Protein in Arabidopsis Confers Enhanced Cold Stress Tolerance in Plants. International journal of molecular sciences *18*, 2546.

Merchant, S.S., Prochnik, S.E., Vallon, O., Harris, E.H., Karpowicz, S.J., Witman, G.B., Terry, A., Salamov, A., Fritz-Laylin, L.K., Marechal-Drouard, L*., et al.* (2007). The Chlamydomonas genome reveals the evolution of key animal and plant functions. Science *318*, 245-250.

Merlot, S., Mustilli, A.-C., Genty, B., North, H., Lefebvre, V., Sotta, B., Vavasseur, A., and Giraudat, J. (2002). Use of infrared thermal imaging to isolate Arabidopsis mutants defective in stomatal regulation. The Plant Journal *30*, 601-609.

Miklasz, K.A., and Denny, M.W. (2010). Diatom sinkings speeds: Improved predictions and insight from a modified Stokes' law. Limnology and Oceanography *55*, 2513-2525.

Miller, A.J., and Zhou, J.J. (2000). Xenopus oocytes as an expression system for plant transporters. Biochimica et Biophysica Acta (BBA) - Biomembranes *1465*, 343-358.

Minagawa, J., and Tokutsu, R. (2015). Dynamic regulation of photosynthesis in Chlamydomonas reinhardtii. The Plant Journal *82*, 413-428.

Minorsky, P.V., and Spanswick, R.M. (1989). Electrophysiological evidence for a role for calcium in temperature sensing by roots of cucumber seedlings. Plant, Cell & Environment *12*, 137-143.

Mitchell, D.R. (2001). Chlamydomonas flagella. Journal of Phycology *36*, 261-273.

Mithöfer, A., and Mazars, C. (2002). Aequorin-based measurements of intracellular Ca2+-signatures in plant cells Biol. Proced. *4*, 105-118.

Miura, K., and Furumoto, T. (2013). Cold signaling and cold response in plants. International journal of molecular sciences *14*, 5312-5337.

Miwa, H., Sun, J., Oldroyd, G.E.D., and Downie, J.A. (2006). Analysis of Nod-Factor-Induced Calcium Signaling in Root Hairs of Symbiotically Defective Mutants of Lotus japonicus. MPMI *19*, 914-923.

Miyawaki, A., Llopsis, J., Heim, R., McCaffery, J.M., Adams, J.A., Ikura, M., and Tsien, R.Y. (1997). Fluorescent indicators for Ca2+ based on green fluorescent proteins and calmodulin. Nature *388*, 882-887.

Mizrachi, A., Graff van Creveld, S., Shapiro, O.H., Rosenwasser, S., and Vardi, A. (2019). Light-dependent single-cell heterogeneity in the chloroplast redox state regulates cell fate in a marine diatom. eLife *8*, e47732.

Moller, I.M., and Sweetlove, L.J. (2010). ROS signalling--specificity is required. Trends Plant Sci *15*, 370-374.

Moran, Y., Barzilai, M.G., Liebeskind, B.J., and Zakon, H.H. (2015). Evolution of voltage-gated ion channels at the emergence of Metazoa. J Exp Biol *218*, 515-525.

Morgan, A.J., and Galione, A. (2014). Two-pore channels (TPCs): current controversies. Bioessays *36*, 173-183.

Mori, K., Renhu, N., Naito, M., Nakamura, A., Shiba, H., Yamamoto, T., Suzaki, T., Iida, H., and Miura, K. (2018). Ca(2+)-permeable mechanosensitive channels MCA1 and MCA2 mediate cold-induced cytosolic Ca(2+) increase and cold tolerance in Arabidopsis. Sci Rep *8*, 550.

Morris, C.E., and Juranka, P.F. (2007). Chapter 11 - Lipid Stress at Play: Mechanosensitivity of Voltage-Gated Channels. In Current Topics in Membranes, O.P. Hamill, ed. (Academic Press), pp. 297-338.

Morris, E.J.S., Jackson, S.L., and Garrill, A. (2011). An investigation of the effects of Ca2+ channel inhibitors on branching and chemotropism in the oomycete Achlya bisexualis: Support for a role for Ca2+ in apical dominance. Fungal Genetics and Biology *48*, 512-518.

Motiwalla, M.J., Sequeira, M.P., and D'Souza, J.S. (2014). Two Calcium-Dependent Protein Kinases fromChlamydomonas reinhardtiiare transcriptionally regulated by nutrient starvation. Plant Signaling & Behavior *9*, e27969.

Mueller-Tribbensee, S.M., Karna, M., Khalil, M., Neurath, M.F., Reeh, P.W., and Engel, M.A. (2015). Differential Contribution of TRPA1, TRPV4 and TRPM8 to Colonic Nociception in Mice. PLoS One *10*, e0128242.

Murata, N., and Los, D.A. (1997). Membrane Fluidity and Temperature Perception. Plant physiology *115*, 875-879.

Murata, N., and Los, D.A. (2006). Histidine kinase Hik33 is an important participant in cold-signal transduction in cyanobacteria. Physiologia Plantarum *126*, 17-27.

Murata, N., Takahashi, S., Nishiyama, Y., and Allakhverdiev, S.I. (2007). Photoinhibition of photosystem II under environmental stress. Biochimica et Biophysica Acta (BBA) - Bioenergetics *1767*, 414-421.

Murchie, E.H., and Ruban, A.V. (2020). Dynamic non-photochemical quenching in plants: from molecular mechanism to productivity. The Plant Journal *101*, 885-896.

Murray, P., Hayward, S.A.L., Govan, G.G., Gracey, A.Y., and Cossins, A.R. (2007). An explicit test of the phospholipid saturation hypothesis of acquired cold tolerance in <em>Caenorhabditis elegans</em&gt. Proceedings of the National Academy of Sciences *104*, 5489.

Murthy, S.E., Dubin, A.E., Whitwam, T., Jojoa-Cruz, S., Cahalan, S.M., Mousavi, S.A.R., Ward, A.B., and Patapoutian, A. (2018). OSCA/TMEM63 are an evolutionarily conserved family of mechanically activated ion channels. eLife *7*, e41844.

Nagarajan, S., Schuler, E.E., Ma, K., Kindt, J.T., and Dyer, R.B. (2012). Dynamics of the gel to fluid phase transformation in unilamellar DPPC vesicles. J Phys Chem B *116*, 13749-13756.

Nagata, T., Iizumi, S., Satoh, K., Ooka, H., Kawai, J., Carninci, P., Hayashizaki, Y., Otomo, Y., Murakami, K., Matsubara, K.*, et al.* (2004). Comparative Analysis of Plant and Animal Calcium Signal Transduction Element Using Plant Full-Length cDNA Data. Molecular Biology and Evolution *21*, 1855-1870.

Nakai, J., Ohkura, M., and Imoto, K. (2001). A high signal-to-noise Ca2+ probe composed of a single green fluorescent protein. Nature Biotechnology *19*.

Nakayama, Y., Yoshimura, K., and Iida, H. (2012). Organellar mechanosensitive channels in fission yeast regulate the hypo-osmotic shock response. Nature Communications *3*, 1020.

Nanjappa, D., Sanges, R., Ferrante, M.I., and Zingone, A. (2017). Diatom flagellar genes and their expression during sexual reproduction in Leptocylindrus danicus. BMC Genomics *18*, 813.

Nellaepalli, S., Kodru, S., and Subramanyam, R. (2012). Effect of cold temperature on regulation of state transitions in Arabidopsis thaliana. Journal of Photochemistry and Photobiology B: Biology *112*, 23-30.

Nelson, D.M., Tréguer, P., Brzezinski, M.A., Leynaert, A., and Quéguiner, B. (1995). Production and dissolution of biogenic silica in the ocean: Revised global estimates, comparison with regional data and relationship to biogenic sedimentation. Global Biogeochemical Cycles *9*, 359-372.

Neupert, J., Karcher, D., and Bock, R. (2009). Generation of Chlamydomonas strains that efficiently express nuclear transgenes. Plant J *57*, 1140-1150.

Nievola, C.C., Carvalho, C.P., Carvalho, V., and Rodrigues, E. (2017). Rapid responses of plants to temperature changes. Temperature (Austin) *4*, 371-405.

Norwood, T.H., and Zeigler, C.J. (1982). The Use of Dimethyl Sulfoxide in Mammalian Cell Fusion. In Techniques in Somatic Cell Genetics, J.W. Shay, ed. (Boston, MA: Springer US), pp. 35-45.

Notman, R., den Otter, W.K., Noro, M.G., Briels, W.J., and Anwar, J. (2007). The permeability enhancing mechanism of DMSO in ceramide bilayers simulated by molecular dynamics. Biophys J *93*, 2056-2068.

Notman, R., Noro, M., O'Malley, B., and Anwar, J. (2006). Molecular Basis for Dimethylsulfoxide (DMSO) Action on Lipid Membranes. Journal of the American Chemical Society *128*, 13982-13983.

Nymark, M., Sharma, A.K., Sparstad, T., Bones, A.M., and Winge, P. (2016). A CRISPR/Cas9 system adapted for gene editing in marine algae. Sci Rep *6*, 24951.

Ohkura, M., Sasaki, T., Sadakari, J., Gengyo-Ando, K., Kagawa-Nagamura, Y., Kobayashi, C., Ikegaya, Y., and Nakai, J. (2012). Genetically Encoded Green Fluorescent Ca2+ Indicators with Improved Detectability for Neuronal Ca2+ Signals. PLOS ONE *7*, e51286.

Okita, N., Isogai, N., Hirono, M., Kamiya, R., and Yoshimura, K. (2005). Phototactic activity in Chlamydomonas: non-phototactic; mutants deficient in Ca2+-dependent control of flagellar dominance or in inner-arm dynein. Journal of Cell Science *118*, 529.

Ono, T.A., and Murata, N. (1981). Chilling Susceptibility of the Blue-green Alga Anacystis nidulans: Stimulation of the passive permeability of cytoplasmic membrane at chilling temperatures. Plant physiology *67*, 182-187.

Orio, P., Parra, A., Madrid, R., González, O., Belmonte, C., and Viana, F. (2012). Role of Ih in the firing pattern of mammalian cold thermoreceptor endings. Journal of Neurophysiology *108*, 3009-3023.

Örvar, B.L., Sangwan, V., Omann, F., and Dhindsa, R.S. (2000). Early steps in cold sensing by plant cells: the role of actin cytoskeleton and membrane fluidity. The Plant Journal *23*, 785-794.

Ovide, C., Kiefer-Meyer, M.C., Berard, C., Vergne, N., Lecroq, T., Plasson, C., Burel, C., Bernard, S., Driouich, A., Lerouge, P*., et al.* (2018). Comparative in depth RNA sequencing of P. tricornutum's morphotypes reveals specific features of the oval morphotype. Sci Rep *8*, 14340.

Owttrim, G.W. (2006). RNA helicases and abiotic stress. Nucleic acids research *34*, 3220-3230.

Paasche, E. (1973). Silicon and the ecology of marine plankton diatoms. II. Silicate-uptake kinetics in five diatom species. Marine Biology *19*, 262-269.

Parag, H.A., Raboy, B., and Kulka, R.G. (1987). Effect of heat shock on protein degradation in mammalian cells: involvement of the ubiquitin system. The EMBO journal *6*, 55-61.

Paredes, R.M., Etzler, J.C., Watts, L.T., Zheng, W., and Lechleiter, J.D. (2008). Chemical calcium indicators. Methods *46*, 143-151.

Park, S., Lee, Y., Lee, J.H., and Jin, E. (2013). Expression of the high light-inducible Dunaliella LIP promoter in Chlamydomonas reinhardtii. Planta. *238*, 1147-1156.

Parrotta, L., Faleri, C., Cresti, M., and Cai, G. (2015). Heat stress affects the cytoskeleton and the delivery of sucrose synthase in tobacco pollen tubes. Planta *243*.

Patapoutian, A., Peier, A.M., Story, G.M., and Viswanath, V. (2003). ThermoTRP channels and beyond: mechanisms of temperature sensation. Nature Reviews Neuroscience *4*, 529-539.

Patel, S. (2015). Function and dysfunction of two-pore channels. Science Signaling *8*, re7.

Patel, S., Penny, C.J., and Rahman, T. (2016). Two-pore Channels Enter the Atomic Era: Structure of Plant TPC Revealed. Trends Biochem Sci *41*, 475-477.

Paulsen, C.E., Armache, J.P., Gao, Y., Cheng, Y., and Julius, D. (2015). Structure of the TRPA1 ion channel suggests regulatory mechanisms. Nature *520*, 511-517.

Pazour, G.J., Agrin, N., Leszyk, J., and Witman, G.B. (2005). Proteomic analysis of a eukaryotic cilium. J Cell Biol *170*, 103-113.

Pearson, G.A., Lago-Leston, A., Cánovas, F., Cox, C.J., Verret, F., Lasternas, S., Duarte, C.M., Agusti, S., and Serrão, E.A. (2015). Metatranscriptomes reveal functional variation in diatom communities from the Antarctic Peninsula. The ISME journal *9*, 2275-2289.

Pedersen, S.F., Owsianik, G., and Nilius, B. (2005). TRP channels: an overview. Cell Calcium *38*, 233-252.

Pei, Z.M., Murata, Y., Benning, G., Thomine, S., Kluesener, B., Allen, G.J., Grill, E., and Schroeder, J.I. (2000). Calcium channels activated by hydrogen peroxide mediate abscisic acid signalling in guard cells. Nature *406*, 731-734.

Peier, A.M., Moqrich, A., Hergarden, A.C., Reeve, A.J., Andersson, D.A., Story, G.M., Earley, T.J., Dragoni, I., McIntyre, P., Bevan, S*., et al.* (2002). A TRP Channel that Senses Cold Stimuli and Menthol. Cell *108*, 705-715.

Peiter, E., Maathuis, F.J.M., Mills, L.N., Knight, H., Pelloux, J., Hetherington, A.M., and Sanders, D. (2005). The vacuolar Ca2+-activated channel TPC1 regulates germination and stomatal movement. Nature *434*, 404-408.

Pereira, G.J., Hirata, H., Fimia, G.M., do Carmo, L.G., Bincoletto, C., Han, S.W., Stilhano, R.S., Ureshino, R.P., Bloor-Young, D., Churchill, G*., et al.* (2011). Nicotinic acid adenine dinucleotide phosphate (NAADP) regulates autophagy in cultured astrocytes. J Biol Chem *286*, 27875-27881.

Perozeni, F., Stella, G.R., and Ballottari, M. (2018). LHCSR Expression under HSP70/RBCS2 Promoter as a Strategy to Increase Productivity in Microalgae. Int J Mol Sci *19*.

Petroutsos, D., Busch, A., Janssen, I., Trompelt, K., Bergner, S.V., Weinl, S., Holtkamp, M., Karst, U., Kudla, J., and Hippler, M. (2011). The chloroplast calcium sensor CAS is required for photoacclimation in Chlamydomonas reinhardtii. Plant Cell *23*, 2950-2963.

Pfitzer, E. (1871). Untersuchungen über Bau und Entwicklung der Bacillariaceen (Diatomaceen). Hansteins Bot. Anhandl. *2*, 1-189.

Pitt, S.J., Funnell, T.M., Sitsapesan, M., Venturi, E., Rietdorf, K., Ruas, M., Ganesan, A., Gosain, R., Churchill, G.C., Zhu, M.X*., et al.* (2010). TPC2 is a novel NAADP-sensitive Ca2+ release channel, operating as a dual sensor of luminal pH and Ca2+. J Biol Chem *285*, 35039-35046.

Pitt, S.J., Lam, A.K.M., Rietdorf, K., Galione, A., and Sitsapesan, R. (2014). Reconstituted Human TPC1 Is a Proton-Permeable Ion Channel and Is Activated by NAADP or Ca2+. Sci. Signal. *7*, 46.

Plieth, C., Hansen, U.-P., Knight, H., and Knight, M.R. (1999). Temperature sensing by plants: the primary characteristics of signal perception and calcium response. The Plant Journal *18*, 491-497.

Podolsky, R.D. (1994). Temperature and Water Viscosity: Physiological Versus Mechanical Effects on Suspension Feeding. Science *265*, 100.

Pologruto, T.A., Yasuda, R., and Svoboda, K. (2004). Monitoring neural activity and [Ca2+] with genetically encoded Ca2+ indicators. J Neurosci *24*, 9572-9579.

Popov, V.N., Antipina, O.V., Pchelkin, V.P., and Tsydendambaev, V.D. (2017). Changes in fatty acid composition of lipids in chloroplast membranes of tobacco plants during cold hardening. Russian Journal of Plant Physiology *64*, 156-161.

Popova, A.V., and Hincha, D.K. (2005). Effects of the sugar headgroup of a glycoglycerolipid on the phase behavior of phospholipid model membranes in the dry state. Glycobiology *15*, 1150-1155.

Pottosin, I.I., Dobrovinskaya, O.R., and Muñiz, J. (2001). Conduction of Monovalent and Divalent Cations in the Slow Vacuolar Channel. J Membrane Biology *181*, 55-56.

Poulsen, N., Chesley, P.M., and Kröger, N. (2006). Molecular Genetic Manipulation of the Diatom Thalassiosira Pseudonana (Bacillariophyceae). Journal of Phycology *42*, 1059-1065.

Poulsen, N.C., Spector, I., Spurck, T.P., Schultz, T.F., and Wetherbee, R. (1999). Diatom gliding is the result of an actin-myosin motility system. Cell Motility *44*, 23-33.

Poveda, J.A., Giudici, A.M., Renart, M.L., Molina, M.L., Montoya, E., Fernandez-Carvajal, A., Fernandez-Ballester, G., Encinar, J.A., and Gonzalez-Ros, J.M. (2014). Lipid modulation of ion channels through specific binding sites. Biochim Biophys Acta *1838*, 1560-1567.

Pristerá, A., and Okuse, K. (2011). Building Excitable Membranes: Lipid Rafts and Multiple Controls on Trafficking of Electrogenic Molecules. The Neuroscientist *18*, 70-81.

Privalov, P.L. (1990). Cold Denaturation of Protein. Critical Reviews in Biochemistry and Molecular Biology *25*, 281-306.

Pu, R., and Robinson, K.R. (1998). Cytoplasmic calcium gradients and calmodulin in the early development of the fucoid alga Pelvetia compressa. Journal of Cell Science *111*, 3197.

Purves, D., Augustine, G.J., Fitzpatrick, D., Katz, L.C., LaMantia, A., McNamara, J.O., and Williams, S.M. (2001). Neuroscience, 2nd edn (Sinauer Associaties Inc.).

Purvis, A.C., Shewfelt, R.L., and Gegogeine, J.W. (1995). Superoxide production by mitochondria isolated from green bell pepper fruit. Physiologia Plantarum *94*, 743-749.

Qi, Z., Stephens, N.R., and Spalding, E.P. (2006). Calcium entry mediated by GLR3.3, an Arabidopsis glutamate receptor with a broad agonist profile. Plant Physiol *142*, 963-971.

Qiu, Y., Li, M., Kim, R.J., Moore, C.M., and Chen, M. (2019). Daytime temperature is sensed by phytochrome B in Arabidopsis through a transcriptional activator HEMERA. Nat Commun *10*, 140.

Quarmby, L.M. (1996). Ca 2+ Influx Activated by Low pH in Chlamydomonas. J. Gen. Physiol. *108*, 351-361.

Raghavan, M., Fee, D., and Barkhaus, P.E. (2019). Chapter 1 - Generation and propagation of the action potential. In Handb Clin Neurol, K.H. Levin, and P. Chauvel, eds. (Elsevier), pp. 3-22.

Rahman, T., Cai, X., Brailoiu, G.C., Abood, M.E., Brailoiu, E., and Patel, S. (2014). Two-pore channels provide insight into the evolution of voltage-gated Ca2+ and Na+ channels. Sci Signal *7*, ra109.

Ranade, S.S., Syeda, R., and Patapoutian, A. (2015). Mechanically Activated Ion Channels. Neuron *87*, 1162-1179.

Ranf, S., Wunnenberg, P., Lee, J., Becker, D., Dunkel, M., Hedrich, R., Scheel, D., and Dietrich, P. (2007). Loss of the vacuolar cation channel, AtTPC1, does not impair Ca2+ signals induced by abiotic and biotic stresses. Plant J *53*, 287-299.

Rasala, B.A., Lee, P.A., Shen, Z., Briggs, S.P., Mendez, M., and Mayfield, S.P. (2012). Robust expression and secretion of Xylanase1 in Chlamydomonas reinhardtii by fusion to a selection gene and processing with the FMDV 2A peptide. PLoS One *7*, e43349.

Rastogi, A., Murik, O., Bowler, C., and Tirichine, L. (2016). PhytoCRISP-Ex: a web-based and stand-alone application to find specific target sequences for CRISPR/CAS editing. BMC Bioinformatics *17*, 261.

Rastogi, A., Vieira, F.R.J., Deton-Cabanillas, A.-F., Veluchamy, A., Cantrel, C., Wang, G., Vanormelingen, P., Bowler, C., Piganeau, G., Hu, H.*, et al.* (2019). A genomics approach reveals the global genetic polymorphism, structure and functional diversity of ten accessions of the marine model diatom Phaeodactylum tricornutum. bioRxiv, 176008.

Ratcliff, W.C., Herron, M.D., Howell, K., Pentz, J.T., Rosenzweig, F., and Travisano, M. (2013). Experimental evolution of an alternating uni- and multicellular life cycle in Chlamydomonas reinhardtii. Nat Commun *4*, 2742.

Raven, J.A., and Waite, A.M. (2004). The evolution of silicification in diatoms: inescapable sinking and sinking as escape? New Phytologist *162*, 45-61.

Regaudie-de-Gioux, A., Lasternas, S., Agustí, S., and Duarte, C.M. (2014). Comparing marine primary production estimates through different methods and development of conversion equations. Frontiers in Marine Science *1*, 19.

Reiff, D.F., Ihring, A., Guerrero, G., Isacoff, E.Y., Joesch, M., Nakai, J., and Borst, A. (2005). In vivo performance of genetically encoded indicators of neural activity in flies. J Neurosci *25*, 4766-4778.

Rensink, W.A., Iobst, S., Hart, A., Stegalkina, S., Liu, J., and Buell, C.R. (2005). Gene expression profiling of potato responses to cold, heat, and salt stress. Funct Integr Genomics *5*, 201-207.

Reuter, H., and Seitz, N. (1968). The dependence of calcium efflux from cardiac muscle on temperature and external ion composition. J Physiol *195*, 451-470.

Ridone, P., Vassalli, M., and Martinac, B. (2019). Piezo1 mechanosensitive channels: what are they and why are they important. Biophysical Reviews *11*, 795-805.

Rietdorf, K., Funnell, T.M., Ruas, M., Heinemann, J., Parrington, J., and Galione, A. (2011). Two-pore channels form homo- and heterodimers. J Biol Chem *286*, 37058-37062.

Robinson, P.K. (2015). Enzymes: principles and biotechnological applications. Essays in biochemistry *59*, 1-41.

Rochaix, J.-D. (1995). Chlamydomonas reinhardtii as the Photosynthetic Yeast. Annual Review of Genetics *29*, 209-230.

Roux, B. (2017). Ion channels and ion selectivity. Essays Biochem *61*, 201-209.

Ruas, M., Rietdorf, K., Arredouani, A., Davis, L.C., Lloyd-Evans, E., Koegel, H., Funnell, T.M., Morgan, A.J., Ward, J.A., Watanabe, K.*, et al.* (2010). Purified TPC Isoforms Form NAADP Receptors

with Distinct Roles for Ca(2+) Signaling and Endolysosomal Trafficking. Current Biology *20*, 703-709.

Ruban, A.V., Johnson, M.P., and Duffy, C.D. (2012). The photoprotective molecular switch in the photosystem II antenna. Biochim Biophys Acta *1817*, 167-181.

Rudd, J.J., and Franklin-Tong, V.E. (2001). Unravelling response-specificity in Ca2+ signalling pathways in plant cells. New Phytol. *151*, 7-33.

Russell, N.J. (2008). Membrane Components and Cold Sensing. In Psychrophiles: from Biodiversity to Biotechnology, R. Margesin, F. Schinner, J.-C. Marx, and C. Gerday, eds. (Berlin, Heidelberg: Springer Berlin Heidelberg), pp. 177-190.

Rybalchenko, V., Ahuja, M., Coblentz, J., Churamani, D., Patel, S., Kiselyov, K., and Muallem, S. (2012). Membrane potential regulates nicotinic acid adenine dinucleotide phosphate (NAADP) dependence of the pH- and Ca2+-sensitive organellar two-pore channel TPC1. J Biol Chem *287*, 20407-20416.

Sabir, J.S.M., Theriot, E.C., Manning, S.R., Al-Malki, A.L., Khiyami, M.A., Al-Ghamdi, A.K., Sabir, M.J., Romanovicz, D.K., Hajrah, N.H., El Omri, A*., et al.* (2018). Phylogenetic analysis and a review of the history of the accidental phytoplankter, Phaeodactylum tricornutum Bohlin (Bacillariophyta). PLoS One *13*, e0196744.

Sakato, M., Sakakibara, H., and King, S.M. (2007). Chlamydomonas Outer Arm Dynein Alters Conformation in Response to Ca2+. mol biol cell *18*, 3620-3634.

Sanders, D., Pelloux, J., Brownlee, C., and Harper, J.F. (2002). Calcium at the crossroads of signaling. Plant Cell *14 Suppl*, S401-417.

Sangwan, V., Foulds, I., Singh, J., and Dhindsa, R.S. (2001). Cold-activation of Brassica napus BN115 promoter is mediated by structural changes in membranes and cytoskeleton, and requires Ca2+ influx. The Plant Journal *27*, 1-12.

Sarno, D., Kooistra, W.H.C.F., Balzano, S., Hargraves, P.E., and Zingone, A. (2007). Diversity in the Genusskeletonema(Bacillariophyceae): Iii. Phylogenetic Position and Morphological Variability Ofskeletonema Costatumandskeletonema Grevillei, with the Description Ofskeletonema Ardenssp. Nov. Journal of Phycology *43*, 156-170.

Saro, G., Lia, A.-S., Thapliyal, S., Marques, F., Busch, K.E., and Glauser, D.A. (2020). Specific Ion Channels Control Sensory Gain, Sensitivity, and Kinetics in a Tonic Thermonociceptor. Cell Reports *30*, 397-408.e394.

Sasaki, K., and Imai, R. (2011). Pleiotropic roles of cold shock domain proteins in plants. Front Plant Sci *2*, 116.

Sasaki, T., Naka, M., Nakamura, F., and Tanaka, T. (1992). Ruthenium red inhibits the binding of calcium to calmodulin required for enzyme activation. Journal of Biological Chemistry *267*, 21518-21523.

Schneider, E.R., Anderson, E.O., Gracheva, E.O., and Bagriantsev, S.N. (2014). Temperature sensitivity of two-pore (K2P) potassium channels. Current topics in membranes *74*, 113-133.

Schobert, B. (1980). Proline catabolism, relaxation of osmotic strain and membrane permeability in the diatom Phaeodactylum tricornutum. Physiologia Plantarum *50*, 37-42.

Schonknecht, G. (2013). Calcium Signals from the Vacuole. Plants (Basel) *2*, 589-614.

Schulz, P., Herde, M., and Romeis, T. (2013). Calcium-dependent protein kinases: hubs in plant stress signaling and development. Plant Physiol *163*, 523-530.

Schulze, C., Sticht, H., Meyerhoff, P., and Dietrich, P. (2011). Differential contribution of EF-hands to the Ca2+-dependent activation in the plant two-pore channel TPC1. The Plant Journal *68*, 424-432.

Scranton, M.A., Ostrand, J.T., Georgianna, D.R., Lofgren, S.M., Li, D., Ellis, R.C., Carruthers, D.N., Dräger, A., Masica, D.L., and Mayfield, S.P. (2016). Synthetic promoters capable of driving robust nuclear gene expression in the green alga Chlamydomonas reinhardtii. Algal Research *15*, 135-142.

Scrase-Field, S.A.M.G., and Knight, M.R. (2003). Calcium: just a chemical switch? Current Opinion in Plant Biology *6*, 500-506.

Sehrawat, A., Gupta, R., and Deswal, R. (2013). Nitric oxide-cold stress signalling cross-talk, evolution of a novel regulatory mechanism. PROTEOMICS *13*, 1816-1835.

Seki, M., Narusaka, M., Abe, H., Kasuga, M., Yamaguchi-Shinozaki, K., Carninci, P., Hayashizaki, Y., and Shinozaki, K. (2001). Monitoring the expression pattern of 1300 Arabidopsis genes under drought and cold stresses by using a full-length cDNA microarray. The Plant cell *13*, 61-72.

Seki, M., Narusaka, M., Ishida, J., Nanjo, T., Fujita, M., Oono, Y., Kamiya, A., Nakajima, M., Enju, A., Sakurai, T.*, et al.* (2002). Monitoring the expression profiles of 7000 Arabidopsis genes under drought, cold and high-salinity stresses using a full-length cDNA microarray. The Plant Journal *31*, 279-292.

Sekimoto, H. (2017). Sexual reproduction and sex determination in green algae. Journal of Plant research *130*, 423-431.

Sengupta, P., and Garrity, P. (2013). Sensing temperature. Current biology : CB *23*, R304-R307.

Sharma, A.K., Nymark, M., Sparstad, T., Bones, A.M., and Winge, P. (2018). Transgene-free genome editing in marine algae by bacterial conjugation - comparison with biolistic CRISPR/Cas9 transformation. Sci Rep *8*, 14401.

Sharma, P., Jha, A.B., Dubey, R.S., and Pessarakli, M. (2012). Reactive Oxygen Species, Oxidative Damage, and Antioxidative Defense Mechanism in Plants under Stressful Conditions. Journal of Botany *2012*, 217037.

Sharma, V., He, C., Sacca-Schaeffer, J., Brzozowski, E., Martin-Herranz, D.E., Mendelowitz, Z., Fitzpatrick, D.A., and O'Halloran, D.M. (2013). Insight into the family of Na+/Ca2+ exchangers of Caenorhabditis elegans. Genetics *195*, 611-619.

Shaya, D., Findeisen, F., Abderemane-Ali, F., Arrigoni, C., Wong, S., Nurva, S.R., Loussouarn, G., and Minor, D.L., Jr. (2014). Structure of a prokaryotic sodium channel pore reveals essential gating elements and an outer ion binding site common to eukaryotic channels. J Mol Biol *426*, 467-483.

Shen, J., Zeng, Y., Zhuang, X., Sun, L., Yao, X., Pimpl, P., and Jiang, L. (2013). Organelle pH in the Arabidopsis endomembrane system. Mol Plant *6*, 1419-1437.

Silva, D.F., de Almeida, M.M., Chaves, C.G., Braz, A.L., Gomes, M.A., Pinho-da-Silva, L., Pesquero, J.L., Andrade, V.A., Leite Mde, F., de Albuquerque, J.G.*, et al.* (2015). TRPM8 Channel Activation Induced by Monoterpenoid Rotundifolone Underlies Mesenteric Artery Relaxation. PLoS One *10*, e0143171.

Sims, P.A., Mann, D.G., and Medlin, L.K. (2006). Evolution of the diatoms: insights from fossil, biological and molecular data. Phycologia *45*, 361-402.

Singh, A.K., McGoldrick, L.L., Demirkhanyan, L., Leslie, M., Zakharian, E., and Sobolevsky, A.I. (2019). Structural basis of temperature sensation by the TRP channel TRPV3. Nature Structural & Molecular Biology *26*, 994-998.

Slattery, S.S., Diamond, A., Wang, H., Therrien, J.A., Lant, J.T., Jazey, T., Lee, K., Klassen, Z., Desgagné-Penix, I., Karas, B.J.*, et al.* (2018). An Expanded Plasmid-Based Genetic Toolbox Enables Cas9 Genome Editing and Stable Maintenance of Synthetic Pathways in Phaeodactylum tricornutum. ACS Synthetic Biology *7*, 328-338.

Soattin, L., Fiore, M., Gavazzo, P., Viti, F., Facci, P., Raiteri, R., Difato, F., Pusch, M., and Vassalli, M. (2016). The biophysics of piezo1 and piezo2 mechanosensitive channels. Biophys Chem *208*, 26-33.

Somerville, C. (1995). Direct tests of the role of membrane lipid composition in low-temperature-induced photoinhibition and chilling sensitivity in plants and cyanobacteria. Proceedings of the National Academy of Sciences of the United States of America *92*, 6215-6218.

Sonoike, K. (1999). The different roles of chilling temperatures in the photoinhibition of photosystem I and photosystem II. Journal of Photochemistry and Photobiology B: Biology *48*, 136-141.

Stael, S., Wurzinger, B., Mair, A., Mehlmer, N., Vothknecht, U.C., and Teige, M. (2012). Plant organellar calcium signalling: an emerging field. Journal of experimental botany *63*, 1525-1542.

Steponkus, P.L. (1984). Role of the Plasma Membrane in Freezing Injury and Cold Acclimation. Annual Review of Plant Physiology *35*, 543-584.

Stewart, T.A., and Davis, F.M. (2019). An element for development: Calcium signaling in mammalian reproduction and development. Biochim Biophys Acta Mol Cell Res *1866*, 1230-1238.

Suarez, G., Santschi, C., Slaveykova, V.I., and Martin, O.J. (2013). Sensing the dynamics of oxidative stress using enhanced absorption in protein-loaded random media. Sci Rep *3*, 3447.

Südhof, T.C. (2012). The presynaptic active zone. Neuron *75*, 11-25.

Sumper, M., and Brunner, E. (2008). Silica Biomineralisation in Diatoms: The Model Organism Thalassiosira pseudonana. ChemBioChem *9*, 1187-1194.

Suto, K., and Gotoh, H. (1999). Calcium signaling in cold cells studied in cultured dorsal root ganglion neurons. Neuroscience *92*, 1131-1135.

Suttangkakul, A., Sirikhachornkit, A., Juntawong, P., Puangtame, W., Chomtong, T., Srifa, S., Sathitnaitham, S., Dumrongthawatchai, W., Jariyachawalid, K., and Vuttipongchaikij, S. (2019). Evaluation of strategies for improving the transgene expression in an oleaginous microalga Scenedesmus acutus. BMC Biotechnology *19*, 4.

Suzuki, N., and Mittler, R. (2006). Reactive oxygen species and temperature stresses: A delicate balance between signaling and destruction. Physiologia Plantarum *126*, 45-51.

Takahashi, K., Minoru, I., Knight, M.R., Trewavas, A.J., and Muto, S. (1997). Hypoosmotic Shock lnduces lncreases in Cytosolic Ca2+ in Tobacco Suspension-Culture Cells. Plant Physiol *113*, 597-594.

Talevich, E., Mirza, A., and Kannan, N. (2011). Structural and evolutionary divergence of eukaryotic protein kinases in Apicomplexa. BMC Evolutionary Biology *11*, 321.

Tanaka, R., Kikutani, S., Mahardika, A., and Matsuda, Y. (2014). Localization of enzymes relating to C4 organic acid metabolisms in the marine diatom Thalassiosira pseudonana. Photosynthetic Researh *121*, 251-263.

Tang, J., Jia, Y., Ma, J., and Yi, M. (2008). Numerical study of IP3-dependent Ca2+ spiral waves in Xenopus oocytes. EPL (Europhysics Letters) *83*, 68001.

Tattersall, E.A.R., Grimplet, J., DeLuc, L., Wheatley, M.D., Vincent, D., Osborne, C., Ergül, A., Lomen, E., Blank, R.R., Schlauch, K.A*., et al.* (2007). Transcript abundance profiles reveal larger and more complex responses of grapevine to chilling compared to osmotic and salinity stress. Functional & Integrative Genomics *7*, 317-333.

Taylor, A.R. (2009). A Fast Na+/Ca2+-Based Action Potential in a Marine Diatom. PLOS ONE *4*, e4966.

Taylor, A.R., Chrachri, A., Wheeler, G., Goddard, H., and Brownlee, C. (2011). A Voltage-Gated H+ Channel Underlying pH Homeostasis in Calcifying Coccolithophores. PLOS Biology *9*, e1001085.

Taylor, A.R., Manison, N.F.H., Fernandez, C., Wood, J., and Brownlee, C. (1996). Spatial Organization of Calcium Signaling Involved in Cell Volume Control in the Fucus Rhizoid. The Plant Cell *8*, 2015.

Thomashow, M.F. (1999). Plant Cold Acclimation: Freezing Tolerance Genes and Regulatory Mechanisms. Annual Review of Plant Physiology and Plant Molecular Biology *50*, 571-599.

Toivola, D.M., Strnad, P., Habtezion, A., and Omary, M.B. (2010). Intermediate filaments take the heat as stress proteins. Trends Cell Biol *20*, 79-91.

Toseland, A., Daines, S.J., Clark, J.R., Kirkham, A., Strauss, J., Uhlig, C., Lenton, T.M., Valentin, K., Pearson, G.A., Moulton, V*., et al.* (2013). The impact of temperature on marine phytoplankton resource allocation and metabolism. Nature Climate Change *3*, 979-984.

Tsai, C.-J., Maizel, J.V., and Nussinov, R. (2002). The Hydrophobic Effect: A New Insight from Cold Denaturation and a Two-State Water Structure. Critical Reviews in Biochemistry and Molecular Biology *37*, 55-69.

Tsien, R.Y., Pozzan, T., and Rink, T.J. (1984). Measuring and manipulating cytosolic Ca2+ with trapped indicators. Trends in Biochem. Sc*. 9*, 263-266.

Tsuda, A., Takeda, S., Saito, H., Nishioka, J., Nojiri, Y., Kudo, I., Kiyosawa, H., Shiomoto, A., Imai, K., Ono, T*., et al.* (2003). A Mesoscale Iron Enrichment in the Western Subarctic Pacific Induces a Large Centric Diatom Bloom. Science *300*, 958.

Tsuruda, P.R., Julius, D., and Minor, D.L., Jr. (2006). Coiled coils direct assembly of a cold-activated TRP channel. Neuron *51*, 201-212.

Tugba Durlu-Kandilci, N., Ruas, M., Chuang, K.T., Brading, A., Parrington, J., and Galione, A. (2010). TPC2 proteins mediate nicotinic acid adenine dinucleotide phosphate (NAADP)- and agonist-evoked contractions of smooth muscle. J Biol Chem *285*, 24925-24932.

Underwood, G., Phillips, J., and Saunders, K. (1998). Distribution of estuarine benthic diatom species along salinity and nutrient gradients. European Journal of Phycology *33*, 173-183.

van Creveld, S.G., Rosenwasser, S., Schatz, D., Koren, I., and Vardi, A. (2015). Early perturbation in mitochondria redox homeostasis in response to environmental stress predicts cell fate in diatoms. The ISME Journal *9*, 385-395.

van Meer, G., Voelker, D.R., and Feigenson, G.W. (2008). Membrane lipids: where they are and how they behave. Nature Reviews Molecular Cell Biology *9*, 112-124.

Vardi, A., Formiggini, F., Casotti, R., De Martino, A., Ribalet, F., Miralto, A., and Bowler, C. (2006). A stress surveillance system based on calcium and nitric oxide in marine diatoms. PLoS Biol *4*, e60.

Véron, B., Billard, C., Dauguet, J.-C., and Hartmann, M.-A. (1996). Sterol composition of Phaeodactylum tricornutum as influenced by growth temperature and light spectral quality. Lipids *31*, 989-994.

Verret, F., Wheeler, G., Taylor, A.R., Farnham, G., and Brownlee, C. (2010). Calcium channels in photosynthetic eukaryotes: implications for evolution of calcium-based signalling. New Phytol *187*, 23-43.

Vincent, T.R., Avramova, M., Canham, J., Higgins, P., Bilkey, N., Mugford, S.T., Pitino, M., Toyota, M., Gilroy, S., Miller, A.J.*, et al.* (2017). Interplay of Plasma Membrane and Vacuolar Ion Channels, Together with BAK1, Elicits Rapid Cytosolic Calcium Elevations in Arabidopsis during Aphid Feeding. The Plant Cell *29*, 1460.

Virta, L., Gammal, J., Järnström, M., Bernard, G., Soininen, J., Norkko, J., and Norkko, A. (2019). The diversity of benthic diatoms affects ecosystem productivity in heterogeneous coastal environments. Ecology *100*, e02765.

Voets, T., Droogmans, G., Wissenbach, U., Janssens, A., Flockerzi, V., and Nilius, B. (2004). The principle of temperature-dependent gating in cold- and heat-sensitive TRP channels. Nature *430*, 748-754.

Waadt, R., Krebs, M., Kudla, J., and Schumacher, K. (2017). Multiparameter imaging of calcium and abscisic acid and high-resolution quantitative calcium measurements using R-GECO1-mTurquoise in Arabidopsis. New Phytologist *216*, 303-320.

Wang, C., Xu, W., Jin, H., Zhang, T., Lai, J., Zhou, X., Zhang, S., Liu, S., Duan, X., Wang, H.*, et al.* (2016a). A Putative Chloroplast-Localized Ca(2+)/H(+) Antiporter CCHA1 Is Involved in Calcium and pH Homeostasis and Required for PSII Function in Arabidopsis. Mol Plant *9*, 1183-1196.

Wang, L., Yamano, T., Takane, S., Niikawa, Y., Toyokawa, C., Ozawa, S.-I., Tokutsu, R., Takahashi, Y., Minagawa, J., Kanesaki, Y.*, et al.* (2016b). Chloroplast-mediated regulation of CO2-concentrating mechanism by Ca2+-binding protein CAS in the green alga Chlamydomonas reinhardtii. Proceedings of the National Academy of Sciences of the United States of America *113*, 12586-12591.

Wang, Q., Yang, S., Wan, S., and Li, X. (2019). The Significance of Calcium in Photosynthesis. Int J Mol Sci *20*.

Wang, S.S., and Thompson, S.H. (1995). Local positive feedback by calcium in the propagation of intracellular calcium waves. Biophys J *69*, 1683-1697.

Wang, W., Li, H., Lin, X., Zhang, F., Fang, B., and Wang, Z. (2016c). The effect of polar auxin transport on adventitious branches formation in Gracilaria lichenoides in vitro. Physiologia Plantarum *158*, 356-365.

Wang, X., Zhang, X., Dong, X.P., Samie, M., Li, X., Cheng, X., Goschka, A., Shen, D., Zhou, Y., Harlow, J.*, et al.* (2012). TPC proteins are phosphoinositide- activated sodium-selective ion channels in endosomes and lysosomes. Cell *151*, 372-383.

Wang, Y.J., Yu, J.N., Chen, T., Zhang, Z.G., Hao, Y.J., Zhang, J.S., and Chen, S.Y. (2005). Functional analysis of a putative Ca2+ channel gene TaTPC1 from wheat. J Exp Bot *56*, 3051-3060.

Ward, J.M., and Schroeder, J.I. (1994). Calcium-Activated K+ Channels and Calcium-Induced Calcium Release by Slow Vacuolar Ion Channels in Guard Cell Vacuoles Implicated in the Control of Stomatal Closure. The Plant Cell *6*, 669.

Weber, T., and Deutsch, C. (2012). Oceanic nitrogen reservoir regulated by plankton diversity and ocean circulation. Nature *489*, 419-422.

Wehner, F., Olsen, H., Tinel, H., Kinne-Saffran, E., and Kinne, R. (2003). Cell volume regulation: osmolytes, osmolyte transport, and signal transduction. Reviews of physiology, biochemistry and pharmacology *148*, 1-80.

Weiner, I., Atar, S., Schweitzer, S., Eilenberg, H., Feldman, Y., Avitan, M., Blau, M., Danon, A., Tuller, T., and Yacoby, I. (2018). Enhancing heterologous expression in Chlamydomonas reinhardtii by transcript sequence optimization. Plant J *94*, 22-31.

Weinl, S., and Kudla, J. (2009). The CBL-CIPK Ca2+-decoding signaling network: function and perspectives. New Phytologist *184*, 517-528.

Westbroek, P., Young J, R., and Linschooten, K. (2007). Coccolith Production (Biomineralization) in the Marine Alga Emiliania huxleyi. The Journal of Protozoology *36*, 368-373.

Wetsel, W.C. (2011). Sensing hot and cold with TRP channels. Int J Hyperthermia *27*, 388-398.

Whalley, H.J., and Knight, M.R. (2013). Calcium signatures are decoded by plants to give specific gene responses. New Phytologist *197*, 690-693.

Wheeler, G., Helliwell, K.E., and Brownlee, C. (2019). Calcium signalling in algae. Perspectives in Phycology *6*, 1-10.

Wheeler, G.L., and Brownlee, C. (2008). Ca2+ signalling in plants and green algae - changing channels. Trends in Plant Science *13*, 506-514.

Wheeler, G.L., Joint, I., and Brownlee, C. (2008). Rapid spatiotemporal patterning of cytosolic Ca2+ underlies flagellar excision in Chlamydomonas reinhardtii. Plant J *53*, 401-413.

Whitaker, M. (2006). Calcium at fertilization and in early development. Physiol Rev *86*, 25-88.

Willis, A., Chiovitti, A., Dugdale, T.M., and Wetherbee, R. (2013). Characterization of the extracellular matrix of Phaeodactylum tricornutum (Bacillariophyceae): structure, composition, and adhesive characteristics. Journal of Phycology *49*, 937-949.

Winfield, M.O., Lu, C., Wilson, I.D., Coghill, J.A., and Edwards, K.J. (2009). Cold- and light-induced changes in the transcriptome of wheat leading to phase transition from vegetative to reproductive growth. BMC Plant Biology *9*, 55.

Winfield, M.O., Lu, C., Wilson, I.D., Coghill, J.A., and Edwards, K.J. (2010). Plant responses to cold: transcriptome analysis of wheat. Plant Biotechnology Journal *8*, 749-771.

Wu, J., Yan, Z., Li, Z., Qian, X., Lu, S., Dong, M., Zhou, Q., and Yan, N. (2016). Structure of the voltage-gated calcium channel Ca(v)1.1 at 3.6 A resolution. Nature *537*, 191-196.

Xu, L., Han, Y., Chen, X., Aierken, A., Wen, H., Zheng, W., Wang, H., Lu, X., Zhao, Z., Ma, C.*, et al.* (2020). Molecular mechanisms underlying menthol binding and activation of TRPM8 ion channel. Nature Communications *11*, 3790.

Xu, L., Tripathy, A., Pasek, D.A., and Meissner, G. (1999). Ruthenium Red Modifies the Cardiac and Skeletal Muscle Ca2+ Release Channels (Ryanodine Receptors) by Multiple Mechanisms. Journal of Biological Chemistry *274*, 32680-32691.

Xu, X., Bittman, R., Duportail, G., Heissler, D., Vilcheze, C., and London, E. (2001). Effect of the structure of natural sterols and sphingolipids on the formation of ordered sphingolipid/sterol domains (rafts). Comparison of cholesterol to plant, fungal, and disease-associated sterols and comparison of sphingomyelin, cerebrosides, and ceramide. J Biol Chem *276*, 33540-33546.

Yamauchi, T. (2005). Neuronal Ca2+ Calmodulin-Dependent Protein Kinase II Discovery, Progress in a Quarter of a Century, and Perspective: Implication for Learning and Memory. Biological and Pharmaceutical Bulletin *28*, 1342-1354.

Yancey, P.H. (2005). Organic osmolytes as compatible, metabolic and counteracting cytoprotectants in high osmolarity and other stresses. Journal of Experimental Biology *208*, 2819-2830.

Yáñez, M., Gil-Longo, J., and Campos-Toimil, M. (2012). Calcium Binding Proteins. In Calcium Signaling, M.S. Islam, ed. (Dordrecht: Springer Netherlands), pp. 461-482.

Yang, F., and Zheng, J. (2014). High temperature sensitivity is intrinsic to voltage-gated potassium channels. eLife *3*, e03255.

Yang, M., Lin, X., Liu, X., Zhang, J., and Ge, F. (2018). Genome Annotation of a Model Diatom Phaeodactylum tricornutum Using an Integrated Proteogenomic Pipeline. Mol Plant *11*, 1292-1307.

Yin, J., and Kuebler, W.M. (2010). Mechanotransduction by TRP channels: general concepts and specific role in the vasculature. Cell Biochem Biophys *56*, 1-18.

Yin, Y., Wu, M., Zubcevic, L., Borschel, W.F., Lander, G.C., and Lee, S.Y. (2018). Structure of the cold- and menthol-sensing ion channel TRPM8. Science *359*, 237-241.

Yoshida, Y., and Imai, S. (1997). Structure and Function of Inositol 1,4,5-Trisphosphate Receptor. Jpa. J. Pharmacol. *74*, 125-137.

Yoshimura, K., and Sokabe, M. (2010). Mechanosensitivity of ion channels based on protein-lipid interactions. J R Soc Interface *7 Suppl 3*, S307-320.

Yuan, F., Yang, H., Xue, Y., Kong, D., Ye, R., Li, C., Zhang, J., Theprungsirikul, L., Shrift, T., Krichilsky, B.*, et al.* (2014). OSCA1 mediates osmotic-stress-evoked Ca2+ increases vital for osmosensing in Arabidopsis. Nature *514*, 367-371.

Yuan, P., Du, L., and Poovaiah, B.W. (2018). Ca(2+)/Calmodulin-Dependent AtSR1/CAMTA3 Plays Critical Roles in Balancing Plant Growth and Immunity. Int J Mol Sci *19*.

Zagotta, W.N. (2006). Permutations of permeability. Nature *440*, 427-429.

Zarka, D.G., Vogel, J.T., Cook, D., and Thomashow, M.F. (2003). Cold Induction of Arabidopsis CBF Genes Involves Multiple ICE (Inducer of CBF Expression) Promoter Elements and a Cold-Regulatory Circuit That Is Desensitized by Low Temperature. Plant Physiology *133*, 910.

Zhang, C., and Hu, H. (2014). High-efficiency nuclear transformation of the diatom Phaeodactylum tricornutum by electroporation. Mar Genomics *16*, 63-66.

Zhang, S., Liu, H., Ke, Y., and Li, B. (2017). Effect of the Silica Content of Diatoms on Protozoan Grazing. Frontiers in Marine Science *4*.

Zhang, X., Hu, Y., Yang, X., Tang, Y., Han, S., Kang, A., Deng, H., Chi, Y., Zhu, D., and Lu, Y. (2019). Foerster resonance energy transfer (FRET)-based biosensors for biological applications. Biosens Bioelectron *138*, 111314.

Zhao, Y., Araki, S., Wu, J., Teramoto, T., Chang, Y.F., Nakano, M., Abdelfattah, A.S., Fujiwara, M., Ishihara, T., Nagai, T*., et al.* (2011). An expanded palette of genetically encoded Ca(2)(+) indicators. Science *333*, 1888-1891.

Zheng, J. (2013). Molecular Mechanism of TRP Channels. Comprehensive Physiology, 221-242.

Zheng, L., and Mackrill, J.J. (2016). Calcium Signaling in Oomycetes: An Evolutionary Perspective. Frontiers in Physiology *7*.

Zhu, M.X., Ma, J., Parrington, J., Calcraft, P.J., Galione, A., and Evans, A.M. (2010). Calcium signaling via two-pore channels: local or global, that is the question. Am J Physiol Cell Physiol *298*, C430-441.

Zhu, X., Dunand, C., Snedden, W., and Galaud, J.P. (2015). CaM and CML emergence in the green lineage. Trends Plant Sci *20*, 483-489.

Zimmerman, R.C., and Kremer, J.N. (1984). Episodic nutrient supply to a kelp forest ecosystem in Southern California. Journal of Marine Research *42*, 591-604.